Department of Structural Engineering
Faculty of Engineering Science and Technology
NTNU- Norwegian University of Science and Technology

ACCESSIBILITY
OPEN

MASTER'S THESIS 2010

SUBJECT AREA:	DATE:	NO. OF PAGES:
Structural Engineering	June 7, 2010	145 pages + 71 appendix pages

TITLE: **Hybrid Concrete Structures**
Experimental Testing and Numerical Simulation of Structural Elements

Hybride betongkonstruksjonar
Laboratorieforsøk og numerisk simulering av konstruksjonselement

BY: Ole Georg Skjølberg
Anders Hansson

ABSTRACT:

The Composite Sandwich Slab (CSS) studied in this report is a hybrid concrete structure with different concrete types in zones of high versus low stresses. The CSS is a combination of a precast concrete formwork and in-situ concrete, where a structural top layer is supposed to be cast at the construction site. It is intended that the precast concrete formwork would be lifted directly into position before the structural top layer is cast. The precast concrete formwork consist of a relatively thin bottom layer in reinforced normal concrete with a thicker steel fiber reinforced lightweight concrete layer above.

The CSS concept is supposed to be an alternative to today's existing slab solutions in buildings and harbor structures. The CSS concept is lighter than a traditional concrete slab, but with maintained load carrying capacity. For a typical 250mm thick slab the weight reduction would be up to 35% compared to a traditional concrete slab. The precast CSS elements are also stiffer than today's existing precast products, which means that the number of temporary supports needed during the construction phase can be reduced or eliminated. This reduction would lead to saved time, space and money at the construction site.

The lightweight concrete used in the precast formwork has an approximate density of 900kg/m^2–1150kg/m^2 with a compressive strength in the range of 15-20 MPa. The lightweight concrete is relatively new product and is therefore first studied through laboratory tests with respect to compressive strength, tensile strength and shear capacity. Since the material properties for the lightweight concrete is going to be used in numerical analyses, the first laboratory tests are analyzed numerically in order to verify that agreement can be obtained and that the material models used are valid for this specific concrete. The results indicate good agreement.

A concept CSS beam is then designed, tested and analyzed both by hand and numerically in order to state the CSS capacity as a slab construction. The concept CSS beam is both tested and analyzed with and without the structural top layer, i.e. as a finished product and during construction phase respectively. The laboratory tests indicate competitive capacities for both types. Hand calculations and numerical analysis performed after the test had good correlation with respect to the capacities and displacements obtained in the laboratory when testing the concept beam.

The numerical analyses are therefore valid and can be used in further analyses of the CSS concept. The numerical model used in the post analysis of the CSS has been exposed to realistic loading. Both analysis of the precast part of the CSS during construction phase and analysis of the CSS with top layer and loading according to NS 3491-1 has been performed. Material and load factors have also been taken into account. The results from these analyses are promising with respect to the CSS general capacity. Results show that it is possible to use the precast formwork without temporary supports during the construction phase for a typical concrete slab with a span of 6m.

RESPONSIBLE TEACHER: Terje Kanstad

SUPERVISOR: Linn Grepstad Nes

CARRIED OUT AT: Department of Structural Engineering, NTNU

MASTEROPPGÅVE 2010

for

Anders Hansson og Ole Georg Skjølberg

Hybride betongkonstruksjonar

–laboratorieforsøk og numerisk simulering av konstruksjonselement

Hybride concrete structures

- experimental testing and numerical simulation of structural elements

Oppgåve:

Litteraturstudium:	Skildring av forsøksmetodar for bøyeprøving og strekkprøving av fiberarmert betong etter Norsk Standard og metode frå Sintef. Matematisk modellering av ikkje-lineær betongoppførsel etter eit utval artiklar og delar av pensum til Ph.d.-faget "Numerisk simulering av armert betong". Litteratur på fiberarmert betong.
Forsøk i lab:	Hovudmålet med oppgåva er å gjennomføre forsøk på ein hybrid betongbjelke. I tillegg blir det støypt ut mindre prøvestykker for å finne eigenskapar til dei ulike materiala som inngår i den hybride bjelken; trykkfasthet, strekkfasthet, bøyestrekkfasthet samt reststrekkfastheten.
FEM-analysar:	Forsøka i lab utgjer grunnlaget for numeriske analysar utført med elementmetodeprogrammet Abaqus. Numeriske analysar blir utført på dei små konstruksjonselementa for å finne materialeigenskapar og resultata frå desse analysane blir deretter brukt i FEM-analysar av ein større hybrid betongbjelke og samanlikna med resultat frå labforsøk.

Oppgåva organiserast etter gjeldande retningslinjer og leverast til Institutt for Konstruksjonsteknikk innan 14.juni 2010.

Rettleiar: Ph.d. stipendiat Linn Grepstad Nes

Faglærar: Professor Terje Kanstad

NTNU, 18.januar, 2010

Terje Kanstad — Linn Grepstad Nes

Terje Kanstad — Linn Grepstad Nes

Faglærar — Rettleiar

Abstract

The Composite Sandwich Slab (CSS) studied in this report is a hybrid concrete structure with different concrete types in zones of high versus low stresses. The CSS is a combination of a precast concrete formwork and in-situ concrete, where a structural top layer is supposed to be cast at the construction site. It is intended that the precast concrete formwork would be lifted directly into position before the structural top layer is cast. The precast concrete formwork consist of a relatively thin bottom layer in reinforced normal concrete with a thicker steel fiber reinforced lightweight concrete layer above.

The CSS concept is supposed to be an alternative to today's existing slab solutions in buildings and harbor structures. The CSS concept is lighter than a traditional concrete slab, but with maintained load carrying capacity. For a typical 250mm thick slab the weight reduction would be up to 35% compared to a traditional concrete slab. The precast CSS elements are also stiffer than today's existing precast products, which means that the number of temporary supports needed during the construction phase can be reduced or eliminated. This reduction would lead to saved time, space and money at the construction site.

The lightweight concrete used in the precast formwork has an approximate density of 900kg/m^2–1150kg/m^2 with a compressive strength in the range of 15-20 MPa. The lightweight concrete is relatively new product and is therefore first studied through laboratory tests with respect to compressive strength, tensile strength and shear capacity. Since the material properties for the lightweight concrete is going to be used in numerical analyses, the first laboratory tests are analyzed numerically in order to verify that agreement can be obtained and that the material models used are valid for this specific concrete. The results indicate good agreement.

A concept CSS beam is then designed, tested and analyzed both by hand and numerically in order to state the CSS capacity as a slab construction. The concept CSS beam is both tested and analyzed with and without the structural top layer, i.e. as a finished product and during construction phase respectively. The laboratory tests indicate competitive capacities for both types. Hand calculations and numerical analysis performed after the test had good correlation with respect to the capacities and displacements obtained in the laboratory when testing the concept beam.

The numerical analyses are therefore valid and can be used in further analyses of the CSS concept. The numerical model used in the post analysis of the CSS has been exposed to realistic loading. Both analysis of the precast part of the CSS during construction phase and analysis of the CSS with top layer and loading according to NS 3491-1 has been performed. Material and load factors have also been taken into account. The results from these analyses are promising with respect to the CSS general capacity. Results show that it is possible to use the precast formwork without temporary supports during the construction phase for a typical concrete slab with a span of 6m.

Preface

This master's thesis is the final project for receiving the Master of Science degree in Civil and Environmental Engineering at the Norwegian University of Science and Technology. It has been carried out at the Department for Structural Engineering with supervision from Ph.D. student Linn Grepstad Nes and Professor Terje Kanstad between January and June 2010.

The theme for the thesis, "Hybrid Concrete Structures", was chosen on the basis of the possibilities to combine innovative laboratory research work with numerical analyses. The Composite Sandwich Slab that we ended up working with is our own concept which is a result from workshops with concrete products producers, SINTEF and NTNU researchers and initial literature studies.

Our first acknowledgement is given to Linn and Terje who supervised us and made it possible to work with innovative research during our master's thesis project. They should both have special thanks since they believed in our project from day one and pushed the right buttons so that the project could be realized the way we wanted.

The laboratory work was made possible due to partial funding from COIN – The Concrete Innovation Center, Weber and The Department of Structural engineering. Many thanks for the financial support.

Geir Norden and Weber should also have special thanks for guidance and help related to the production of test specimens and recipes for their special foam concrete.

All the people working in the laboratory should also receive acknowledgements. One should search a long time to find more helpful, service minded and flexible laboratory employees. Special thanks to Ove Loraas and Steinar Seehuus who were the people helping us the most.

Thanks to Håvard Nedrelid for supporting us through the whole project, from the brainstorming phase to the bitter end. Somehow you almost became part of our project and had always time to answer questions and share your own thoughts.

Thanks to Sindre Sandbakk for sharing of your laboratory experience and supporting us with our first unsteady steps in the laboratory.

Our final thanks go to our families for your support and patience through this hectic and challenging last semester.

Trondheim, June 7, 2010

Ole Georg Skjølberg

_____

Anders Hansson

_____

Contents

APPENDICES

1 Introduction

Hybrid concrete structures and fiber reinforced structures are in the focus for several Ph.D. and graduate students working with their thesis at NTNU. These are also themes that COIN – The Concrete Innovation Center sanctions and researchers in the concrete group at SINTEF are working with.

NTNU, SINTEF and COIN have a close cooperation and from this innovative environment grew the ideas of an optimized, partly fiber reinforced hybrid concrete structure. A concrete sandwich slab with fiber reinforced lightweight core and tension and compression zones of normal concrete. This report will focus on this new concept, purely developed by the authors of this report.

The report will start by describing concrete and other existing hybrid concrete structures in brief. This will be followed by a close study of the special lightweight concrete used in the middle layer, a study containing both laboratory experiments and numerical analyses. Finally a concept lightweight concrete composite slab is designed, produced, tested and analyzed numerically. The results from the study of the middle concrete layer are used as basis for the design and analysis of the final concept.

The scope of this report is to design an optimized hybrid concrete structure. Perform laboratory experiments on the structure and verify the experiments numerically in order to establish documentation of the behavior and capacity. Since the concrete material used in the middle layer is a relatively new product, a secondary goal is to establish necessary material properties for this concrete, in order to have correct input for the design and analyses of the final hybrid structure. To establish a basis of knowledge, literature studies on concrete, hybrid concrete structures and numerical analysis of concrete are done.

2 Nomenclature

CMOD	Crack Mouth Opening Displacement
CSS	Concrete Sandwich Slab
FE	Finite Element
FEA	Finite Element Analysis
FEM	Finite Element Method
FRP	Fiber Reinforced Polymer
LECA	Light Expanded Clay Aggregate (Weber product)
LWAC	Light Weight Aggregate Concrete
LWC	Light Weight Concrete
LVDT	Linear Variable Differential Transformer
OSMD	Optical Strain Measuring Device
SLS	Service ability Limit State
ULS	Ultimate Limit State
W1150	Light weight aggregate concrete developed by Weber with approximate wet density of 1150 kg/m^3. Added foam to reduce density and increase concrete strength.
W900	Light weight aggregate concrete developed by Weber with approximate wet density of 1150 kg/m^3. Added foam to reduce density and increase concrete strength.
"NC30"	Concrete used in the top and bottom layer in the concept CSS beams. Normal concrete with mean theoretically cylindrical pressure capacity close to 30Mpa.

3 Concrete in General

Concrete is as of today one of the most important building materials worldwide and it is estimated that the global yearly production is more than 2 billion cubic meters [1]. Economical, versatility and durability aspects makes concrete to a competitive building material in many structures world over.

Concrete is a mixture of cement and stone aggregate in different fractions. When water is added to the mixture the cement turns into a cement paste which encases the stone aggregate. The cement also reacts chemically with the water in a process called hydration. This is what makes the cement paste solid and turns the mixture of cement paste and stone aggregate into a rigid structure.

Concrete is characterized by its poor tensile capacity, which traditionally is compensated by steel reinforcement. In order to construct a strong, ductile and durable structure it is important to use reinforcement with high tensile strength. The steel must also have approximately the same thermal properties as concrete and be durable in the concrete environment [1].

As a substitute for steel reinforcement it is possible to use fiber reinforcement which is mixed in together with the cement and stone aggregate. This reduces or replaces the need of traditional steel reinforcement. However, fiber reinforcement is not yet accepted by the market as a substitute for traditional steel reinforcement in load-bearing structures and more research and documentation has to be done on the field. Fiber reinforcement is today mostly used in slabs on ground and sprayed concrete for rock support.

Normal concrete has usually a density of approximately 2400 kg/m^3. Concrete with density under 2000 kg/m^3 is in Norway classified as Light Weight Concrete (LWC). LWC is added lighter aggregate in order to reduce the concrete density. This aggregate can be natural products as pumice stone or volcanic slag.

The aggregate can also be artificially produced. The most common light weight aggregate in Norway is expanded clay aggregate, where LECA (Light Expanded Clay Aggregate) is a registered trade mark by the Weber group. LECA is a typical example of an artificially produced light weight aggregate. In this report, this kind of concrete is referred to as Light Weight Aggregate Concrete (LWAC). In common for most LWAC's are their less ductile behavior, compared to normal concrete, which makes LWAC's more vulnerable for cracking [1].

When designing concrete structures, it is important to consider many aspects. The structure must be designed to withstand the design load, both in the *Ultimate Limit State* (ULS) and *Serviceability Limit State* (SLS). Long term effects from loading must be considered. It is also important to have control over the crack widths and reinforcement coverage in a concrete structure, in order obtain sufficient long term durability. Concrete design in Europe is mainly regulated by Eurocode 2 [2].

4 Hybrid Concrete Structures

*Hybrid Concrete Structure*s can be complicated to define as a specific group of concrete structures. In the literature it is referred to hybrid concrete structures when describing everything from steel/carbon - concrete composites to beams and slabs with different kind of concrete over the cross section. In this report, hybrid concrete structures will be defined as structures in which concrete works together with another material or another concrete quality. In order to narrow down the definition, traditional steel reinforced cross sections with a homogenous concrete cross section as well as homogenous fiber reinforced cross sections are here chosen to be excluded from the hybrid definition. Hybrid concrete structures are then categorized in the following three groups:

- *Steel-Concrete Composites*. Structures where steel is used in addition to reinforcement bars or fiber reinforcement.

- *Polymer-Concrete Composites*. Structures where carbon or polymer is used in addition to reinforcement bars or fiber reinforcement.

- *Concrete-Concrete Composites*. Structures with different concrete qualities over the structural cross section.

Common for all of these structures is the importance of a complete, or at least partial, connection between the different materials in order to utilize the full potential of the materials working together. The differences between full connection and no connection between two material layers are shown in Fig. 1. In the figure it is shown how the second moment of area increases four times from no shear connection to full shear connection between the two material layers.

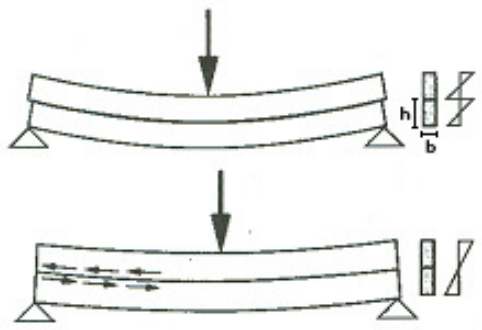

No connection

$$I = 2 \times \frac{1}{12} bh^3 = \frac{1}{6} bh^3$$

Full connection

$$I = \frac{1}{12} b(2h)^3 = \frac{4}{6} bh^3$$

Fig. 1: Second moment of area as a function of shear connection between material layers [3].

4.1 Steel-Concrete Composites

Steel-concrete composites are today one of the most common types of hybrid concrete structures. Well proven solutions are among others; steel beams together with a concrete slab or a concrete compression flange, thin walled corrugated steel plates with in-situ concrete cast and different kind of pillar solutions with internal or external steel. Some examples of these kinds of structures are shown in Fig. 2.

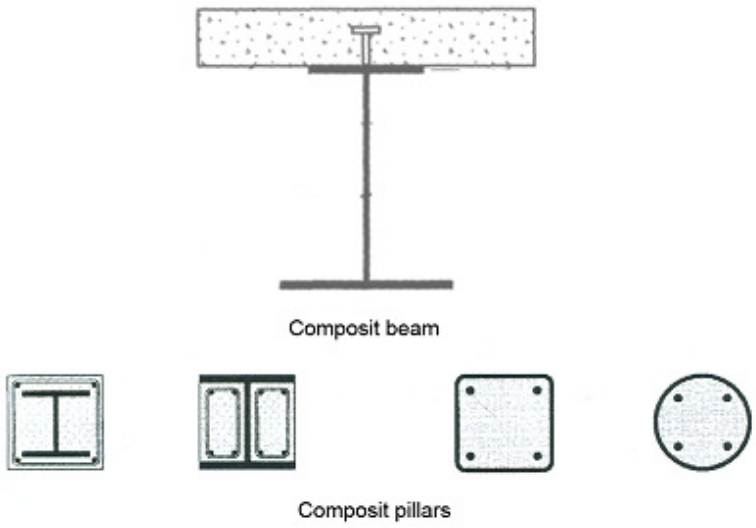

Fig. 2: Example of steel-concrete composites beam and pillars [3].

4.1.1 Beams

The beam example shown in the top in Fig. 2 utilizes the best properties from both of the two materials to attain an optimal structure. All the tensile and shear forces will in this case be carried by the steel beam. The flexural compression on the other hand will be carried by the concrete which is well known to withstand high pressures compared to the price of the material needed. To ensure full connection between the steel and concrete, dowels may be used as shear connectors. The dowels are shown as T-pins welded to the steel beam in Fig. 2. Dowels are common shear connectors in these structures and must be designed to ensure full connection between the materials in order to utilize the beam to its maximum level.

This kind of beam structure is widely used in bridge constructions where the structural system is a high steel beam in combination with a bridge deck in concrete. Fig. 3 shows a typical example of steel beam-concrete bridge. It is possible to save a lot of time in building a bridge like in Fig. 3 compared to a bridge purely in concrete. However, steel is more expensive than concrete and the steel-concrete composites are most popular in times of low steel prices.

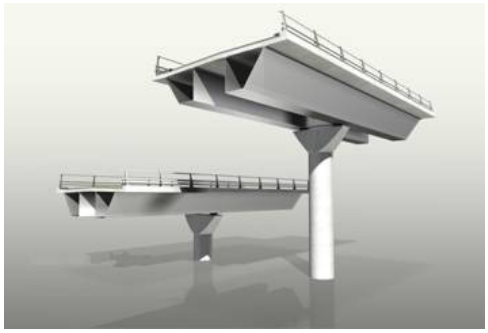

Fig. 3: Steel case bridge with concrete deck. Typical steel-concrete composite [4].

4.1.2 Pillars

Pillars can be optimized by combining steel and concrete in different ways. The pillar with the concrete encased H-section in Fig. 2, combines the higher capacity of steel with concrete characteristics to achieve better durability and fire resistance. This result in a more slender pillar compared to a traditional concrete pillar and a more durable and resistant construction compared to a true steel solution.

Steel encased concrete solutions as the pillars shown to the right in Fig. 2 will obtain extra strength due to confining effects on the concrete. When encased pillars are loaded in axial direction, the concrete will be subjected to radial pressure since it is restrained to expand within the steel case. This will lead to a triaxial stress condition which will increase the compressive capacity of the concrete [3].

In constructions where high performance concrete is used are often vulnerable to brittle failure which is an effect that is not desirable in structures in general. A combination of a confining circular steel section and high performance concrete will reduce the brittle problem and result in a more ductile and stronger composite structure [5]. Composite pillars are usually used where the designer wants a combination of a slender and strong structure.

Design rules for steel-concrete composites can be found in Eurocode 4, part 1-1 [6].

4.1.3 Slabs

Composite floor slabs are widely used in multi-storey buildings all over the world. Examples of different composite slabs are shown in Fig. 4. This construction consists of a thin steel sheet which serves as shuttering in the production phase and tension reinforcement in the final structure.

This way of producing slabs is time efficient due to no need of temporary shuttering in the construction phase. It also makes it possible to build thin structures compared to the obtained capacity. However, a numerous number of supports are needed in the building phase due to the poor flexural tensile capacity of the steel plates alone before the cured concrete can take

compressive forces. According to the thin steel sheet producer Plannja, their standard slab system must be supported on every 1500 mm in the building phase for a 240 mm thick slab [7]. Being able to reduce or eliminate the need for such supports could reduce the production costs.

In order to obtain full shear connection between the steel and concrete, the sheets are usually embossed with projections repeated indefinitely or corrugated in such a way that shear connection is obtained [8]. This is shown in Fig. 4, in the top and bottom respectively. Design rules for thin steel plate-concrete composites can be found in Eurocode 4, part 1-1 [6] and Eurocode 3, part 1-3 [9].

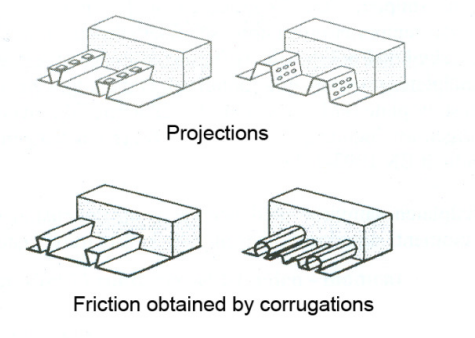

Fig. 4. Thin steel sheet - concrete composites [3].

4.1.4 Challenges Connected To Steel-Concrete Composites

Common for almost all of the steel-concrete composites is the unprotected steel part on the tension side. Steel is well known for its severe shortage when it comes to fire resistance and corrosion. This is the main reason why pure concrete structures often can compete with steel-concrete composites when such serviceability aspects are taken into account.

The thin steel-concrete composite slabs are more dependent of temporary supports in the construction phase, compared to a hollow core deck or a combination of structural precast concrete formwork and in-situ concrete. Another esthetic issue with this kind of slabs is the corrugated plate which in many cases will be visible in the ceiling. A lowered ceiling will be needed in cases where a visual steel plate is not acceptable.

4.2 Polymer-Concrete Composites

Fiber Reinforced Polymer (FRP) ribbed planks is the most common commercial polymer-concrete hybrid product on the market. It is widely used in bridge decks and other infrastructure applications in North America [10]. The concept is in many ways similar to the thin steel plate - concrete slabs described in Section 4.1.3, except that the thin steel plate is replaced by an FRP structure. Example of FRP ribbed planks are shown in Fig. 5.

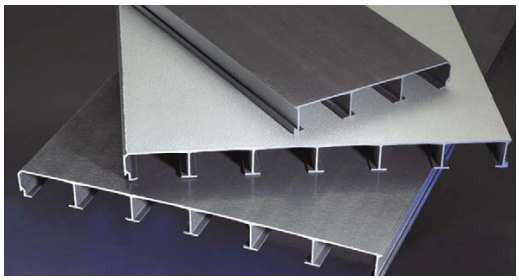

Fig. 5: Typical FRP ribbed planks [10].

Advantages with the ribbed FRB are the relatively high flexural stiffness of the plank with the ribs and the low weight compared to its strength. In the construction phase, this system requires less supports compared to the thin steel plate system due to its relatively high flexural stiffness. The planks can be delivered in any color and are versatile since they easily can be produced in arbitrary shapes and with different surface structure. Shear connection is here obtained by the shape of the polymer ribs connecting to the concrete. Fig. 6 shows a FRP plank with a concrete slab.

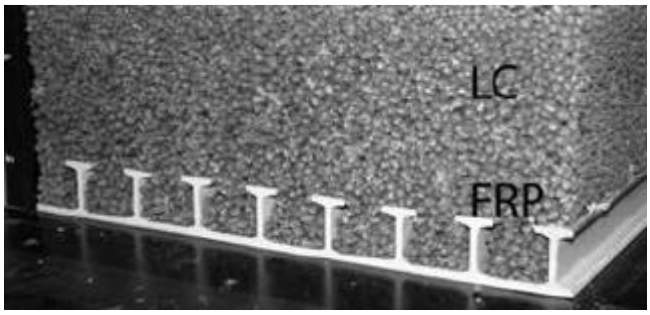

Fig. 6: FRP ribbed plank with concrete slab [11].

4.3 Concrete-Concrete Composites

Concrete-concrete composites can be subdivided into structures with different concrete over the structure cross section, combination of precast and in-situ concrete and combinations of the two.

4.3.1 Precast Concrete Formwork with In-situ Concrete Top Cast

A very common slab solution is a combination of precast concrete formwork and in-situ concrete. In Norway this kind of system is delivered by Con-Form and Unicon among others. This system is based on precast slabs with lattice girder reinforcement which acts like formwork in the construction phase. A typical example of precast concrete formwork is shown in Fig. 7.

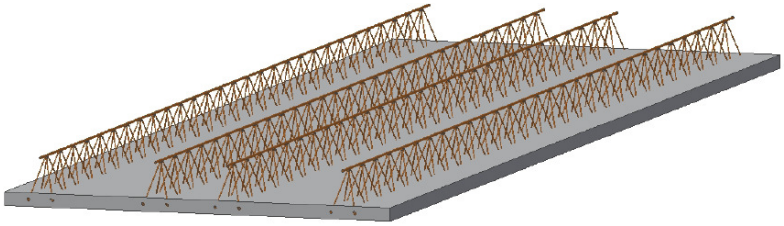

Fig. 7: Typical precast concrete formwork [12].

The main tension and minimum transversal reinforcement is located in the precast slab. The lattice girder reinforcement acts like shear connectors between the precast and in-situ layer. The girder also stabilizes the slab during the construction phase and the top steel reinforcement of the girder takes the compression forces alone through the construction phase. The rest of the structural reinforcement is put in place after the precast slabs are mounted. Finally the top layer is cast over the whole concrete formwork, turning it to a monolithic slab after the final cast has cured.

Fig. 8: Installation of precast concrete formwork in Sweden [13].

Since the top steel reinforcement only can take small pressure forces due to its dimension and slenderness, the concrete formwork requires temporary supports through the construction phase, unless the spans are short. A typical 7m Con-form precast slab requires 3 supports during construction. This is illustrated in Fig. 8. The support beams are usually supported by floor props placed on the underlying deck. The work with the temporary supports is a time

demanding job and solutions where the amount of supports could be reduced partly or completely would save a lot of money.

Precast concrete formwork is usually delivered in widths up to 2.4m and spans up to 7.2m with normal reinforcement. Spans up to 12m can be delivered when pre stressed reinforcement is used [14]. These kinds of slabs can be designed to resist very large loads, with limitations usually related to serviceability aspects of crack width and maximum displacement.

4.3.2 Weber's LECA Byggeplank

The LECA Byggeplank is delivered as construction elements with widths of 0.6m and in lengths up to 8.1m. The elements are purely precast and are lifted into place at the construction site. No extra structural cast is needed on the LECA Byggeplank. However, it is not uncommon to do a level cast on the very top which will increase the capacity somewhat, due to monolithic behavior of the structure. Steel reinforcement is used both in the tensile and compressive zone as shown in Fig. 9.

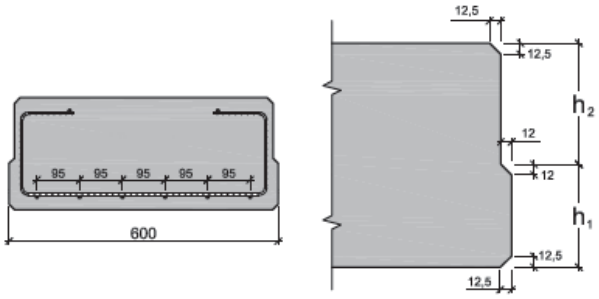

Fig. 9: Principles of Weber's Leca Byggeplank 250T [15].

Limitation in this system is the relatively low load capacity. As an example the 6 m element with height of 250 mm can only carry a little over 5 kN/m^2 [15]. This can be compared to a hollow core slab, with height of 220 mm and 6 m span, which can carry up to 18kN/m^2 [16].

5 Concrete Sandwich Slab

5.1 The Concept

The Concrete Sandwich Slab (CSS) which is going to be tested and analyzed in this report, is a new concept which is based on ideas from existing products like the LECA Byggeplank, combinations of precast concrete formwork and in-situ concrete and ideas from hollow deck solutions. The concept is developed purely by the authors of this report.

The CSS is meant to be an alternative to the today existing products of concrete precast formwork. This product will be able to carry heavy loads and can be used in rough environments due to its surface qualities, for example industrial or harbor structures.

The cross sectional principles of the CSS concept are shown in Fig. 10. The CSS concept is built on the hybrid structure idea of different materials in high stress versus low stress zones. In a general load case in which the tensile stresses are localized to the cross sectional bottom and compressive to the top, normal reinforced concrete is carrying the tension and pressure in the bottom and top respectively. In the low stress zone, typically in the cross sectional middle, a LWAC is used to reduce the structural weight. In order to assure shear connection between the different layers, shear connectors are placed through the three layers as shown in Fig. 10. Confer the principles of the lattice girder in Section 4.3.1.

If the load case would be such that tensile forces would appear in the top, it is easy to add additional reinforcement in the top before the top cast is done, i.e. continuous slab construction with monolithic behavior over supports.

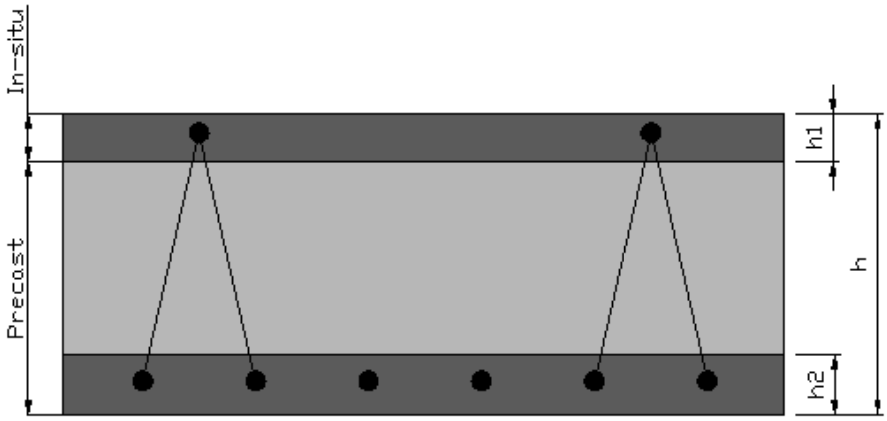

Fig. 10: Principles of the Lightweight Concrete Sandwich Slab concept.

The CSS is meant to be constructed as a combination of precast and in-situ concrete. The precast part is cast in two stages, the first stage with a normal reinforced concrete and the second stage with a lightweight concrete. The two precasting stages are done within a short time period, before the bottom layer has started to cure in order to obtain maximum shear connection between the layers.

The precast part will then be delivered to construction site, lifted on place and installed in the same manner as the above mentioned existing products. The top layer (h1 in Fig. 10) will be cast at the construction site.

5.2 Bottom and Top Layer

The bottom and top layer of the CSS is in this study chosen to be steel bar reinforced normal concrete. This is chosen on the basis of reliability in dimensioning rules and good bonding ability between concrete and reinforcement. A normal concrete surface without open pores will also give the structure good durability characteristics and cover for the reinforcement.

5.3 Middle Layer

Since tensile forces will be carried by traditional reinforcement and the compressive forces almost exclusively by the top layer, the middle layer does not have to withstand high stresses induced from bending moment. This reduces the need of compression capacity of the middle material layer. However, the material must be strong enough to assure shear connection between the layers and withstand the shear forces acting on the slab structure.

5.3.1 Lightweight Concrete

One of the best LWAC with acceptable strength, cost efficiency and available in Norway, is a special concrete developed by Weber. This LWAC is used in a beam product to be used over windows and doors in LECA masonry structures. Compared to a normal concrete this concrete contains LECA aggregate, steel fiber reinforcement and weight reducing foam. Some characteristics are wet density of approximately 1150kg/m^3 and compressive capacity of approximately 20 MPa.

In this project it is chosen to use the well proven Weber recipe that is used in production today as well as a new similar Weber recipe with wet density of approximately 900 kg/m^3 and compressive capacity estimated to 15 MPa.

In the rest of the report these two concretes are referred to as the W900 and W1150 concrete, as in Weber and approximate density of 900 kg/m^3 and 1150 kg/m^3 respectively.

The first test program in this project, described in Chapter 6, contains mixtures of both the W1150 and the W900 concrete with different fiber content in order to find the optimal recipe and material parameters for the CSS middle layer. The recipe of the W1150 concrete is based on earlier research at NTNU [17] and at Weber's research laboratory. The W900 recipe is purely developed by Weber in Lillestrøm in February 2010 for this specific study.

5.3.2 Foam

Information about the content of the weight reduction foam is restricted by Weber. Its positive characteristics when added to concrete are its stabilizing, strength increasing and weight reducing effects. The foam adds air pores to the concrete mixture, with size approximately 10^{-6} m. These air pores result in swelling of the cement paste and makes the paste better distributed in the concrete mix. This is the main cause of increased strength. It also stabilizes the mixture which has a tendency to separate before the foam is added.

The consistency of the foam can be compared to shaving foam. However, it is very stable and the foam volume is only reduced by half when added to the concrete.

Fig. 11: Adding foam to the mixture.

5.3.3 Fiber

The LWAC is added steel fiber reinforcement to increase shear and moment capacity. In addition the ductility of the concrete is substantially increased. The steel fiber used is Dramix 65/35 produced by Bekaert. This fiber type is chosen on the basis on research done at NTNU in 2009 [18] where it was concluded that the LECA-foam concrete benefitted the most capacity wise when the Dramix 65/35 steel fiber was used. Dramix fiber is shown in Fig. 12 and its characteristics are presented in Table 1.

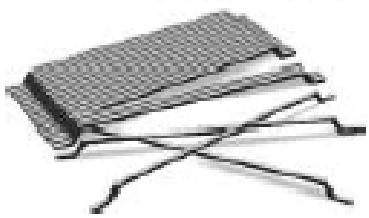

Fig. 12: Dramix 65/35.

Table 1: Product data Dramix steel fiber 65/35.

Parameter	Value
Description	Cold drawn, wire fiber, hooked ends, glued in bundles
Length	35 mm
Diameter	0.55 mm
Aspect ratio (l/d)	64
no. Fibers/kg	14500
Bond type	End hooks
Tensile strength	1100 MPa

The LWAC is also added polypropylene micro fiber mesh in order to increase the concrete stability and avoid separation issues. This was done on the basis from recommendations from Weber's R&D section in Lillestrøm and earlier research carried out at NTNU [18]. The fiber added was Polypropylene Fiber Mesh 150 produced by BASF, the fiber is shown in Fig. 13 and its characteristics are summarized in Table 2.

Fig. 13: BASF Polypropylene Fiber Mesh 150.

Table 2: Product data BASF polypropylene fiber mesh 150.

Parameter	Value
Description	100% polypropylene, monofilament fiber
Length	12 mm
Diameter	0.001 mm
Ductility (CN/dtex)	34.0min

5.4 CSS Advantages and Comparison with Today Existing Products

The precast part of the CSS concept will, as mentioned above, be delivered to the construction site in modules and be lifted in place to form a slab. This slab will then act as formwork for the final casting of the top layer, which will give the slab monolithic behavior after the top layer has cured. This means no need of traditional formwork which saves time, people, space and money at the construction site. The CSS would also be more favorable in an environmental perspective because of less produced waste related to formwork used in production of pure in-situ slabs.

The CSS is very similar to traditional precast concrete formwork but the finished CSS structure is lighter due to the LWAC. For a 250 mm slab, the CSS concept with the W900 LWAC described later in Section 5.3, will be 38% lighter compared to a slab with normal concrete through the whole cross sectional area.

The precast part of the CSS is thicker compared to traditional concrete formwork which means that the CSS will have a concrete compressive zone, also in the construction phase. This is illustrated in Fig. 14. This result in less or no need at all for temporary supports in the construction phase for the CSS concept, compared to the traditional precast concrete formwork which requires many supports during construction, confer Section 4.3.1.

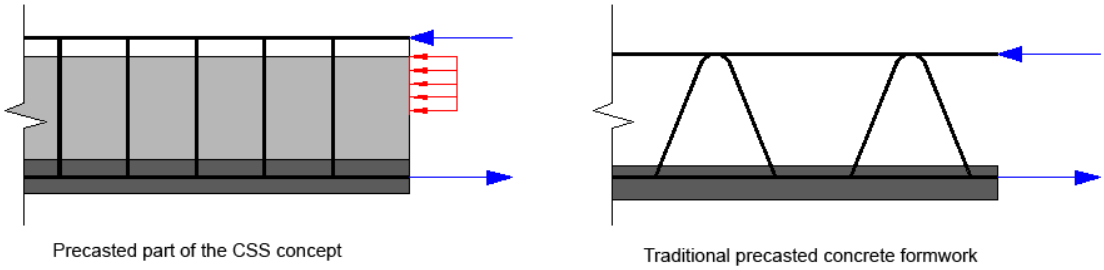

Fig. 14: Comparison between the CSS concept and traditional precast concrete formwork. The picture shows that the CSS has a concrete compressive zone (red) in the construction phase.

Compared to a hollow core slab solution, the CSS concept is only slightly heavier. However, a massive structure with no cavities leads to better properties when it comes to sound transmission [19]. This is favorable in constructions that are sensitive for sound transmission between storeys.

The CSS concept will also be heavier than Weber's LECA Byggeplank. However, the CSS concept has a much higher carrying capacity and stiffness, due to the high capacity top and bottom zone. This makes the CSS more versatile when it comes to structural design, due to the possibilities of longer spans and larger loads without an increase in slab thickness. The CSS top

and bottom surface will also have a dense structure without open pores and will therefore have better durability properties compared to the LECA Byggeplank.

5.5 Challenges

The most obvious structural challenge for the CSS concept is the bonding resistance between the different layers. Steel shear connectors will be used to assure sufficient bond properties. However, the bond between the LWAC, the normal concrete and the steel shear connectors is hard to predict. This is an unsure factor in this project. All the calculations through this report assume full shear connection between the layers. More detailed studies on this field should be carried out in later research.

Another well known challenge is material shrinkage. Due to different shrinkage properties in the LWAC versus normal concrete, problems might arise when the layers in the precast part of the CSS starts to shrink when curing. Different shrinkage strains in the layers might lead to unwanted stresses and curvature on the precast part of the CSS. Theory related to this field is discussed in Chapter 12.

6 Test Phase 1: Test Program for Material Data Determination

In order to establish a basis for hand calculations and numerical analysis of the CSS, material parameters had to be obtained. The main motivation behind the test phase 1 was to document the behavior of the W900 and W1150 concrete and simultaneously establish material parameters to be used in hand calculations and numerical analyses later in the report.

6.1 Overview of Test Phase 1

The first test phase contained four different concrete mixtures. The mixtures are summarized in Table 3.

Table 3: Overview of concrete batches.

Batch Nr.	Approximate Wet Density [kg/m^3]	Fiber Volume [%]	Batch Volume [l]
B0	900	0	125
B1a	900	0.5	200
B1b	900	0.5	125
B2a	900	1	200
B2b	900	1	125
B3	1150	1	200

6.1.1 Specimens

6 different types and a total of 66 test specimens were cast in test phase 1, all these castings are summarized in Table 4. Since the LWAC used in this project differ a lot from traditional LWAC's, it was chosen to do several different types of test to establish all necessary material parameters.

In Table 5 the different types of test methods for the specimens are listed, together with their governing regulations/methods.

Table 4: Overview of test specimens.

Specimen Type	Number of Specimens	Batch Nr.	Approximate Wet Density [kg/m^3]	Fiber Volume [%]
Comp. cube	3	B0	900	0
	3	B1b	900	0.5
	3	B2b	900	1
	6	B1a	900	0.5
	6	B2a	900	1
	6	B3	1150	1
Comp. cylinder	3	B1a	900	0.5
	3	B2a	900	1
	3	B3	1150	1
Uniaxial tensile prism	3	B1a	900	0.5
	3	B2a	900	1
	3	B3	1150	1
Flexural tensile prism	3	B1a	900	0.5
	3	B2a	900	1
	3	B3	1150	1
Round panel*	3	B1a	900	0.5
	3	B2a	900	1
	3	B3	1150	1
Shear beam	1	B0	900	0
	1	B1b	900	0.5
	1	B2b	900	1

*Round panels were primary cast by us on behalf our supervisor Linn Grepstad Nes. Testing was later performed in collaboration with her. The results from the round panel test are presented, but not discussed further in this report.

Table 5: Test specimen geometry, aim for testing and governing regulations.

Specimen Type	Geometry [mm]	Aim	Governing Regulation
Comp. cube	100x100x100	Cube Compressive strength	European standard [20],[21]
Comp. cylinder	Ø100x200	Cylinder compressive strength	European standard [20], [21]
Uniaxial tensile prism	100x100x600	Uniaxial tensile strength	SINTEF method [22]
Flexural tensile prism	150x150x550	Flexural tensile strength	European standard [23]
Round panel*	Ø800x75	Flexural toughness	ASTM standard [24]
Shear beam	150x250x2900	Shear capacity	No regulation**

*Round panels were primary cast for our supervisor Linn Grepstad Nes. Testing was later performed in collaboration with her. The results from the round panel test are presented, but not discussed further in this report.

**No regulation for testing of LWAC shear capacity exists. The testing is therefore performed in accordance to earlier research at SINTEF. [25]

6.1.2 Shear Beam Reinforcement

The only specimens with traditional steel reinforcement are the shear beams. The reinforcement in the shear beams is illustrated in Fig. 15. The reinforcement is chosen on the basis on earlier similar studies on beams with the same measurements performed by SINTEF, where LWAC beams were tested with respect to their shear capacity [25].

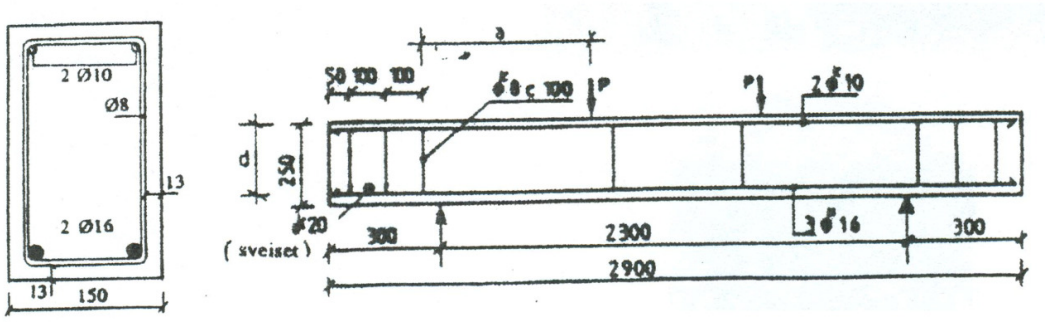

Fig. 15: Sketch of shear beams, illustrating measurements and position of reinforcement.

6.2 Production of Test Specimens

The test specimens were cast at Weber's premises in Lillestrøm 19.02.2010 after several weeks of planning. Initially the test specimens were to be cast at the laboratory at NTNU, but since the machine that generates the foam could not be transported to Trondheim, it was decided that the casting should be done in Lillestrøm.

Temperature- and moisture conditions were adapted for indoor casting since this was the same premises where Maxit produce their lightweight concrete beams for use in masonry structures. During the mixing and casting of the test specimens the following people were present:

- Geir Norden, R&D manager, Saint-Gobain Weber Federals
- Trygve Berger, laboratory employee, Weber
- Oddbjørn Nylænden, laboratory employee, Weber
- Ole Georg Skjølberg, Graduate Student, NTNU
- Anders Hansson, Graduate Student, NTNU

6.2.1 Proportioning

The recipes for the W900 and W1150 concrete were prepared by Geir Norden. The recipe for the W1150 concrete is, as mentioned earlier, a well proven mixture. The W900 concrete on the other hand is newly developed and until the casting of the test specimen, untested in larger batches than 5 liters. The W900 recipe was tested the week before by Geir Norden in Weber's laboratory to ensure good quality with respect to strength and casting abilities. However,

during the mixing of the W900 concrete the recipe was modified due to observations made related to separation and unwanted latent air.

The recipes used are summarized in Table 6.

Table 6: Overview of the W900 and W1150 recipes.

Recipe	W1150	W900
w/c	0.474	0.457
Unit	**kg/m^3**	**kg/m^3**
Norcem Industri (Cement)	114.0	101.0
Norcem Anlegg(Cement)	266.0	221.0
Elkem Microsilica	35.0	9.0
Leca 2-4mm (LWA)	230.0	184.0
Leca 4-10mm (LWA)	0	110.0
Sand Lillestrøm 0-4mm	400.0	92.0
BASF MECH PP 150 (polypro. fiber)	1.5	1.5
BASF Glenium SKY 550 (SP)	7.2	3.7
BASF Glenium Steam (Stabilisator)	2.0	1.7
Defoaming Agent	0.123	0.12
Bekaert 30/35 Steel Fiber	78.5	0/39.25/78.5
Water	180.0	147.0
Foam	at random*	at random*

***Foam was added during mixing until wanted wet density was obtained.

6.2.2 Mixing and Casting

The concrete was mixed in a simple concrete mixer (Fig. 16) with rigid chamber. This kind of mixer does not mix as good as a mixer with rotating chamber. This resulted in a lower quality of the actual mixing procedure compared to what one could expect with a better concrete mixer. The mixer was also inadequate with respect to overall quality since it was leaking water/cement-paste which resulted in less control of the W/C relation.

The details of the mixing procedures for test phase 1 are attached in Appendix A.1.

Fig. 16: Simple concrete mixer at Weber Lillestrøm.

6.2.2.1 W900 Concrete

The first batch to be mixed was B0 (W900 with 0% fiber). It quickly became evident that a 100+ liter batch did not have the same characteristics as a small testing batch of 5 liters in the Weber laboratory. The recipe could not simply be scaled up from 5 to 100+ liters. The first mixture B0 had light separation problems and very high air content. The big amount of latent air almost made the concrete look like it was boiling. The most likely cause of this problem was the high amount of super plasticizer. In order to stabilize the mix; sand, cement, water and air reducing chemicals were added. This resulted in a fairly stable mix which had relatively good casting properties.

To compensate for the separation and high air content in the other W900 mixes, the amount of water, sand and cement was increased while the amount of super plasticizer was reduced for the rest of the batches (B1-B2). Both problems were reduced after the small recipe changes, but some separation was still observed. It was concluded that the low quality mixer together with the new recipe was the cause of the remaining separation problems. The W900 recipe presented in Table 6 is the final adjusted recipe used in Lillestrøm.

The W900 concrete also became very difficult to work with when steel fibers were added. This was not expected since the W1150 concrete had good working properties even though fiber usually is added. This resulted in casting difficulties since the W900 concrete behaved more or less like a stiff mass. The casting was performed by hand and the concrete was compacted with steel rods. No external vibration was applied since unwanted separation was expected.

6.2.2.2 W1150 Concrete

The W1150 recipe is a well tested Weber product. When batch B3 was mixed, no separation problems or problems with latent air arose. The steel fiber content of 1% by volume did not result in any bad casting properties. The casting with this concrete was done in the same way as described in Section 6.2.2.1 but without any complications at all.

It should be noted that because of the very good flow ability of the W1150 concrete, the steel fibers could have adjusted itself parallel with the direction of the flow when the concrete was poured into the formwork.

6.3 Transportation of Test Specimens

Since the specimens were cast in Lillestrøm they had to be transported to Trondheim. By practical and economical reasons, this had to be done the following day. The transportation of the specimens was a critical phase because of the low material strength at this point, due to short curing time. This applies especially for the shear beams because of the arising bending moments when the beams were to be lifted, even though they were still lying in the formwork. Extra care was taken while handling the shear beams to minimize the arising bending moments. The rest of the test specimens were cast in such a stiff formwork that bending moments could be more or less neglected.

All specimens were properly packed in wet cloths and plastic to ensure a relative air humidity of approximately 100% during transportation. During transport the outdoor temperature was between 5-10˚C below freezing. To protect the concrete from freezing, insulating padding were placed on top of the plastic. Because of the ongoing curing, the concrete produced enough heat itself from the hydration process to keep the temperature above 0˚C. After arrival at Trondheim the temperature was controlled and found to be several degrees above freezing.

6.4 Removing Formwork and Storage until Testing

The formwork was removed after three days of curing and the revealed surface finish of the bigger test specimens showed that the overall quality was good (shear beams, flexural tensile beams and round panels). The W1150 specimens looked excellent while the W900 concrete with 1% steel fiber content naturally had the worst surface finish due to the concrete's bad casting abilities. In Fig. 17 there is an example of the consequence of the bad castability of the W900. The figure shows the shear beam with the highest percentage of steel fiber by volume.

Fig. 17: A cavity had developed because of bad castability in one of the shear beams.

This defect will most likely not affect the results significantly since the cavity is located at the top of the cross section at the end of the beam. This part of the beam is localized outside the bearing zone and its primary purpose is to secure sufficient bonding of the tensile reinforcement located at the lower part of the beam. No such similar defects were found on the other specimens.

After removing the formwork for the small test specimens (cubes and cylinders) it became evident that the quality of the W900 concrete was a severe problem. The surface finish for several of the specimens was so bad that they could be classified as unsuccessfully cast. However, the tests of the W900 specimens will still be carried through.

A comparison of the surface finish of the compression cubes are shown in Fig. 18. It can easily be seen how the higher steel fiber volume leads to a worse surface finish, because of the poor castability of the concrete. The cubes are positioned with increasing steel fiber volume from 0% at the left, to 1% volume for the three rightmost cubes. The two cubes stacked on top of each other represent the same batch, B2b - W900 with 1% fibers by volume, even though the exterior quality of the two cubes is completely different. This may be a result of the varying quality of the concrete within each batch and in combination with difficult and poor casting.

Fig. 18: Comparison of compression cubes after removed formwork. The cubes are positioned with increasing steel fiber volume from 0% at the left, to 1% volume for the three rightmost cubes. W900 concrete in the first three columns and W1150 in the rightmost cube.

In Fig. 18 it is clearly shown how the W1150 concrete recipe results in an overall better quality. This is shown even clearer in Fig. 19 where the rightmost cylinder is W1150 concrete.

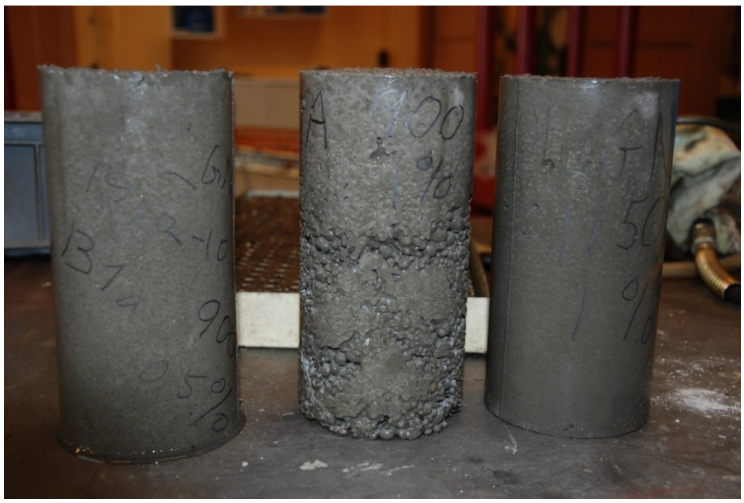

Fig. 19: Comparison of the three different batches for the compressive cylinders in the following order from the left: B1a, B2a, B3.

Immediately after removing all the formwork the smallest test specimens (cubes and cylinders) were submerged in water to be stored until testing. The other test specimens were covered in wet cloths and wrapped in plastic in order to ensure air humidity close to 100%.

6.5 Final Preparation before Testing

6.5.1 Flexural Tensile Prisms

The governing standard for the testing of the flexural tensile beams [23] specifies that a notch is to be cut in the test specimen, as shown in Fig. 20, in order to predict the location of the failure crack.

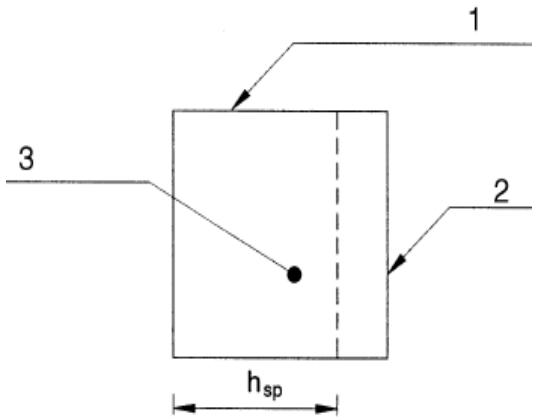

Fig. 20: Cross section of bending specimen with notch [23]. 1: Top surface during casting. 2: Notch. 3: Cross section.

According to the standard, the notch should be cut to ensure a cross sectional height, h_{sp} of 125 mm ± 1 mm and a notch width ≤ 5 mm. This notch was cut 2 days before testing with a notch width of 4 mm.

6.5.2 Tension Prisms

A similar notch was cut in all of the tension prisms. The tension prisms were cut on all four sides so that the final cross sectional width was 80mm x 80mm (± 1mm). The notch width was 4 mm.

The notches are primarily made in order to define the location where the specimen will crack. The notch forces the crack to develop within the location of reduced net area, which makes it possible to measure strains more correctly since the crack always will appear where it is predicted.

6.6 Calculation of Shear Beam Capacities

Since there are no regulations regulating the testing procedure of the shear beams, it was chosen to do capacity estimations before testing, in order to predict the failure load and determine an a/d relation (Fig. 21) that for sure would trigger a shear failure.

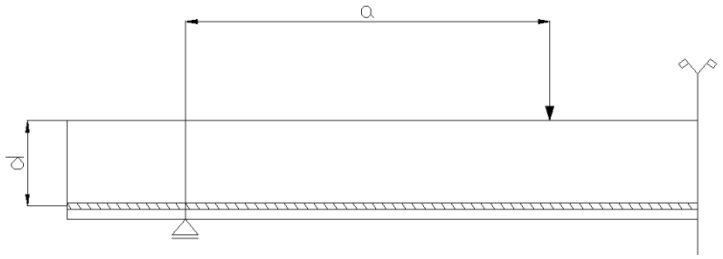

Fig. 21: Schematic sketch of a/d relation.

The testing of the shear beams was performed in the end of test phase 1 which means that material properties for the W900 concrete, obtained early in test phase 1, could be used in the final capacity estimations for the shear beams. In the following sections the theory behind the capacity estimation is described along with theory of the extraction of material data needed from the laboratory testing of the flexural tensile beams.

The hand calculations are principally performed in accordance to the design rules in Eurocode 2 [2]. The measured mean values have been used as material strength parameters. No partial safety factors with respect to loading or materials have been used.

6.6.1 Residual tensile strength

The residual tensile strength had to be calculated in order to estimate the steel fiber contribution to both shear and moment capacity of the shear beams. In order to calculate the residual tensile strength, the results from the laboratory test of the flexural tensile beams were used. By processing the results from these laboratory tests, the residual flexural tensile strength is obtained, which constitutes the basis for calculation of the residual tensile strength.

All calculations related to the steel fiber contribution are done on the basis of the Steel Fiber Draft “Stålfiberarmering i betong; Veiledning for prosjektering, utførelse og kontroll” [26] based on advice from supervisors at NTNU. The Steel Fiber Draft is based on the old Norwegian Standard series NS-EN 12390 which assumes a different specimen geometry compared to the specimens cast. This leads to additional challenges which are discussed further in the following section.

6.6.1.1 Calculation of residual flexural tensile strength

A relation between the results obtained in the laboratory for the flexural tensile beams and the Steel Fiber Draft [26] needs to be established. This is because the flexural tensile beams cast in this report is based on NS-EN 14651 [23] which assumes different specimen geometry and testing method than what is assumed in the Steel Fiber Draft. The differences between the two specimens and their correlating testing methods therefore need to be studied in detail.

Fig. 22.1 illustrates the specimen of which the draft is based, while Fig. 22.2 illustrates the specimens used in this report. The main difference except specimen length and loading, is the 25mm notch (Fig. 22.2) cut in the specimens used in this report.

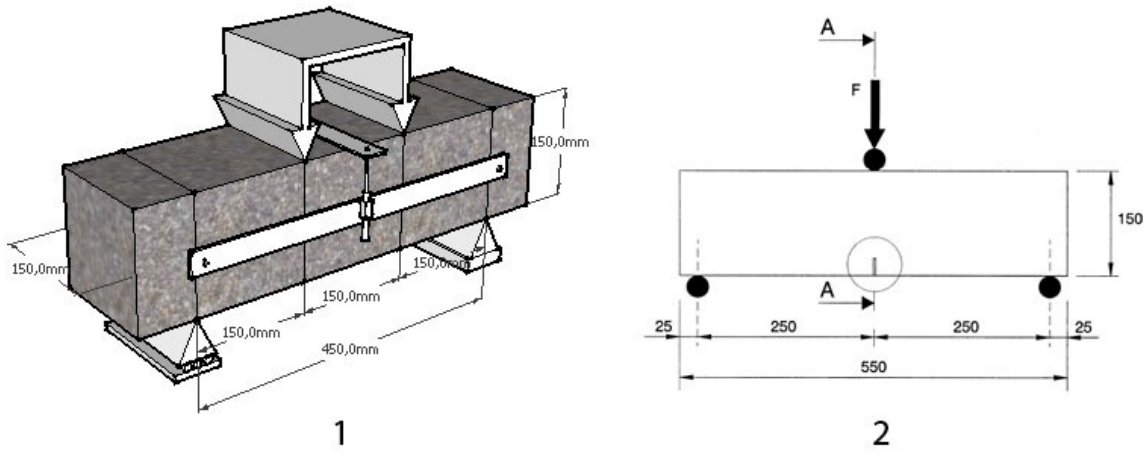

Fig. 22: 1: Specimen as described by the Steel Fiber Draft [26].
2: Specimen as described by NS-EN 14651 [23].

The Steel Fiber Draft calculates the residual flexural tensile strength on the basis of the mean load measured between 0.5mm and 2.5mm deflection at the crack tip. Since the degree of pull-out suffered from the concrete is governing for the performance of most steel fibers and the degree of pull-out is governed by the angle of crack rotation [27], it is necessary to establish corresponding deflections for the two beam types which gives the same Crack Mouth Opening Displacement (CMOD), i.e. displacement measured at the crack tip is not directly comparable for the two beams, but the CMOD is.

It must also be noted that for the beam specimen used in this report the crack starts at a height y=25mm from the bottom of the specimen because of the notch cut in the beam. This effect needs to be accounted for. A relation between displacement and CMOD exists in NS-EN 14651 as described by Equation (6.1) [23]:

$$\delta = 0.85 \times CMOD + 0.04 \qquad (6.1)$$

In NS-EN 14651, CMOD is defined to be measured at the bottom of the specimen, i.e. at y=0mm, even though the crack really would arise at y=25mm. Equation (6.1) could therefore not be used as a relation between the two beam specimens, hence the derivation of the relation in the following section.

Calculation of CMOD

When assuming small angles, which is a reasonable assumption for such small displacements, the relation in Equation (6.2) is found between the displacement δ and the angle of rotation/crack rotation. Equation (6.2) refers to Fig. 23.

$$\tan\frac{\varphi}{2} = \frac{\delta}{\frac{L}{2}} = \frac{\varphi}{2} \qquad \rightarrow \qquad \varphi = 4\frac{\delta}{L} \tag{6.2}$$

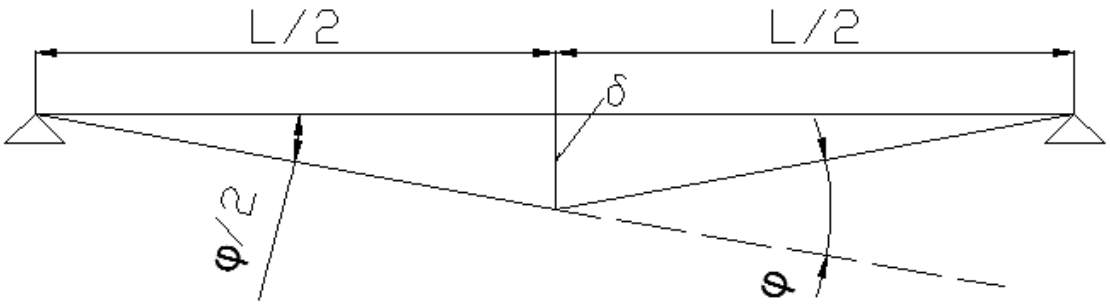

Fig. 23: Angles used for calculations of CMOD.

When considering the beam specimen described by the Steel Fiber Draft in Fig. 24, the relation between the mid displacement and the CMOD is found as described by Equation (6.3).

$$\sin\frac{\varphi}{2} = \frac{\frac{CMOD}{2}}{h} = \frac{\varphi}{2} \qquad \rightarrow \qquad CMOD = \varphi \times h = 4\frac{\delta_1 \times h}{L_1} \tag{6.3}$$

It must be noted that the two following assumptions have been made:

- Rigid body rotation, with assumed infinitesimal compression zone height.
- Small angles

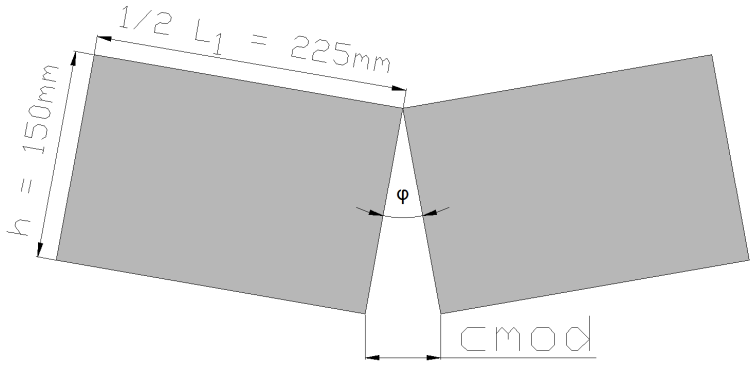

Fig. 24: Assumed deformation of specimen described by the draft.

Using the same assumptions when considering the specimen described by NS-EN 14651 (Fig. 25), Equation (6.4) could be established.

$$\sin\frac{\varphi}{2} = \frac{\frac{CMOD_{sp}}{2}}{h_{sp}} = \frac{\varphi}{2} \quad \rightarrow \quad CMOD_{sp} = \varphi \times h_{sp} = 4\frac{\delta_2 \times h_{sp}}{L_2} \tag{6.4}$$

and the corresponding displacement which satisfies the requirement $CMOD = CMOD_{sp}$ in Equation (6.5).

$$\delta_2 = \frac{CMOD_{sp} \times L_2}{4 \times h_{sp}} \tag{6.5}$$

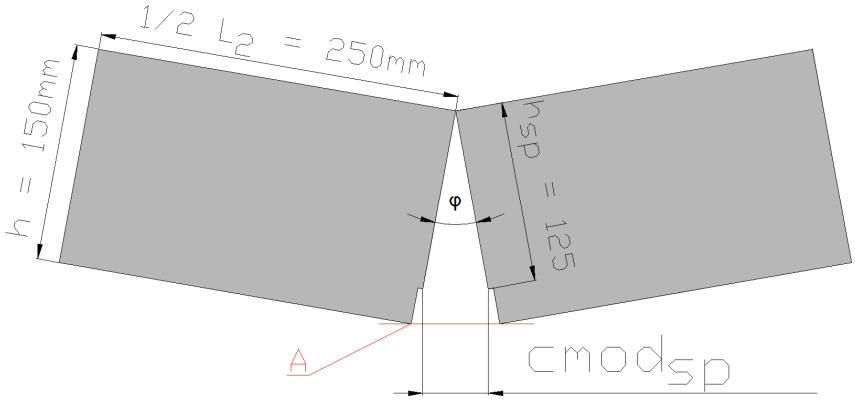

Fig. 25: Assumed deformation of specimen described by NS-EN 14651:2007.

By substituting values for L_2 and h_{sp}, as shown in Fig. 25, Equation (6.5) reduces to the simple expression (6.6).

$$\delta_2 = CMOD_{sp} \tag{6.6}$$

Using the derived relations, the displacement at which the residual flexural tensile strength is to be based could be calculated. The results are summarized in Table 7.

Table 7: Summarized displacement relation between draft specimen and NS-EN 14651 specimen.

Sampling point no.	Displ. Draft [mm]	CMOD = CMODsp [mm]	Displ. NS-EN 14651 Specimens [mm]
1	0.5	$\frac{2}{3}$	$\frac{2}{3}$
2	2.5	$\frac{10}{3}$	$\frac{10}{3}$

The calculated displacement which constitutes the basis for the residual flexural tensile strength calculations should be measured at the mid-section. In this report the displacement was measured along the horizontal line noted “A” in Fig. 25. Calculating the residual flexural tensile strength on the basis of the mean load at the displacement measured along line “A” leads to a small error, but to the conservative side. This error has been neglected in this report since it only constitutes about 0.8% of the measured displacement. In addition the elastic contribution to the total deformation has been neglected for simplicity.

The contribution from steel fibers connecting the bottom part of the beam specimen and across the notch has not been accounted for, see Fig. 26. This is a simplification to the conservative side with respect to capacity contribution from the steel fibers and further study is needed to incorporate this effect into the residual flexural tensile strength.

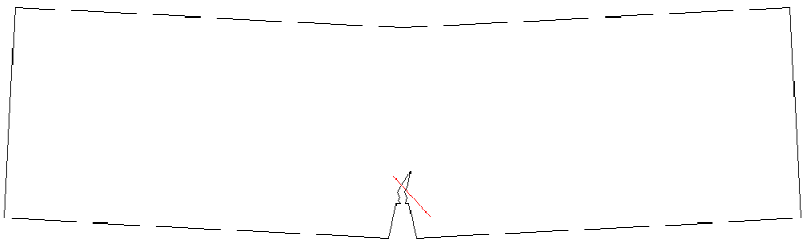

Fig. 26: Illustration of steel fiber contribution which has been neglected.

Residual Flexural Tensile Strength

The mean load level for the flexural tensile beams has been calculated by assuming a linear variation of the load in the range of 0.67mm to 3.33mm displacement from the laboratory results. This is a reasonable assumption as seen in the laboratory results of the flexural tensile beams in Fig. 43. It is seen that the load varies more or less linearly in this displacement range. The residual flexural tensile strength is then calculated as in Equation (6.7).

$$M = T_c \times z \quad \rightarrow \quad f_{ftk,eq} = \frac{3 \times F \times L_2}{2 \times b \times d^2} \tag{6.7}$$

$$M = \frac{F(\delta_{12}) \times L_2}{4}$$

$$T_c = \frac{1}{4} \times f_{ftk,eq} \times b \times d$$

As illustrated in Fig. 27.

$$z = \frac{2}{3} d$$

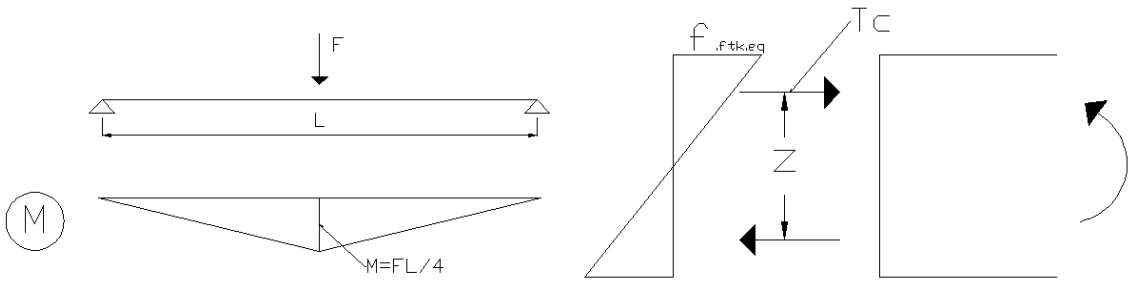

Fig. 27: Moment diagram and stress distribution over the cross section for the flexural tensile beam specimens used in this report.

Once the residual flexural tensile strength has been calculated according to Equation (6.7), the residual tensile strength is easily calculated according to Equation (6.8) [26]:

$$f_{ftk,res} = 0.37 \times f_{ftk,eq} \tag{6.8}$$

Where $f_{ftk,eq}$ is based on the mean calculated value, corrected with standard deviation, see Appendix E.1-E.3. Equation (6.8) is based on a minimum reinforcement requirement when comparing Stadium I (not cracked section) with Stadium II (cracked section) and requiring horizontal equilibrium as shown in Fig. 28.

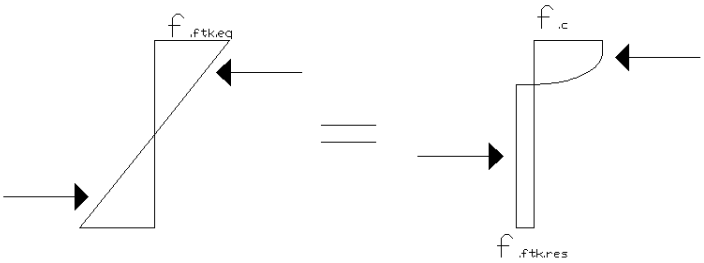

Fig. 28: Basis for derivation of Equation (6.8).

Theoretical Residual Flexural Tensile Strength

On basis of the Steel Fiber Draft a theoretical residual flexural tensile strength can be calculated according to Equation (6.9).

$$f_{ftk,eq} = 2.7\, v_f\, \eta_0\, \sigma_{fk.mid} \tag{6.9}$$

v_f	Steel fiber content in percent
$\eta_0 = \frac{1}{3}$	Orientation factor, assumed value according to the steel fiber draft [26]
$\sigma_{fk.mid}$	Average stress in steel fibers intersecting a crack at random direction and anchorage length.

Pull-out tests need to be performed in advance in order to estimate this capacity. Such tests have been performed with several different steel fibers at NTNU, in students work with master thesis. For the W1150 concrete using the Dramix 65/35 steel fiber, $\sigma_{fk.mid} = 193$ MPa was obtained [28]. How these pull-out tests have been performed or how the results have been interpreted will not be discussed further in this report. The results from these calculations regarding residual strengths are summarized in Table 16 in Section 0.

6.6.2 Estimated Shear Beam Capacity

The capacity of the beam itself, disregarding the steel fibers, was calculated according to Eurocode 2. All calculations related to the steel fiber contribution are done on the basis of the Steel Fiber Draft[26] together with the derivations in Section 6.6.1. In addition, the anchorage capacity has been calculated according to both Eurocode 2 [2] and the old Norwegian concrete standard NS 3473 [29]. Except for the results, the anchorage calculations will not be commented further in this report, but are enclosed in Appendix F.3 and F.4.

6.6.2.1 Moment Capacity Disregarding Steel Fiber Contribution

The method used for calculating the moment capacity disregarding the steel fiber contribution will not be given in detail, only assumptions used will be cited. The calculations are enclosed in Appendix F.1.

The compressive strain at maximum strength of the LWAC has conservatively been calculated according to Eurocode 2.

It has been assumed a rectangular stress distribution for the LWAC. The correctness of this assumption could be discussed, but as shown later in Section 6.8.5, this seems realistic with respect to the laboratory results.

6.6.2.2 Shear Capacity Disregarding Steel Fiber Contribution

The method used for calculating the shear capacity disregarding the steel fiber contribution will not be given in detail, only assumptions used will be cited. The calculations are enclosed in Appendix F.2.

In the expression for the shear capacity for LWC in Eurocode 2, see Equation (6.10), the coefficient η_1 has been neglected since it principally is a coefficient for determining the tensile strength for LWC on the basis of NC compressive strength [2]. This has been compensated by using the real measured average compressive strength for the LWAC produced in this report, see Appendix F.2.

$$V_{lRd,c} = \left[C_{lRd,c}\eta_1 k(100\rho_1 f_{lck})^{\frac{1}{3}} + k_1\sigma_{cp}\right] b_w d \geq \left(v_{l,min} + k_1\sigma_{cp}\right) b_w d \qquad (6.10)$$

6.6.2.3 Steel Fiber Capacity Contribution to Moment

For simplicity the capacity contribution from the steel fibers has been calculated separately as described in the Steel Fiber Draft [26] and shown in Fig. 29. It is here assumed that the residual tensile strength is mobilized over a height of 0.8h with an internal moment arm of 0.5h.

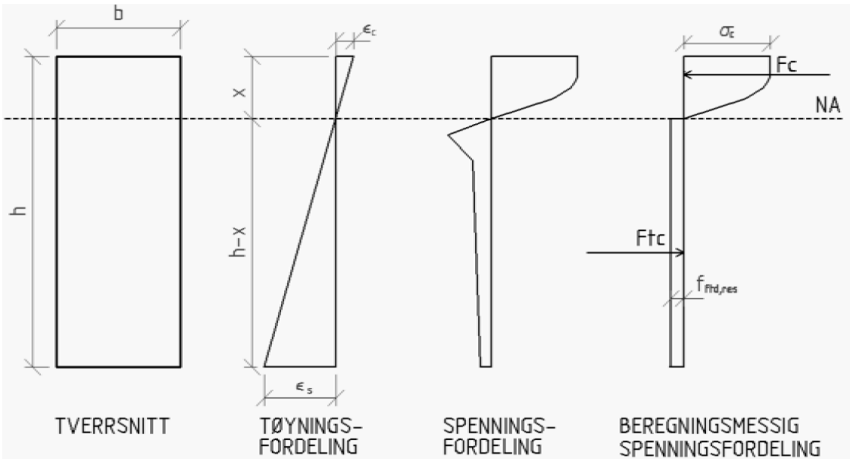

Fig. 29: Stress and strain relations for non-reinforced cross section induced by pure bending [26].

The moment contribution is calculated on basis of Fig. 29 and as described in Equation (6.11).

$$M_{ftk} = 0.4 \times f_{ftk,res} \times b \times h^2 \times p \times e \qquad (6.11)$$

$p = 1.1 - 0.7h \geq 0.75$ P dimensionless scale coefficient

$e = 1.0$ $e = 1.0$ for self compacting concrete

The moment contribution should in reality be calculated according to the stress and strain relation illustrated in Fig. 30. The error made by simplifying the calculation will not affect the predicted capacity to a big amount since the steel fiber contribution to the overall moment capacity is modest as compared to the capacity of the beam itself.

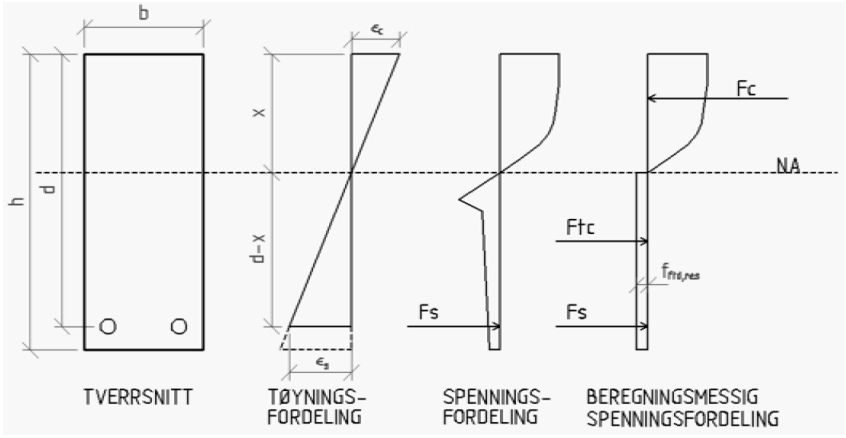

Fig. 30: Stress and strain relation for reinforced cross section induced by pure bending [26].

6.6.2.4 Steel Fiber Capacity Contribution to Shear

The contribution to the overall shear capacity from the steel fibers is calculated according to the Steel Fiber Draft [26] with Equation (6.12).

$$V_{fk} = 0.8 \times f_{ftk,res} \times b \times d \times p \qquad (6.12)$$

6.7 Laboratory Testing

All of the testing in phase 1, except for the shear beams (tested April 21 2010), was carried out during the period of March 17-19, 2010 in the laboratory at The Department of Structural Engineering at NTNU.

The following tests were performed:

- Compressive strength; compression of standard cylinders and cubes.
- Flexural tensile strength; 3-point bending of small scale bending prisms.
- Uniaxial tensile strength; tensile test of small scale tension prisms.
- Shear strength; 4-point bending of shear beams.
- Flexural toughness; centric point loaded round panels supported on three pivots.

When unpacking all the test specimens the storage conditions was been found to be adequate according to the requirements set by the governing standards, i.e. ≥95% humidity.

All the results from test phase 1 is summarized and discussed further in Chapter 6.8.

6.7.1 Compressive Strength

A total of 12 cubes and 9 cylinders were tested March 17-19 in order to establish the compressive strength of the different concrete recipes. A secondary objective was to compare the correlation between cylinder and cube compression strength for the W900 and W1150 with the LWC correlations in Eurocode 2 [2]. The tests were performed in accordance with the European Standard NS-EN 12390-3 [20] in a uniaxial compression testing machine. The testing rig is made by Galdabini and is shown in Fig. 31. This is an analog machine so no other logging than the actual failure load and visual observation was done.

The rest of the cube specimens which had not been tested were cured until the day of the shear beam testing (April 21) in order to have reference data on the compression strength development for the W900 and W1150 concrete. In this second curing phase from 28 to 62 days of curing, the cubes were not stored submerged in water. The cubes were stored in wet cloths and wrapped in plastic to ensure sufficient humidity, i.e. ≥95% humidity. During these compression test, the Galdabini machine stopped working. The rest of the compression tests were then performed with another equivalent analog uniaxial compression machine. More specifically a Mohr Federhaff Losenhausen with a maximum capacity of 300 000 kilopond.

Fig. 31: Galdabini analog uniaxial compression testing machine.

6.7.2 Flexural Tensile Strength

A total of 9 small scale beams for testing of flexural tensile strength were tested in test phase 1. The main objective of these tests was to determine the residual tensile strength of the LWAC with different fiber volume and density. A sketch of the testing arrangement and specimen geometry is shown in Fig. 32. A photo of the arrangement which was used in the laboratory at NTNU is shown in Fig. 33.

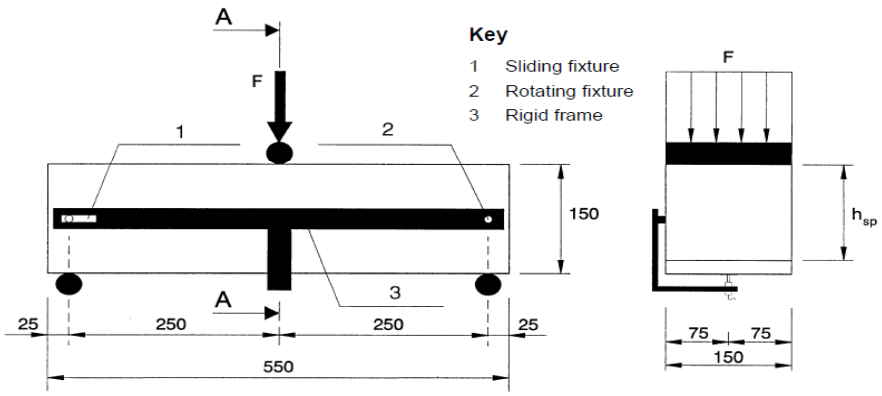

Fig. 32: Sketch of the testing arrangement for flexural tensile capacity of small scale beams [23].

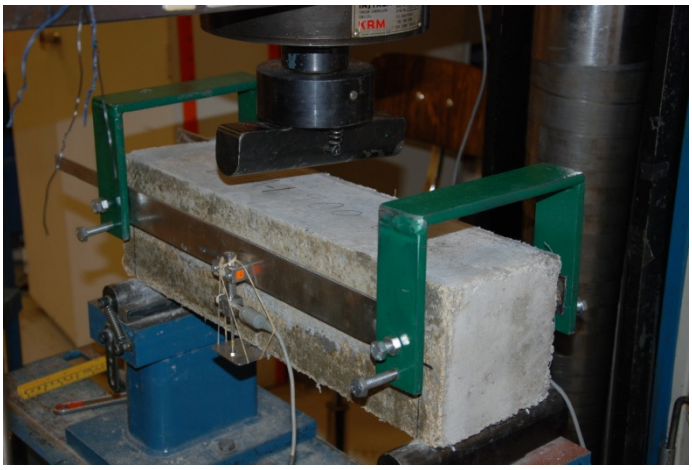

Fig. 33: Photo of the flexural tensile test arrangement in the laboratory at NTNU.

The bending specimens were tested with an Instron 1126 multipurpose testing machine with a maximum load capacity of 250kN (hydro mechanical drive) together with an Instron 8800 controller for logging purposes. A universal bearing rig with sufficient stiffness especially made for these kinds of experiments were used to ensure a simply supported boundary condition for the beams. The bearing rig fulfills the requirements set by the governing standard NS-EN 14651[23].

The test was performed by applying the load indirectly by displacing the specimen at a constant rate. The load was measured by a load cell mounted behind the loading piston. The displacement was measured with two *Linear Variable Differential Transformers* (LVDT) mounted at a bracket at each side of the specimen in the longitudinal center over the notch. The vertical displacement is then measured as illustrated in Fig. 33 by a rigid steel plate mounted at the bottom the specimen, across the notch.

The tests were performed in accordance with the European Standard NS-EN 14651 [23], but with the exceptions shown in Table 8. The modifications were done in order to reduce testing time and reduce the number of sampling data points. This has been done since SINTEF researchers claimed that the specified modifications had a small/no influence on the test results, based on earlier experience [30].

Table 8: Exceptions made when testing the small scale flexural tensile beams.

Control Parameter	Governing method	Method used
Operating speed	0-0.13mm deflection: 0.08mm/min 0.13–3.44mm deflection: 0.21mm/min	constant 0.21mm/min
Sampling rate	0-0.13mm deflection: 5 Hz 0.13–3.44mm deflection: ≥ 1 Hz	constant 2 Hz

6.7.3 Uniaxial Tensile Strength

A total of 9 uniaxial tensile prisms were tested in test phase 1 for determination of tensile strength and Young's Modulus. The test was performed in accordance to a procedure developed by SINTEF at NTNU [22] mainly because of good experience gained with this testing procedure and the available rig equipment at the NTNU laboratory. This test method does not suggest a notch to be cut in the specimen, even though this is common in more well known testing methods such as RILEM TC 162-TDF [31].

To be able to measure the displacements in the cracked region it is decided to make an exception from the SINTEF method and cut a notch as described in Section 6.5.2. Previous experiments using the same exception have been carried out at NTNU with good results. No negative effects of the notch have been observed [32].

Other exceptions from the SINTEF method used in this report are summarized in Table 9.

Table 9: Exceptions made when testing uniaxial tension prisms.

Control Parameter	Governing method	Method used
Operating Speed	SINTEF: 5mm/min RILEM: 0-0.1mm deflection: 0.005mm/min 0.1mm→ deflection: 0.1mm/min	0.5mm/min
Sampling Rate	RILEM: 0.5Hz	2 Hz

The uniaxial tensile specimens were tested with the same Instron testing machine and logging equipment as described in Section 0, but with another testing rig especially made for uniaxial tension testing. The bearing rig is made for this particular type of test and has been thoroughly tested at NTNU. The tension specimen is held in the rig by rubber covered steel plates with applied pressure by hydraulic jacks. No sliding was observed or recorded during the testing. A sketch of the testing arrangement and specimen geometry is shown in Fig. 34 together with the arrangement used at NTNU.

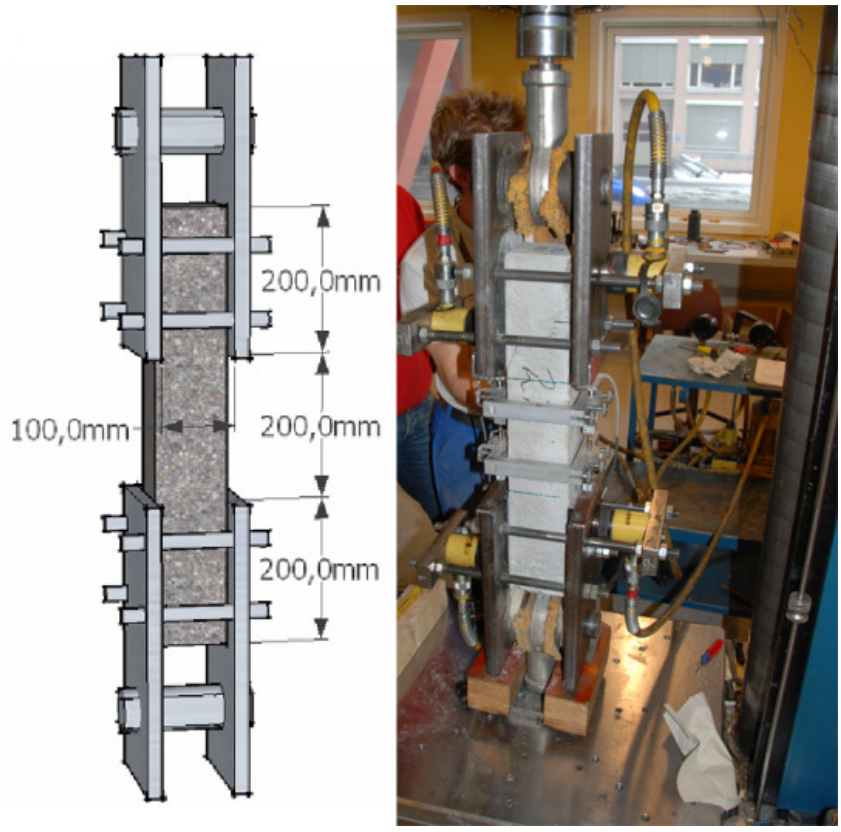

Fig. 34: Left: Sketch of tension test arrangement [13]. Right: Photo of the tension rig used in the laboratory at NTNU.

The test was performed by applying the load indirectly by displacing the specimen at a constant rate. The load was measured by a load cell mounted behind the load piston while the displacement was measured with two LVDT's mounted at a bracket at two of the specimen sides over a distance of 100mm over the notch, see Fig. 35. The measuring rig was removed when the LVDT measuring devices were outside their measuring range, approximately at a displacement of 6-7mm. After the LVDT's had been removed the displacement was measured directly by the machine.

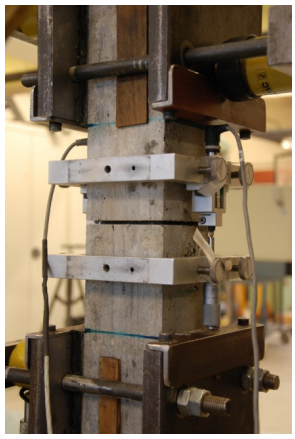

Fig. 35: Measuring bracket mounted on the uniaxial tensile specimen within the test rig.

6.7.4 Flexural Toughness

A total of 9 round panels were tested for determination of flexural toughness, expressed through the energy absorption in the post crack phase of the fiber reinforced concrete. The tests were performed in accordance with the ASTM standard C1550-08 [24] with a minor exception related to the data sampling rate. The control parameters used during the tests are summarized in Table 10.

Table 10: Machine properties used during tests of round panels.

Control Parameter	Governing method	Method used
Operating Speed	ASTM: 4.0±1.0 mm/min	4mm/min
Sampling Rate	ASTM: 1.33Hz	2 Hz

The round panels are centrally loaded by a point load while being supported on three symmetrically placed pivots. The testing arrangement is shown in a sketch in Fig. 36.1. A photo of the rig used in the laboratory at NTNU is shown in Fig. 36.2.

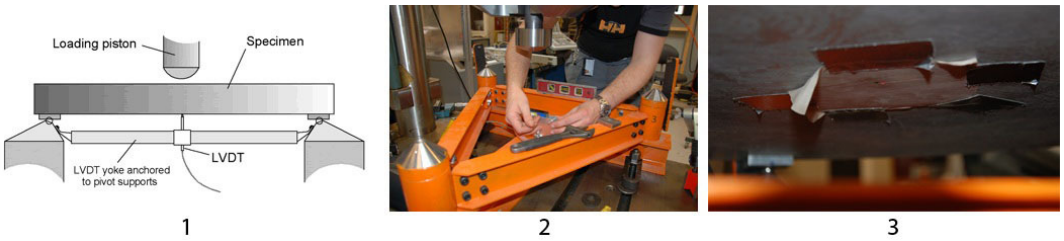

Fig. 36: 1: Recommended testing arrangement ASTM [24]. 2: Testing arrangement used at NTNU. 3: Deflection recorded by use of a laser pointed to a piece of latex fabric.

The machine used during the tests was a Dartec RE500 multipurpose testing machine (hydraulic drive) with a maximum load capacity of 500kN. An Instron 8800 controller was used for logging purposes. The load was applied indirectly through a loading piston with a hemispherical end which was displaced at a constant speed.

The displacement of the round panels were not recorded using a LVDT, as indicated in Fig. 36.1. Instead the displacement was measured with laser equipment, measuring the displacement at the specimen center.

Since the development of cracks could interfere with the laser, a piece of latex fabric was glued to the base of the round panel. In this way the measuring surface was kept flat through the whole laboratory test. The latex fabric is mounted and hit by the laser as shown in Fig. 36.3.

6.7.5 Shear Strength

A total of three beams, cast with the W900 concrete with 0, 0.5% and 1% fiber content, were tested. The purpose for performing the shear beam tests were primarily to test the shear capacity of the W900 concrete with varying steel fiber reinforcement volume.

The shear beams were initially to be run in the end of the same testing period as the rest of the testing done in phase 1. However, a mishap in the laboratory with the rig controller resulted in a delay. An error in the rig controller software, led to unintentional crushing of beam B0 and no data was recorded for this beam. The error was later corrected and the whole testing rig was calibrated and controlled before the two remaining beams were tested. The testing of these two beams was carried out April 21.

6.7.5.1 Loading, Boundary Conditions and Data Logging

The tests were performed using an Alfred J. Amsler & CO. 100kN hydraulic jack together with an Instron 8800 controller for logging purposes. The testing rig is shown in Fig. 37.

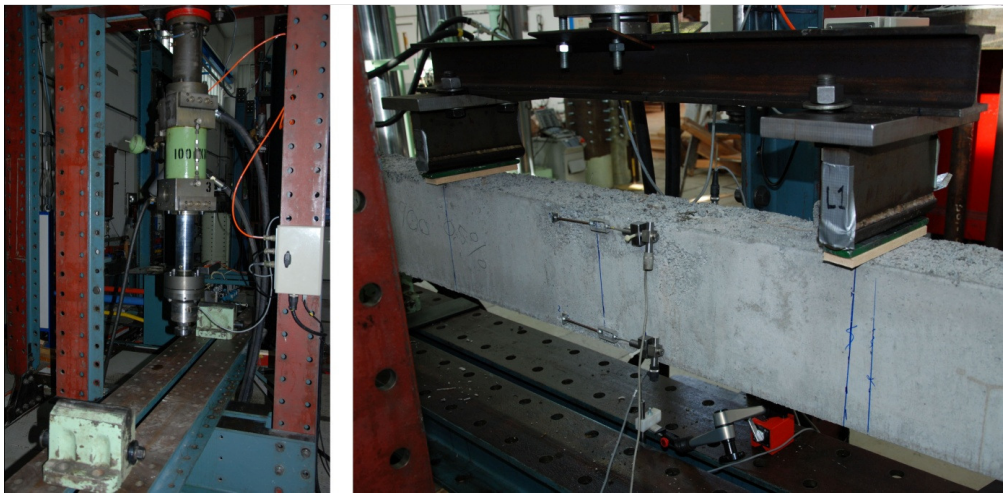

Fig. 37: Left: Testing rig used for testing of the shear beams at NTNU. Right: Arrangement of loading and LVDT placement.

The calculations performed prior to testing in Section 6.6 concluded that an a/d relation equal to 3 should be used in order to assure pure shear failure instead of a flexural tensile failure or a combination failure. This resulted in load positions as shown in Fig. 38.

A total of 5 LVDT's were mounted on the beams during testing for displacement and strain logging purposes. The LVTD's were placed as shown in Fig. 38. The horizontally placed LVDT's were placed parallel to the longitudinal reinforcement and had a matching pair on the opposite side of the beam. Confer Fig. 15 for reinforcement placement. The vertical LVDT was placed at the beam center beneath the beam to measure the vertical displacement.

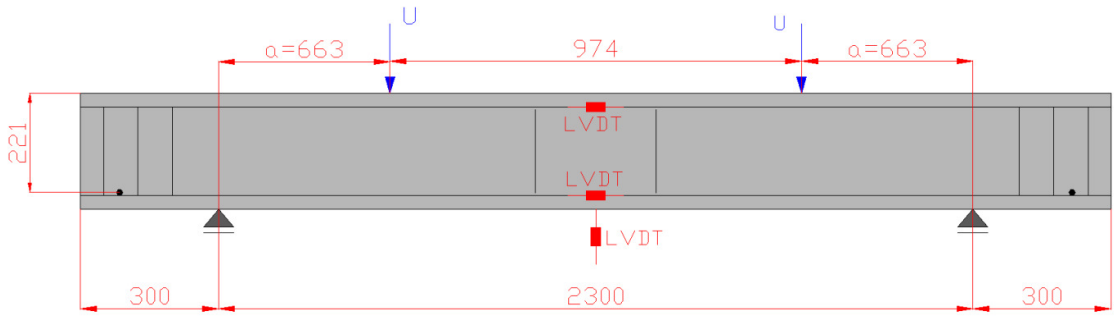

Fig. 38: Sketch of load placing and placing of LVDT's during laboratory testing on shear beams.

The load level was measured by a load cell in the hydraulic jack piston. The load was applied by displacing the specimen at a constant rate, using two symmetrically placed steel rollers. Between the rollers and the concrete specimen, a 10mm thick steel plate and a 10mm thick wood fiber plate was placed, in order to distribute the load, see Fig. 37. This somewhat reduced the risk of local deformations and unwanted failure. A detailed sketch of the loading and boundary condition arrangement can be seen in the test setup for the CSS beams in Fig. 86, where a similar test arrangement has been used. Control parameters used during the testing are summarized in Table 11.

Table 11: Control parameters used for testing of shear beams.

Control Parameter	Value
Operating Speed	2mm/min
Sampling Rate	1 Hz

During testing the beams were inspected constantly in order to determine the crack load. Once the first crack was observed the test was paused and crack bandwidth was recorded using a crack binocular. The load was then applied in adequate intervals in order to record the crack bandwidth and to draw the crack development.

At 75-80% of the calculated failure load, recording of the crack development was stopped and the specimen was displaced non-stop until failure occurred. It is assumed in this report that these intermissions did not influence the capacity or behavior of the beam in any negative way.

6.8 Summary of Laboratory Results

In this chapter the results from test phase 1 are summarized and commented. Description of the different batches and test methods are done earlier in Chapter 6.

6.8.1 Compressive Strength

6.8.1.1 Cubes

Measures: 100x100x100mm

28 Days:

Table 12: Average compressive strength from laboratory testing of 28 days cured cubes.

Batch	Achieved Average True Density [kg/m^3]	Average Capacity [MPa]
BO (W900 0%)	945	9.38
B1A (W900 0.5%)	996	8.11
B2B (W900 1%)	1020	12.36
B3 (W1150 1%)	1231	17.23

62 Days:

Table 13: Average compressive strength from laboratory testing of 62 days cured cubes.

Batch	Achieved Average True Density [kg/m^3]	Average Capacity [MPa]
B1A (W900 0.5%)	996	7.42
B1B (W900 0.5%)	975	10.77
B2A (W900 1%)	964	7.3
B3 (W1150 1%)	1231	27.27

The results from compression testing of cubes are summarized in Table 12 and Table 13, in terms of average values from the different batches and different curing time. A complete overview of the results can be found in Appendix C.1.

After studying the compressive strength values sampled for the W900 concrete, the general conclusion is inconsistency in the results. The quality of the specimens cast from both batch B1A and B2A was not satisfying. Since the concrete was supposed to be self compacting, no external vibration was applied when casting. Externally applied vibration could be considered for later work, even though research show that external vibration leads to worse fiber

anchorage and fiber orientation than for a self compacting concrete [33]. More could probably be gained by refining and establishing a stable recipe for the W900 concrete.

The higher capacity observed for the W900 concrete from batch B2B and B1B compared to the rest of the batches with W900 concrete, correlated with the quality of the specimens. The specimens from batch B2B and B1B had a better quality and fewer imperfections. The higher capacity is therefore most likely related to the concrete's casting abilities. More carefully cast specimens could also be one of the contributing factors since several persons were involved in the process, which could have resulted in various quality in the work done.

A remarkable observation was done when the results from the W1150 concrete with 62-days strength was studied. The W1150 concrete had a pronounced increase in strength after 62 days of curing compared to the strength obtained after 28 days. Further research is necessary in order to state a conclusion on this concern, but the results from this study is promising. Whether this increase is related to the storage conditions from 28-62 days (wrapped in wet cloths and plastic) or if the concrete has a natural increase of capacity past 28 days is too early to tell. The W1150 concrete's compressive capacity appears to be more than 35% higher than expected according to Table 12 and Table 13 after 62 days of curing.

No general increase in strength was observed for the W900 concrete when comparing 28 and 62 days of curing. However, this observation should be taken with caution because of the inconsistency of the specimen quality and results. The most representative capacity for the W900 concrete would be related to batch B1B and B2B which had the best quality. It should also be noted that the most probable reason why a higher capacity is noted for batch B1A at 28 days than at 62 days is because it was chosen deliberately to test the specimens with the best overall quality at 28 days.

In general the overall specimen quality for the W1150 concrete was good and could not be compared to the poor quality of the W900 concrete, this also explains the big differences in capacity within the W900 batches.

6.8.1.2 Cylinders (28 days cured)

Measures: Ø100x200mm

Table 14: Average compressive strength from laboratory testing of 28 days cured cylinders.

Batch	Achieved Average True Density [kg/m^3]	Average Capacity [MPa]
B1A	1001	10.66
B2A	907	5.12
B3	1206	16.37

The results from compression test of cylinders are summarized in Table 14, in terms of average values from the different batches and different curing time. A complete overview of the results can be found in Appendix C.1.

Studying the results from the cylinder test, the same tendency is observed as for the cubes. Really bad specimen quality was observed for the W900 concrete which again resulted in inconsistency in the results, while the W1150 concrete results were very consistent. Batch B1A was the most representative for the W900 concrete due to the specimen's relatively higher quality.

6.8.1.3 General Comments about Compression Strength Test

The varying quality of the casting for the compression test specimens lead to non consistent results for some of the batches. The tendency was clear, good casting quality lead to higher compressive strength independent of the steel fiber content. This makes sense since the steel fibers only contributes to the overall capacity when cracks have formed, which in this case will be after the maximum compression load is reached. In this specific case the increase of steel fiber content had only negative effects because of worse casting abilities for the concrete.

Comparing the cube- and cylinder compressive strength, a slightly higher capacity was observed for the cubes from the batch with the W1150 concrete. The deviation between the two measures matches good with a LWAC with similar strength in Eurocode 2 and gives approximately the same ratio between cube and cylinder compressive strength [2]. However, the number of specimens in this study is not enough to make a conclusion on the cylinder – cube compressive strength relation since all the specimens made of W900 concrete could not be used as a comparison due to their bad quality.

The governing standard for compressive strength testing [20] describes which failure modes that can be characterized as satisfactory or unsatisfactory failure modes. Examples are shown in the right of Fig. 39. Most of the specimens had a failure mode which resembles what is described as unsatisfactory failures. One could initially believe that the steel fibers could prevent this satisfactory failure mode to arise since the fibers would counteract the deformation. This is probably not the case since the test specimens with no fiber content had the same observed failure modes as the rest of the specimens as shown in the rightmost cube in Fig. 39. The most likely cause for these observed failure modes might be caused by the failure arising in the lightweight aggregate instead of in the cement paste because of its relatively low bearing capacity. It is however unclear if the failure modes are valid for this specific LWAC.

Even though there are uncertainties related to the compressive failure modes, the results are used further in the report.

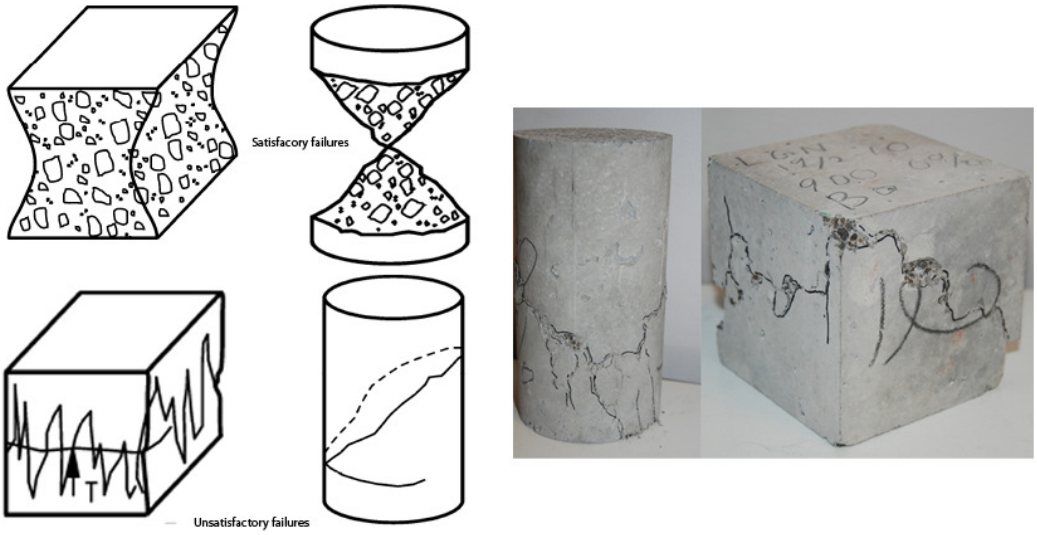

Fig. 39: Left: Satisfactory (top) and unsatisfactory (bottom) failures. Right: Example of "unsatisfactory" failure modes from the laboratory testing.

6.8.2 Tensile Strength

Measures: 100x100x600mm

The results from the laboratory tension tests are shown in Fig. 40 in terms of tension load (measured by the load cell) versus displacement (measured over the notch with two LVTD'S placed on two opposite sides).

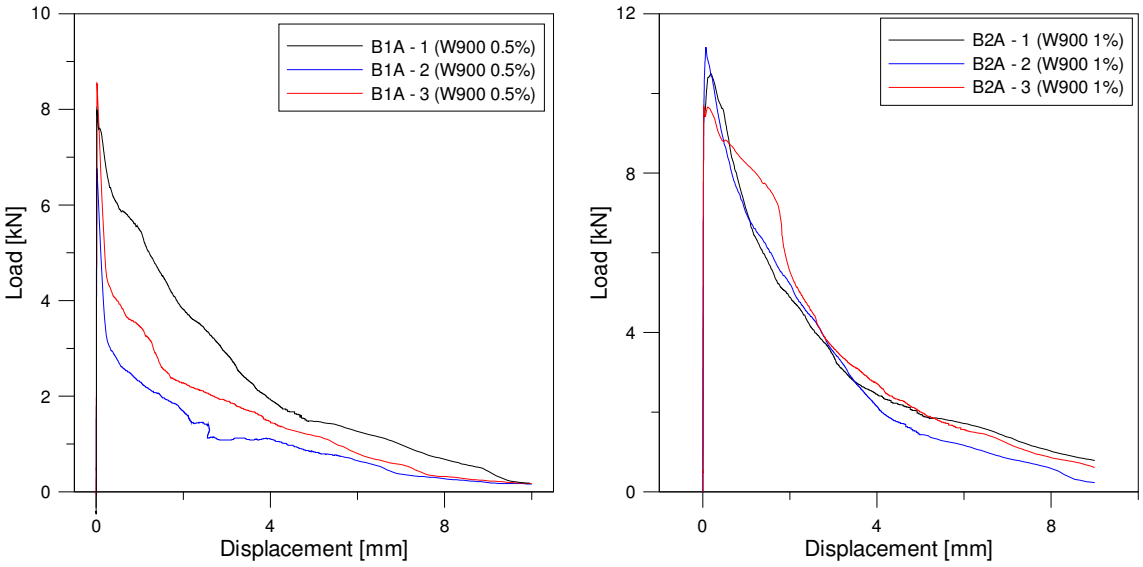

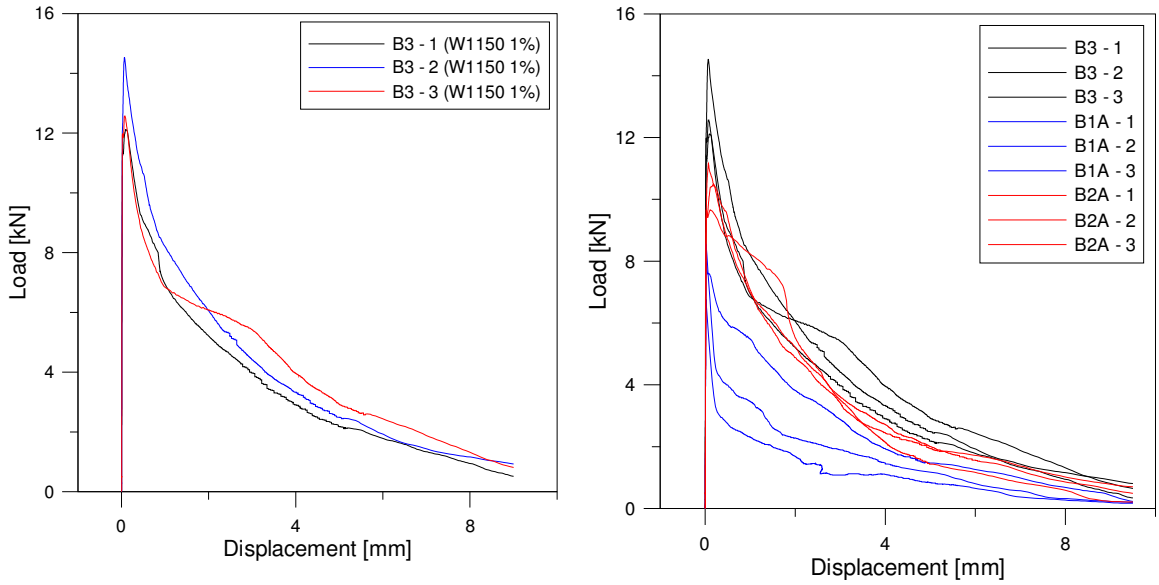

Fig. 40: Load-displacement curves from laboratory testing of tensile prisms.

The quality of the tensile specimens cast with the W900 concrete was especially varying for batch B1A while specimens cast from batch B2A had higher and more uniform quality. This is also reflected in the results presented in Fig. 40 where it is seen that the results for batch B1A is not as consistent as the results from batch B2A.

In general a higher tensile strength is observed for 1% steel fiber content as compared to 0.5% and thereby the steel fiber content not only increases the post crack capacity, but also the tensile strength in general. However, this conclusion should be taken with some caution due to the varying quality of the W900 specimens with 0.5% fiber content (B1A).

Studying the results just post cracking, the specimens with 1% steel fiber content experience initial hardening before reaching their maximum capacity as illustrated in Fig. 41. The hardening effect was a little more pronounced for the W1150 concrete, probably due to its better quality.

The same hardening effect is not observed for the specimens with 0.5% steel fiber content. This could indicate that the amount of steel fibers across the crack, together with their low pullout capacity, not fulfills the minimum reinforcement requirement when moving from pre to post crack behavior. It therefore appears that a fiber content higher than 0.5% is desirable in order to achieve a more predictable behavior with no sudden drop in post crack capacity.

Earlier research at NTNU with the same concrete and steel fiber type has shown that a fiber content of 2.5% is above the upper desired limit because of reduced ductility and sudden loss of capacity [17]. On the basis on the earlier work at NTNU and the observations done in this report, it can be anticipated that the most favorable fiber content would be in the range 1% - 2.5%, in order to obtain hardening effects and desired behavior. Further research with a larger number of consistent specimens of higher quality is needed to state a conclusion on the lower limit.

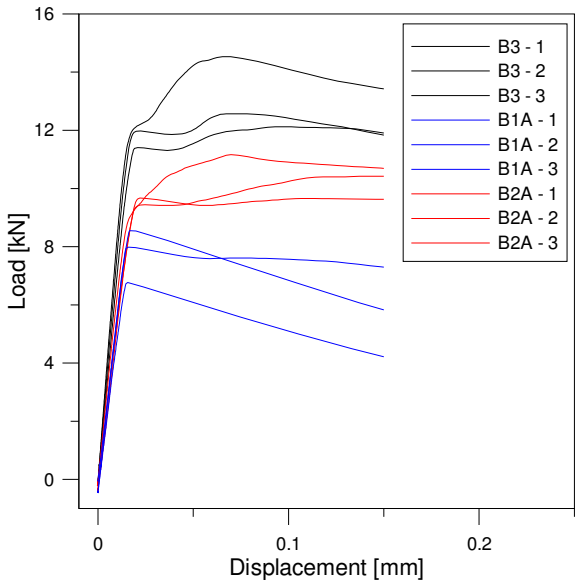

Fig. 41: Behavior just post cracking of tensile specimens. (zoom of the top of the summarizing plot in Fig. 40.)

All but one of the test specimens behaved as anticipated during testing, i.e. the crack started within the notch and the specimen experienced more or less uniform deformation. For specimen B2A-2 the crack started from outside of the notch, at one side of the specimen, and eventually ended in the notch on the opposite side as shown to the left in Fig. 42.

This unwanted crack growth could be related to uneven steel fiber distribution. As attempted illustrated to the right in Fig. 42, a denser cluster of steel fibers are located at the part of the specimen where the crack started outside the notch. This cluster could have caused higher capacity in the notched section compared to the non cut section just outside, which then led to the start of the crack outside the notch.

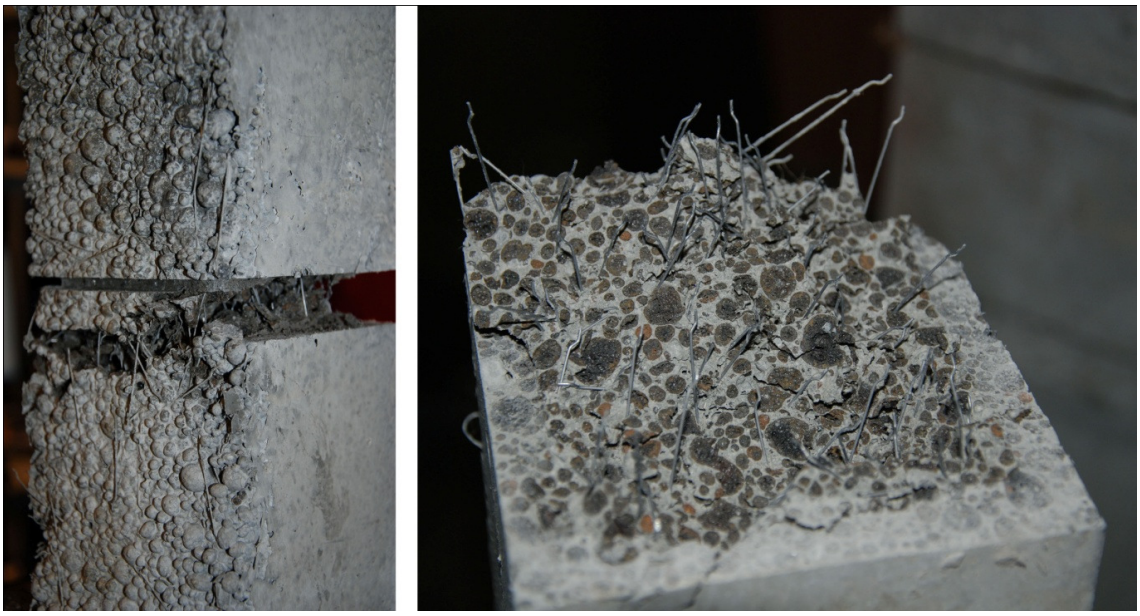

Fig. 42: Left: Crack starting from outside of the notch on specimen B2A-2.
Right: Higher density of steel fibers on one end of the specimen.

When studying the fracture surfaces after the testing, it was observed that pullout capacity of the fibers were critical for the global specimen capacity. In general for the tensile specimens most of the steel fibers were more or less undeformed after testing, which could indicate that the anchorage capacity in general for the W900 and the W1150 concrete is poor.

However, some steel fibers with straightened end hooks were observed for the B1A specimens with 0.5% steel fiber content. This indicates that a steel fiber content of approximately 1% and higher increases the risk of collective anchorage failure for this specific concrete, while the anchorage capacity is sufficient for steel fiber contents around 0.5%.

A summary of the obtained mean tensile yield strength for each batch is summarized in Table 15.

Table 15: Summary of mean tensile capacities from tension tests.

Batch	Average Tensile Capacity [MPa]
B1A	1.22
B2A	1.44
B3	1.87

6.8.3 Flexural Tensile Strength

Measures: 150x150x550mm

The results from the laboratory flexural tensile tests are shown in Fig. 43, in terms of load (measured by the load cell) versus vertical displacement (measured over the notch with two LVTD'S placed on each side of the beam). The overall quality of the flexural tensile beams was good. No major defects were found in any of the specimens.

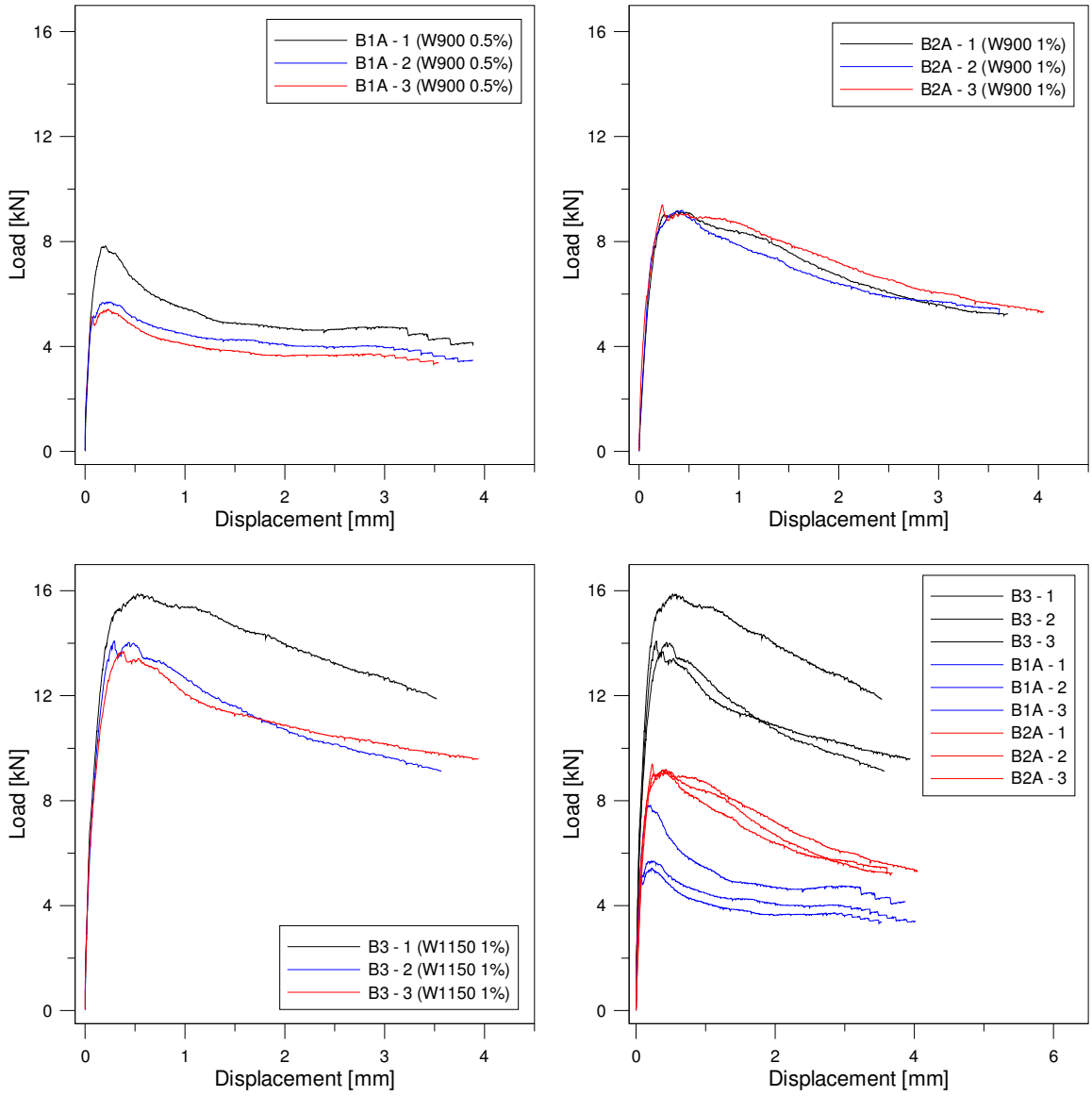

Fig. 43: Load-displacement curves from laboratory testing of flexural tensile beams.

When casting the three beams with the W1150 concrete, it was hard to distribute the concrete in the formwork as described in the European standard [23], due to very good flow abilities of

the concrete. This might have lead to a more favorable steel fiber distribution compared to the beams cast with the W900 concrete. This could be part of the explanation of the higher capacity for the W1150 concrete, even though most of the extra capacity probably has its origin in the general better quality and w/c relation of the W1150 concrete. Studying the effect of this possible favorable steel fiber distribution will not be a further focus in this report due to a small basis of comparison.

The crack started in the notch base in all the test specimens, except for specimen B2A-1. In specimen B2A-1, the crack initially started from outside of the notch at one side of the beam. However, the crack eventually propagated towards the notch as shown in Fig. 44. This could be related to a local defect within the beam, for example locally uneven distributed steel fibers, similar to what is described earlier with the crack outside the notch for the uniaxial tensile specimen in Section 6.8.2.

Fig. 44: Notch propagated from outside of the notch.

6.8.3.1 Residual Flexural Tensile Strength: Comparison with Earlier Research

Research done at NTNU through COIN concluded in 2009 that the increase from 0.5% to 1% steel fiber content not increased the flexural residual tensile strength correspondingly for the W1150 concrete [17]. The COIN report actually concludes with a decrease in the residual flexural tensile strength when increasing the fiber content from 0.5% to 1% for some of the test series.

The results shown in Fig. 43 and in Table 16 indicate that the COIN results are partially contradicted. An increase of approximately 60% is observed for the residual flexural tensile strength when doubling the fiber content from 0.5% to 1% for the W1150 concrete. The achieved residual flexural tensile strength in this report is nearly 75% higher than the corresponding strength achieved in earlier research with the same concrete [28]. It is not possible to state whether this observation is related to different specimen geometry, testing method or higher achieved concrete quality.

The values in Table 16 are calculated as described in section 6.6.1.

Table 16: Summarized results from flexural tensile beams.

Specimen ID	Fiber Volume	$f_{ftk,eq}$[1]		$f_{ftk,eq}$[2]	f_{ck}
		Specimen	Mean	[MPa]	[MPa]
B1A-1	0.5% Dramix 65/35	1.674			
B1A-2	0.5% Dramix 65/35	1.387	1.442	0.8685	10.66
B1A-3	0.5% Dramix 65/35	1.266			
B2A-1	1% Dramix 65/35	2.235			
B2A-2	1% Dramix 65/35	2.229	2.272	1.737	5.12
B2A-3	1% Dramix 65/35	2.352			
B3-1	1% Dramix 65/35	4.469			
B3-2	1% Dramix 65/35	3.637	3.929	1.737	16.37
B3-3	1% Dramix 65/35	3.682			

$f_{.ftk,eq}$[1] : Residual flexural tensile strength determined directly from standard beam testing

$f_{.ftk.eq}$[2]: Residual flexural tensile strength determined from pullout test results from similar LWAC [17], confer Section 6.6.1.1.

As seen in Table 16 the theoretically calculated residual flexural tensile strength is far lower than the obtained capacity calculated on basis of the flexural tensile beams. The obtained residual flexural tensile strengths in this report corresponds to an average stress in the steel fibers across the crack of approximately 437 MPa whereas earlier research at NTNU obtained 193 MPa when performing pull-out tests [28].

Further research with fiber counting and a more thorough test program is needed, in order to state a conclusion on the exact effects that the fiber content will have on the residual flexural tensile strength.

6.8.4 Round Panels

Measures: Ø800x75mm

Round panels were primary cast by us on behalf our supervisor Linn Grepstad Nes. Testing was later performed in collaboration with her. The results from the round panel test are presented but discussed very briefly since the round panels not are a focus in this report.

The results from the laboratory round panel tests are shown in Fig. 45, in terms of load (measured by the load cell) versus vertical displacement (measured in the round panel center base with a laser).

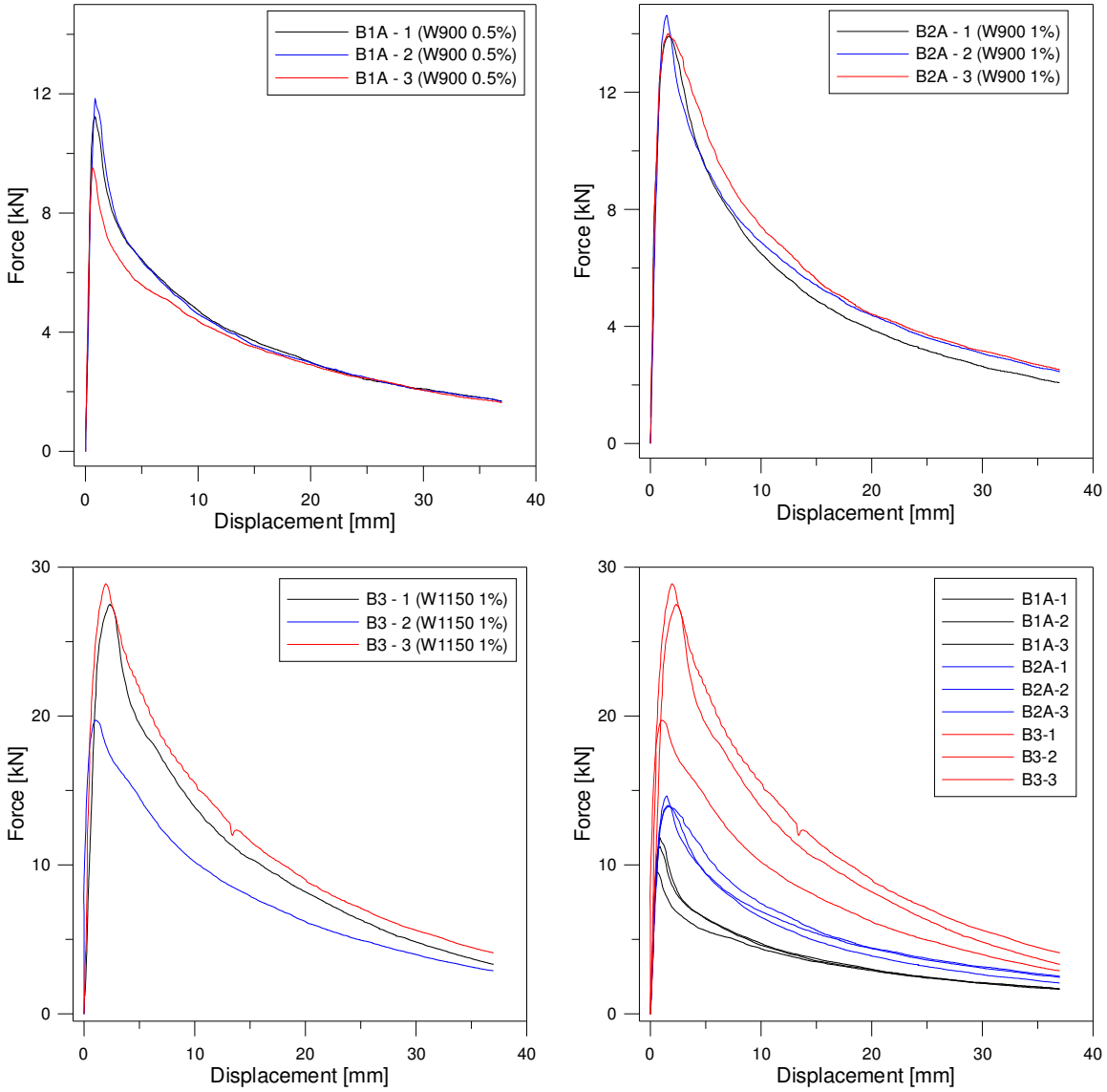

Fig. 45: Load-displacement curves from laboratory testing of round panels.

The anticipated crack pattern, shaped as a Mercedes star, described in the ASTM standard [24] was obtained for the all the W900 concrete round panels. On two out of the three round panels tested with the W1150 concrete the anticipated crack pattern was not obtained. Examples of the cracking patterns are shown in Fig. 46. It was no correlation with the higher capacities obtained for two of the W1150 specimens with the unexpected crack pattern, i.e. one of the specimens reaching almost 30kN had Mercedes star shaped pattern and the other one did not.

Fig. 46: Leftt: Anticipated crack pattern shaped as a Mercedes star. Right: Crack pattern obtained in two of the specimens cast with the W1150 concrete.

Because of the good flow ability for the W1150 concrete, the steel fibers could have been distributed in an unfavorable position during casting. While filling the formwork, the concrete flowed in radial direction from the center of the formwork towards the outer walls. This might have led to an orientation of the steel fibers, parallel to the cracks which could have reduced the post crack capacity in this direction. This should be studied further in later research and actions should be taken to avoid this effect during casting.

6.8.5 Shear Beams

Measures: 150x250x2900mm

As mentioned earlier, the shear beam cast without steel fiber reinforcement (B0) was crushed in a laboratory accident. Therefore no laboratory data can be presented for that beam.

The results from the laboratory shear beam tests are shown in Fig. 47, in terms of load (measured by the load cell) versus vertical displacement (measured with a LVTD placed in the beam mid span, base center). Very similar behavior was observed for the two beams until the ultimate load was reached for the B1A beam, which drops while the B2A beam has additional capacity. The sudden drop in capacity was anticipated because of an expected failure mechanism as a sudden shear failure.

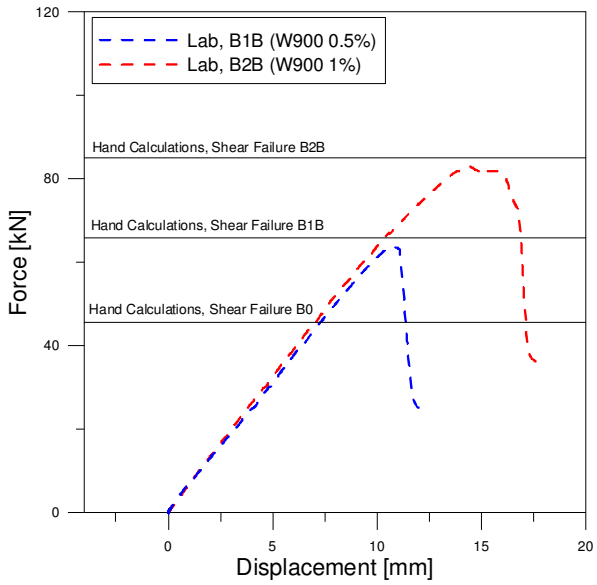

Fig. 47: Load-displacement curves from laboratory testing of shear beams. Compared to predicted capacities from hand calculations.

The capacity of the shear beams was calculated in advance according to Section 6.6. The predicted shear capacities for all three beams (B0, B1A and B2A) are indicated with horizontal lines in Fig. 47. The capacities are also summarized in Table 17 and Table 19. The tables indicate that shear failure was estimated for all three beams and that an anchorage length of 300mm is sufficient in all three cases.

Extremely good agreement is observed between predicted and real capacity. Predicted load is a small fraction to big and is most likely related to the capacity contribution from the steel fibers and uncertainty in the material parameters. The fiber contribution is prominent as seen in Table 17 and increases the total capacity theoretically in magnitude of 45% and 85% for beam B1A and B2A respectively as compared to the theoretical capacity of shear beam B0. The mishap with shear beam B0 was very unfortunate since laboratory test results should have been available to validate the actual steel fiber contribution to the overall capacity.

Table 17: Summary of shear beam shear capacities.

Specimen ID	Fiber volume	V_{ck} [kN]	V_{fk} [kN]	$V_{Rk} = V_{ck} + V_{fk}$ [kN]	V_{lab} [kN]	V_{lab}/V_k
B0	0%	22.774	0	22.774	-	-
B1B	0.5% Dramix 65/35	22.774	10.156	32.930	31.830	0.967
B2B	1% Dramix 65/35	22.774	19.649	42.424	41.466	0.977

V_{ck}: Theoretical shear capacity for the beam itself, without fiber contribution.
V_{fk}: Theoretical steel fiber contribution to the shear capacity.
V_{lab}: Total shear capacity achieved by testing.

Table 18: Summary of shear beam moment and anchorage capacities.

Beam	M_{Rk} [kNm]	$l_{anchorage,Euro}$ [mm]	$l_{anchorage,NS}$ [mm]
B0	26.553	160	116
B1B	27.969	160	150
B2B	29.312	160	157

$M_{Rk,B0}$ = 26.553kNm corresponds to V_{max} = 40.02kN > **$V_{Rk,BO}$ → Shear failure.**
$M_{Rk,B1B}$ = 27.969kNm corresponds to V_{max} = 42.19kN > **$V_{Rk,BO}$ → Shear failure.**
$M_{Rk,B2B}$ = 29.312kNm corresponds to V_{max} = 44.21kN > **$V_{Rk,BO}$ → Shear failure.**

The pure shear failures from the laboratory tests are illustrated in Fig. 48. The failure arose suddenly in a typical shear failure pattern growing in a 45 degree angle from the tension zone towards the point load. The horizontal crack in the tension zone developed after failure and grew towards the left bearing. The same pattern is observed for both beams, however the crack is not as distinct in beam B2B as in beam B1B, see Fig. 48. This could be related to the larger steel fiber content in beam B2B which increases the capacity substantially, making the beam nearly just as strong with respect to both shear and moment failure. Arising cracks induced by bending during testing of beam B2B emphasize this fact. Such cracks did not develop to the same degree of beam B1B.

Fig. 48: Shear failures from the laboratory testing. Left: B1B W900 concrete with 0.5% steel fiber content. Right: B2B W900 concrete with 1% steel fiber content.

6.8.6 Density

The density of the Weber concrete was controlled during mixing. Foam was added until an approximate density of 900 kg/m^3 and 1150 kg/m^3 was reached for the two concretes respectively.

This means that the density after the concrete has cured, in theory should be a bit lower because of evaporating humidity. However, the achieved true dry densities were in general higher than the searched 900 kg/m^3 and 1150 kg/m^3 density.

The reason for this is most likely related to a higher grade of compaction when the concrete is cast, compared to when the density was measured during mixing. More foam must be added until densities <900 kg/m^3 and <1150 kg/m^3 is reached in order to produce concrete with

density closer to the theoretical. This issue could also be related to the efficiency of the weight reducing foam which could diminish since the concrete is mixed and treated further when being cast into the formwork.

7 Numerical Analysis

The Finite Element Method (FEM) is today a common tool to predict and re-examine capacity and behavior of structures. In this report, FEM is used in order to analyze and test the possibilities to predict the behavior and capacity of some of the laboratory tests.

In this report the Finite Element Analysis (FEA) program Abaqus has been used, mainly because of the authors experience with this software and because it is one of the most complete and powerful suites of FEA software available on the market.

Static implicit direct integration is used to solve the nonlinear problems in this report because of the smooth nonlinearities (plasticity problem) and no dynamic effects in the laboratory tests. The Concrete Damage Plasticity model in Abaqus is used as materiel model and is chosen on the basis of advice from the authors supervisors.

7.1 Nonlinear Solution Algorithms

Calculating the response for a concrete structure is not easily achieved by solving a single system of linear equations. Concrete is a highly nonlinear material which is both strain, load and time dependant. Calculating the response through FEA therefore makes it necessary to solve a system of nonlinear equations. Solving the system equations can be done in several ways. In briefness, a simplified summary of an implicit solution algorithm is summarized below.

The solution of the nonlinear equations is found by making the load time dependant. Then by incrementing the time, and thereby the load, equilibrium is found by an iterative process at the end of each time increment until the whole load is applied [34]. There are several solution methods for nonlinear FEA, but the most frequently used method consist of a predictor step followed by a corrector step. The predictor step increments the load, usually by a forward Euler method, while the corrector step use some sort of iteration scheme, for example Newton-Raphson, in order to achieve equilibrium [35]. Abaqus uses, among others, a Newton-Raphson iterative method to solve nonlinear systems. To the left in Fig. 49, a sketch of the general procedure for solving a nonlinear equation system is shown.

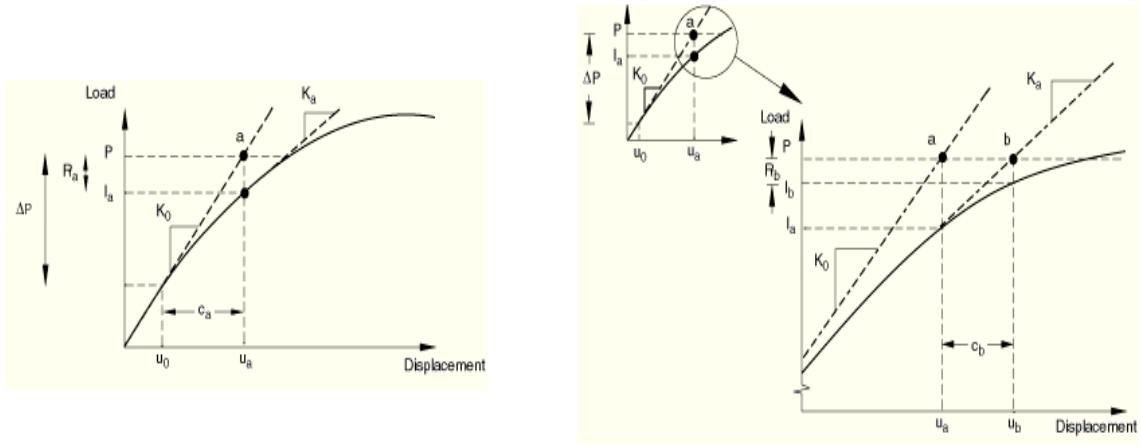

Fig. 49: First two iterations in an increment using a Newton-Raphson solution scheme [25].

The iterative process is done in order to achieve equilibrium between internal and external forces as shown in Fig. 49. The external applied load P is not in equilibrium with the internal force I_a and more iterations are necessary in order to reduce the residual, denoted R_a and R_b in Fig. 49, towards a given tolerance. When this tolerance, or convergence criteria, is satisfied, the whole procedure is repeated by incrementing the load and performing new iterations until the whole load is applied. The number of iterations needed, and increment size, varies with the degree of nonlinearity of the governing system, and in many cases a more advanced solution algorithm has to be applied in order to achieve convergence, for example some sort of arc-length method.

7.2 Numerical Analysis of Concrete in General

A well known characteristic for concrete is its non-linear stress-strain behavior, especially in the compressive range. The behavior in compression and tension is quite different comparing both stress and stress-strain linearity. The ratio between maximum tensile and compressive strength is typically in the range 0.05 to 0.1. In addition the tensile behavior is typically far more linear than the compressive behavior.

Because of concrete's varying behavior at different stress states, it has been chosen to briefly describe the concrete's behavior and characteristics in uniaxial, biaxial and triaxial stress states in the following sections. The descriptions are mainly based on the book "*Plasticity in Reinforced Concrete*" by W.F. Chen [36].

7.2.1 Uniaxial Behavior

Effects from mixing/casting and chemical reactions in the concrete during curing (that being for example; segregation, shrinkage and thermal effects) results in several microcracks in the concrete, mainly between the aggregate and mortar . These microcracks affect the concrete behavior to a big degree, especially the tensile behavior. A typical stress-strain relation at a uniaxial stress state is shown to the left of Fig. 50.

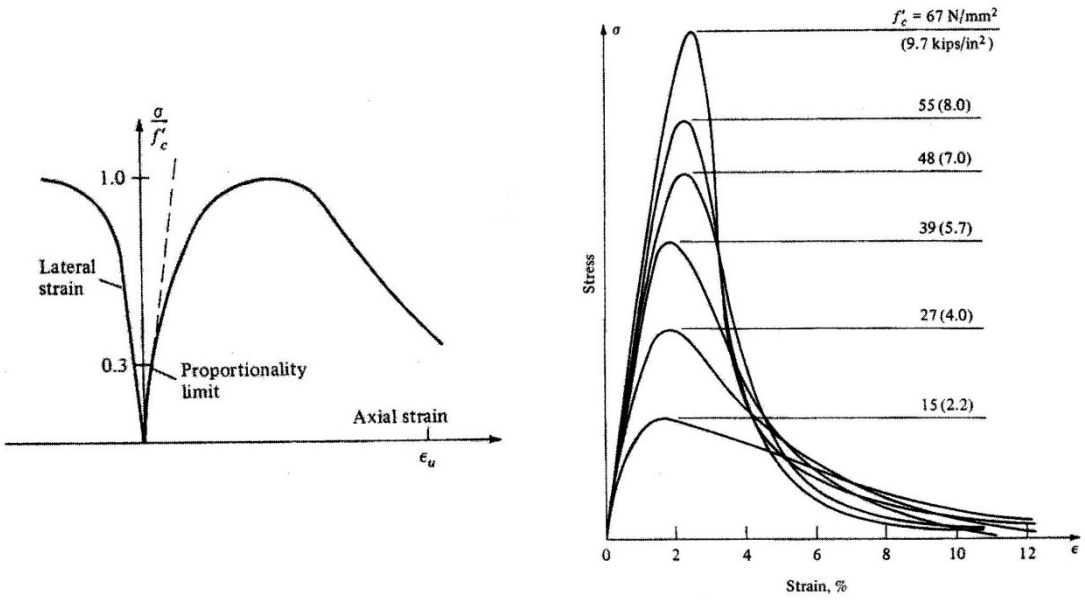

Fig. 50: Left: Stress-strain relation, uniaxial stress state [36]. Right: Comparison of stress-strain relations for different concrete qualities (Normal Concrete) [36].

7.2.1.1 Compressive Behavior

The microcracks in the concrete make the concrete behave more or less linearly up to the proportionality limit as shown to the left in Fig. 50. Major crack growth initiate at the proportionality limit and grow at an increasing rate until a stress level of approximately 75% of the maximum capacity. At this level the crack propagation becomes unstable. The fracture which then develops as the stresses increase towards maximum, is a result of microcracks which bond together and result in internal damage.

To the right in Fig. 50, the stress-strain relationship for increasing concrete quality is illustrated. Increasing compressive capacity leads to a more brittle behavior and the concrete behaves linear to a higher stress level, but the maximum capacity is attained at approximately the same strain. In the case of a LWAC as used in this report, the behavior resembles that of a high strength normal concrete.

7.2.1.2 Tensile Behavior

The tensile behavior is more or less linear nearly until brittle failure. The corresponding proportionality limit as for the compressive behavior is at approximately 60%. At this level further crack growth from micro cracking initiates and continues until the stability limit at 75% of the maximum capacity. As opposed to compressive failure due to numerous micro cracks, the tensile failure is a consequence of a few bridging cracks which arise perpendicular to the principal stress direction.

When the concrete section has cracked and reached yield in tension, it is usually assumed that the tensile capacity immediately drops to zero for a non-reinforced concrete. This is on the other hand, a conservative assumption since concrete has the capability to resist tensile

stresses to a certain degree in the cracked zone. This effect is often referred to as tension softening.

For reinforced concrete the concrete has a more significant capacity post cracking. Shear forces are established along the contact surface between the reinforcement and the concrete within a cracked concrete section. These shear forces contribute to the overall capacity and is often referred to as the tension stiffening effect.

7.2.2 Biaxial Behavior

Since the biaxial behavior is strongly dependant of the stress situation, the biaxial behavior is best described by Fig. 51. An example worth mentioning is the distinct increase of compressive strength of 25% and 16% at a stress ratio of $\frac{\sigma_1}{\sigma_2} = 0.5$ and $\frac{\sigma_1}{\sigma_2} = 1$ respectively.

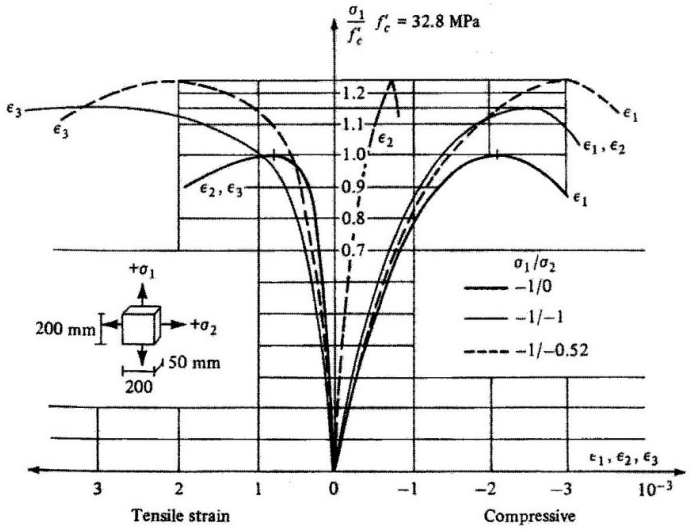

Fig. 51: Stress-strain relation, biaxial stress state [36].

When the concrete has cracked after yielding in tension, the concrete has a significant capacity in the direction parallel to the crack, especially for reinforced concrete. This effect is known as aggregate interlock and can for a reinforced normal concrete make the concrete retain about 40-60% of its shear capacity parallel to a crack. It should be noted that this effect is not as prominent for high-strength or lightweight concrete since the cracked surface often is not as coarse, making the aggregate interlock effect less significant.

7.2.3 Triaxial Behavior

Concrete affected by large triaxial compressive stresses is able to achieve very high axial compressive stresses as compared to a uniaxial or biaxial stress state due to the confining pressure. This is because the failure mode in the concrete changes from cleavage to crushing of the cement paste which greatly increases the capacity. This effect is best illustrated by Fig. 52.1.

In Fig. 52.2 and Fig. 52.3 the deviatoric and plane failure surface is shown respectively. The deviatoric stress space illustrates planes perpendicular to the hydrostatic axis shown in Fig. 52.1. At a low hydrostatic stress level the failure surface is convex and noncircular. At increasing hydrostatic stress level the deviatoric planes take on a circular shape.

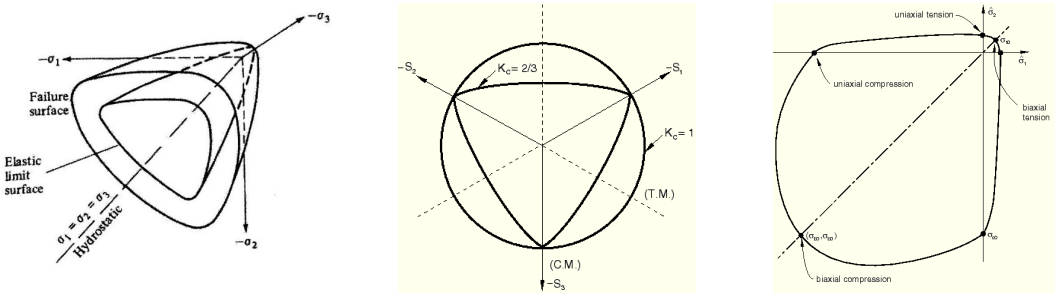

1 2 3

Fig. 52: 1: Failure Surface in 3D stress space [36]. 2: Failure surface deviatoric stress space[34]. 3: Failure surface plane stress space ($\sigma_3 = 0$) [34].

7.2.4 Compressive Interpretation

In order to implement the compressive behavior of concrete into a FEM-software one has to take the multiaxial stress state into consideration. This is because the different pure stress states, that being compressive, tensile and shear, affect the multiaxial stress state in a negative or positive way as described in the previous sections.

A fracture criterion has to be established which takes the three principal stress invariants (I_1, J_1, J_2) into account. There exists several fracture criteria's which interpret the compressive behavior with varying success dependant on how many parameters the fracture criteria's account for.

The simplest models (one-parameter models) only account for typically maximum tensile or shear stress. Typical for these models is that they do not describe the concrete behavior to a satisfying degree and that the fracture surface typically is non-smooth. This might lead to severe convergence issues in FEA.

Two-parameter models as for example the Mohr-Coulomb or Drucker-Prager describes the compressive behavior of the concrete to a more satisfying degree, but they are far from perfect. The Mohr-Coulomb model has a non-smooth fracture surface as most of the one-parameter models. The Drucker-Prager model describes on the other hand a smooth fracture surface, but it assumes only circular fracture surfaces in the deviatoric plane.

In order to describe the compressive behavior to a more satisfying degree one has to use more advanced models which account for more parameters. Whether they give a better result numerically depends on the degree of complicated stress state.

7.2.5 Tensile Interpretation

As for the compressive interpretation, tensile interpretation of concrete in the FEM has to account for the multiaxial stress state effects. The FE-software has to account for effects such as tension softening, tension stiffening (for reinforced concrete), aggregate interlock and opening/closing of cracks.

There exist numerous numerical models which interpret the tensile behavior of concrete with varying success. Common for most of these models is that they are established on basis of one of the following principal models/approaches:

- Smeared Cracking Model
- Discrete Cracking Model
- Fracture-Mechanics Model
- Plasticity Model

In this report it has been chosen to use a plasticity model and it will be discussed in detail in Section 7.3. The rest of the models will only be described briefly in the following sections.

7.2.5.1 Smeared Cracking Model

The smeared crack model resembles a plasticity model in the way that the concrete is assumed to remain a continuum. As the name indicates, the model smears the cracks across the concrete section. Sudden drop in tensile capacity, aggregate interlock and opening/closing of cracks is well accounted for in this model.

7.2.5.2 Discrete Cracking Model

The major drawback with the discrete cracking model is that the location and orientation of the cracks has to be specified in advance. When performing a FEA to for example re-examine laboratory tests where and the result/crack-location is known in advance, one can use the discrete crack model with great result.

7.2.5.3 Fracture-Mechanics Model

Fracture-mechanics models have generally had great success when being used for analyzing metals and geo-materials. When crack formulation and crack growth is of special interest a fracture mechanics model is appropriate.

7.3 Material Model

When analyzing concrete and other quasi brittle materials in Abaqus, there are mainly three different material models which are applicable. In the work with this report it has been chosen

to use the Concrete Damaged Plasticity model which could be used with both Abaqus/Implicit and Abaqus/Explicit. (Abaqus/Explicit uses an explicit solution algorithm.)

The other two models in the Abaqus material library are the smeared crack model in Abaqus/Implicit and the brittle cracking model in Abaqus/Explicit [34], which both are based on the smeared crack approach. These two models will not be discussed any further in this report.

The Concrete Damaged Plasticity model in Abaqus is based on a plastic damage model for concrete established by J. Lubliner et.al. in 1989 [37]. This model has later been modified with respect to cyclic loading and damage parameters in the late 90's [38]. The model is fairly complex and is based on plasticity theory. It is primarily made for analyzing reinforced concrete structures under cyclic or dynamic loading, but can be used on unreinforced concrete structures as well. It should be noted that convergence issues most likely will arise when unreinforced concrete is analyzed [34].

The material model assumes two main failure mechanisms, which is tensile cracking and compressive crushing. In contrast to the smeared crack approach, no crack would directly arise in the Concrete Damaged Plasticity model. As indicated by the name of the model, cracks are represented by damaged material by locally degrading the material where the maximum capacity of the material has been exceeded.

7.3.1 Yield Criterion, Yield Surface and Flow Rule

The yield criteria used for the Concrete Damaged Plasticity model has the same principal objectives as the Mohr Coulomb and Drucker Prager yield criteria [37] which has the form as following (7.1):

$$F(\sigma) = c \tag{7.1}$$

Where $F(\sigma) = c$ is a function of the stress components. By setting the cohesion $c = f_{c0}$ the initial yield surface is described. The failure surface is described as the cohesion c attains its maximum value along a given loading path [37]. The yield surface adopted in this model is described by the following Equation (7.2) in terms of effective stresses, where α and γ are dimensionless constants:

$$F(\sigma) = \frac{1}{1-\alpha}\left[\bar{q} - 3\alpha\bar{p} + \beta\left(\tilde{\varepsilon}^{pl}\right)\langle\hat{\bar{\sigma}}_{max}\rangle - \gamma\langle-\hat{\bar{\sigma}}_{max}\rangle\right] - \bar{\sigma}_c\left(\tilde{\varepsilon}_c^{pl}\right) \tag{7.2}$$

α and γ	are dimensionless constants, see 7.3.2
$\bar{p} = -\frac{1}{3}\bar{\boldsymbol{\sigma}}:\boldsymbol{I}$	is the effective hydrostatic pressure
$\bar{q} = \sqrt{\frac{3}{2}\bar{\boldsymbol{S}}:\bar{\boldsymbol{S}}}$	is the Mises equivalent effective stress
$\bar{\boldsymbol{S}} = \bar{p}\boldsymbol{I} + \bar{\boldsymbol{\sigma}}$	is the deviatoric part of the stress tensor $\bar{\boldsymbol{\sigma}}$
$\hat{\bar{\sigma}}_{max}$	is the algebraically maximum eigenvalue of $\bar{\boldsymbol{\sigma}}$
$\beta\left(\tilde{\varepsilon}^{pl}\right) = \frac{\bar{\sigma}_c\left(\tilde{\varepsilon}_c^{pl}\right)}{\bar{\sigma}_t\left(\tilde{\varepsilon}_t^{pl}\right)}(1-\alpha) - (1+\alpha)$	in which $\bar{\sigma}_c$ and $\bar{\sigma}_t$ are the effective compressive and tensile cohesion stresses, respectively. $\bar{\sigma}_c$ and $\bar{\sigma}_t$ are dependant of the hardening variables $\tilde{\varepsilon}_c^{pl}$ and $\tilde{\varepsilon}_t^{pl}$.

The yield function used in the Concrete Damaged Plasticity model reduces to the Drucker Prager yield condition in biaxial compression with $\hat{\bar{\sigma}}_{max} = 0$. The yield surfaces in the deviatoric plane and plane stress are shown in Fig. 53, to the right and left respectively.

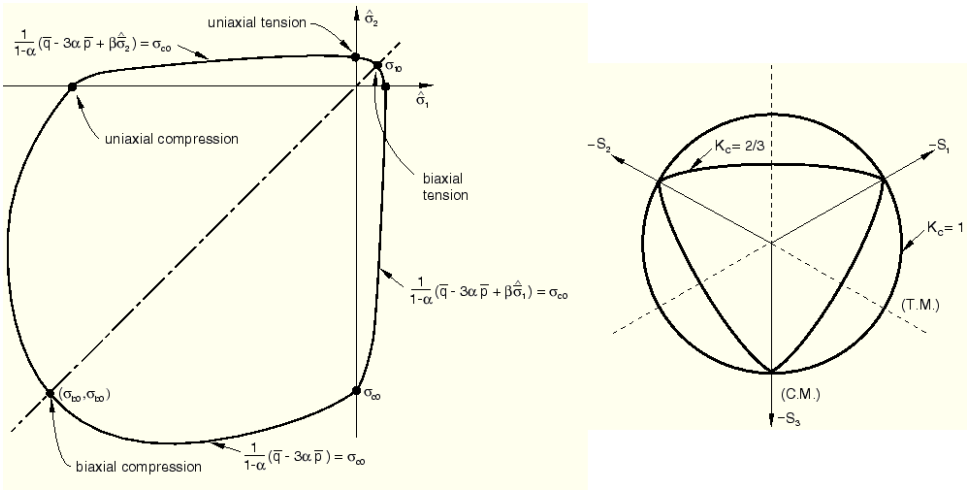

Fig. 53: Left: Yield surface plane stress. Right: Yield surface deviatoric plane [34].

The Concrete Damaged Plasticity model assumes non-associated potential flow (7.3):

$$\dot{\varepsilon}^{pl} = \dot{\lambda}\frac{\partial G(\bar{\boldsymbol{\sigma}})}{\partial \bar{\boldsymbol{\sigma}}} \tag{7.3}$$

where the flow potential G is chosen as the Drucker Prager hyperbolic function (7.4):

$$G = \sqrt{(\epsilon\sigma_{t0}\tan\psi)^2 + \bar{q}^2} - \bar{p}\tan\psi \tag{7.4}$$

As mentioned in Section 7.3, the Concrete Damaged Plasticity model is especially made for cyclic and dynamic loading where damage and stiffness degradation is introduced through damage parameters in both tension and compression. These parameters will not be discussed further because the material model is only used for static loading cases in this report.

7.3.2 Defining the Material Model in Abaqus

When defining the Concrete Damaged Plasticity material model in Abaqus one must specify tensile behavior, compressive behavior and parameters controlling plasticity.

7.3.2.1 Compressive and Tensile Behavior

Both compressive and tensile capacity and behavior is provided as input to Abaqus through tabular data.

The compressive stress data is given as a tabular function of inelastic strain, which in this case is identical to the plastic compressive strain since no compressive damage is defined. The compressive plastic strain (hardening) is defined as the following Equation (7.5):

$$\tilde{\varepsilon}_c^{pl} = \tilde{\varepsilon}_c^{in} - \frac{d_c}{(1-d_c)}\frac{\sigma_c}{E_0} \tag{7.5}$$

d_c is the compressive damage variable

$\tilde{\varepsilon}_c^{in} = \varepsilon_c - \varepsilon_{0c}^{el}$ is the inelastic strain

$\varepsilon_{0c}^{el} = \frac{\sigma_c}{E_0}$ is the elastic strain

The definitions used for defining the compression hardening data are shown in Fig. 54.

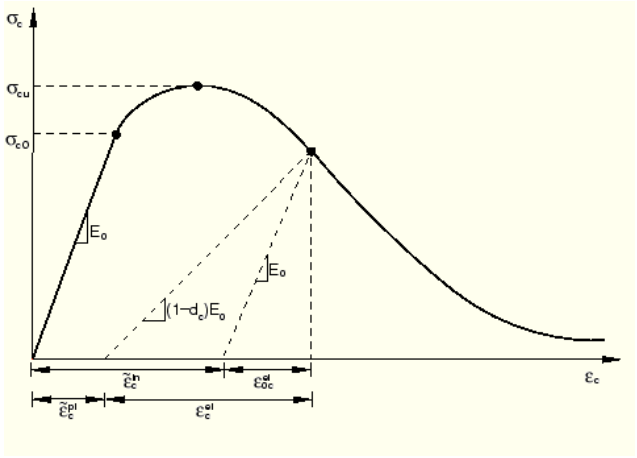

Fig. 54: Strain parameters used for definition of compression hardening data [34].

The tensile behavior in Abaqus is modeled by a tension stiffening model and through this model tension softening is defined. The tensile stress data can be given in the same way as the compressive data by a tabular form of cracking strain given by Equation (7.6):

$$\tilde{\varepsilon}_t^{ck} = \varepsilon_t - \varepsilon_{0t}^{el} \tag{7.6}$$

where:

$\varepsilon_{0t}^{el} = \frac{\sigma_t}{E_0}$ is the elastic strain

Abaqus converts the given tensile cracking strain into tensile plastic strain in the same way as compressive plastic strain is defined in Equation (7.7), except that d_c is replaced by a tensile damage variable d_t, see equation :

$$\tilde{\varepsilon}_t^{pl} = \tilde{\varepsilon}_t^{ck} - \frac{d_t}{(1-d_t)}\frac{\sigma_t}{E_0} \tag{7.7}$$

d_t	is the tensile damage variable
$\tilde{\varepsilon}_t^{ck} = \varepsilon_t - \varepsilon_{0t}^{el}$	is the cracking
$\varepsilon_{0t}^{el} = \frac{\sigma_t}{E_0}$	is the elastic strain

The definitions used for defining the tension stiffening data are shown in Fig. 55.

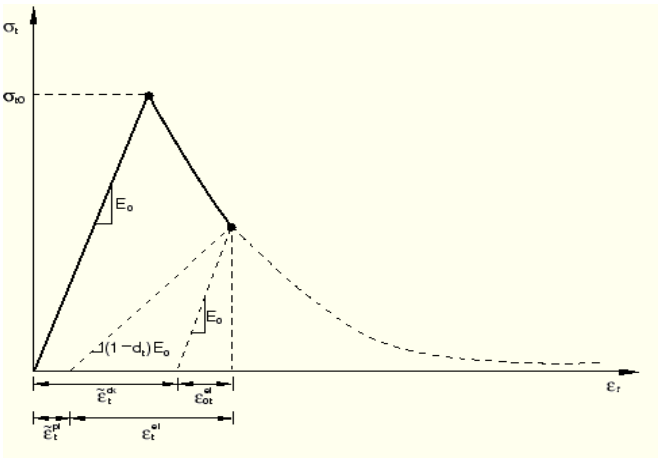

Fig. 55: Strain parameters used for definition of tension stiffening data [34].

Introducing tensile stress data into Abaqus by means of a stress – strain relation as described above will introduce mesh sensitivity into the results. Refining the mesh will not lead to convergence towards a unique solution because mesh refinement leads to narrower crack bands for the concrete [34]. This could be especially troublesome when modeling the notched specimens from test phase 1 because refining the mesh locally at the notch should not lead to formation of additional cracks. For unreinforced concrete mesh sensitivity might also be a problem because of the small amount of tension stiffening which results in an unstable behavior. This might be of less concern in this report since the concrete is steel fiber reinforced which introduces a big amount of tension stiffening in the post-critical range.

In order to reduce the mesh sensitivity one can define a fracture energy cracking criterion to describe the tensile behavior in Abaqus. The fracture energy cracking criterion can be invoked by specifying the post-failure stress as a tabular function of either crack displacement, u^{ck}, or by directly specifying the associated fracture energy, G_f. For the notched specimens in this report, the crack displacement would correlate directly with the crack mouth opening displacement. When specifying tensile behavior with the stress – crack displacement concept, a characteristic crack length needs to be defined. Abaqus automatically chooses a crack length which is based on element geometry associated with an integration point. For first order elements the crack length is the length of a line across an element, i.e. $\sqrt{A}$ for a square element; where A is the element area.

In this report both the stress – strain and the stress – displacement method of defining tensile behavior has been used and compared.

7.3.2.2 Plasticity Parameters

A total of 5 parameters need to be specified for the Concrete Damaged Plasticity model. These parameters modify the plasticity behavior of the material model by controlling plastic flow, the yield function and viscoplastic regularization. The plasticity parameters will be discussed in briefness in the following sections.

Dilation Angle

The dilation angle, ψ, governs the amount of volumetric plastic strain in the analysis and is best described by geometrical interpretation in Fig. 56, where β is the internal material friction angle. For shear loading the dilation angle is simply the ratio of plastic volumetric strain rate divided by plastic shear strain rate, see Hobbs et.al. [39]. In Fig. 56, the yield surface is plotted in linear form in the meridional plane (p-t plane). The Concrete Damaged Plasticity assumes non-associated potential flow as described in Section 7.3.1. This is only the case when $\psi \neq \beta$. When the dilation angle and the internal material friction angle coincide, a fully associated flow rule is assumed and thereby the model is of the type first introduced by Drucker Prager [34]. If ψ = 0 the material is non-dilational, which corresponds to no volumetric strain.

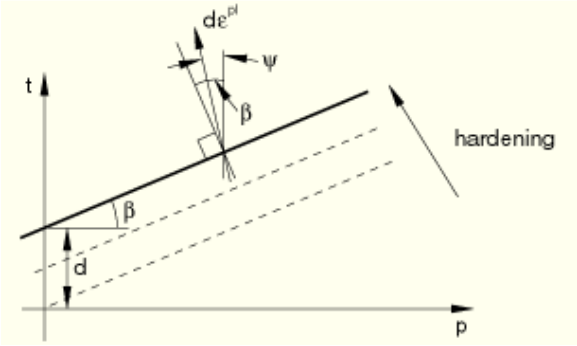

Fig. 56: Geometrical interpretation of the dilation angle in the p-t plane [34].

Since the dilation angle cannot be determined from the experimental results in test phase 1, the dilation angle has been chosen on basis of hand calculations and recommended values in FEM software manuals [34] and [40]. Since the dilation angle is always smaller than the friction angle for geomaterials [41], hand calculations for the friction angle has been carried out in order to have an initial estimate of a reasonable dilation angle for the concrete of interest. The calculations are attached in Appendix D.1. It has also been chosen to include the dilation angle into the parameter study in order to determine a more correct value with respect to the laboratory results.

Flow Potential Eccentricity

The eccentricity, ε, is a parameter which defines at what rate the flow potential function approaches the linear Drucker Prager flow potential asymptote. In other words, if a low value is given for the eccentricity the dilation angle shown in Fig. 56 varies little over a wide range of confining pressure stress values, vice versa if a high value is given [34].

$\sigma_{b0} / \sigma_{c0}$

σ_{b0}/σ_{c0} is the ratio between initial equibiaxial compressive yield stress to initial uniaxial compressive yield stress and is described in Equation (7.8). Experimental values for this ratio lie between 1.10-1.16 [37]. The ratio is used to define the dimensionless constant α in the material model yield function.

$$\alpha = \frac{\left(\frac{\sigma_{b0}}{\sigma_{c0}}\right) - 1}{2\left(\frac{\sigma_{b0}}{\sigma_{c0}}\right) - 1}; 0 \leq \alpha \leq 0.5 \tag{7.8}$$

K_c

By varying the parameter K_c the yield surface takes on a different shape as illustrated by Fig. 53 and can be interpreted as a constant. The dimensionless constant K_c controls the tension and compression meridians in the meridian plane through the dimensionless constant γ in Equation (7.2) as follows in Equation (7.9).

$$\gamma = \frac{3(1 - K_c)}{2K_c - 1} \tag{7.9}$$

By setting $K_c = 1$ and $\psi = \phi$, the original Drucker Prager model is recovered [34].

Viscoplastic Regularization

The viscoplastic regularization parameter could be used in order to overcome typical convergence issues for material models where material softening is defined. In Abaqus/Standard defining viscoplastic regularization leads to acceptance of stresses outside the yield surface to a certain degree which could reduce the convergence difficulties [34]. This parameter will not be studied further in this report since most of the convergence issues which arose were overcome by applying an arc length solution control to the Newton-Raphson iteration scheme.

7.3.3 Extraction of Material Data from the Laboratory Results

In order to perform a FEA in Abaqus, material data for both tensile and compressive behavior needs to be specified both in the elastic and in the plastic domain. The material data is based on the experiments done in test phase 1 where the raw data was sampled as described in Section 6.7. In this section the procedure used for extracting and processing the necessary material data from the raw data, is described.

7.3.3.1 Tensile Data

Tension specimens cast in phase 1 are the basis for the tensile data used in this report. As described in Section 6.7.3, displacement was measured by two LVDTs attached at two sides opposite of each other. Once the test specimen has cracked at the notch, the displacement measured at each side of the specimen will not increase at the same rate relative to each LVDT. This is because the crack could be skew within the notch and because the steel fiber reinforcement is not equally distributed over the cross section. This leads to unsymmetrical displacement. Because of this, the mean calculated displacement has been used as a basis for calculating both cracking displacement, u^{ck} , and cracking strain, ε_t^{ck}.

The load applied to the test specimen was measured by a load cell in the testing rig and the weight of the test specimen has been accounted for during the processing of the raw data. When giving material properties in a Finite Element (FE) model, true stress (Cauchy stress) is usually defined. This is typical when defining metal plasticity where necking occurs after yielding. When concrete yields it tension it cracks, and thereby reducing the load carrying area to zero if the concrete is unreinforced. For fiber reinforced concrete the area is reduced to the load carrying steel fiber area. In the Concrete Damaged Plasticity model no cracks will form, instead the material is degraded. Thereby the load carrying area in the FEA is kept constant equal to the initial area, A_0. Due to this the calculated stresses used in the material model of this report are nominal stresses (Engineering Stresses), as defined by Equation (7.10).

$$\sigma_{nom} = \frac{F}{A_0} \tag{7.10}$$

Stress-Cracking Displacement

Once the tension specimens have cracked, it is assumed that all the deformation measured by the two LVDTs, are localized at the crack, i.e. crack mouth opening displacement. This is a reasonable assumption since the cross section is drastically reduced after cracking and because the elastic contribution from the rest of the specimen within the measuring area contributes in the order of 10^{-5} compared to the cracking displacement. Crack displacement is assumed equal to zero at first yield.

Stress-Cracking Strain

When defining strain in a FE model, the true strain is usually used, but as for the stresses, the calculated cracking/plastic strain is based on nominal values in this report. As described in Section 7.3.3.1, the deformation of the specimens in the FEA is uniform and thereby makes the nominal values valid. An attempt of analyzing both the tension specimen and the 3 point bending specimen with true stress/strain values confirms this fact and a far too stiff behavior was observed. The cracking strain has therefore been calculated as follows (7.11):

$$\varepsilon = \frac{\Delta L}{L_0}$$
$$\varepsilon^{ck} = \varepsilon - \frac{F}{A_0 E_0} \tag{7.11}$$

As for the cracking displacement, the cracking strain is calculated using the assumption that all deformation is located at the crack once the specimen has reached the tensile yield stress. When calculating the total strain ε, the length L_0 has been chosen with respect to the element size used in the FEA. The same stress-strain input data is given for both 4mm and 2mm element size since uniform deformation of the elements is observed in the numerical analysis. This makes the stress-strain relation used for 4mm element size valid for 2mm element size as well. In Section 8.1.3 the choice of method for describing tensile behavior is seen in comparison with used element size.

Since the concrete is not perfectly elastic to the point of first yield, there is a contribution to plastic strain before yielding takes place. This contribution has been neglected because the contribution was of such a small order.

7.3.3.2 Young's Modulus

Young's modulus has been calculated according to the governing testing standard developed by SINTEF [22]. It is based on the secant modulus between σ_t = 0 and 40% of the yield stress.

7.3.3.3 Compressive Data

The compressive data has been calculated according to the governing concrete standard, Eurocode 2 [2]. The basis of the calculations is the achieved mean compressive cylinder strength as described in Section 6.8.1.2. The compressive data has been calculated according to the following stress – strain relation (7.12):

$$\sigma_{lc} = f_{lcd}\left[1 - \left(1 - \frac{\varepsilon_{lc}}{\varepsilon_{lc2}}\right)^{n}\right] \text{ for } 0 \le \varepsilon_{lc} \le \varepsilon_{lc2} \qquad (7.12)$$

$$\sigma_{lc} = f_{lcd} \text{ for } \varepsilon_{lc2} \le \varepsilon_{lc} \le \varepsilon_{lcu2}$$

7.3.3.4 Summary Material Parameters W1150 Concrete

On basis of the previous sections the necessary material parameters for the material model in Abaqus could be established. It has been chosen to perform all the numerical analysis on the basis of the W1150 concrete because of the generally good specimen and concrete quality achieved as compared to the W900 concrete. The compressive behavior is based on the mean measured cylinder compressive strength, see Section 6.8.1.2. The tensile behavior was chosen to be based on tensile specimen B3-2 because no unexpected situations arose while testing this specimens and it generally had the best overall physical quality.

All the material data are given to Abaqus as tabular values. The material data defining the plastic behavior of the concrete is shown in Fig. 57. The elastic behavior of the LWAC is described by the material parameters summarized in Table 19.

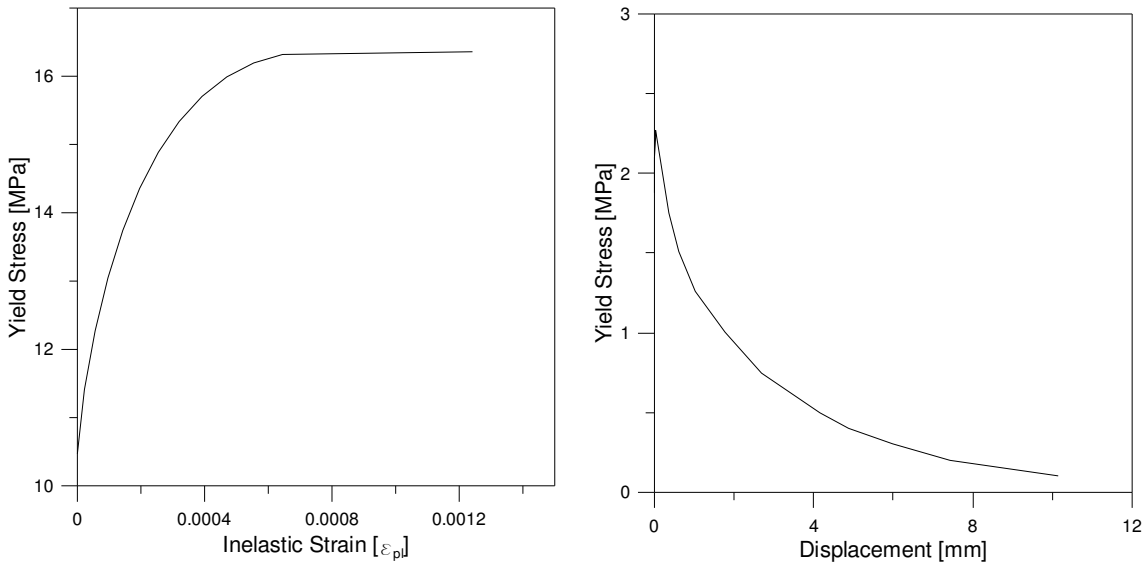

Compressive Input Data
W1150

Tensile Input Data
W1150

Fig. 57: Tensile and compressive data for the W1150 concrete used for numerical analysis in phase 1.

Table 19: Summary of material parameters for the W1150 concrete.

Parameter	Value	Note
$E_{cm,28}$	13000 MPa	Calculated according to Section 7.3.3.2.
$f_{cm,28}$	16.4 MPa	Mean measured cylinder strength phase 1, see Appendix C.1.
$f_{ctm,28}$	1.88 MPa	Tensile yield strength. Based on specimen B3-2.
υ	0.2	Recommended value Abaqus manual [34].

In some of the parameter studies in the numerical analysis it has been chosen to describe the tensile behavior of the W1150 concrete with a stress-strain relation. The tensile stress-strain curve, based on tension specimen B3-2, is shown in Fig. 58.

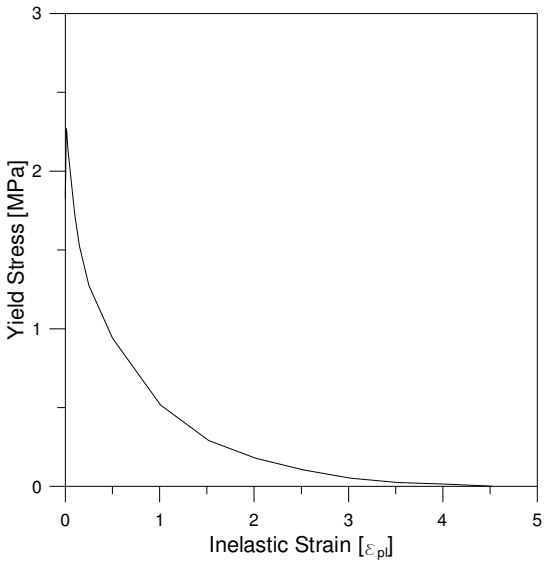

Fig. 58: Tensile input for the W1150 concrete, based on a stress-strain relation.

8 Test Phase 1: Numerical Analyses

In order to validate the input data given in the material model, boundary conditions and element-/mesh selections it is chosen to do analyses of the tension prisms and flexural tension beams and compare the numerical results with the results from the laboratory.

8.1 Analysis of Tension Specimen

The tension specimen is at first modeled with the basic setup described in Table 20. A parameter study is later performed in Section 8.1.3 with the basic setup in Table 20 as reference.

8.1.1 Numerical Model

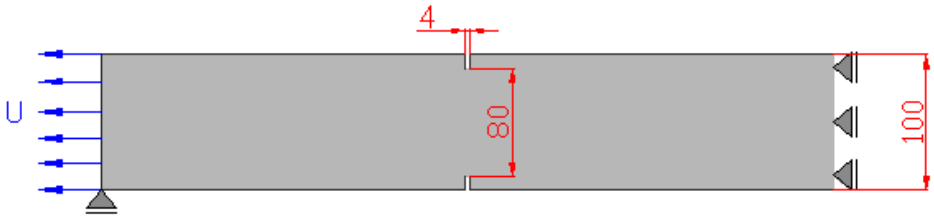

Fig. 59: Numerical model of tension specimen.

It is chosen to model the full tension specimen in order to get full notch width in the model. This will make it possible to model the notch with element size up to 4 mm. Utilizing symmetry would not be more efficient computational wise, because 2mm elements would have been necessary in order to model half the notch geometry. The measures, load conditions and boundary conditions are shown in Fig. 59. The parameters used in the analysis are listed in Table 20.

Table 20: Summary of input parameters for analysis performed in Section 8.1 and 8.2.

Parameter	Value
Element	CPS4 (4node plane stress element, full integration)
Mesh	2 & 4 mm elements, structured meshing technique
Material	As described in Section 7.3.3.4.
Dilation angle	36°*
Eccentricity	0.1**
σ_{b0}/σ_{c0}	1.16**
K_c	2/3**

*Abaqus recommended value for normal concrete.

**Abaqus default value.

8.1.2 Comparison Analysis with Basic Setup versus Laboratory

A comparison between the analysis and the laboratory result is presented Fig. 60. The correlation is fairly good and indicates that the FEM program interpret the material input correctly.

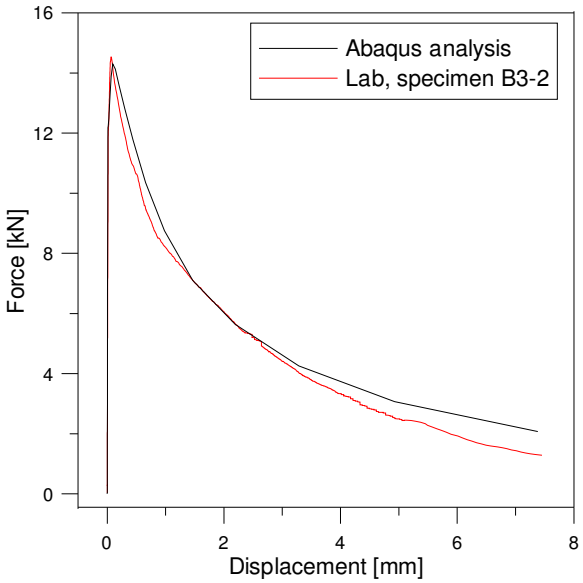

Fig. 60: Comparison between Abaqus analysis and laboratory result of tension specimen.

8.1.3 Parameter Study

In order to study the sensitivity of mesh size and influence of material input data a parameter study is done on the tension specimen analysis.

8.1.3.1 Mesh Size and Material Tensile Input

As mentioned in Section 0, the material tensile input can be defined either by a stress-displacement or stress-strain relationship in the Concrete Damage Plasticity model in Abaqus. These two ways of defining tensile behavior together with different mesh size are studied in this section. The different parameter combinations in these analyses are shown in Table 21. The meshes used are shown in Fig. 61.

Table 21: Overview of parameter combinations used in parameter study of mesh size and tensile input.

Analysis Reference ID	Mesh Size	Tensile Input
CPS4_2mm_disp	2 mm	stress-displacement
CPS4_4mm_disp	4 mm	stress-displacement
CPS4_2mm_strain4	2mm	stress-strain (L_0 = 4mm)
CPS4_4mm_strain4	4mm	stress-strain (L_0 = 4mm)

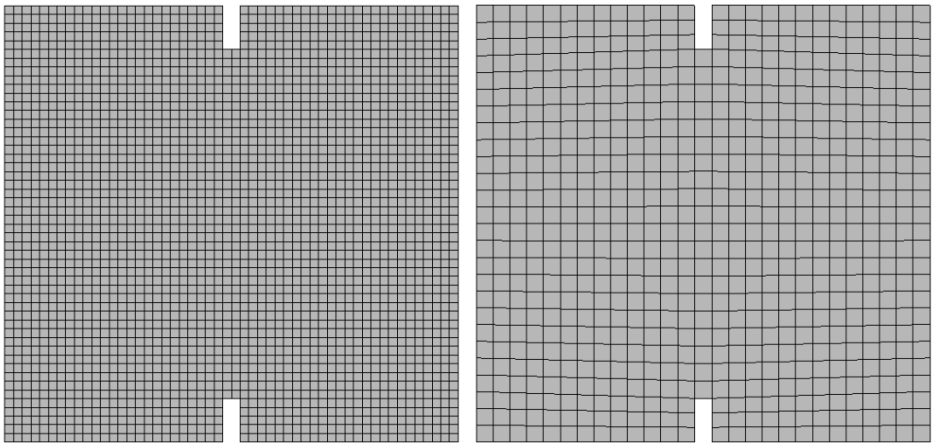

Fig. 61: 2 mm and 4 mm structured mesh used in analyses of tension specimen.

The result from this parameter study is shown in Fig. 62. When the input is given in terms of stresses and displacement, the program calculates the strain in the element based on a reference length L_0, which is related to the element size. This means that the stresses calculated in elements with size 4 mm, with tensile input based on displacement, will be the same as the stresses calculated in elements with size of both 2 mm and 4 mm with tensile data based on strain with L_0=4 mm. This is shown in Fig. 62 where all the analyses in which the stresses are calculated with L_0=4 mm have the same response. However, the result with mesh size equal to 4mm and 2mm differ when tensile input is described by the stress-displacement relation. This means that the model is somewhat mesh sensitive for the stress-displacement approach. However, this is only critical in the post critical region and the peak load can be predicted with good reliability independent of mesh and input approach.

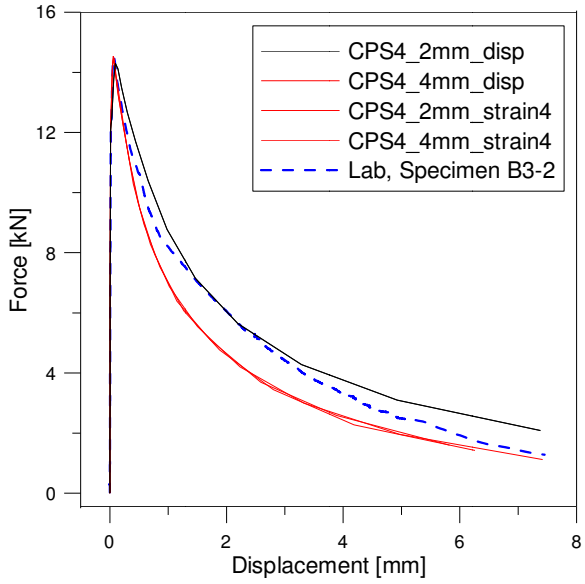

Fig. 62: Result from parameter study of mesh size and tension input on tension specimen.

When refining the mesh to 1 mm or smaller, the model starts to get more mesh sensitive, especially when the tensile data is base on stress-strain relations. This is shown in Fig. 63 where the behavior of the tension specimen is compared when modeled with mesh size 1 mm versus 2 mm and tension data based on stress-strain (Fig. 63.1 and Fig. 63.2) and stress-displacement (Fig. 63.3 and Fig. 63.4). Fig. 63.1 shows how the Concrete Damage Plasticity model, based on stress-strain tensile data, fails to distribute the localized crack over the full notch when the mesh is refined (compared to Fig. 63.2). This results in more tensile softening in the elements with large strain (Fig. 63.1) and a decrease in capacity in the post critical region, compared to Fig. 63.2 where the strain is distributed more evenly over the notch.

Fig. 63.3 shows how the Concrete Damage Plasticity model, based on stress-displacement tensile data, also have some problems when distributing the displacement over all the elements in the notch (all strain is localized to two element columns of a total of four), even though the representation here will be better compared to Fig. 63.1, due to less localized strain in single elements. This is a result that was somewhat expected, due to what is described in the Abaqus manual and also discussed earlier in Section 0. From the study in this section, it can be concluded that the Concrete Damage Plasticity model can describe cracks in localized regions when the element size is equal to the size of the expected crack region. If the mesh is refined the tensile input should be described by a strain-displacement relationship to decrease the mesh sensitivity problems.

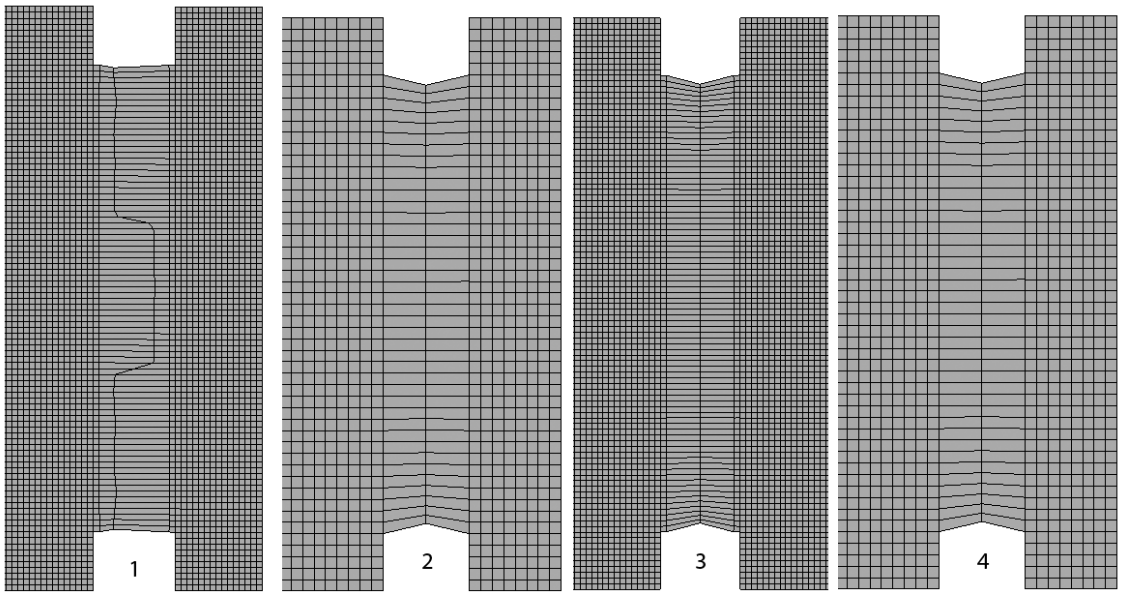

Fig. 63: Deformed shapes of tension specimen modeled with; 1: 1 mm elements, stress-strain tensile input. 2: 2 mm elements, stress-strain tensile input. 3: 1 mm elements, stress-displacement tensile input. 4: 2 mm elements, stress-displacement tensile input.

8.1.3.2 Plasticity Parameters

The different plasticity input parameters have also been studied.

- Dilation angle
- Eccentricity
- σ_{b0}/σ_{c0}
- K_c

Varying each and all of these parameters does not affect the response in any way for the analyses of the tension specimens.

8.2 Analysis of Flexural Tensile Beam

The flexural tensile beam is at first modeled with the same basic input setup as the tension specimen. The details are shown in Table 20. It is then performed a parameter study on the beam of the same parameters as studied in Section 8.1.3.

8.2.1 Numerical Model

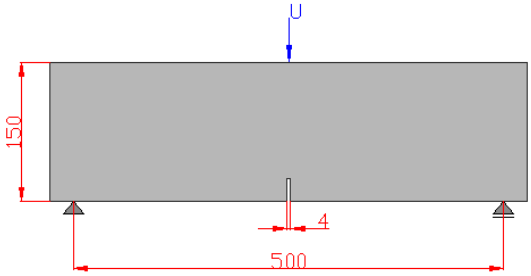

Fig. 64: Numerical model of flexural tensile beam.

The geometry, load conditions and boundary conditions of the flexural tensile beam are shown in Fig. 64. It is also here chosen to model the full beam to have the option to model the notch with just one 4mm element

8.2.2 Comparison Analysis with Basic Setup versus Laboratory

A comparison between the basic analysis and the laboratory result is presented in Fig. 65. The correlation could definitely have been better. The parameter study that is done in the following Section 8.2.3 did not result in any obvious improvements that could lead to better correlation.

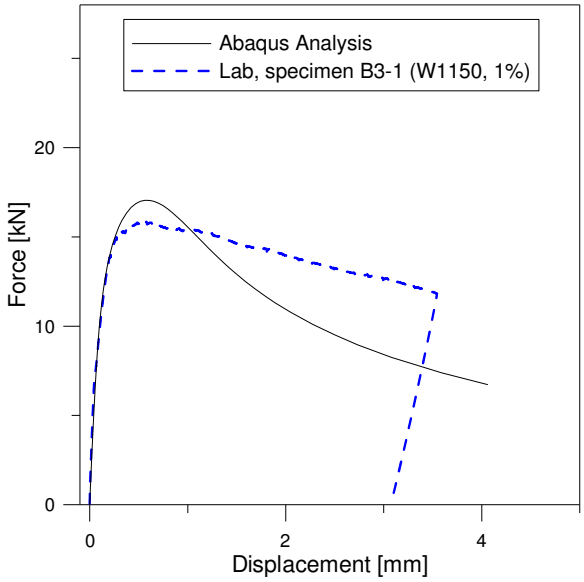

Fig. 65: Comparison between Abaqus analysis and laboratory result of flexural tensile beam.

The deviation could be explained by the dimensional relationship between the elements and the plane stress/strain thickness in the 2 dimensional analyses. It is not sure that the response is 100% correct when the element size is 4 mm or even less and the plane stress/strain thickness is 150 mm. Because of this, 3-dimensional analyses are done in Section 8.3 in order to see if the analyses could be improved with respect to the laboratory results.

Another explanation to the deviation could be membrane effects from the beam "hanging" on the supports by friction. This could to a certain degree introduce membrane effects. When tested, the beams are supported by steel supports. The friction coefficient between steel and concrete is about 0.45 [42]. These effects could be an explanation to why the laboratory response appears to be stiffer in the post critical region.

8.2.3 Parameter Study

In order to examine if the parameters studied in Section 8.1.3 will give the same trends in flexural tensile behavior, these parameters are varied in a similar study on the flexural tensile beam.

8.2.3.1 Mesh Size and Material Tensile Input

The same parameters as in the parameter study of the tensile specimens are varied in analyses of the flexural tensile beam. An overview of the parameter combinations are found in Table 21. The meshes used are shown in Fig. 67.

The results from the parameters studied in this section are presented in Fig. 66. Due to the same limitations in the Concrete Damage Plasticity model that was shown earlier, a refined mesh will not lead to more accurate solutions in this case either. The green and red curves in Fig. 66 is a result of the same effect as described in Fig. 63.1, where the force drops due to

tension softening when all the deformation is localized in one element column and the strains become large. Even though the blue curves is far off from the laboratory results, this must be the most correct result of these 2 dimensional analyses due to correct definitions of tensile data with notch and element size of 4 mm.

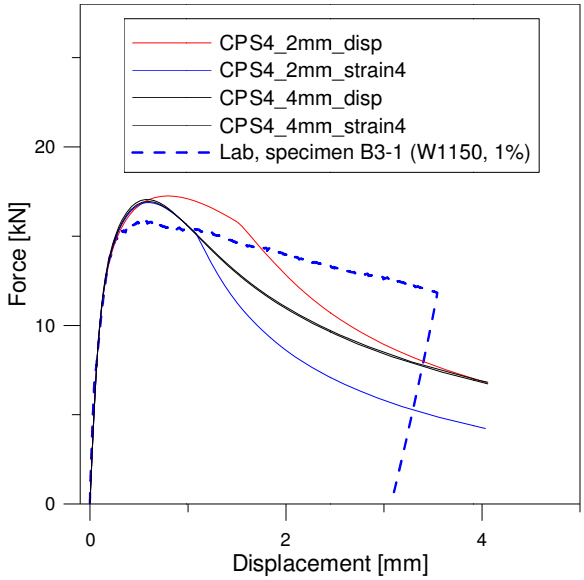

Fig. 66: Result from parameter study of mesh size and tension input on flexural tensile beam.

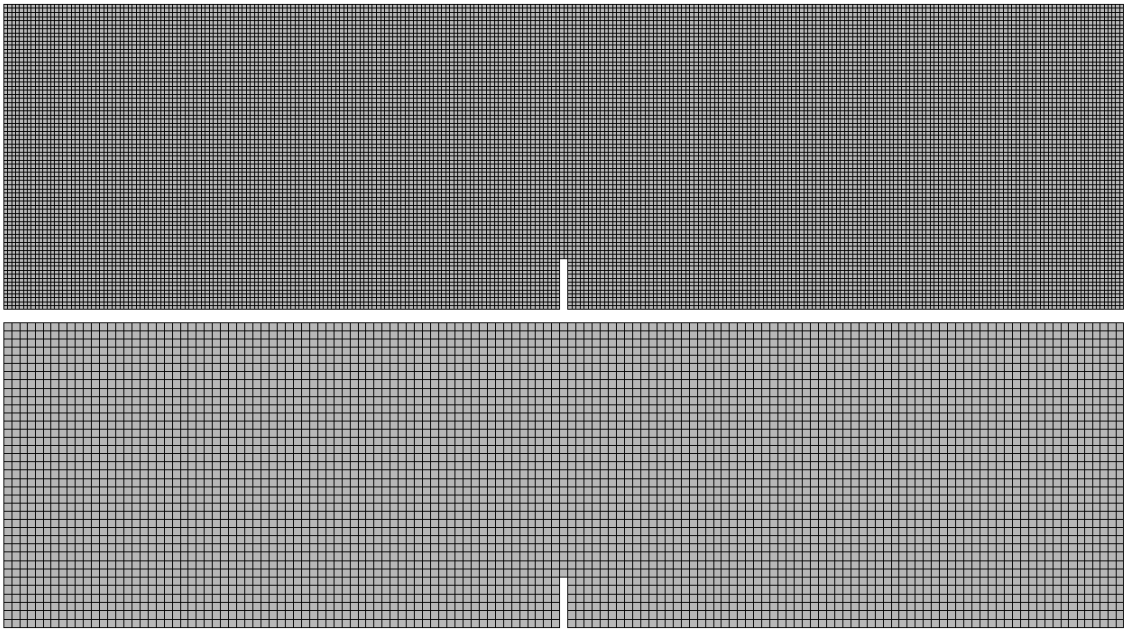

Fig. 67: 2 mm and 4 mm structured mesh used in analyses of flexural tensile beam.

8.2.3.2 Plasticity Parameters

The different plasticity input parameters have also been studied.

- Dilation angle
- Eccentricity
- σ_{b0}/σ_{c0}
- K_c

Varying each and all of these parameters does not affect the response in any way.

8.3 Analysis of Flexural Tensile Beam, 3D

In order to achieve better correlation between the numerical analysis and the laboratory experiments, it was chosen to perform a 3D analysis. Multiaxial stress states are better represented by a 3D analysis than in a 2D analysis. In addition the effect of varying the plasticity parameters could be studied since some of them mainly affect the results in a 3D analysis where a more realistic stress state is achieved.

8.3.1 Numerical Model

The numerical model used when modeling the flexural tensile beams is best illustrated in 2 dimensions by Fig. 64 where both loading and boundary conditions are shown.

A 3D analysis is far more demanding when it comes to computational expense compared to 2D analysis because of the increased number of elements and d.o.f. (Degrees of Freedom). In order to perform a 3D analysis on the flexural tensile beams it has been chosen to use the tied constraint feature in Abaqus. By introducing a tied constraint condition between two parts in Abaqus, they can be meshed independently. Modeling the flexural tensile beam in three parts and by using a more dense mesh at the notch where the crack would arise, while meshing the rest of the specimen with a coarse mesh, the computational expense is drastically reduced. An illustration of the mesh used in the reference analysis is shown in Fig. 68. It is seen that the notch itself is modeled as an independent part and the rest of the beam is tied to its surfaces.

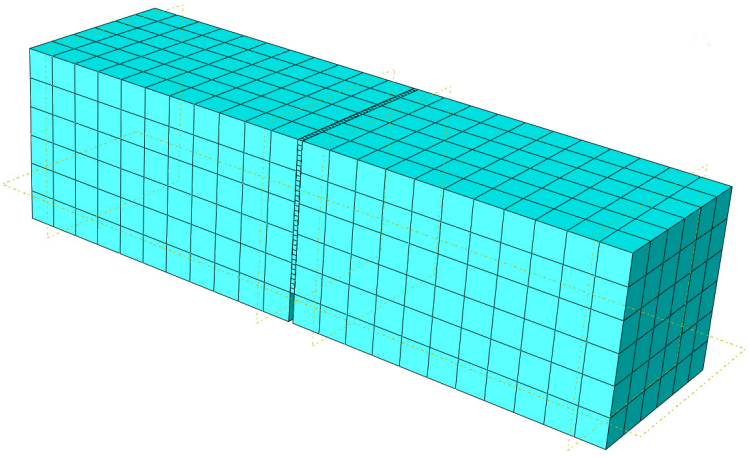

Fig. 68: Tied constraint feature applied in 3D analysis of the flexural tensile beam. Notch meshed independently of the rest of the specimen.

It has been chosen to model the full beam in order to use just one element across the notch. In Fig. 69 the three parts which constitutes the numerical model is shown. It has been chosen to use a node-to-surface contact technique for the tied constraints with the refined notch surfaces as slave surface in order to reduce computational expense. The choice of master and slave surfaces is shown in Fig. 69. The master surface is colored red while the slave surface colored purple.

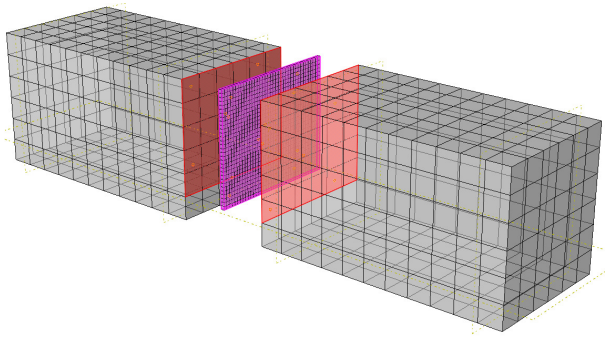

Fig. 69: Three parts using the tied constraint feature in Abaqus constitutes the numerical model. The master surface is colored red while the slave surface colored purple.

The input parameters used for the reference analysis is summarized in Table 22.

Table 22: Summary of input parameters for reference analysis performed in Section 8.3.

Parameter	Value
Element	C3D8R (8 node volume element with reduced integration)
Mesh	4 mm structured notch. 25mm structured elsewhere. Confer Fig. 68.
Material	As described in Section 7.3.3.4.
Dilation angle	36°*
Eccentricity	0.1**
σ_{b0}/σ_{c0}	1.16**
K_c	2/3**

*Abaqus recommended value for normal concrete.

**Abaqus default value.

8.3.2 Comparison Analysis with Basic Setup versus Laboratory Results

A comparison between the reference analysis based on the input parameters summarized in Table 22 and the laboratory results are shown in Fig. 70. It is seen that fairly good correlation is achieved, but it is a clear potential for improvement. The most distinct disadvantage is the predicted maximum capacity, but it should be noted that the capability of predicting the post critical behavior is better for the 3D analysis as compared to the 2D analysis performed in Section 8.2.

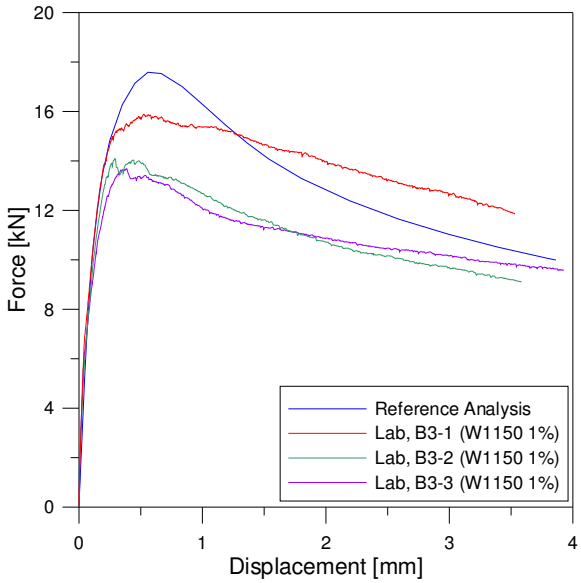

Fig. 70: Comparison between the reference analysis in Abaqus and the laboratory results for the flexural tensile beams.

The tensile input is, as described in Section 8.1.1, based on tensile specimen B3-2 which achieved the highest capacity. Using tensile specimen B3-2 as a basis for the tensile input may not be representable for the flexural tensile beams. (Note: The numbering of the tensile specimens and the flexural tensile specimens has been done at random, i.e. tensile specimen B3-2 does not correspond especially to flexural tensile beam B3-2)

8.3.3 Parameter Study

In order to achieve better correlation between the 3D numerical analysis and the laboratory results, a parameter study has been performed. The 2D analysis concluded earlier in the report that more or less no effect was achieved by varying the plasticity input parameters in a plane stress analysis.

8.3.3.1 Dilation Angle

On basis of recommended values in FEM software manuals [40] and [34] together with hand calculations enclosed in Appendix D.1, the dilation angle was varied as shown in Table 23.

Table 23: Summary of parameter study of the dilation angle.

Basis	Dilation Angle Value
Recommended Value Abaqus software manual [34]	36° *
Recommended Value Diana software manual [40]	10°
Hand Calculations, Appendix D.1.	~10°
Extreme Value	50°

*Reference Analysis

The result of varying the dilation angle is illustrated in Fig. 71. The parameter study indicated that a dilation angle equal to 10° could be considered most appropriate. The maximum capacity is lowered together with a slight increase in post critical capacity. Performing numerical analyses with a dilation angle lower than 10° did not lead to any change in the results.

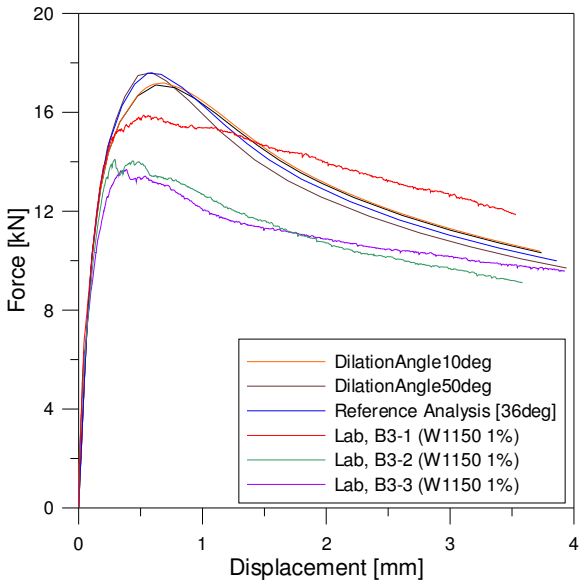

Fig. 71: Parameter study of dilation angle.

8.3.3.2 σ_{b0} / σ_{c0}

Experimental values for the ratio between equibiaxial compressive yield stress and initial uniaxial compressive yield stress lie between 1.10-1.16 [37]. It has been chosen to vary the ratio from 1.0 to 1.2 in this parameter study. As shown in the analysis results in Fig. 72, increasing the value from the reference value of 1.16 to 1.2 had no effect. Decreasing the value on the other hand gives a slight increase in predicted capacity. The parameter study indicated that the chosen default value of 1.16 seems appropriate.

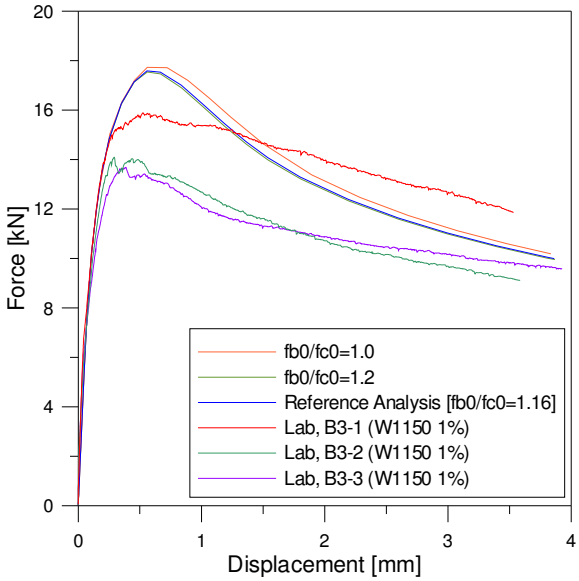

Fig. 72: Parameter study of σ_{bo}/σ_{co}.

8.3.3.3 Flow Potential Eccentricity

By varying the flow potential eccentricity parameter exclusively, it is seen in the left of Fig. 73 that the capacity of the numerical analysis is generally lowered when the eccentricity is increased. Increasing the flow potential eccentricity will as described in Section 7.3.2.2 affect at which rate the dilation angle varies at different confining pressures. Since the flow potential eccentricity affects the behavior through the dilation angle, it would be natural to study the influence of varying the flow potential eccentricity at a dilation angle of for example 10^o. Little or no variation in the numerical results is observed in the right of Fig. 73 when the flow potential eccentricity is varied at a dilation angle of 10^o. This observation does not motivate any change in the flow potential eccentricity from the default value since a dilation angle of about 10^o has been found appropriate.

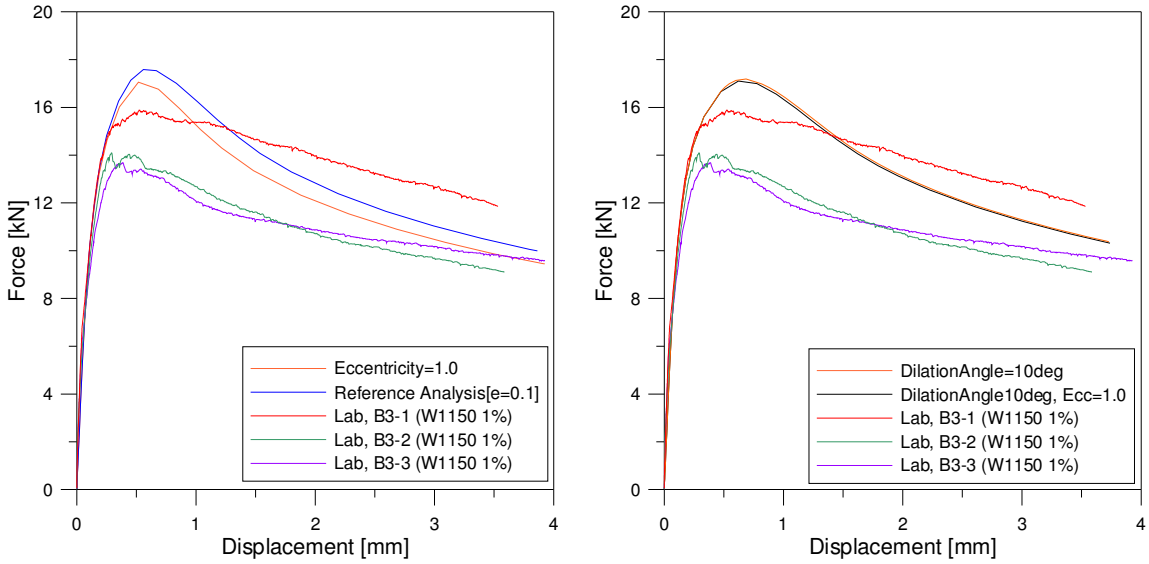

Fig. 73: Left: Parameter study flow potential eccentricity. Right: Effect of Eccentricity at a dilation angle of 10°.

8.3.3.4 K_c

Variation of the parameter K_c will alter the shape of the yield surface. As seen in the left of Fig. 74, choosing a K_c value equal to unity will lower the maximum capacity predicted by the numerical analysis. As mentioned in Section 7.3.2.2, when choosing the dilation angle equal to the internal material friction angle and K_c equal to unity, the Drucker Prager yield criterion is recovered. As seen to the right in Fig. 74, using the Drucker Prager yield criterion leads to better agreement between the laboratory results and the numerical analysis. If this observation is incidental for this specific analysis, or if it actually describes the LWAC better than the default yield criterion in the Concrete Damaged Plasticity model is too early to tell. Further numerical analysis is needed in order to conclude on this issue.

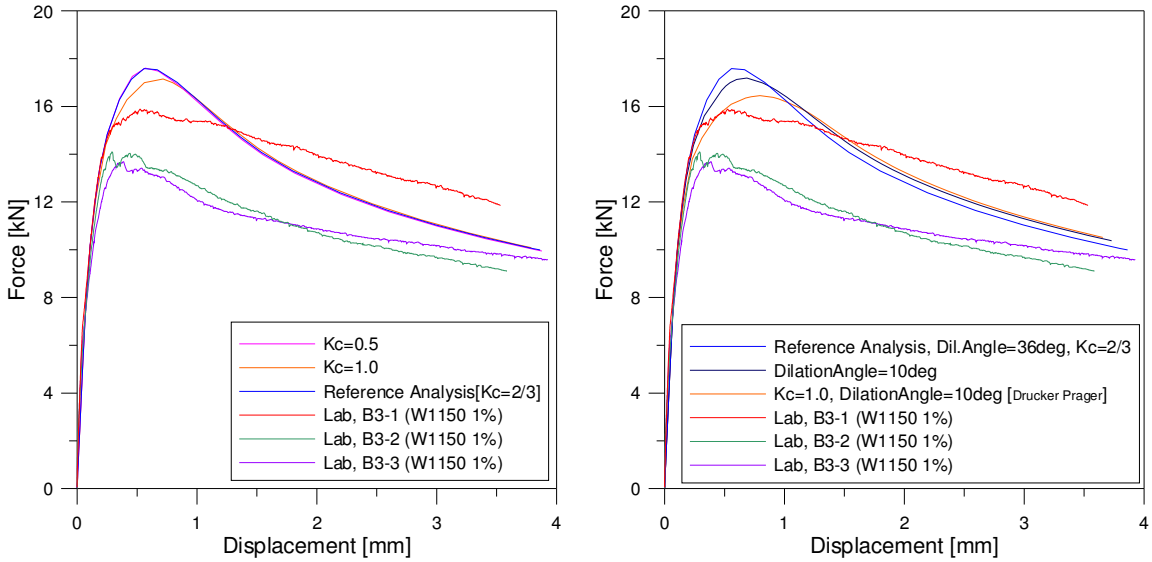

Fig. 74: Left: Parameter study of parameter K_c. Right: Drucker Prager yield criterion enabled.

8.3.4 Discussion/Modification of Numerical Analysis of Flexural Tensile Beams

It is clear that several of the plasticity parameters affect the numerical results in a positive matter when more accurate values are assumed than the default program values. It should on the other hand be noted that the combined effect of changing all the plasticity parameters simultaneously not necessarily is positive. Giving a clear statement of an exact value for each of the plasticity parameters which is best suited for the specific LWAC used in this project, difficult at this point. Further extensive research is needed for each of the plasticity parameters, but through the numerical analysis an indication of a suitable approximate value has been be obtained.

A more optimal numerical analysis is attempted later in this section by using the experience obtained in the parameter study later in this section.

As mentioned earlier in Section 0, it seems as the tensile input should be chosen on the basis of the average achieved capacity of the tensile specimens rather than on one specific tensile specimen as done earlier in this report. Basing the tensile input on tensile specimen B3-2 was done purely because the physical quality of the specimen was better than the rest. It has been chosen to use the laboratory results of tensile specimen B3-1 as the basis for the tensile input in Abaqus in the remaining analysis of this report because it best represents the average achieved tensile capacity. It has also been experimented with applying the tensile input by specifying a stress-strain relation, as for the 2D analysis, rather than the analysis default using stress-displacement.

When performing the numerical analyses it has been chosen to apply the load indirectly by displacing the top of the specimen in the direction of the load. This displacement has been applied on the area marked red (4mm x 150mm) as illustrated to the left in fig Fig. 75. Applying the load over such a small area made local deformations and stress concentrations arise, confer the right of Fig. 75. To counteract this effect, the load/displacement has been applied over a larger area, avoiding local stress concentration problems.

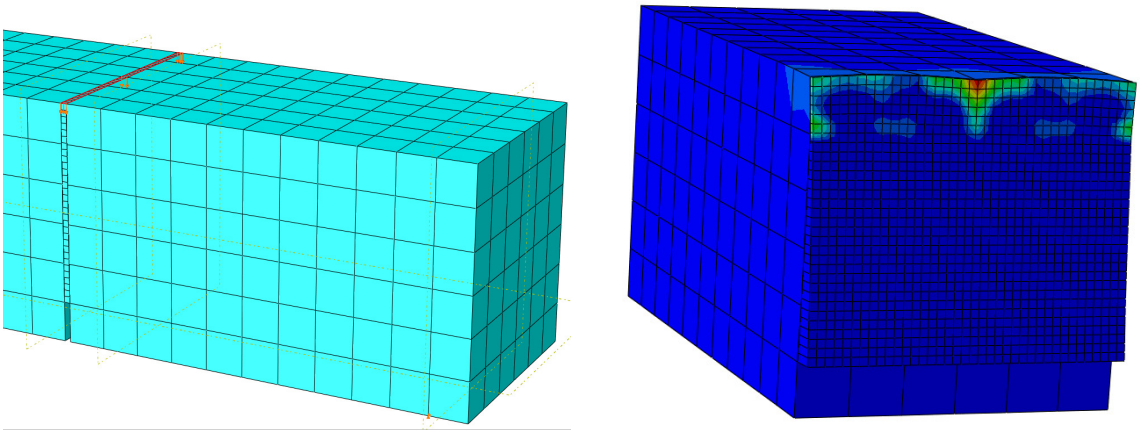

Fig. 75: Left: Displacement applied over the area of the notch (Marked red). Right: Local stress concentration at the notch [Mises].

In order to apply the load/displacement over a larger area, the mesh had to be redefined such that the load area would be of a realistic size. The input parameters used for the improved numerical analysis is summarized in Table 24.

Table 24: Summary of input parameters for the improved analyzes performed in Section 8.3.4.

Parameter	Value
Element	C3D8R (8 node volume element with reduced integration)
Mesh	4 mm structured notch. 12.5mm structured elsewhere. Confer Fig. 77.
Material	As described in Section 7.3.3. Based on tensile specimen B3-1. Compression parameters as summarized in Section 7.3.3.4.
Dilation angle	10˚
Eccentricity	1.0
σ_{b0}/σ_{c0}	1.16*
K_c	1.0

*Abaqus default value.

The results from the improved numerical analyses are illustrated in Fig. 76 where it is seen that the correlation between the laboratory results and the numerical analyses are very satisfying. In order to achieve better numerical results, inverse numerical analysis with respect to both tensile and compressive input data has to be performed. Whether the results achieved with an inverse analysis are more correct than the results presented in this report could be a theme of discussion. More could be gained with performing more accurate and numerous laboratory tests to establish true material parameters.

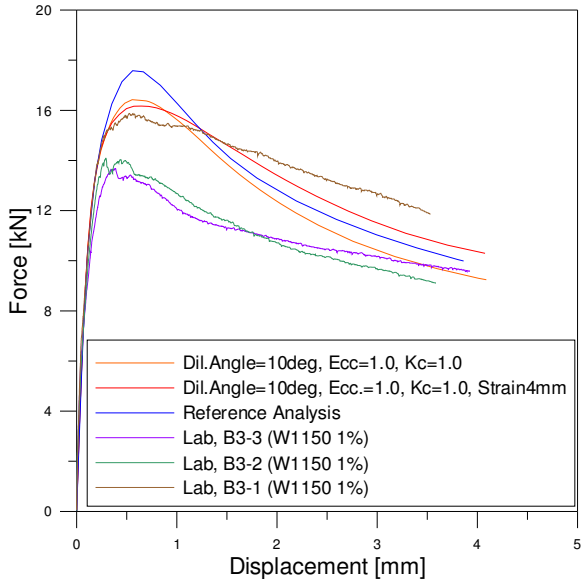

Fig. 76: Results from improved numerical analyses of the tensile flexural beams.

As for the 2D analysis of the flexural tensile beams, it was also chosen to characterize the LWAC's tensile behavior by a stress-strain relation for the 3D analysis. The results are shown in Fig. 76 together with the corresponding stress-displacement analysis and the reference analysis. The results using stress-strain and stress-displacement differ quite a lot, especially in the post critical range. When doing corresponding analysis in 2D there was no observed difference in the numerical results.

The difference observed in the 3D analysis is most likely related to how Abaqus interprets and processes the tensile input data when stress-displacement is defined. When the mesh is defined as described by Table 22 and Table 24, Abaqus calculates an equivalent element (crack) length of 12.4mm and 11.1mm respectively. Considering the fact that the crack initiates in the notch with an element size of only 4mm, it is only natural that the two numerical results differ. When using the stress-strain relation, the input data has been based on a crack length of 4mm equal to the notch.

As seen to the right in Fig. 77, the stress concentration at the notch takes on a more realistic distribution when the displacement is applied across a larger area. No unphysical local deformation or stress concentration arose in this case. In the left of Fig. 77 the area over which the displacement was applied is shown marked in red. Applying the displacement/load over an area of 29mm x 150mm might have yielded a too stiff solution and could be a contributing factor to why the maximum predicted load is higher than desired. Nonetheless, it is more realistic than the reference analysis since the physical print of the loading piston from the laboratory testing was in the range of 10-15mm.

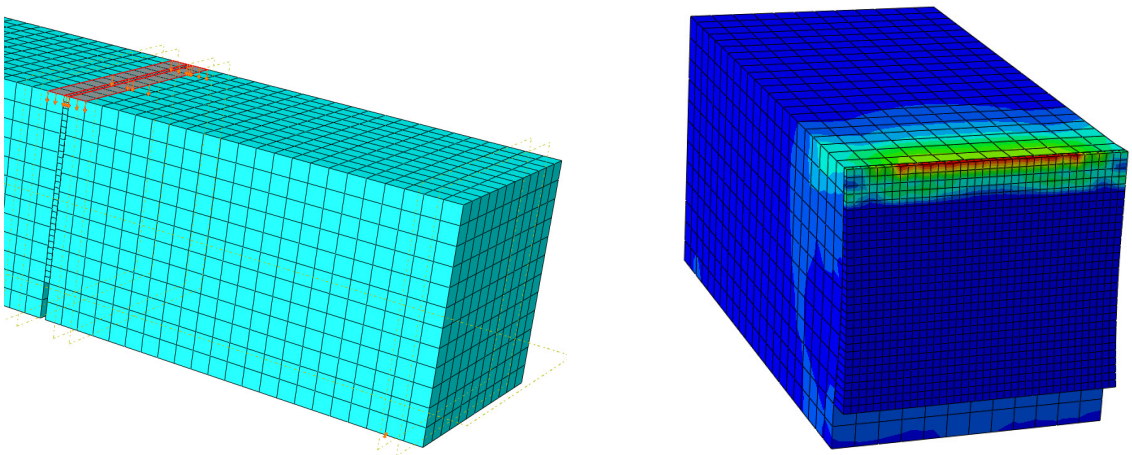

Fig. 77: Left: Displacement applied over a larger area around the notch [Marked red]. Right: Local stress concentration at the notch [Mises stresses].

9 Test Phase 2: Test Program for Concept CSS Beams

With material parameters from test phase 1, a concept CSS is designed, cast and tested. Hand calculations of the basic design are performed in advance, prior to the testing, in order to predict the CSS capacity. The calculations were also used to decide load and boundary position that would ensure a pure flexural tensile failure.

Since test phase 1 revealed severe shortages in the W900 concrete recipe, it is chosen to only do laboratory tests with the W1150 concrete at this stage. Therefore all of the CSS concept beams are cast with the W1150 concrete in the middle layer.

For the top and bottom layer it was chosen to use a normal concrete with mean cylinder compressive capacity close to 30 MPa. The normal concrete is henceforth named “NC30”. The normal concrete will be referred to with quotation marks since its real capacity is not known in advance.

9.1 Estimation of Capacities

As for the shear beams in test phase 1, hand calculations was carried out in advance for the Concept CSS beams. This was done in order to ensure pure flexural tensile failure which was the desired failure mode for the Concept CSS beams. The beam geometry, reinforcement amount and load placement was chosen on the basis of these hand calculations. The capacity of the beam itself, disregarding the steel fibers, was calculated according to Eurocode 2. All calculations related to the steel fiber contribution are done on the basis of the Steel Fiber Draft as in Section 6.6.2. In addition to moment and shear capacities, the anchorage capacity has been calculated according to both Eurocode 2 [2] and the old Norwegian concrete standard NS3473 [29]. Except for the results, the anchorage calculations will not be commented further in this report, but are attached in Appendix G.4 - G.5.

The mean measured values from the laboratory have been used for material strength parameters. No partial safety factors with respect to loading or materials have been used in order to obtain as accurate and realistic calculations as possible, compared to the laboratory tests.

The material parameters and capacities for the middle layer are based on results from test phase 1. The parameters for the top and bottom layer are based on an assumed mean cylindrical capacity of 30 MPa for normal concrete, i.e. $f_{cm} \sim 30$ MPa. This means that the 28-days strength values which all the parameters in Table 26 are based on, are interpolated from table 3.1 in Eurocode 2 [2] in order to correspond to $f_{cm} \sim 30$ MPa.

In production, the CSS concept is intended to be cast in two stages. The first stage includes the precast part, i.e. bottom and middle layer. The second stage is the final in-situ top cast.

As a consequence it was decided to cast the concept CSS test beams in two rounds with one week delay between the two casting stages. Due to a tight time schedule it was decided to test the beams three weeks after the first two layers were cast. This means that the bottom and middle layer will have cured for 21-days when tested and the top layer 14-days.

Therefore all material data were adjusted for 21-days strength for the bottom and middle layer and for 14-days strength for the top layer. Values for 14 and 21-days strength are obtained by interpolating according to Eurocode 2 [2] on basis of the 28-days strength. This is shown in the notations of Table 25 and Table 26. The material data used in the estimation calculations are summarized in Table 25 and Table 26.

Table 25: Summary of material parameters for W1150 used in estimation calculations.

Parameter	Value	Note
f_{cm21}	15.5 MPa	Adjusted for 21 days strength *
$f_{lctm,21}$	1.214 MPa	Adjusted for 21 days strength**
$f_{ftk,res,21}$	1.12 MPa	Adjusted for 21 days strength***
$E_{cm,21}$	12800 MPa	Adjusted for 21 days strength ****
υ	0.2	

*$f_{cm,i} = [e^{0.38(1-\sqrt{\frac{28}{i}})}] \times f_{cm,28}$ (Cylindrical strength after "i" days, $f_{cm,28}$ = 16.4 MPa from test phase 1)

**$f_{lcm,i} = [e^{0.38(1-\sqrt{\frac{28}{i}})}] \times f_{lcm,28}$ (Residual tensile strength after "i" days, $f_{lcm,28}$ = 1.28 MPa from test phase 1)

***$f_{ftk,res,i} = [e^{0.38(1-\sqrt{\frac{28}{i}})}] \times f_{ftk,res,28}$ (Residual tensile strength after "i" days, $f_{ftk,res,28}$ = 1.187 MPa from test phase 1)

****$E_i = (f_{cm,i}/f_{cm})^{0.3} \times E_{cm,28}$ (Young's modulus after "i" days, $E_{cm,28}$ = 13000 MPa from test phase 1)

Table 26: Summary of material parameters for "NC30" used in estimation calculations.

Parameter	Value	Note
$f_{cm,14}$	25.6 MPa	Adjusted for 14 days strength *
$f_{cm,21}$	28.3 MPa	Adjusted for 21 days strength *
$f_{ctm,21}$	2.2 MPa	Adjusted for 21 days strength **
$E_{cm,14}$	26150 MPa	Adjusted for 14 days strength ***
$E_{cm,21}$	28900 MPa	Adjusted for 21 days strength ***
υ	0.2	

*$f_{cm,i} = [e^{0.38(1-\sqrt{\frac{28}{i}})}] \times f_{cm,28}$ (cylindrical strength after "i" days, $f_{cm,28}$ = 30 MPa; Assumed value)

**$f_{ctm,i} = [e^{0.38(1-\sqrt{\frac{28}{i}})}] \times f_{ctm,28}$ (tensile strength after "i" days, $f_{ctm,28}$ = 2.36 MPa; based on $f_{cm,28}$ = 30 MPa)

***$E_i = (f_{cm,i}/f_{cm})^{0.3} \times E_{cm,28}$ (Young's modulus after "i" days, $E_{cm,28}$ = 30600 MPa; based on $f_{cm,28}$ = 30 MPa)

9.1.1 Moment Capacity

The moment capacity has been calculated using the same assumptions and method as for the shear beams in Section 6.6 except for a few minor modifications. Worth mentioning are:

- Moment capacity contribution from the steel fibers: The contribution has been calculated according to the Steel Fiber Draft [26], but the formulas has been modified to account for the fact that only the middle layer of the Concept CSS beams contain steel fibers.

9.1.2 Shear Capacity

The shear capacity has been calculated using the same assumptions and method as for the shear beams in Section 6.6 except for a few minor modifications. Worth mentioning are:

- Shear capacity of the beam itself: For simplicity the capacity has been calculated assuming a homogenous cross section using the LWAC. This is a conservative and fairly realistic assumption since the middle layer (LWAC) would be most exposed with respect to shear.

- Shear capacity contribution from steel fibers: The contribution has been calculated according to the Steel Fiber Draft [26], but the formulas has been modified to account for the fact that only the middle layer of the Concept CSS beams contain steel fibers. For the two beams where the top layer is established it is assumed on basis of the calculated compression zone height, that the entire middle layer contributes to the shear capacity as illustrated in Fig. 78.

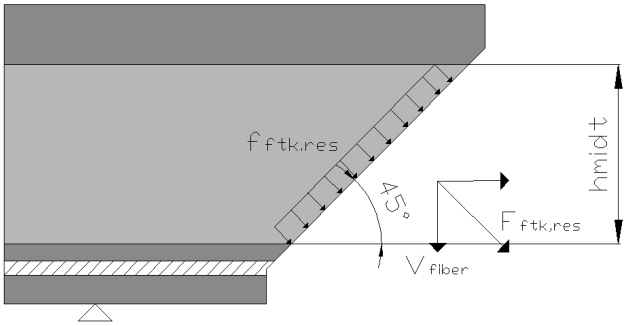

Fig. 78: Assumed shear capacity contribution from the steel fibers in the Concept CSS beams.

9.2 Overview of Test Phase 2

The concept was tested as a beam width with of 150 mm, rather than a slab shaped structure with larger width to thickness ratio. This was done due to limitations in production capacity of foam for the Weber concrete. However, the beam will act as a good approximation for the capacity and behavior of a slab. The CSS test beams will have measures as shown in Fig. 79 and Fig. 80.

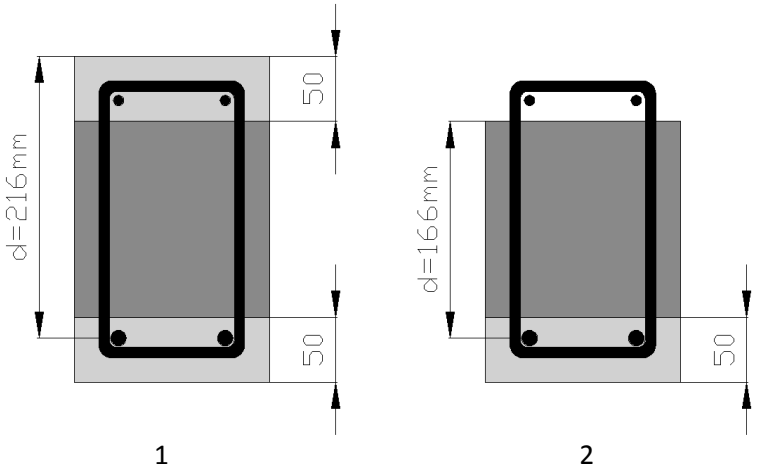

Fig. 79: Cross sectional measures of concept CSS beams, with (1) and without top cast (2).

The second test phase contains a total of 4 specimens and is summarized in Table 27. Two of the specimens are with top cast (left figure in Fig. 79). The top cast is cast 7 days after the bottom and middle layer in order to simulate realistic behavior of the top bonding capacity, since the top would be cast at a later time in a real construction phase.

Two of the beams are tested without the top layer (right figure in Fig. 79). This will make it possible to study the increase in capacity from the top layer, and test the capacity of the precast part of the CSS concept.

Table 27: Overview of test phase 2, concept CSS beams.

Specimen ID	Top cast	Middle layer	Top/bottom layer
HB 1	No	W1150 concrete, 1% fiber	"NC30"
HB 2	No	W1150 concrete, 1% fiber	"NC30"
HB 3	Yes	W1150 concrete, 1% fiber	"NC30"
HB 4	Yes	W1150 concrete, 1% fiber	"NC30"

9.3 Design of the Concept CSS

The minimum height of the top and bottom layer was set to 50 mm due to practical reasons related to the casting process and by regulations of reinforcement placing according to Eurocode 2. The hand calculations indicated that no increase in capacity was achieved by increasing the size of the bottom and top layer. The hand calculations actually reveal that the effective compressive zone is smaller than the total height of the top layer. Reducing the height of the top layer while increasing the height of the middle layer could then load to a lighter slab without reducing the load bearing capacity.

Using the "NC30" concrete in the bottom layer will not increase the post crack (Stadium II) capacity. In fact, using the W1150 in the bottom layer could increase the overall capacity because of the W1150's post crack capacity, but at the sacrifice of the durability properties of the concept CSS slab.

9.3.1 Reinforcement

The structural tension reinforcement was chosen on the basis to maintain the characteristics of an under reinforced concrete structure. The amount of reinforcement should also be similar to a traditional reinforced concrete slab. For the concept beams it was chosen to use 2Ø12mm which will correspond to 1508 mm^2/m for a slab structure. The top reinforcement, 2Ø8mm, is only placed in the structure for mounting purposes.

The positioning of the reinforcement is governed by the rules in Eurocode 2 [2]. Even though this is a laboratory test, the rules are followed in order to be on the safe side when it comes to bonding capacity of the reinforcement. The position of the reinforcement is shown in Fig. 80.

The loops are nonstructural with respect to shear and are placed in the structure with respect to mounting of longitudinal reinforcement and bonding capacity behind the support and between the concrete layers. The four loops which are placed 442mm and 884mm from the each of the bearings respectively, are used to ensure sufficient bonding strength between the three concrete layers. Calculations were performed to decide the necessary number of loops to avoid bonding problems between the layers. The loops are placed in such a way that they theoretically should not affect the shear capacity. When calculating the necessary number of loops it has conservatively been assumed that the loops should be able to carry a horizontal shear force between the layers of the same magnitude as the maximum vertical shear force.

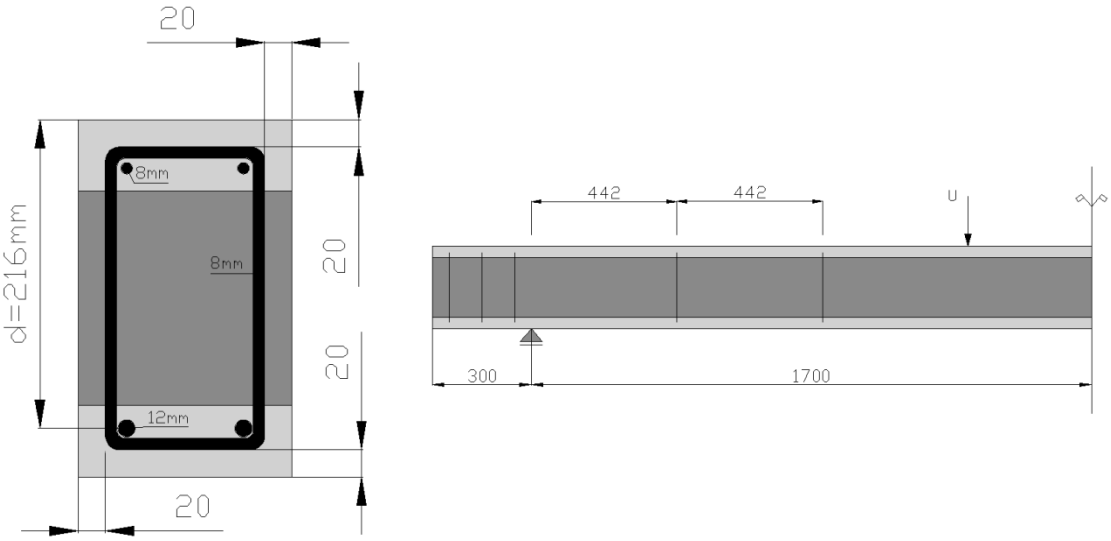

Fig. 80: Position of reinforcement in concept CSS beams.

9.3.2 Overview Estimated Capacities Concept CSS Beams

The predicted capacities from the hand calculations for the concept CSS beams are summarized in Table 28. The predicted values indicate flexural tensile failure in both cases.

Table 28: Summary of estimated hand calculation for CSS beams, based on assumed material parameters.

Beam	V_{Rk} [kN]	M_{Rk} [kNm]	$l_{anchorage,Euro}$ [mm]	$l_{anchorage,NS}$ [mm]
CSS with top cast	43.65	25.25	120	93
CSS without top cast	36.75	17.48	120	≤93

$M_{Rk,w.top}$ = 25.25kNm corresponds to V_{max} = 19.05kN < **$V_{Rk,w.top}$ → Flexural tensile failure.**
$M_{Rk,wo.top}$ = 17.48kNm corresponds to V_{max} = 13.19kN < **$V_{Rk,wo.top}$ → Flexural tensile failure.**

9.4 Production of Concept CSS Beams

The whole production of the concept CSS beams was carried out in the M-Lab facility at The Department of Structural Engineering at NTNU. All of the preparatory work was carried out by the authors of this report, this being preparing materials and manufacturing both the formwork and the reinforcement. During the mixing and casting of the concept CSS beams the following people were present:

- Ole Georg Skjølberg, Graduate Student, NTNU
- Anders Hansson, Graduate Student, NTNU
- Ove Loraas, Sectional Engineer, Concrete Laboratory NTNU
- Steinar Seehuus, Engineer, Concrete Laboratory NTNU
- Linn Grepstad Nes, PhD student, COIN SINTEF

9.4.1 Proportioning

Two recipes were used when casting the concept CSS beams, a normal structural concrete ("NC30") and the W1150 concrete. Some small adjustments to the recipes were done during casting because of observations made while mixing. The basic recipes used are summarized in Table 29.

Table 29 Overview of recipes, test phase 2

Recipe	W1150	"NC30"
w/c	0.474	0.580
Unit	**kg/m^3**	**kg/m^3**
Norcem Industri (cement)	114.0	0
Norcem Anlegg(cement)	266.0	0
Norcem Standard FA (cement)	0	311.2
Elkem Microsilica	35.0	0
Leca 2-4mm (LWA)	230.0	0
Sand Årdal 0-4 mm	400.0*	0
Sand Årdal 0-8 mm	0	1112.5*
Rock Årdal 8-16 mm	0	740.2
BASF MECH PP 150 (polypro. fiber)	1.5	0
BASF Glenium SKY 550 (SP)	7.2	0
Mighty 150 (SP)	0	0.031
BASF Glenium Stream (Stabilisator)	2.0	0
Defoaming Agent	0.123	0
Bekaert 30/35 Steel Fiber	78.5	0
Water	180.0*	180.5*
Foam	At random (~210L)**	0

*It must be noted that these recipes are not adjusted with respect to the moisture in the sand. Adjustments were done during weighing. The final adjusted recipes are attached in Appendix B.2.

**Foam was added during mixing until sufficient wet density was obtained.

9.4.2 Mixing and Casting

The casting of the bottom and middle layer for all of the CSS beams was done April 12, 2010. Since the middle layer was cast right after the bottom, two concrete mixers was used in order to avoid waiting time between the castings and assure maximum bonding capacity between the layers.

The casting of the top on beam HB3 and HB4 was done April 19, 2010.

Cylinders representing each batch were also cast for testing of the concrete's compressive strength.

9.4.2.1 Bottom Layer

The bottom layer was mixed using a smaller concrete mixer with a maximum capacity of 50L, Gustav Eirich SKG 1, shown to the left in Fig. 81. The mixing procedure is attached in Appendix A.2.

The mixing and casting of the "NC30" concrete had no complications or deviations from the casting plan. An external vibrator was used to distribute the concrete evenly in the formwork and to ensure good bond with the reinforcement. The "NC30" concrete was not self-compacting. The thickness of the bottom layer was controlled manually along the beam length using a ruler. Spacers were placed on both sides of the reinforcement in order to keep the reinforcement centered in the formwork through the casting process, this is shown to the right in Fig. 81. The spacers were later raised a little before the middle layer was cast and finally removed in order to avoid cavities not filled with concrete.

Fig. 81: Left: Mixer used for the bottom layer. Right: Casting of the bottom layer. The spacers centering the reinforcement are shown in the picture.

9.4.2.2 Middle layer

When the W1150 concrete was produced at Weber's premises for test phase 1, a foam generator was available. The fact that this generator was not available when producing the specimens in test phase 2 at NTNU led to additional challenges.

The foam was instead produced using a Kenwood Titanium Major food mixer and a Hobart A 200 food mixer. Production of the foam concrete developed by Weber has previously been attempted in master theses and research at NTNU. In this context the Kenwood food mixer had been tested and found to be adequate by Weber.

Because of the big production volume needed for the test program in this report, the Hobart A 200 food mixer was tested. The tests showed that it was possible to obtain the same quality foam with the Hobart as with the Kenwood mixer. Both density and behavior was the same as the foam produced by the Kenwood.

To produce a sufficient volume of foam, the foam had to be mixed in two turns. This seemed to have no negative influence on the foam itself. It only resulted in the foam production starting approximately 10 minutes before the foam was added to the concrete mix. The mixers used for the foam production are shown in the middle and right picture in Fig. 82.

The W1150 concrete itself was mixed in a professional concrete mixer with a maximum capacity of 100-250L (Gustav Eirich EBG 3), shown to the left in Fig. 82.

Fig. 82: Left: Concrete mixer used for middle and top layer. Center: Kenwood mixer used to produce foam. Right: Hobart mixer used to produce foam.

No problems occurred during the mixing procedure of the W1150 concrete. The concrete seemed to have the same characteristics as the concrete produced in Lillestrøm. The amount of superplasticizer used was reduced compared to the recipe shown in Table 29 for the W1150 concrete because the flow ability was found to be adequate before all of the superplasticizer was added. The detailed mixing procedure for both the foam and the W1150 concrete itself is attached in Appendix A.2.

As for the mixing in phase 1, the density of the W1150 concrete was controlled during mixing to verify that the correct amount of foam was added to achieve a wet density of about 1150 kg/m^3. All batches achieved a density in the range of 1160-1180 kg/m^3. The final recipes used are attached in Appendix B.2.

Casting of the middle layer did not result in any problems. The concrete had really good flow ability and was stable. The effects of adding the steel fibers to the W1150 concrete were more or less insignificant with respect to fresh state properties. No external vibration was applied during casting of the middle layer since the concrete basically was self compacting. Trowels were used to ensure that the concrete was properly compacted and distributed along the sides of the formwork and around the reinforcement loops. This is illustrated in the right of Fig. 83. The height of the layer was controlled accurately through the casting process.

When filling the formwork, using a wheelbarrow, it was observed that the good flow ability of the concrete made it flow longitudinally in the formwork as attempted illustrated in the left figure in Fig. 83. This might have resulted in a more favorable steel fiber distribution than one could expect when casting a slab like structure, where it is more likely that the fiber orientation will be more random.

Fig. 83: Left: Filling the formwork using a wheelbarrow. W1150 concrete flowing longitudinally inside the formwork. Right: Measuring layer height and distributing concrete using a trowel.

9.4.2.3 Top Layer

Exactly one week after the two first layers were cast the top cast was carried out for beam HB3 and HB4. The concrete was mixed using the same concrete mixer as for the middle layer, shown to the left in Fig. 82.

No complications arose during mixing or casting. Experience gained when casting the bottom layer lead to an increase in the amount of superplasticizer. This made the concrete more workable, but an external vibrator (shown in Fig. 84) was still used to ensure that the concrete was sufficiently compacted. A screed was used to achieve an even surface and exact beam height.

Fig. 84: Compacting the concrete using a vibrator.

9.4.3 Removing Formwork and storage until testing

For the two beams without the top cast the formwork was removed after 3 days of curing. No defects were found and the surface finish quality of the beams was satisfying.

All of the four beams, two of which still laying in the formwork, were wrapped in wet cloths and plastic to maintain 100% humidity during curing. 3 days after the top was cast on beam HB3 and HB4, the formwork was removed and the beams were yet again properly wrapped in wet cloths and plastic. Since theoretically 100% humidity was maintained during curing, only autogenous shrinkage is expected to affect the specimens before testing.

The overall quality of all four beams was good, but some surface defects were observed for beam HB3 and HB4 as shown in Fig. 85. These defects most likely arose due to the spacers which were placed in the formwork in order to keep the reinforcement in the correct position. These spacers should have been removed earlier when casting the bottom layer. The defect found on beam HB4 will most likely not influence the results since it will be located outside of

the bearing during testing. The effect of the defect in the CSS beam HB3 will be discussed further in Section 9.5.2.2.

Fig. 85: Left: Defect in CSS beam HB3, mid span. Right: Defect in CSS beam HB4, on the outside of the bearing.

9.5 Laboratory Testing of Concept CSS Beams

The CSS beams were tested 3-4 May 2010 in the laboratory at The Department of Structural Engineering at NTNU. The purpose for testing these beams was primarily to test the capacity and behavior of the CSS concept with and without the final top cast.

During testing the following persons were present:

- Ole Georg Skjølberg, Graduate Student, NTNU
- Anders Hansson, Graduate Student, NTNU
- Steinar Seehuus, Engineer, Concrete Laboratory NTNU
- Linn Grepstad Nes, PhD student, COIN SINTEF

9.5.1 Loading, Boundary Conditions and Logging of Strains and Displacements

The testing method used is not governed by any regulations or standards. The test was performed as a 4 point bending test where the failure mode was intended to be a pure flexural tensile failure. The a/d relationship was 6.13 and 7.98 for the CSS with and without the top cast respectively. The positioning of the loads and supports are shown in Fig. 86. The load position is based on the hand calculations described in Section 9.1.

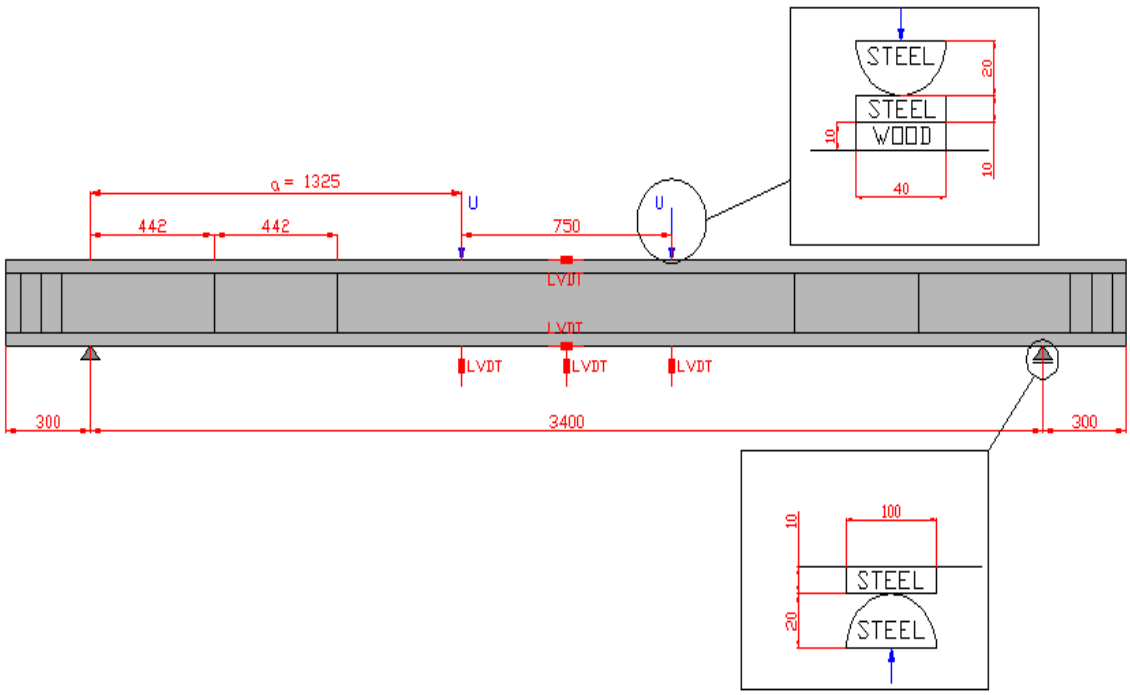

Fig. 86: Overview of load and LVDT position.

The test was performed using an Aflred J. Amsler & CO 100kN hydraulic jack together with an Instron 8800 controller for logging purposes. The load was applied from the jack to the test specimen through a stiff steel beam with two symmetrically placed rollers, se Fig. 87. The loading can be considered to be quasi-static and was applied with a rate of 2mm per minute. The load was applied with the same speed through the whole test with no intermissions.

The logging performed throughout the test was done with a total of five LVDT's. These were placed as shown in Fig. 86. For the CSS without the top cast, the LVDT on the top was placed on top of the middle layer. The LVDT's was all placed in the center of the beams in respect to the horizontal plane.

In addition to the LVDT's, an Optical Strain Measuring Device (OSMD) was used to log the strains on one of the sides of the beams. The OSMD measured strains over the whole beam height and between the loads in the beam's longitudinal direction. This area is painted in white on the beam in Fig. 87.

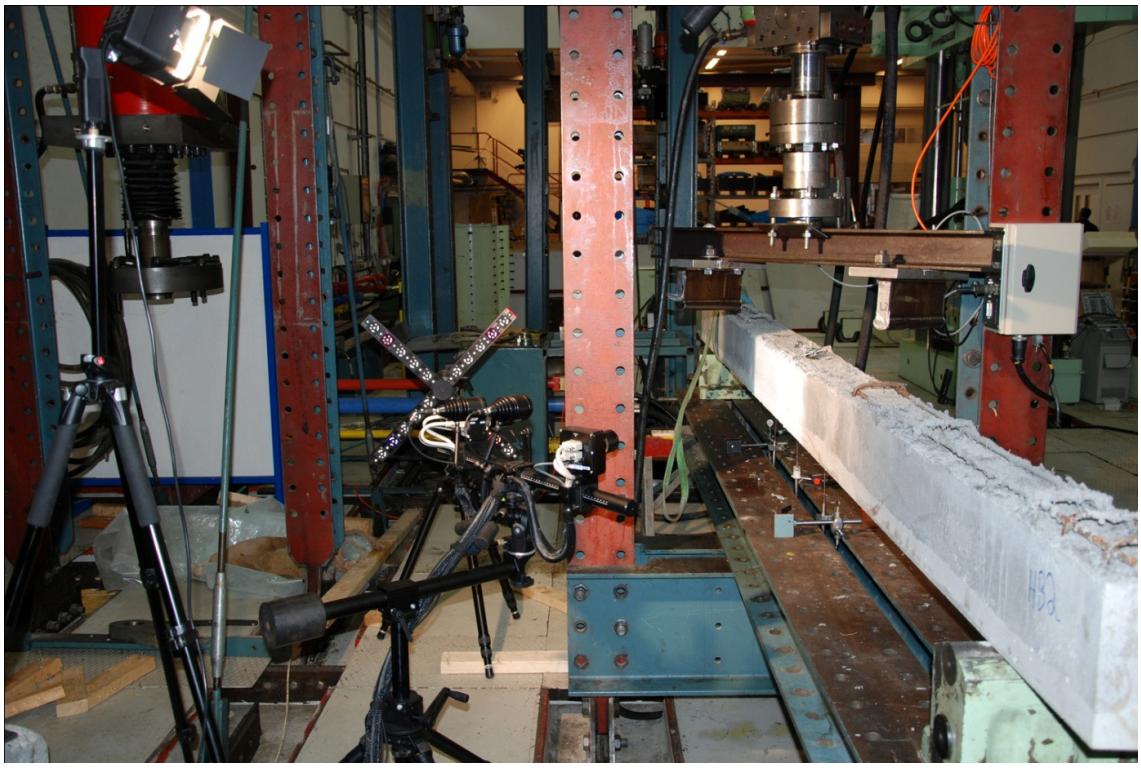

Fig. 87: Test rig with beam, LVDT's and optical strain measuring device. The beam shown in this figure is without the top cast.

9.5.2 Test Observations and Deviations

9.5.2.1 Cracks

During the test, cracks induced by bending occurred continuously across most of the beam length. The cracks where more or less spread evenly over the beam length, although the length between the cracks were a bit smaller in the zone of constant moment between the loads. An overview of the crack distribution is found in Table 30 and in Fig. 88 and Fig. 89.

Table 30: Overview of crack spacing from beams tested in phase two.

Specimen ID	Average Length Between Cracks [mm]	Average Length Between Cracks in Zone With Constant Moment [mm]	Total Length of Crack Zone [mm]	Number of Cracks	Load at First Crack Observation [kN]
HB 1	78	63	2188	29	6.6
HB 2	96	72	2500	27	7
HB 3	83	58	2483	31	9.5
HB4	83	55	2480	31	12.8

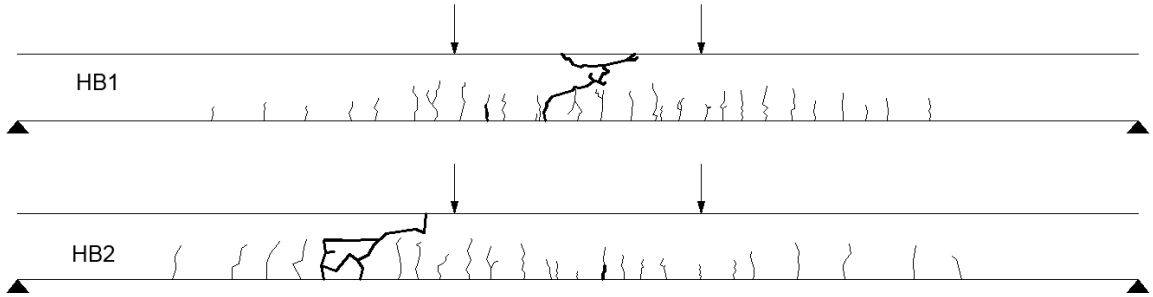

Fig. 88: Crack distribution after failure for the beams without top cast (HB1 and HB2). The failure crack is marked in bold. The short bold line between the loads indicates the position of first crack. The sketch is a reproduction from many photos from the test since a similar photo as Fig. 89 was missing for these beams.

Fig. 89. Crack distribution after failure for the beams with top cast (HB3 and HB4). The failure is marked in bold. The short bold line indicates the position of first crack.

9.5.2.2 Failure

The failures during the testing were pure flexural tensile failures for all beams except for HB2. The HB2 failure reminds more of a shear failure even though it most likely is a flexural tensile failure. The failure for HB2 occurred outside the zone of constant moment between the loads, in difference from the rest of the beams. The failures are shown in detail in Fig. 90 and Fig. 91.

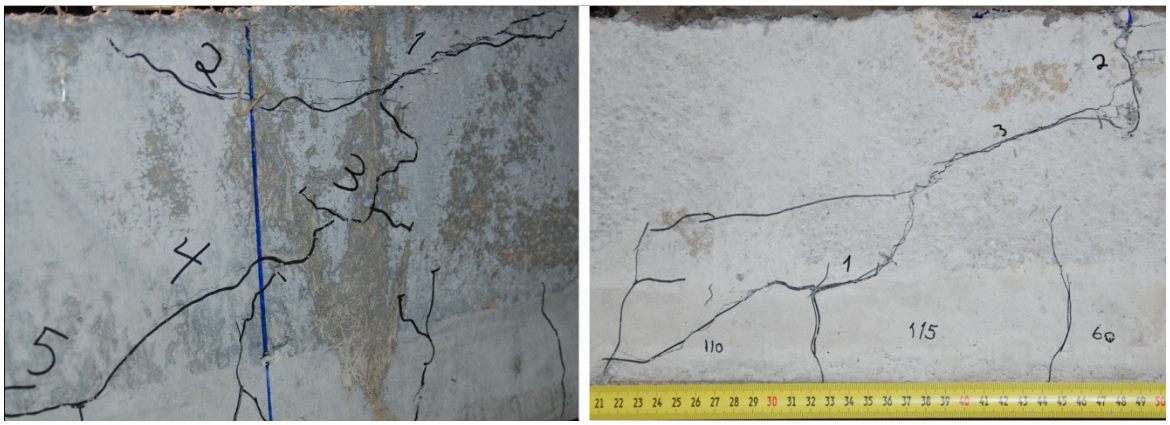

Fig. 90: Failure for HB1 and HB2, left and right respectively.

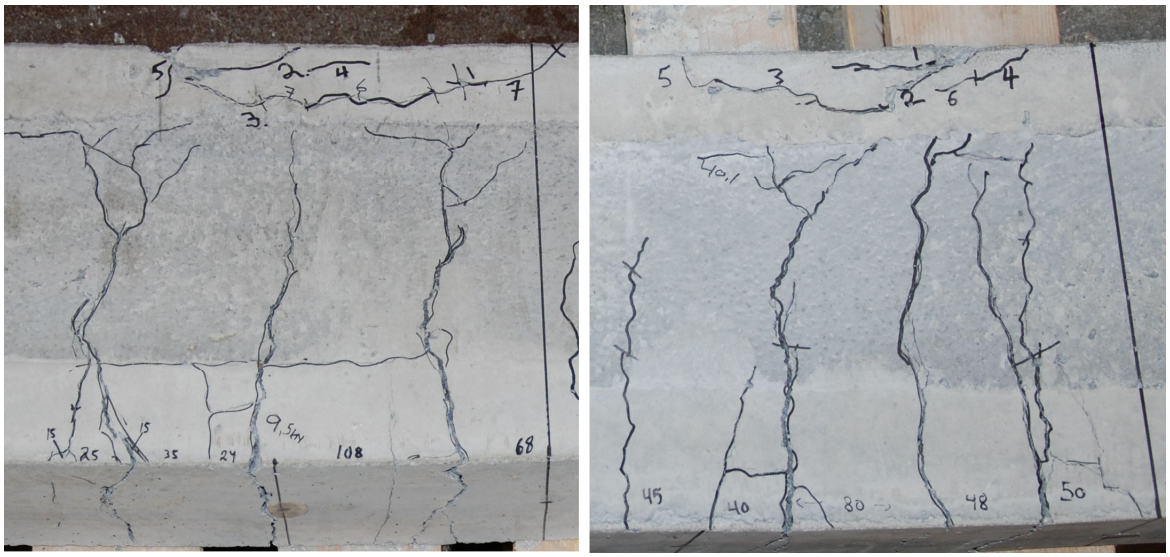

Fig. 91: Failure for HB3 and HB4, left and right respectively.

The reason for the nonconformity failure on HB2 is hard to explain. The a/d relationship equal to 7.98 together with longitudinal reinforcement percentage of 0.75% will, according to the literature [43] and hand calculations, trigger a flexural tensile failure. However, the failure could be a combination of internal imperfections and reduced capacity from cracks. This theory is strengthened by the progression of the failure shown in the right figure in Fig. 90.

1. The failure starts with a crack progressing from the bottom.

2. Then the pressure zone collapses.
3. After the pressure zone collapses, the cracks are connected.

This progress is similar to the other failure paths from the test (Fig. 90 and Fig. 91) where the failure starts at the top and the progresses downwards before the failure connects with a crack from underneath.

The failure of beam HB2 progressed in a way totally opposite to a normal shear failure. A shear failure usually progress from the tensile zone and towards the compressive zone [43].

The argumentation above strengthens the theory that the HB2 failure also is a flexural tensile failure. The failure is most likely placed outside the zone of constant moment, due to initial imperfections or imperfections caused by the loading, which differed from the loading of the other beams in the test. The loading for HB2 was induced without wood plates between the steel plates and the concrete. This could have caused askew loading or loading through single stones in the concrete, rather than over a larger area.

Fig. 92: HB2 were loaded without wood plates between the steel plate and the concrete. This could have caused askew loading or loading through single stones in the concrete, rather than over a larger area.

None of the observed defects on beams HB3 and HB4 as described in Section 9.4.3 seemed to influence the failure capacity in any negative way. The failure patterns had no connection to the observed defects.

9.5.2.3 Removal of LVDT's while Tests were Running

The LVDT measuring longitudinal strain at the bottom of the beam as well as the two LVDT's measuring vertical displacement under the loads were removed when the deformations became so large that they could damage the LVDT's.

9.5.2.4 Compressive Strength

The compression cylinders which were cast in relation to each batch in test phase 2 was tested as described in Section 6.7.1 using a Mohr Federhaff Losenhausen analog uniaxial compression machine. Cylinders were tested at 15, 22, 29 and at 49 days strength for the different batches. Detailed results are shown in Appendix C.2.

9.6 Test Phase 2: Summary of Laboratory Results

9.6.1 CSS Beams

The results of the laboratory testing of the CSS beams are shown in Fig. 93 in terms of machine force and vertical displacement of beam at mid span. The beams with top cast, HB3 and HB4, reached their maximum capacity long before failure. This is an expected behavior and an essential feature for normal concrete structures due to safety requirements. Normal or under reinforced structures should have similar behavior of HB3 and HB4 since a failure without premonition is not desired.

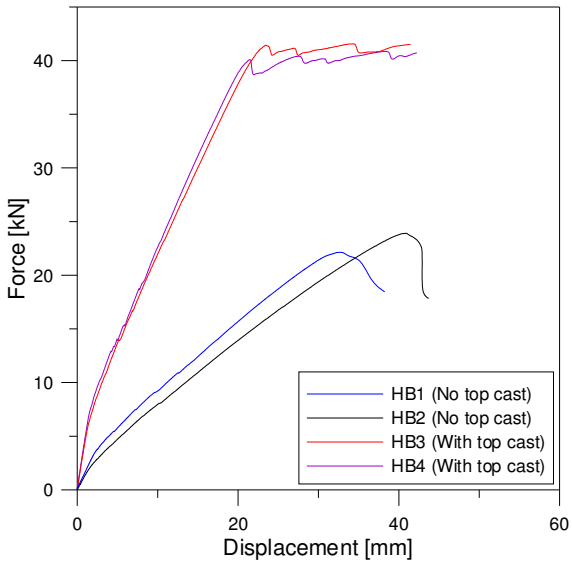

Fig. 93: Results from laboratory testing of CSS concept beams in terms of machine force and vertical displacement measured in the mid span of the beams.

This is not the case for the beams without the top cast, HB1 and HB2. From Fig. 93 it is clear that failure for the beams without top cast occurs close to the point where maximum load is reached. This could be an indication that the failure takes place before the reinforcement yields, or at least simultaneously. The sudden drop could also be related to the brittle behavior of the LWAC. The beams without the top cast were concluded to just barely being under reinforced when the hand calculations were performed.

9.6.2 Compression Cylinders

A total number of 26 compression cylinders were cast during the production of the CSS beams. The results from the compression tests are summarized in Table 31. Detailed results from the testing are attached in Appendix C.2.

Table 31: Average compressive strength from laboratory testing of cylinders in phase 2.

ID	Curing Time [days]	Achieved Average True Density [kg/m^3]	Average Capacity [MPa]
W1150	22	1215	11.6
W1150	29	1215	11.8
W1150	49	1215	12.0
“NC30” bottom	22	2400	26.8
“NC30” bottom	29	2400	26.2
“NC30” top	15	2402	25.5
“NC30“ top	28	2402	27.0

The obtained compression strength for the W1150 concrete was approximately 30% less in phase 2 compared to phase 1, i.e $\sim$ 12Mpa in phase 2 versus $\sim$ 17Mpa in phase 1. The reason for this is however hard to state. The production of the concrete was done with the same recipes at both occasions. The concrete mixed in phase 2 was produced more carefully compared to phase 1 which means that the production most likely not is the cause. However, the foam was produced by hand in phase 2 compared to phase 1 were a foam generator was used. The foam production is therefore the most likely cause to the reduced strength, even though this is hard to state.

After 49 days of curing there was no increase in strength compared to the strength measured after 28 days for the W1150 concrete in phase 2. This must be compared to phase 1 were an increase in almost 60% was observed from 28 to 62 days of curing, i.e 17.2 MPa at 28days compared to 27.3 MPa at 62 days. This is also an interesting observation which indicates that the W1150 concrete produced in phase 2 was of a different quality, strength wise, compared to what was produced in phase 1.

It should also be noted that the 28 days cylinder compressive strength for the “NC30” was 3-4 MPa less than the 30 MPa that was expected.

10 Test Phase 2: Analysis of Concept CSS Beams

The CSS beams are also analyzed with Abaqus as the test specimens from phase 1. It was only performed 2-dimensional analyses of the CSS. All analyses were run as implicit analyses as described earlier in Chapter 7.

10.1 Numerical Model

The numerical model used for the analyses of the CSS is shown in Fig. 94. It was chosen to analyze half the beam due to symmetry. When the analyses of the beams without the top cast was performed, the same model was used but without the top layer. The parameters used in the analysis are listed in Table 32.

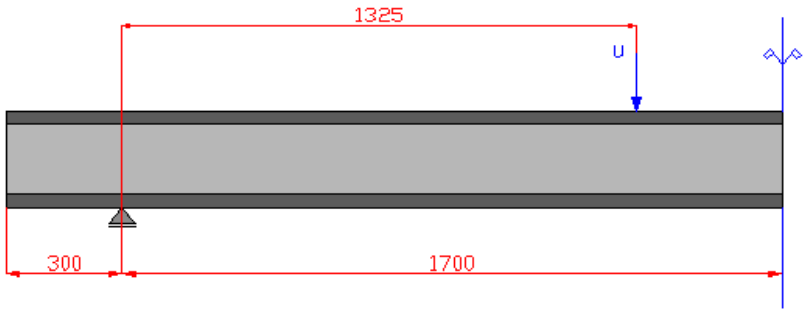

Fig. 94: Numerical model used in analyses of CSS beams. In the analyses of the beams without the top cast, the same model is used but without the top layer.

Table 32: Summary of plasticity parameters and element properties used in analyses of CSS beams.

Parameter	Value
Element	CPS4
Mesh	50 mm, structured
Material	As described in Section 10.2
Dilation angle	10˚ for LWAC, 36° for "NC30"
Eccentricity	0.1*
σ_{b0}/σ_{c0}	1.16*
K_c	2/3*

*Abaqus default value.

10.2 Material Input

The material input data for the analyses are based on the results from the laboratory testing in phase 1 (phase 2 for compression), Eurocode rules [2] and experience from the parameter

study in Chapter 7. All material data are given to Abaqus as tabular values. The material data defining the plastic behavior of the concretes are shown in Fig. 95. The elastic behavior of the LWAC and the "NC30" are described by the material values summarized in Table 33 and Table 34 respectively.

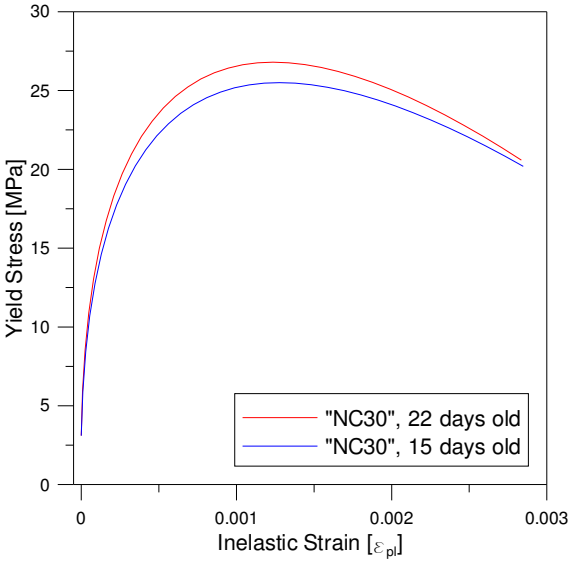

Compressive Input Data
"NC30"

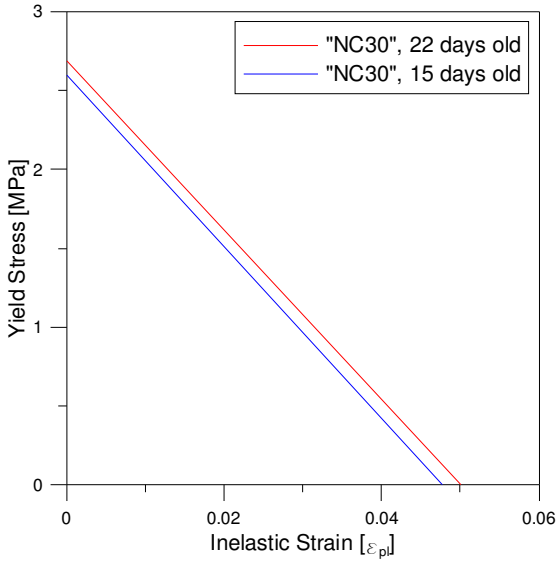

Tensile Input Data
"NC30"

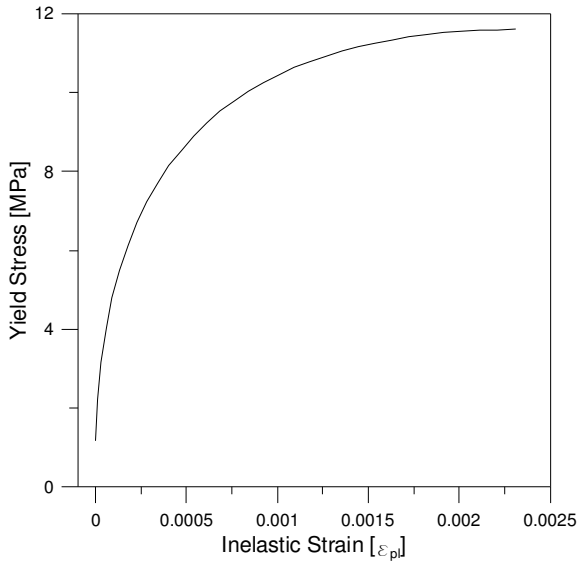

Compressive Input Data
W1150 (22 days old)

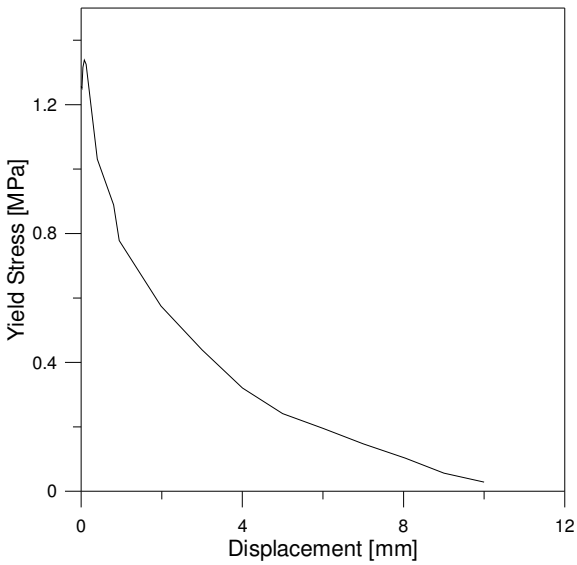

Tensile Input Data
W1150 (22days old)

Fig. 95: Tension and compression data for the W1150 and "NC30" concrete, used in analyses of concept CSS beams.

10.2.1 W1150 Concrete

The material parameters which constitutes the basis for the numerical analysis for the W1150 concrete is summarized in Table 33.

Table 33: Summary of W1150 material parameters.

Parameter	Value	Note
$E_{cm,22}$	11700 Mpa	Adjusted according to $f_{cm,22}$*
$f_{cm,22}$	11.6 Mpa	Mean measured cylinder strength Phase 2, see Appendix C.2.
$f_{ctm,22}$	1.26 Mpa	Adjusted according to $f_{cm,22}$**
ε_{c1}	0.0033	Adjusted for LWAC***
υ	0.2	

*$E_{cm,22} = (f_{cm,22}/f_{cm})^{0.3} \times E_{cm}$ E_{cm}= 13000 Mpa from test phase 1

** $f_{ctm,22} = (f_{cm,22}/f_{cm}) \times f_{ctm}$ f_{cm}= Mean measured cylinder strength W1150 phase 1, f_{ctm} = measured tensile strength W1150 specimen B3-1 phase 1

*** According to Table 11.3.1 in Eurocode 2 [2]

10.2.1.1 Tensile Data

The tensile data is based on tension specimen B3-1 in test phase 1 which was concluded to represent the W1150 concrete with 1% fiber in an appropriate way. The tensile data is in this case defined in Abaqus in terms of stress-displacement for chosen values from first yield to failure of the tension specimen.

10.2.1.2 Compression Data

In the previous analyses in Chapter 7, the simplified stress-strain relationship in Eurocode 2 [2], have been used to define the compressive path. Based on recommendations from supervisors it is here instead chosen to use the stress-strain relation that is suggested for non-linear analyses in Eurocode 2. This should in theory be a more correct way of describing the compressive behavior of concrete. The schematic representation of the stress-strain relation from Eurocode 2 is shown in Fig. 96.

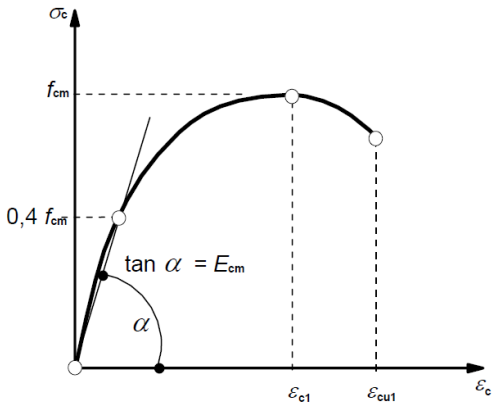

Fig. 96: Schematic representation of the stress-strain relation for structural analysis (the use of 0,4fcm for the definition of E_{cm} is approximate) [2].

The compression data in the analyses of the concept CSS beams is based on the measured compressive strength from the test cylinders that were sampled during the production of the CSS beams. The compression data is given to Abaqus in terms of yield stress and inelastic strain from first yield to ultimate strain ε_{cu1} according to the recommendations in Eurocode 2 [2]. The compressive data given to Abaqus is shown as plotted values in the top left diagram in Fig. 95 and is based on equation (10.1) [2] together with the values in Table 33:

$$\sigma_c = f_{cm,ii} \times \frac{k\eta - \eta^2}{1 + (k-2)\eta} \qquad (10.1)$$

where:

$$\eta = \varepsilon_c / \varepsilon_{c1}$$

$$k = 1.05 E_{cm,ii} \times |\varepsilon_{c1}| / f_{cm,ii}$$

10.2.2 "NC30" Concrete

The material parameters which constitutes the basis for the numerical analysis for the "NC30"concrete is summarized in Table 34.

Table 34: Summary of "NC30" material parameters.

Parameter	Value	Note
$E_{cm,22}$	29570 MPa	Calculated on basis of $f_{cm,i}$ [2] *
$E_{cm,15}$	29130 MPa	Calculated on basis of $f_{cm,i}$ [2] *
$f_{cm,22}$	26.8 MPa	Mean measured cylinder compressive strength
$f_{cm,15}$	25.5 MPa	Mean measured cylinder compressive strength
$f_{ctm,22}$	2.1 MPa	Calculated on basis of $f_{cm,i}$ **
$f_{ctm,15}$	2.0 MPa	Calculated on basis of $f_{cm,i}$ **
$G_{f,22}$	67.2 N/m	From Abaqus manual [34]
$G_{f,15}$	62 N/m	From Abaqus manual [34]
ε_{c1}	0.0035	Table 3.1 Eurocode 2 [2]
υ	0.2	

*$E_{cm,I} = 22[(f_{cm,i})/10]^{0.3}$ (Based on mean measured cylinder compressive strength in phase 2)

**Linearly interpolated according to Table 3.1 in Eurocode 2 [2] on basis of $f_{cm,i}$.

10.2.2.1 Tensile Data

The tensile data for the "NC30" concrete is based on fracture energy values, G_f, recommended in the Abaqus manual [34] for normal concrete, together with values for tensile strength f_{ctm} from Eurocode 2[2]. The values are adjusted for curing time of 15 and 22 days respectively.

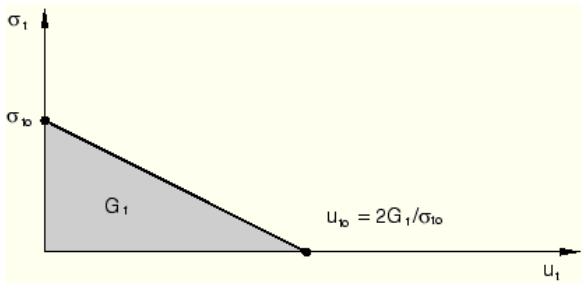

Fig. 97: Schematic representation of postfailure stress-fracture energy curve [34].

The tensile data is given to Abaqus in terms of stress and displacement with values from Table 33 together with the relationship expressed in (10.2) [34]. Fig. 97 explains the content of expression (10.2).

$$u = 2\frac{G_{f,ii}}{f_{ctm,ii}} \quad (10.2)$$

10.2.2.2 Compression Data

The compressive data is given as described in Section 10.2.1.2 but based on values from Table 34.

10.2.2.3 Reinforcement and Bond Between Concrete Layers

The yield stress for the reinforcement is given as 500MPa on basis of Eurocode 2 [2]. Only longitudinal reinforcement is included in the numerical model. The vertical reinforcement is excluded, instead perfect bond is assumed between the different concrete layers. Perfect bond is also assumed between the reinforcement and the concrete. The longitudinal reinforcement is added as embedded objects and placed in equivalent amount on correct center distances matching Fig. 80.

10.3 Element and Mesh

All analyses of the CSS are run with the CPS4 element. The element size is chosen on the bases of the thickness of the top and bottom layer and this resulted in global structured mesh with an element size of 50mm. Using an element size of approximately 50mm seems appropriate on basis of the distance measured between the bending induced cracks as summarized in Table 30.

10.4 Comparison between Numerical and Experimental Result of the Concept CSS Beams

Analyses with the above described parameters gave good correlation between the numerical analysis and the laboratory results. The results are plotted and compared with laboratory results Fig. 98. Since the CSS with top cast is under reinforced, it is easy to analyze the behavior of this structure after maximum load, due to reinforcement yielding controlling the deformation.

The CSS without the top cast is harder to analyze after top load since this structure failure is purely related to fracture mechanisms in the compression zone rather than reinforcement yielding. When studying the reinforcement stresses numerically it is seen that the reinforcement reaches yield more or less just as the maximum capacity is reached. This indicates good agreement with the hand calculations which concluded that the CSS without the top cast just barely is under reinforced.

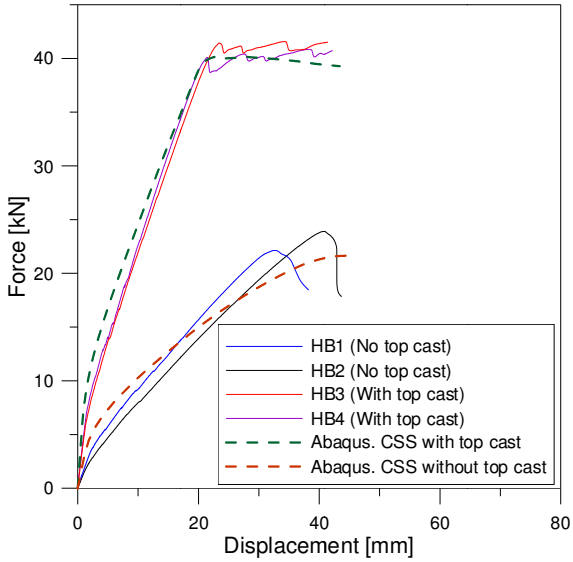

Fig. 98: Result from Abaqus analyses of CSS beams, with and without top cast, compared with laboratory results of CSS beams.

The crack pattern direction and variations generated in Abaqus also correlates well to the pattern from the laboratory tests. However, the concrete damage plasticity model cannot predict physical cracks and it is therefore not possible to compare crack widths and distances between single cracks with what was observed during the laboratory testing. The analysis crack pattern direction and variations can be read from an Abaqus symbol plot of the minimum in plane principle plastic strains as shown in Fig. 99.

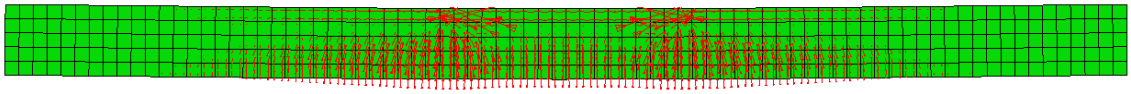

Fig. 99: Abaqus symbol plot of minimum in plane principle plastic strains from analysis of CSS beam.

10.5 Comparison between Hand Calculations and Experimental Result of the Concept CSS Beams

Hand calculations were performed after all material parameters for the Concept CSS beams in phase 2 had been established. As seen in Fig. 100 the correlation between the hand calculations and the numerical results is good.

In general the hand calculations were conservatively performed, as mentioned in Section 9.1. This is though not reflected in the results for the hand calculations for the Concept CSS beam without the top cast. This is most likely related to the brittle behavior of the LWAC and the fact

that the LWAC most likely would not be able to establish a fully utilized compression zone, as assumed for the hand calculations.

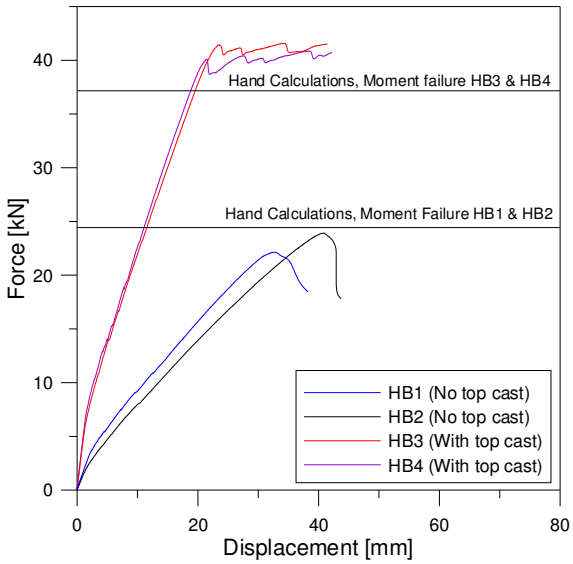

Fig. 100: Comparison between hand calculations and experimental results of the Concept CSS beams.

The results from the hand calculations are summarized in Table 35:

Table 35: Summarized capacities Concept CSS beams, based on measured material strengths.

Beam	V_{Rk} [kN]	M_{Rk} [kNm]	$l_{anchorage,Euro}$ [mm]	$L_{anchorage,NS}$ [mm]
CSS with top cast	38.205	24.62	120	94
CSS without top cast	32.236	16.19	120	≤94

$M_{Rk,w.top}$ = 24.62kNm corresponds to V_{max} = 18.58kN < **$V_{Rk,w.top}$ → Flexural tensile failure.**
$M_{Rk,wo.top}$ = 16.19kNm corresponds to V_{max} = 12.22kN < **$V_{Rk,wo.top}$ → Flexural tensile failure.**

11 Numerical Analyses of 6m Example CSS Beams

Until now, the Concept CSS beams have been considered in respect to absolute failure according to the laboratory results. No safety factors on the material or load have been considered.

In order to compare the Concept CSS with other existing products and determine maximum load bearing capacity according to governing regulations, it is essential to include material factors in the calculations and load amplification factors to the loading.

An example is illustrated with a simply supported beam with a span of 6m. The beam height is set to 250mm and 200mm with and without top cast respectively. In this example the same cross sectional properties has been used as the Concept CSS beam as described in Fig. 80. A sketch of the measures and load case used in the example are shown in Fig. 101. A unit width of 1m is used for the example beam.

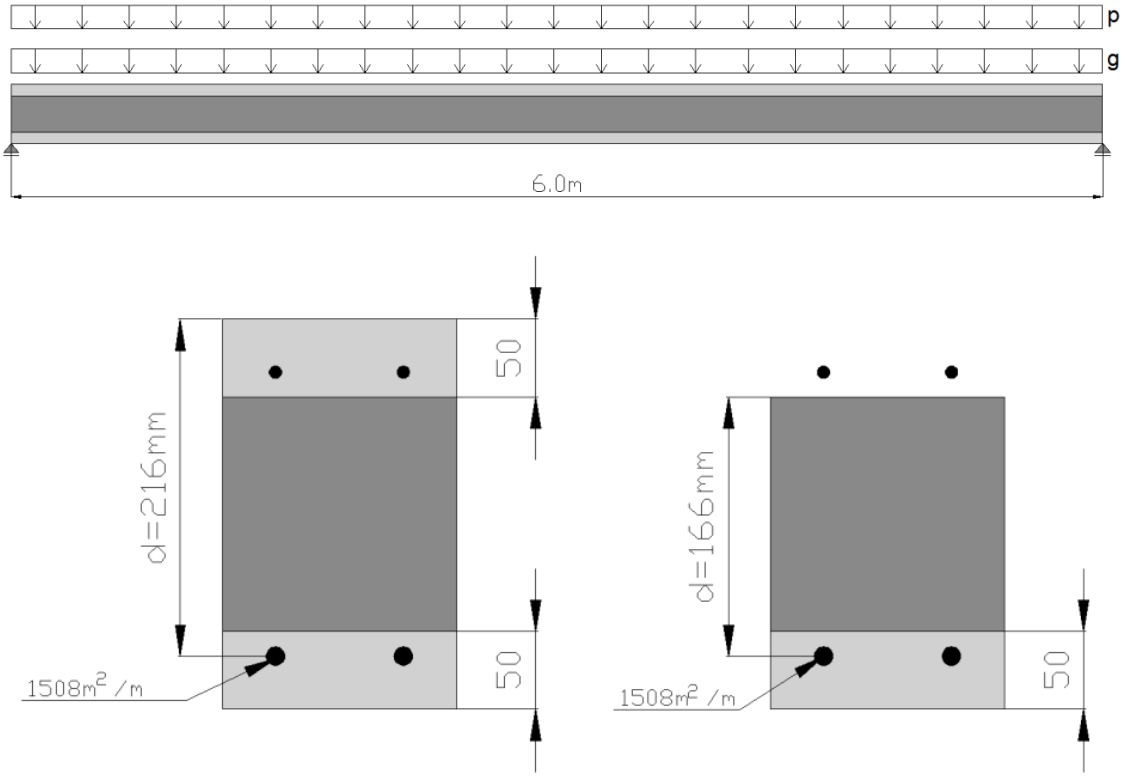

Fig. 101: Sketch of measures and loading for simple supported beam used in the example. Cross sections are assumed to have unit length of 1m.

11.1 Analyses Setup

Since the numerical analyses in Chapter 10 had good correlation with the laboratory results, it is chosen to use FEM analysis with the same basic setup to analyze this example beam. Changes done to the basic setup in Chapter 10 are the following:

- Concrete material input data; same as described in Section 10.2 but reduced with γ_c = 1.5
- Steel material input data; same as described in Section 10.2 but reduced with γ_s = 1.15
- Beam length; changed to 6000mm
- Loading; changed to distributed load

11.2 Analysis of Precast Part without Top Cast of Example CSS in Construction Phase

The 6m beam is analyzed without the top cast to represent the construction phase. Two sets of analyses are performed, one analysis with no supports in the span and one analysis with the beam temporary supported in the mid span.

During the construction phase the slab is going to be loaded with the weight from construction workers and necessary equipment in addition to the precast element's own dead and weight of the top cast. The following values are assumed:

- Dead weight including top cast:4.1 kN/m^2 with γ_g=1.2 (g = γ_g x 4.1 kN/m^2 = 5 kN/m^2)
- Workers and equipment: 3 kN/m^2 with γ_p = 1.5 (p = γ_p x 3 kN/m^2 = 4.5 kN/m^2)

This means a total distributed load of g+p = 9.5 kN/m^2 during the construction phase in the ULS and 7.1 kN/m^2 in the SLS.

11.2.1 Analysis Without Temporary Support

The example beam is first analyzed without temporary supports. The results from this analysis are presented in Fig. 102 in terms of distributed load versus mid span displacement. The analysis results are also compared with the assumed construction phase loading in ULS and SLS.

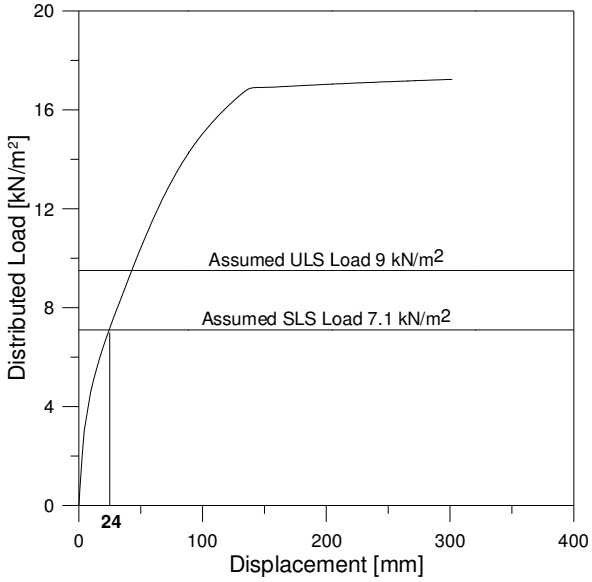

Fig. 102: Result from FEM analysis of example beam without top cast and temporary support. Results are presented in terms of distributed load versus mid span displacement and compared with the assumed construction phase loading in ULS and SLS.

At this load level the displacement is nearly 25mm which is just under the 30mm that is generally accepted, i.e. L/200 = 30mm. This is close to the maximum displacement accepted. In addition, contributions from creep and shrinkage will be added to the total displacement. This could possibly be solved by initial curvature on the precast element.

The result from this analysis looks promising with respect to use the CSS concept without temporary supports in the construction phase. However, it is difficult to state from only this analysis if it is possible to install the precast element without temporary supports and maintain acceptable displacements and crack widths.

11.2.2 Analyses With Temporary Support in Midspan

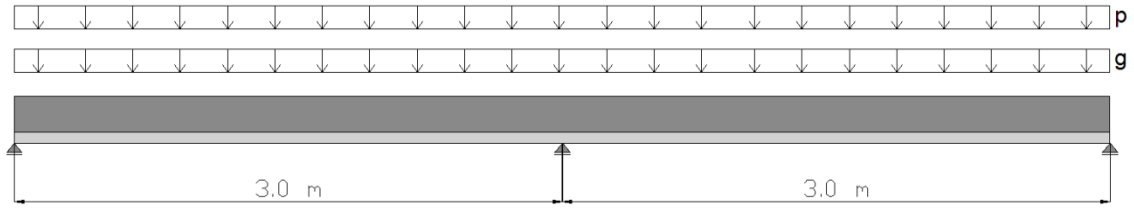

Fig. 103: Sketch of example beam with temporary support in mid span during construction phase.

An initial curvature on the precast element could be considered to reduce the final displacement, but the most efficient way of solving the problem would most likely be to use temporary supports at mid span.

The example beam is therefore analyzed with temporary support in mid span, i.e. a continuous beam with three support as shown in Fig. 103. The results from this analysis are presented in Fig. 104 in terms of distributed load versus maximum displacement in the span. The analysis results are also compared with the assumed construction phase loading in the ULS and the SLS.

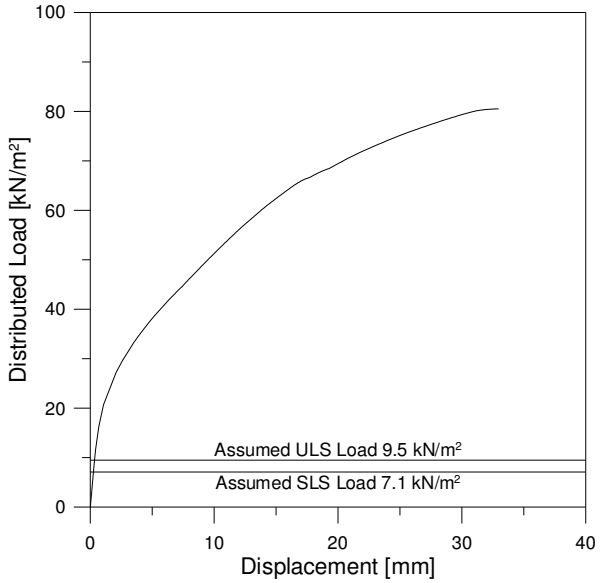

Fig. 104: Result from FEM analysis of example beam without top cast but with temporary support in mid span. Results are presented in terms of distributed load versus side span maximum displacement and compared with the assumed construction phase loading in the ULS and SLS.

The results from this analysis looks very promising with respect to displacement and utilization of the precast part of the example CSS beam. However, there is no structural steel reinforcement in the top of the example beam, which means only fiber reinforcement in the tension zone over the temporary support. This is not allowed according to today's existing design rules.

The plastic tension strains in the W1150 concrete over the temporary mid span support are approximately 0.27 ‰ according to the FEM analysis at a load level of 7.1kN/m^2. This seems to be at an acceptable level, especially since the top cast will cover cracks that might have formed. However, the result from these analyses should be taken with some caution since there are no documentation that can verify the results. It is encouraged to study the behavior of this beam without tension reinforcement in the top when it is supported in mid span.

11.3 Analysis of 6m Example CSS with Top Cast

The 6m example beam is also analyzed after the top is cast in order to show the final capacity. When the slab is taken in use, the type of loading defines the load case. In this example it is chosen to use the load case that NS 3491-1 [44] recommends for shopping centers and similar buildings, i.e. category D according to the standard. The following values are used:

- Dead weight including top cast:4.1 kN/m^2 with γ_g=1.2 (g = γ_g x 4.1 kN/m^2 = 5 kN/m^2)
- Loading: 5 kN/m^2 with γ_p = 1.5 (p = γ_p x 5 kN/m^2 = 7.5 kN/m^2)

This corresponds to a total distributed load in ULS of g+p = 12.5 kN/m^2 and 9.1kN/m^2 when the SLS is considered.

The results from the analysis are shown in Fig. 105 in terms of distributed load versus mid span displacement and compared with the example loading. These results look promising in respect to load level and displacement. The displacement from the loading is less than one third of the allowed L/200=30mm. However, additional displacement from creep and shrinkage must be considered as well.

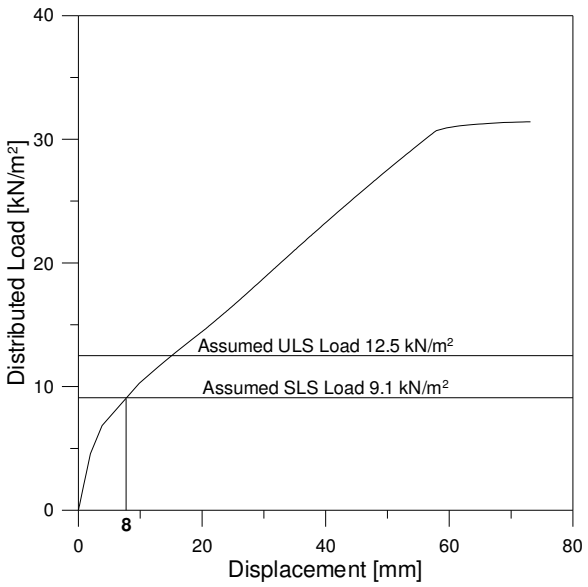

Fig. 105: Result from FEM analysis of example beam with top cast. Results are presented in terms of distributed load versus mid span displacement and compared with the example ULS usage loading of 12.5kN/m^2 and the corresponding SLS load case.

11.4 Comments

One goal with the design of the concept CSS slab is to be able to use the precast part with a minimum amount of supports during the construction phase. The initial analyses show that it is possible to use none or only one set of temporary supports in spans around 6m. This can be compared with today's existing products of combination of precast formwork and in-situ concrete, like the Con-form "Plattendekke" solution, which requires 2-3 sets of supports in the same span length.

Most slab constructions are limited by serviceability aspects related to maximum displacement. This means that it is hard to compare the maximum load level allowed on the concept CSS with other products at this point. The service ability limit state has been given some comments in Chapter 12 but it has not been a main focus in this report. Therefore further studies are needed in order to define the maximum loading that can be accepted for the CSS.

The initial analyses of the concept indicates that it can be competitive with existing products of combinations of precast and in-situ concrete due to reduced need of temporary supports. The concept also appears to be stronger than a 250mm Leca Byggeplank which has a maximum load carrying capacity of load of 5 kN/m^2 over a 6 m span [15].

12 Service Ability Aspects of the CSS Concept

So far in this report, all aspects considering loading and deflections have been related to the ultimate limit state. However, a very important design aspect for concrete structures is the service ability limit state (SLS) where crack width and deflections from creep and shrinkage must be considered. For concrete slabs with large spans, the design limitations are most commonly defined by SLS properties.

12.1 Shrinkage

In a homogenous unreinforced concrete structure, shrinkage is usually not a problem since it causes the concrete to shrink evenly. As long as the concrete structure can shrink in all directions with no resistance, shrinkage will not cause any stresses or curvature to the structure.

However, concrete structures are usually reinforced with most of the reinforcement on the tension side. This causes resistance when the concrete shrinks which leads to curvature. This is initially not a problem, however too much curvature can cause not acceptable deflections and cracks. The effects of shrinkage in reinforced and unreinforced structures are shown in Fig. 106.

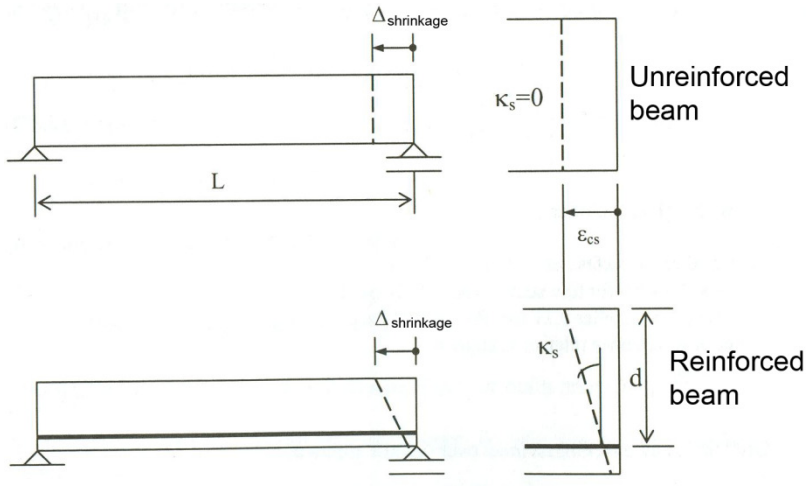

Fig. 106: Effects of shrinkage on unreinforced versus reinforced beam [45].

Total shrinkage ε_{cs} can be separated into two parts, drying shrinkage ε_{cd} and autogenous shrinkage ε_{cs}. Total shrinkage is described of the following relation (12.1):

$$\varepsilon_{cs} = \varepsilon_{cd} + \varepsilon_{cs} \tag{12.1}$$

The curvature can then be calculated easily by the following simplified expression (12.2):

$$\kappa_s = \frac{\varepsilon_{cs}}{d} \tag{12.2}$$

Drying shrinkage starts as soon as the relative humidity of the concrete structure becomes less than 100%. The autogenous shrinkage starts as soon as the curing process of the concrete starts. The drying shrinkage can be reduced by not letting the concrete dry to quick.

Like LWAC in general, the W1150 concrete suffers more from shrinkage than normal concrete. SINTEF Byggforsk has an ongoing shrinkage study in progress [46] for this specific kind of concrete, but with some small modifications regarding the recipe compared to the W1150 concrete used in this report. The results from the first 365 days on this study are plotted in Fig. 107. In the figure, the W1150 shrinkage is compared with theoretical shrinkage of a B30 concrete calculated with Eurocode 2 [2]. As one can see, the shrinkage on the W1150 concrete is approximately twice as large as for the B30.

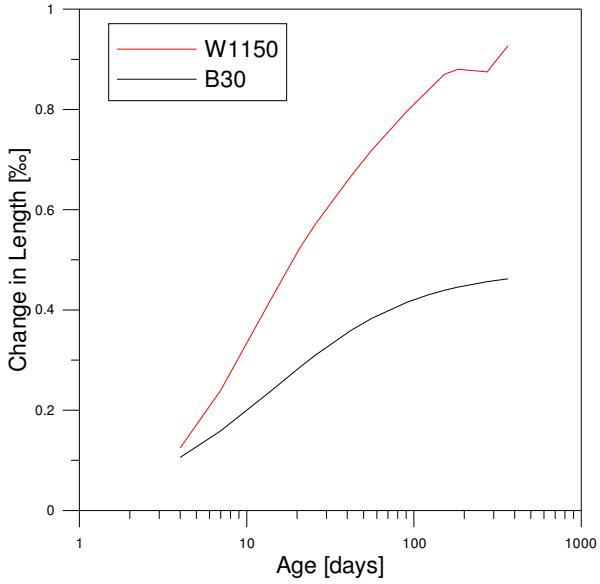

Fig. 107: Results from SINTEF shrinkage study on the W1150 concrete compared to theoretical shrinkage of B30 concrete calculated with Eurocode 2 [2].

12.1.1 Shrinkage of the CSS

A composite structure is very sensitive to shrinkage if the composite materials have different shrinkage properties. With its three layers, the CSS can be compared with a laminate compounded by two different concrete materials with different shrinkage properties.

A general laminate with thickness *h* and laminate stiffness $Q^k_{i,j}$ is shown in Fig. 108. The general expression relating forces and moments to strains and curvatures are shown in Fig. 109.

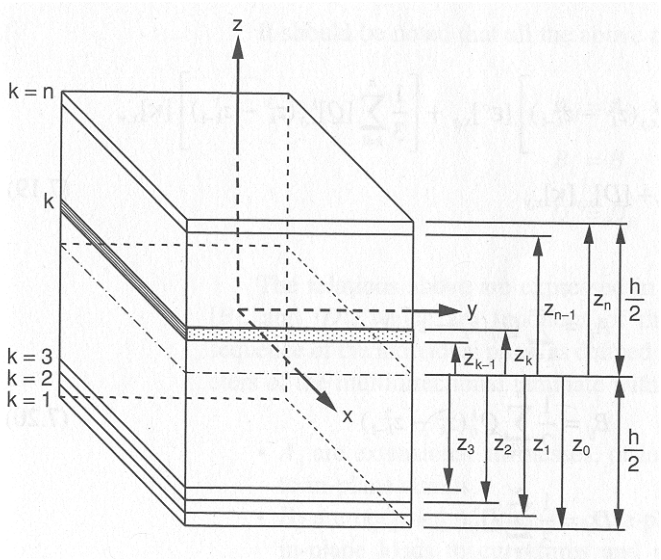

Fig. 108: General multidirectional laminate with coordinate notation of individual plies [47].

$$\begin{bmatrix} N_x \\ N_y \\ N_s \\ \hline M_x \\ M_y \\ M_s \end{bmatrix} = \left[\begin{array}{ccc:ccc} A_{xx} & A_{xy} & A_{xs} & B_{xx} & B_{xy} & B_{xs} \\ A_{yx} & A_{yy} & A_{ys} & B_{yx} & B_{yy} & B_{ys} \\ A_{sx} & A_{sy} & A_{ss} & B_{sx} & B_{sy} & B_{ss} \\ \hline B_{xx} & B_{xy} & B_{xs} & D_{xx} & D_{xy} & D_{xs} \\ B_{yx} & B_{yy} & B_{ys} & D_{yx} & D_{yy} & D_{ys} \\ B_{sx} & B_{sy} & B_{ss} & D_{sx} & D_{sy} & D_{ss} \end{array}\right] \begin{bmatrix} \varepsilon^o_x \\ \varepsilon^o_y \\ \gamma^o_s \\ \hline \kappa_x \\ \kappa_y \\ \kappa_s \end{bmatrix}$$

$$A_{ij} = \sum_{k=1}^{n} Q^k_{ij}(z_k - z_{k-1})$$

$$B_{ij} = \frac{1}{2}\sum_{k=1}^{n} Q^k_{ij}(z_k^2 - z_{k-1}^2)$$

$$D_{ij} = \frac{1}{3}\sum_{k=1}^{n} Q^k_{ij}(z_k^3 - z_{k-1}^3)$$

Fig. 109: General expression to relate in-plane forces and moments to reference plane strains and curvatures [47].

If the CSS is considered, it can be simplified to a symmetric laminate after the top is cast. This means that the coupling matrix, $B_{i,j}$ will have all its elements equal to zero, $B_{i,j} = 0$ because of the symmetry. From Fig. 109 it can be seen how the expression for $B_{i,j}$ only will return zero values for symmetric laminates and that in plane strains, as for example shrinkage strains, will not cause any moment and consequently no curvature.

However, the prefabricated part of the CSS is asymmetric and suffers therefore of severe curvature problems due to changes in plane strains. In this case, the coupling matrix $B_{i,j} \neq 0$

which means correlation between strains and curvature. Since the stiffer material is located in the bottom, the curvature induced by shrinkage will have the same direction as the curvature from later loading. This is not a desired behavior. In addition to this, the reinforcement will increase the curvature effects.

The shrinkage induced curvature on the prefabricated part of the CSS can be evened out by casting it with an initial curvature in the opposite direction. However, this can only be done if the crack widths can be held on a reasonable level. Another solution to the problem could be if the prefabricated part of the CSS could be stored with a relative humidity close to 100% until the top layer is to be cast. Then the drying shrinkage would not start before the top is in place and the structure would have the behavior of a symmetric laminate. The autogenous shrinkage will still cause some curvature, but this part is small compared to the drying part.

12.2 Creep

SINTEF have also performed a study on creep properties for the W1150 concrete [48]. The study concludes that the normal expressions in Eurocode 2 for determination of creep property for LWC are not eligible for the W1150. It is also concluded that the W1150 have a larger creep than traditional LWAC.

12.3 Crack

The CSS will as other concrete structures crack in the tension zones due to large deflections at one point, if the structure is loaded enough. The W1150 concrete in the middle layer of the CSS will also crack when it suffers from drying shrinkage, since it is held back by the top and bottom layer. However, the cracks that will form in the middle layer are of less concern than cracks induced by flexural tensile stresses in the bottom layer. Since the middle layer is protected and encased by the “NC30”, the cracks induced by shrinkage are not a durability related problem in this case.

13 Discussion and Suggestions for Future Work

13.1 Test Phase 1

Even though the W900 concrete has to be developed a lot further, the concrete has potential as a component in the CSS. The weight reduction for the CSS tested in this report would be 10% if the W1150 concrete is swapped for the W900 concrete in the middle layer, a reduction worth considering. A better and more thoroughly developed recipe for the W900 concrete could solve the problem with the poor castability and separation issues. If a new recipe can be developed, it should be considered to perform new laboratory tests with the W900 concrete in the middle layer.

The W1150 concrete showed less compression strength than the predicted 20MPa after 28-days of curing. However, after 62-days this concrete had reached a compression strength of 27 MPa in average for the cubes tested. Whether this increase is a result of a longer curing period, curing conditions or other factors can not be concluded upon. This is an interesting progression and must be studied more closely if this concrete is going to be used in later studies.

The obtained compressive capacities for the W900 concrete were also below the predicted capacity. However, this concrete did not show any increase in capacity after long time of curing.

Results from the tensile specimens indicated that using a steel fiber content lower than 0.5%, does not fulfill the minimum reinforcement requirement for the LWAC. A sudden drop in capacity after yielding in tension was observed for the specimens with just 0.5% steel fiber content, while the specimens with 1% achieved an initial hardening post yielding. The results in this report together with earlier research at NTNU [17], indicate that a favorable steel fiber content is in the range of 1% - 2.5% for this specific type of concrete. It should however be noted that an increase in the steel fiber content beyond 0.5%, seems to increase the risk of collective anchorage failure in the LWAC.

Results from the flexural tensile specimen indicated a pronounced increase in both maximum and post critical capacity when increasing the steel fiber content from 0.5% to 1.0%. In contrast, a decrease was actually observed in earlier research using the same steel fiber type and content [17]. Different specimen geometry, testing method and maybe varying concrete quality makes it difficult to state a conclusion in this case.

The shear beam test also showed that the W900 concrete has potential, due to its relatively large shear capacity. The fact that the shear capacity increased by almost 30%, going from 0.5% fiber by volume to 1% is a remarkably good result even though the design rules in the Steel Fiber Draft [26] indicate such a high increase in capacity. The good correlation between the hand calculations and the laboratory results indicates that the design rules in the Steel Fiber

Draft [26], seems to be valid for the W900 and the W1150 concrete. However, the results should be taken with some caution due to the small test series and the W900 concretes varying quality.

It should also be commented that slab constructions in general, rarely are subjected to large shear forces and the need of up to 1% fiber reinforcement can be discussed. The structural load case must of course be considered from case to case. Using a higher fiber content locally at concentrated point-loads could however be considered.

It was unfortunate that the reference shear beam with 0% fiber was not tested correctly so that it could be compared to the shear beams with fiber. A new shear test with no steel fiber reinforcement should be considered in the future in order to state the need of fiber.

13.2 Test Phase 1: Numerical Analyses

Analyses of the tension specimens showed very good correlation with the laboratory results. The best numerical result was obtained when the element size was set equal to the notch width.

The correctness of setting the element size to 4mm or even smaller in FEM analyses of concrete can be discussed. By using small elements, the concrete is analyzed on aggregate and fiber level rather than being analyzed on the concrete level, i.e. as a conglomerate of cement paste, aggregate and fiber. Setting the element size to 4mm had little influence on the tension specimens were all the deformation was concentrated to uniaxial tension over the notch width. However, if we take this argument into account, a general concrete structure without notches should be analyzed with elements larger than the aggregate and fiber size.

Analyses of the flexural tensile beams were a bit more difficult to perform since the deformations no longer were uniaxial. The 2-dimensional analyses could predict a maximum capacity which was similar to the obtained capacity in the laboratory. However, the post critical behavior differed in the analysis compared to the laboratory results. The reason for this could be many, but most likely the problems are partly related to the plasticity parameters. These parameters are not taken into account correctly in a 2-dimensional plane stress analysis. Another reason could be the element size, due to the previous argument of why an element size of 4mm in the notch might not give a good representation of the concrete conglomerate.

3-dimensional analyses of the flexural tensile beams partly helped to explain the wrong post critical behavior, since the parameter study showed that the plasticity parameters could be chosen more wisely. However, the analysis results are not spot on the results from the laboratory and more work could be done with the mesh selection and element size. Later studies should focus on a wiser meshing approach and maybe another way of defining the notch. This could for example be done by using a discrete modeling approach or by using some sort of interface elements.

The compressive input data given to the analysis is another unsure factor that could affect the results. The compression input stress-strain relation is based on the rules given in Eurocode 2.

Since the Weber foam concrete differ from normal concrete and traditional LWAC's, it is unsure whether the compressive stress-strain relation described in Eurocode 2 can be used to describe this concrete. The only way to figure that out is to do displacement controlled laboratory testing of compression cylinders with the Weber concrete. This is not performed in this report, but is encouraged to do in further research if it is desirable to document the Weber concrete more thoroughly. More carefully chosen material models should also be considered in future work.

In the analyses of the specimen from test phase 1, the simplified relation to interpret compressive behavior from Eurocode 2 was used. By using the nonlinear relation, better correlation could have been obtained. The nonlinear relation was used in the analyses in test phase 2 and the rest of the analyses performed in this study.

13.3 Test Phase 2

The W1150 concrete produced at NTNU during test phase 2 did not obtain similar compressive strength as the W1150 concrete produced in Lillestrøm in test phase 1. The compression testing revealed a 30% reduction in compressive strength for the concrete produced at NTNU even though the recipes used in both productions were identical. This decrease in capacity could be related to the foam production. At NTNU the foam was produced using simple mixers, while the foam was produced using an especially made foam generator in phase 1.

The concrete produced at NTNU had no increase in capacity past 28 days as the W1150 produced in Lillestrøm. This strengthens the theory of worse attained concrete quality for the W1150 concrete in test phase 2.

The force–displacement relation recorded from the laboratory testing of the Concept CSS beams with top cast, shows that they have good post critical capacity with a very predictable and safe behavior. This is a desirable behavior and indicates that the structure is under reinforced. Before the tests it was feared that the beams would suffer from a sudden capacity drop due to brittle behavior of the LWAC. This was not the case and that indicates further that the failure is controlled purely by the top layer with normal concrete and the tension reinforcement.

However, this is not the case for the beams without top cast which show a sudden drop in capacity. This is most likely explained by the fact that the beams were concluded to just being under-reinforced. In addition a more brittle behavior of the compression zone was expected since it in this case purely contains LWAC. The brittle behavior can lead to partially utilized compression zone which causes a different distribution of the compression zone forces. This could make the structure over-reinforced due to a weaker compression zone. If this is the case, more care should be taken in the construction phase if the utilization degree is large. Alternatively, the amount of reinforcement in the CSS should be chosen more carefully to ensure under-reinforced behavior both in the construction and final usage phase.

Another feared behavior was insufficient shear bonding capacity between the different concrete layers. The laboratory tests revealed no signs of such capacity problems. This indicates that the sizes of the estimated shear forces predicted before the tests were to the conservative side. The vertical reinforcement loops together with the concrete's bonding properties were sufficient to handle the acting shear forces between the layers. Studies regarding the bonding properties between the normal concrete and the LWAC are currently being performed at NTNU which might state a final conclusion on the need of the vertical reinforcement loops.

The need of a "high performance" compression zone, i.e. normal concrete in the top layer is obvious. However, the need of normal concrete in the bottom layer can be discussed. If the bonding capacity between the Weber foam concrete and the reinforcement can be shown to be sufficient, there are no limitations in using the W1150 concrete in both the bottom and middle layer capacity wise. The challenges can instead be related to the W1150's relatively more open pore structure compared to the normal concrete, which can result in a less durable structure. Laboratory testing of CSS beams with W1150 concrete in both the bottom and middle layer are recommended to be tested and compared with the results from this report in later work. Calculations associated with the compression zone height also indicate that the height of the top cast could be reduced in order to save further weight without reducing the capacity. Casting aspects could though govern the size of the top layer.

Since the factor of limitation is related to the top layer's compressive strength, one could motivate the use of a more high performance concrete in the top layer.

13.4 Test Phase 2: Numerical Analyses

The analyses performed of the concept CSS showed good correlation with the laboratory results, especially the analyses of the beam with the top cast. This was however expected since a failure caused by yield in the reinforcement naturally is easier to analyze compared to fracture in the compression zone for the beams without the top cast. The maximum capacity predicted by the numerical analysis correlate very good with the laboratory results. These results indicate that the numerical model works fairly well for the Concept CSS beam and that the model can be used as a basis for further calculations.

Assumptions made associated to bond properties (complete bond) between reinforcement and between the different concrete layers seem to be valid on basis of observations made in the laboratory. None of the observed failure mechanisms could be related to the bond properties.

Even though the numerical analysis performed in relation to the concept CSS beams were done in 2D, very good correlation with the laboratory results was obtained. However, in further studies it is recommended to perform 3D analysis of the CSS concept. Experience gained when modeling the small scale test specimens from phase 1 indicated that better correlation and more realistic behavior was predicted by a 3D numerical analysis.

13.5 CSS Beam Example

Very good correlation was observed for the numerical model used for analyzing the concept CSS beams. On basis of this numerical model a CSS beam example was performed for a 6m span. The initial impression was very positive since the CSS concept seemed to have adequate capacity both in the construction phase without top cast, as well as in final use with top cast.

Requirements related to serviceability aspects seemed to be the limiting factor for the CSS, especially displacements, and thereby crack widths, in the construction phase. Such issues could be solved by casting the CSS elements with an initial curvature. However, by using supports in the mid span it is possible to adjust the position of the precast CSS elements before the top is cast, in order to obtain an even ceiling surface. This also reduces the displacements to a more acceptable level.

If the CSS elements are produced using the W900 concrete in the middle layer, an elements weight of approximately 250 kg/m^2 could be achieved. CSS elements could then be produced with similar size of the today's existing "Plattendekke" solution, i.e. 2.4m x 7.2m. These elements would be of an acceptable weight for being installed at the construction site similar as the "Plattedekke" solution, using for example a tower-crane. The complete weight of the CSS concept would be up to 35% lighter than a traditional homogenous concrete slab with thickness of 250mm.

The CSS concept's relatively large stiffness in the construction phase, makes it ideal to be used in for example pier/harbor structures where temporary support in the construction phase is hard to achieve for in-situ concrete slabs which require traditional formwork.

13.6 Service Ability Aspects for the CSS

It can be concluded that a composite structure offers a wide range of challenges when it comes to SLS aspects. These are problems that must be considered, tested and solved before the CSS is ready for the market and can be launched.

Since creep is a bigger issue for the W1150 concrete compared to normal LWAC, a study on creep and perhaps laboratory experiments must be carried through in order to state the behavior of the CSS. It is important to establish data of the behavior of this specific construction under different load cases.

It is also important to study the crack development in this structure and state how big curvatures that are accepted before the crack openings will start to influence the durability properties.

14 Conclusion

Through laboratory experiments and numerical analyses, material parameters and behavior of the special lightweight concrete was documented. The W900 concrete did not have acceptable behavior with respect to strength and cast properties. Nevertheless, seen in relation to the CSS concept, the W900 concrete has greater potential than the W1150 concrete and should be given more focus in later research.

Tensile and 3-point bending tests indicate that a pronounced increase in both maximum and post critical capacity is achieved when increasing the steel fiber content from 0.5% to 1%. The desirable steel fiber content for the specific LWAC and fiber type used in this report seems to be approximately in the range of 1-2.5%. However, it should be noted that using a fiber content higher than 1% would increase the risk of collective anchorage failure in the LWAC.

The concept CSS beams tested in the laboratory together with subsequent numerical analysis indicate that the CSS concept is very competitive to today's existing concrete slab solutions with respect to load carrying capacities. Analyses indicate that the CSS precast elements could be installed without or with a small amount of temporary supports compared to existing similar solutions due to its relatively high stiffness. This would lead to saved time, space and money at the construction site.

Serviceability aspects seem to limit the capacity of the CSS concept with respect to displacements as for most concrete slab structures. Further research is necessary in order to document the CSS concept's behavior when serviceability aspects are taken into account.

Hybrid concrete structures with fiber reinforcement are generally complicated to analyze with concrete hand calculation rules as well as with numerical analysis. The results obtained from hand calculations and numerical analyses in this report, shows however good correlation with laboratory results.

15 References

1. **Jacobsen, Stefan.** *Lecture Notes, BM3.* Trondheim : NTNU, 2006.

2. **CEN, European Standard.** *NS-EN 1992-1-1:2004 "Design of concrete structures, general rules and rules for buildings".*

3. **Larsen, Per Kristian.** *Samvirkekonstruksjoner i stål og betong.* Trondheim : NTNU, 2006.

4. **New Crossing.** *www.newcrossing.gov.bm.*

5. **Johansson, Mathias.** *Composite Action and Confinement Effects in Tubular Steel-Concrete Columns.* Gothenburg : Chalmers University of Technology, 2002.

6. **CEN, European Standard.** *EN 1994-1-1 "Design of composite steel and concrete structures".*

7. **Plannja.** *www.plannja.com.*

8. **Constructalia.** *www.constructalia.com.*

9. **CEN, European Standard.** *EN 1993-1-3 "Supplementary rules for cold-formed thin gage members and sheeting".*

10. **Lawrence C. Bank, et.al.** *Hybrid Pultruded Plank with a Concrete Compression Flange for Pedestrian Bridges.* Tampa, FL, USA : COMPOSITES & POLYCON, 2007.

11. **Schaumann, Erika et.al.** *Shear Resistance of Lightweight Concrete Core of.* s.l. : ACI MATERIALS JOURNAL, 2009.

12. **Arnslett, Hans.** *Master Thesis.* Trondheim : NTNU, 2006.

13. **Svecon Steel AB.** *www.sveconsteel.se.*

14. **Con-Form AS.** *www.con-form.no.*

15. **Weber.** *Brochure "Leca Byggeplank Proff".*

16. **Contiga AS.** *www.contiga.no.*

17. **Kanstad, Terje.** *Fibre Reinforced Superlight Concrete: Testing of Materials and Full Scale Beams.* Trondheim : COIN, SINTEF Building and Infrastructure, 2009.

18. **Engesæter, Rune.** *Masteroppgave.* Trondheim : NTNU, 2009.

19. **Tue, Jan Vincent.** *Professor NTNU, Discussion.*

20. **CEN, European Standard.** *NS-EN 12390-3:2009 "Testing hardened concrete, compressive strength of test specimens".*

21. **CEN, European Standard.** *NS-EN 12390-1:2000 "Testing hardened concrete. Shape, dimensions and other requirements for specimens and moulds".*

22. **SINTEF Byggforsk.** *Strekkprøving av betong- Bestemmelse av E-modul og fasthet ved sentrisk strekk.* 2007.

23. **CEN, European Standard.** *NS-EN 14651:2005 "Test method for metallic fiber concrete, Measuring the flexural tensile strength".*

24. **ASTM.** *Standard Test Method of Flexural Toughness of Fiber Reinforved Concrete (Using Centrally Loaded Round Panel).* 2009.

25. **Stemland, Hans and Thorenfeldt, Erik.** *Lett konstruksjonsbetong, Delprosjekt 2 Konstruktive aspekter, Delrapport 2.3 Skjærkapasitet av lettvektsbetongbjelker uten skjærarmering med Leva 700 grovt tilslag og naturlig sand.* s.l. : SINTEF Bygg og miljøteknikk, 1999.

26. **Thorenfeldt, Erik et.al.** *Stålfiberarmering i betong; Veiledning for prosjektering utførelse og kontroll. Høringsutkast Mai 2006.* 2006.

27. **Banthia, N. and Trottier, J-F.** *Concrete Reinforced with Deformed Steel Fibers, Part 1: Bond-Slip Mechanisms.* s.l. : ACI Materials Journal, Vol 91, No. 5, Sept-Oct, pp.435-446, 1994.

28. **Myhre, Martin Næsgaard.** *Fibre reinforced concrete structures: Materials technology, execution and testing of LWAC beams.* Trondheim : NTNU, 2009.

29. **StandardNorge.** *NS 3473. Prosjektering av betongkonstruksjoner. Beregnings- og konstruksjonsregler.* 2003.

30. **Sandbakk, Sindre.** *COIN/SINTEF Researcher.*

31. **RILEM.** *TC 162-TDF: Uni-axial tension test for steel fibre reinforced concrete.* 2001.

32. **Nes, Linn Grepstad.** *Comments from supervisor.*

33. **Døssland, Åse Lyslo.** *Doctoral thesis; Fibre Reinforcement in Load Carrying Concrete Structures.* Trondheim : NTNU, 2008.

34. **Simulia.** *Abaqus 6.9 Documentation.* 2010.

35. **Mathiesen, Kjell Magne.** *Lecture notes,TKT4197 Nonlinear Finite Element Analysis.* Trondheim : NTNU, 2009.

36. **Chen, Wai-Fah.** *Plasticity in Reinforced Concrete.* New York : McGraw-Hill, 1982.

37. **J. Lubliner, et.al.** *A Plastic-Damage Model For Concrete.* s.l. : University of California, Berkeley, 1989.

38. **Lee, J. and Fevnes, G.L.** *Plastic-Damage Model For Cyclic Loading of Concrete Structures.* Berkeley : University of California, 1998.

39. **Hobbs, B.E. et.al.** *Numerical simulation of shearband formation in frictional-dilatiational materials.* 1989.

40. **Diana 9.4 Users Manual.** s.l. : TNO Diana, 2009.

41. **Poliakov, A.N.B et.al.** *Initiation of salt diapirs with frictional overburdens: numerical experiments.* Amsterdam : Elsevier Science Publishers, 1993.

42. **Serway, Raymond A. et.al.** *Physics for Scientists and Engineers.* s.l. : Thomson Brooks/Cole, 1996.

43. **Pavlovic, M.D. Kotsovos & M.N.** *Ultimate limit state and design of concrete structures, a new approach.* London : Thomas Telford Ltd, 1999.

44. **Standard Norge.** *Basis of design and actions on structures - Part 1: Densities, self-weight and imposed loads.*

45. **Sørensen, Svein I.** *Betongkonstruksjoner.* Trondheim : Tapir, 2000.

46. **SINTEF Byggforsk.** *Reasearch in Progress "Schrinkage Determination of Concrete with Foam".* Trondheim : s.n., 2009 - .

47. **Daniel, Isaac M. and Ishai, Ori.** *Engineering Mechanics of Composite Materials.* New York : Oxford, 2006.

48. **Ola Skjølsvold, Hans Stemland.** *Prøving av lettbetong med skum, bestemmelse av kryptal.* Trondheim : SINTEF Byggforsk, 2010.

A.1 Mixing Procedures, Phase 1

Table A.1.1: Phase 1, Mixing procedure Weber foam concrete (W900 and W1150).

Date	Location	Batch No.	Number of Mixes	What was casted
February 19th, 2010	Weber Lillestrøm	B0 B1a , B2a B1b, B2b B3	One of each batch	Comp. cubes Comp. cylinders Tension prisms Bending prisms Round Panels Shear Beams

All materials had been weighed and prepared in advance by Weber in Lillestrøm. The concrete was mixed using a simple concrete mixer with a maximum capacity of 200L. The foam was produced using a foam generator.

Summarized mixing procedure:

1. Mixing of dry materials, PP fibers and steel fibers.
2. Adding of water
3. Adding of air reducing and superplasticizing additives
4. Measure density
5. Adding of foam until wanted wet density is reached

Both the W900 concrete and the W1150 concrete were casted the same day in Lillestrøm with the same mixing procedure. The W900 concrete (B0, B1a, B1b, B2a, B2b) was developed recently and had not been experimented with in large scale. While mixing it was observed a lot of air bubbles in the concrete, it seemed as it was boiling. It was concluded that the large amount of super plasticizer most likely was the cause. To counteract the effect of artificial air the amount of super plasticizer was reduced while the amount of cement, sand and water was increased. A fairly stable concrete was then achieved with the W900 concrete. The casting ability for the W900 concrete was bad with 0% steel fiber volume and it became even worse when the amount of steel fiber were increased.
The W1150 concrete (B3) has been developed and thoroughly tested in large scale by Weber. Good casting ability was achieved, even with 1vol% steel fiber content.

A.2 Mixing Procedures, Phase 2

Table A.2.1: Phase 2, Mixing procedure middle layer hybrid beams, Weber foam concrete (W1150).

Date	Location	Batch No.	Number of Mixes	What was casted
April 12th , 2010	M-Lab NTNU Trondheim	HB1, HB2 HB3, HB4	1 of each	Middle layer of hybrid beam

All materials had been weighed, prepared and quality controlled in advance by the writers of this report. The concrete was mixed using a professional industrial type concrete mixer with a maximum capacity of 100-250L (Gustav Eirich EBG 3). The foam was produced using a Kenwood Titanium Major food mixer and a Hobart A 200 food mixer. It must be noted that all liquids used in the production of this concrete had a temperature of 20°C. This was done in order to achieve a good effect of the foam on recommendation from Weber.

Summarized mixing procedure foam: Kenwood Titanium Major food mixer

1. Liquid A (245grams) is added to the mixer and run at about 2 minutes at speed 6. Liquid temperature 20°C.
2. Liquid B (23g, stabilizer) is added to the mixer and run at about 2 minutes. Liquid temperature 20°C.

With a density of about 60 grams/liter 4L is produced with the Kenwood

Summarized mixing procedure foam: Hobart A 200 food mixer

1. Liquid A (490grams) is added to the mixer and run at about 3 minutes at speed 3. Liquid temperature 20°C.
2. Liquid B (46g, stabilizer) is added to the mixer and run at about 3 minutes. Liquid temperature 20°C.

With a density of about 60 grams/liter 8L is produced with the Hobart

Summarized mixing procedure concrete:

1. Mixing of dry materials, 1 minute
2. Adding water, air reducing and super plasticizing additives, PP fibers and steel fibers while mixing, 2 minutes. Liquid temperature 20°C.
3. 2 minutes pause
4. 1 minute remixing
5. Adding 15L foam while mixing
6. Measure density
7. Adding foam until wanted wet density is reached (5L foam added)

The W1150 concrete (HB1-HB4) had good casting abilities with 1 vol% steel fibers, no negative qualities worth mentioning was observed during mixing and casting.

Table A.2.2: Phase 2, Mixing procedure bottom layer hybrid beams, normal concrete ("B30").

Date	Location	Batch No.	Number of Mixes	What was casted
April 12th , 2010	M-Lab NTNU Trondheim	HB1, HB2 HB3, HB4	1 of each	Bottom layer of hybrid beam

All materials had been weighed, prepared and quality controlled in advance by the writers of this report. The concrete was mixed using a professional industrial type concrete mixer with a maximum capacity of 50L (Gustav Eirich SKG 1).

Summarized mixing procedure concrete:

1. Mixing of dry materials, 1 minute
2. Adding water and super plasticizing additive, 2 minutes mixing.
3. 2 minutes pause
4. 1 minute remixing

The mixing of the normal concrete did not lead to any problems. The concrete was stable and easy to work with.

Table A.2.3: Phase 2, Mixing procedure top layer hybrid beams, normal concrete ("B30").

Date	Location	Batch No.	Number of Mixes	What was casted
April 19th , 2010	M-Lab NTNU Trondheim	T	1	Top layer of hybrid beam

All materials had been weighed, prepared and quality controlled in advance by the writers of this report. The concrete was mixed using a professional industrial type concrete mixer with a maximum capacity of 100-250L (Gustav Eirich EBG 3).

Summarized mixing procedure concrete:

1. Mixing of dry materials, 1 minute
2. Adding water and superplasticizing additive, 2 minutes mixing.
3. 2 minutes pause
4. 1 minute remixing

The mixing of the normal concrete did not lead to any problems. The concrete was stable and easy to work with.

Proporsjonering på volumbasis — Fyll inn i gule felt — Resept 4.03.2009

TNO 2006-10-18

Oppnådde verdier	Verdi	Verdi	Enhet
Sementlim	504		l/m³
v/(c+Σkp)	0,40	-	-
s/(c1+c2)	0,092	9,21	%
fa/(c1+c2)	0,000	0,00	%
mLWA/(C1+C2)	0,000	0,00	%
kalkfiller/(c1+c2)	0,000	0,00	%
BASF Glenium SKY 550	0,019	1,89	%
Skum	0,000	0,00	%
BASF Glenium Steam	0,005	0,53	%
Luftinnhold		18,0	%
Matriksmengde	514		l/m³

Merknader

Vannabsorpsjon, tilslag (%)	
Leca 2-4 mm	6,0
sand 0-4 mm Lillestrom	1,0
0	0,0
0	7,0
Ingen	
Ingen	

Materiale	Densitet	k
Norcem Industri	3150,0	1
Norcem Anlegg	3150,0	1
Silikastøv	2200	2
Flyveaske	2200	0,7
Micro LWA	2600	1
Kalksteinfiller	2600	0
BASF Glenium SKY	1200	
Skum	1200	
BASF Glenium Ste	1200	

Proporsjonert betong

Materialer	kg/m³	l/m3	kg/0,181m³	40 l bl
Norcem Industri	114,00	36,2	20,634	4,560
Norcem Anlegg	266,00	84,4	48,146	10,640
Silikastøv	35,00	15,9	6,335	1,400
Flyveaske	0,00	0,0	0,000	0,000
Micro LWA	0,00	0,0	0,000	0,000
Kalksteinfiller	0,00	0,0	0,000	0,000
BASF Glenium SKY 550	7,20	6,0	1,303	0,288
Skum	0,00	0,0	0,000	0,000
BASF Glenium Steam	2,00	1,7	0,362	0,080
Tilsatt vann	180,00	180,0	32,580	7,200
Luftinnhold		180,00	0,000	0,000
Sum pasta	604,2	504,2	109,360	24,168
Leca 2-4 mm	230,0	418,2	41,630	9,200
sand 0-4 mm Lillestrom	400,0	149,8	72,400	16,000
0,0	0,0	0,0	0,000	0,000
0,0	0,0	0,0	0,000	0,000
Luftdemper	0,123	0,0	0,022	0,005
BASF MECH PP 150	1,500		0,272	0,060
Bekaert 30/35 Stålfiber	40,0		7,240	1,600
Sum tilslag	671,6	568,0		
Prop. betongdens. (kg/m³)	1,1899	1072		

Tilleggs absorbert vann	17,8
Totalt vann	197,8

Fraksjon	Navn	Densitet	Andel	0
0	0	0	volum	vekt
I	Leca 2-4 mm	550	0,878	0,600
II	sand 0-4 mm Lillestrom	2650	0,122	0,400
III	0	2650	0,000	0,000
IV	0	1450	0,000	0,000
V	Ingen	530	0,000	0,000
VI	Ingen	650	0,000	0,000
VII		2650	0,000	0,000
VIII		2650	0,000	0,000
IX		2650	0,000	0,000
X		2650	0,000	0,000
Sammensatt	0		1,000	1,000

Erfaringer: Meget støpelig betongresept med stor grad av sikkerhet mot sergresjon. Betongen er robust.

Resepten oppgir tilsatt vann og ikke effektivt vann.

Fuktmåling på sand og Leca før oppstart. Bedre innmålingsverktøy for sand og Leca.

Operatørene må vurdere betongen visuelt fortløpende.

Proporsjonering på volumbasis Fyll inn i gule felt Resept 4 - 900kg 19-2-10

FND 2006-10-18

Oppnådde verdier	Verdi	Verdi	Enhet
Sementlim	418		l/m³
v/(c+Σkp)	0,43	-	-
s/(c1+c2)	0,028	2,80	%
fa/(c1+c2)	0,000	0,00	%
mLWA/(C1+C2)	0,000	0,00	%
kalkfiller/(c1+c2)	0,000	0,00	%
BASF Glenium SKY 550	0,011	1,15	%
0,0	0,000	0,00	%
BASF Glenium Stream	0,005	0,53	%
Luftinnhold		16,0	%
Matriksmengde	423		l/m³

Merknader

Vannabsorpsjon, tilslag (%)	
Leca 2-4 mm	6,0
sand 0-4 mm Lillestrom	1,0
Leca 4-10	6,0
0	7,0
Ingen	
Ingen	

Materiale	Densitet	k
Norcem Industri	3150,0	1
Norcem Anlegg	3150,0	1
Silikastøv	2200	2
Flyveaske	2200	0,7
Micro LWA	2600	1
Kalksteinfiller	2600	0
BASF Glenium SKY	1200	
0,0	1200	
BASF Glenium Stre	1200	

Proporsjonert betong

Tilleggs absorbert vann	18,6
Totalt vann	165,6

Materialer	kg/m³	l/m3	kg/200L	4l blanding
Norcem Industri	101,00	32,1	20,2	0,404
Norcem Anlegg	221,00	70,2	44,2	0,884
Silikastøv	9,00	4,1	1,8	0,036
Flyveaske	0,00	0,0	0,0	0,000
Micro LWA	0,00	0,0	0,0	0,000
Kalksteinfiller	0,00	0,0	0,0	0,000
BASF Glenium SKY 550	3,70	3,1	0,7	0,015
	0,00	0,0	0,0	0,000
BASF Glenium Stream	1,70	1,4	0,3	0,007
Tilsatt vann	147,00	147,0	29,4	0,588
Luftinnhold	8,0	160,00	1,6	0,032
Sum pasta	483,4	417,8	96,7	1,934
Leca 2-4 mm	184,00	334,5	36,8	0,736
sand 0-4 mm Lillestrom	92,00	34,5	18,4	0,368
Leca 4-10	110,00	220,0	22,0	0,440
0,0	0,00	0,0	0,0	0,000
Luftdemper	0,12	0,0	0,0	0,000
BASF MECH PP 150	1,50		0,3	0,006
Bekaert 30/35 Stålfiber	40,00		8,0	0,160
Sum tilslag	427,6	589,0		
Prop. betongdens. (kg/m³)	904,9	1007		

Fraksjon	Navn	Densitet	Andel	0
0	0	0	volum	vekt
I	Leca 2-4 mm	550	0,574	0,500
II	sand 0-4 mm Lillestrom	2650	0,048	0,200
III	Leca 4-10	500	0,379	0,300
IV	0	1450	0,000	0,000
V	Ingen	530	0,000	0,000
VI	Ingen	650	0,000	0,000
VII		2650	0,000	0,000
VIII		2650	0,000	0,000
IX		2650	0,000	0,000
X		2650	0,000	0,000
Sammensatt	0		1,000	1,000

B.2 Recipes, Phase 2

Table B.2.1: Recipes middle layer hybrid beams, Weber concrete (W1150).

	HB1, 115 liter		HB1, 125 liter	
Materialer	**kg**	**kg, korr**	**kg**	**kg, korr**
Norcem Industri	13.1100	13.1100	14.2500	14.2500
Norcem Anlegg	30.5900	30.5900	33.2500	33.2500
Silikastøv	4.0250	4.0250	4.3750	4.3750
Flyveaske	0.0000	0.0000	0.0000	0.0000
Micro LWA	0.0000	0.0000	0.0000	0.0000
Kalksteinfiller	0.0000	0.0000	0.0000	0.0000
BASF Glenium SKY 550	0.6223	0.6223	0.7400	0.7400
Skum	0.0000	0.0000	0.0000	0.0000
BASF Glenium Steam	0.2300	0.2300	0.2500	0.2500
Tilsatt vann	20.7000	19.5960	22.5000	21.3000
Sum pasta	**69.4830**	**68.3790**	**75.5250**	**74.3250**
Leca 2-4 mm	26.4500	26.4500	28.7500	28.7500
sand 0-4 mm Lillestrom	46.0000	47.1040	50.0000	51.2000
Luftdemper	0.0141	0.0141	0.0154	0.0154
BASF MECH PP 150	0.1725	0.1725	0.1875	0.1875
Bekaert 30/35 Stålfiber	9.2000	9.2000	10.0000	10.0000
Sum tilslag	**81.8366**	**82.9406**	**88.9529**	**90.1529**

	HB3, 115 liter		HB4, 115 liter	
Materialer	**kg**	**kg, korr**	**kg**	**kg, korr**
Norcem Industri	13.1100	13.1100	13.1100	13.1100
Norcem Anlegg	30.5900	30.5900	30.5900	30.5900
Silikastøv	4.0250	4.0250	4.02500	4.0250
Flyveaske	0.0000	0.0000	0.0000	0.0000
Micro LWA	0.0000	0.0000	0.0000	0.0000
Kalksteinfiller	0.0000	0.0000	0.0000	0.0000
BASF Glenium SKY 550	0.7030	0.7030	0.6430	0.6430
Skum	0.0000	0.0000	0.0000	0.0000
BASF Glenium Steam	0.2300	0.2300	0.23000	0.2300
Tilsatt vann	20.7000	19.5960	20.7000	19.5960
Sum pasta	**69.4830**	**68.3790**	**69.4830**	**68.3790**
Leca 2-4 mm	26.4500	26.4500	26.4500	26.4500
sand 0-4 mm Lillestrom	46.0000	47.1040	46.0000	47.1040
Luftdemper	0.0141	0.0141	0.0141	0.0141
BASF MECH PP 150	0.1725	0.1725	0.1725	0.1725
Bekaert 30/35 Stålfiber	9.2000	9.2000	9.2000	9.2000
Sum tilslag	**81.8366**	**82.9406**	**81.8366**	**82.9406**

Table B.2.2: Recipe bottom layer hybrid beam 1, normal concrete ("B30").

Prosj./id.:	**HB1**

Blandevolum:	40 liter
Dato:	
Tidspunkt for vanntilsetning	
Ansvarlig:	
Utført av:	

Materialer	**Resept** kg/m³	**Sats** kg	**Fukt*** %	**Korr.** kg	**Oppveid**** kg	
Norcem Standard FA	311.2	12.449			12.449	
Elkem Microsilica	0.0	0.000	0	0.000	0.000	
	0.0	0.000	0	0.000	0.000	
Fritt vann	180.5	7.220		-2.768	4.453	*4.734*
Absorbert vann	7.0	0.282			0.282	
Årdal 0-8 mm nat. vask.	1112.5	44.498	6.2	2.759	47.257	
Årdal 0-2 mm nat. vask	0.0	0.000	0.0	0.000	0.000	
Årdal 8-10 mm	0.0	0.000	0.0	0.000	0.000	
Årdal 8-16 mm	740.2	29.606	0.0	0.000	29.606	
	0.0	0.000	0.0	0.000	0.000	
	0.0	0.000	0.0	0.000	0.000	
	0.0	0.000	0.0	0.000	0.000	
	0.0	0.000	0.0	0.000	0.000	
	0.0	0.000	0.0	0.000	0.000	
	0.0	0.000	0.0	0.000	0.000	
Mighty 150	0.3	0.012	72	0.009	0.012	
	0.0	0.000	100	0.000	0.000	
	0.0	0.000	100	0.000	0.000	
	0.0	0.000	100	0.000	0.000	
Stålfiber	0.0	0.000			0.000	
PP-fiber	0.0	0.000			0.000	

*Se fotnote på delark "Proporsjonering" ** NB! Våte mengder, også for pozzolaner og fillere

Table B.2.3: Recipe bottom layer hybrid beam 2, normal concrete ("B30").

Prosj./id.:	**HB2**

Blandevolum:	50 liter
Dato:	
Tidspunkt for vanntilsetning	
Ansvarlig:	
Utført av:	

Materialer	**Resept** kg/m^3	**Sats** kg	**Fukt*** %	**Korr.** kg	**Oppveid**** kg	
Norcem Standard FA	311.2	15.561			15.561	
Elkem Microsilica	0.0	0.000	0	0.000	0.000	
	0.0	0.000	0	0.000	0.000	
Fritt vann	180.5	9.026		-3.436	5.590	*5.942*
Absorbert vann	7.0	0.352			0.352	
Årdal 0-8 mm nat. vask.	1112.5	55.623	6.2	3.425	59.047	
Årdal 0-2 mm nat. vask	0.0	0.000	0.0	0.000	0.000	
Årdal 8-10 mm	0.0	0.000	0.0	0.000	0.000	
Årdal 8-16 mm	740.2	37.008	0.0	0.000	37.008	
	0.0	0.000	0.0	0.000	0.000	
	0.0	0.000	0.0	0.000	0.000	
	0.0	0.000	0.0	0.000	0.000	
	0.0	0.000	0.0	0.000	0.000	
	0.0	0.000	0.0	0.000	0.000	
	0.0	0.000	0.0	0.000	0.000	
Mighty 150	0.3	0.016	72	0.011	0.016	
	0.0	0.000	100	0.000	0.000	
	0.0	0.000	100	0.000	0.000	
	0.0	0.000	100	0.000	0.000	
Stålfiber	0.0	0.000			0.000	
PP-fiber	0.0	0.000			0.000	

*Se fotnote på delark "Proporsjonering" ** NB! Våte mengder, også for pozzolaner og fillere

Table B.2.4: Recipe bottom layer hybrid beam 3 and 4, normal concrete ("B30").

Prosj./id.:	**HB3 og HB4**

Blandevolum:	40 liter
Dato:	
Tidspunkt for vanntilsetning	
Ansvarlig:	
Utført av:	

Materialer	**Resept** kg/m^3	**Sats** kg	**Fukt*** %	**Korr.** kg	**Oppveid**** kg	
Norcem Standard FA	311.2	12.449			12.449	
Elkem Microsilica	0.0	0.000	0	0.000	0.000	
	0.0	0.000	0	0.000	0.000	
Fritt vann	180.5	7.220		-1.477	5.743	*6.025*
Absorbert vann	7.0	0.282			0.282	
Årdal 0-8 mm nat. vask.	1112.5	44.498	3.3	1.468	45.967	
Årdal 0-2 mm nat. vask	0.0	0.000	0.0	0.000	0.000	
Årdal 8-10 mm	0.0	0.000	0.0	0.000	0.000	
Årdal 8-16 mm	740.2	29.606	0.0	0.000	29.606	
	0.0	0.000	0.0	0.000	0.000	
	0.0	0.000	0.0	0.000	0.000	
	0.0	0.000	0.0	0.000	0.000	
	0.0	0.000	0.0	0.000	0.000	
	0.0	0.000	0.0	0.000	0.000	
	0.0	0.000	0.0	0.000	0.000	
Mighty 150	0.3	0.012	72	0.009	0.012	
	0.0	0.000	100	0.000	0.000	
	0.0	0.000	100	0.000	0.000	
	0.0	0.000	100	0.000	0.000	
Stålfiber	0.0	0.000			0.000	
PP-fiber	0.0	0.000			0.000	

*Se fotnote på delark "Proporsjonering" ** NB! Våte mengder, også for pozzolaner og fillere

Table B.2.5: Recipe top layer hybrid beam 1 and 2, normal concrete ("B30").

Prosj./id.:	**Toppstøp HB1 og HB2**

Blandevolum:	100 liter
Dato:	
Tidspunkt for vanntilsetning	
Ansvarlig:	
Utført av:	

Materialer	**Resept** kg/m^3	**Sats** kg	**Fukt*** %	**Korr.** kg	**Oppveid**** kg	
Norcem Standard FA	311.2	31.123			31.123	
Elkem Microsilica	0.0	0.000	0	0.000	0.000	
	0.0	0.000	0	0.000	0.000	
Fritt vann	180.5	18.051		-3.694	14.358	*15.062*
Absorbert vann	7.0	0.704			0.704	
Årdal 0-8 mm nat. vask.	1112.5	111.246	3.3	3.671	114.917	
Årdal 0-2 mm nat. vask	0.0	0.000	0.0	0.000	0.000	
Årdal 8-10 mm	0.0	0.000	0.0	0.000	0.000	
Årdal 8-16 mm	740.2	74.016	0.0	0.000	74.016	
	0.0	0.000	0.0	0.000	0.000	
	0.0	0.000	0.0	0.000	0.000	
	0.0	0.000	0.0	0.000	0.000	
	0.0	0.000	0.0	0.000	0.000	
	0.0	0.000	0.0	0.000	0.000	
	0.0	0.000	0.0	0.000	0.000	
Mighty 150	0.3	0.031	72	0.022	0.031	
	0.0	0.000	100	0.000	0.000	
	0.0	0.000	100	0.000	0.000	
	0.0	0.000	100	0.000	0.000	
Stålfiber	0.0	0.000			0.000	
PP-fiber	0.0	0.000			0.000	

*Se fotnote på delark "Proporsjonering" ** NB! Våte mengder, også for pozzolaner og fillere

C.1 Results from Compression Tests, Phase 1

Table C.1.1: Results from compression tests of cubes, Phase 1.

Batch	Curing Time	Capacity [metric ton]	Capacity [MPa]	Average Capacity [MPa]	Weight [kg]	Immersed Weight [kg]	Density (theoretically) [kg/m3]	Density (true) [kg/m3]	Average True Density [kg/m3]
BO	28 Days	9	8.8	9.4	0.949		949		945
		9.3	9.1		0.952		952		
		10.4	10.2		0.934		934		
B1A	28 Days	7.4	7.3	8.1	1.004		1004		996
		8.8	8.6		1.003		1003		
		8.6	8.4		0.999		999		
	62 Days	7.8	7.7	7.4	0.992		992		
		8.6	8.4		1.003		1003		
		6.3	6.2		0.976		976		
B1B	62 Days		7.0	10.8	0.974		974		975
			13.4		0.971		971		
			11.9		0.981		981		
B2A	62 Days		*	7.3	0.946		946		964
			6.6		0.993		993		
			*		0.978		978		
			*		0.914		914		
			6.5		0.970		970		
			8.8		0.986		986		
B2B	28 Days	10.9	10.7	12.4	1.017		1017		1020
		13.7	13.4		1.029		1029		
		13.2	12.9		1.015		1015		
B3	28 Days	16.4	16.1	17.2	1.217	0.224	1217	1225	1231
		18.8	18.4		1.222	0.227	1222	1228	
		17.5	17.2		1.219	0.228	1219	1230	
	62 Days	28.9	28.4	27.3	1.228	0.232	1228	1233	
		29.1	28.5		1.249	0.243	1249	1241	
		25.4	24.9		1.233	0.229	1233	1229	

Note! For concrete with density < 1000 kg/m3 the average density is based on theoretically volume values due to difficulties of measuring immersed weight.

* These specimens where of to bad quality to be tested.

Table C.1.2: Results from compression tests of cylinders, Phase 1.

Batch	Curing Time	Capacity [metric ton]	Capacity [MPa]	Average Capacity [MPa]	Weight [kg]	Immersed Weight [kg]	Density (theoretically) [kg/m3]	Density (true) [kg/m3]	Average True Density [kg/m3]
B1A	28 Days	7.8	9.7	10.7	1.575		1003		1001
		8.7	10.9		1.562		995		
		9.1	11.4		1.576		1004		
B2A	28 Days	4.7	5.9	5.1	1.447		922		907
		3.1	3.9		1.401		892		
		4.5	5.6		1.425		908		
B3	28 Days	13.3	16.6	16.4	1.906	0.390	1214	1257	1246
		13.4	16.7		1.898	0.376	1209	1247	
		12.6	15.7		1.879	0.357	1196	1235	

Note! For concrete with density < 1000 kg/m3 the average density is based on theoretically volume values due to difficulties of measuring immersed weight.

C.2 Results from Compression Tests, Phase 2

Batch	Weight [kg]	Immersed Weight [kg]	Density (theoretically) [kg/m3]	Density (true) [kg/m3]	Average True Density [kg/m3]	Curing Time	Capacity [MPa]
HB1-LWC	1.900	0.340	1210	1218	1217	22 days	12.1
	1.901	0.342	1211	1220		29 days	12.7
	1.915	0.338	1220	1214		49 days	12
HB1-"B30" (bottom)	3.743	2.179	2384	2393	2390	22 days	27
	3.767	2.188	2399	2386		29 days	26.6
HB2-LWC	1.889	0.336	1203	1217	1212	22 days	11
	1.894	0.333	1206	1213		29 days	12.5
	1.874	0.321	1194	1207		49 days	11.9
HB2-"B30" (bottom)	3.703	2.156	2359	2394	2394	22 days	25.5
	3.716	2.163	2367	2394		29 days	25
HB3-LWC	1.909	0.355	1216	1228	1233	22 days	10.8
	1.911	0.357	1217	1230		29 days	10.9
	1.929	0.374	1229	1240		49 days	12.2
HB3-"B30" (bottom)	3.784	2.220	2410	2420	2416	22 days	28.3
	3.741	2.190	2383	2412		29 days	26.9
HB4-LWC	1.870	0.306	1191	1196	1200	22 days	12.5
	1.883	0.322	1199	1207		29 days	11
	1.874	0.308	1194	1197		49 days	12
HB3-"B30" (bottom)	3.782	2.207	2409	2401	2403	22 days	26.3
	3.759	2.196	2394	2404		29 days	26.3
Top cast "B30"	3.767	2.210	2399	2419	2402	15 Days	25.6
	3.741	2.180	2383	2397			25.7
	3.733	2.169	2378	2387			25.1
	3.752	2.188	2390	2399		28 Days	26.7
	3.737	2.183	2380	2405			26.7
	3.736	2.181	2380	2403			27.7

Average Capacities		
Batch Type	Curing Time	Average Capacity [Mpa]
LWC	22 days	11.6
	29 days	11.8
	60 days	12.0
"B30" bottom	22 days	26.8
	29 days	26.2
"B30" top	15 days	25.5
	28 days	27.0

D.1 Derivation of Friction Angle

Friction Angle: B3-2

$f_t = 2.27$ MPa

$f_c = 16.36$ MPa

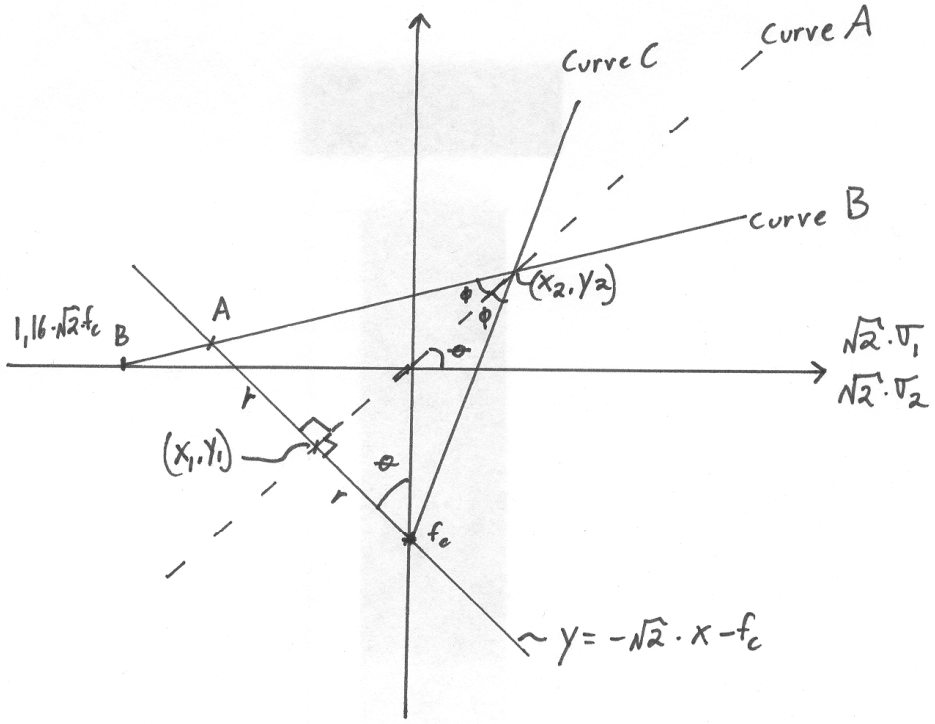

(x_1, y_1)

$$\left.\begin{aligned} \frac{1}{\sqrt{2}} \cdot x_1 &= -\sqrt{2} \cdot x_1 - f_c \\ \left(\frac{1}{\sqrt{2}} + \sqrt{2}\right) x_1 &= -f_c \end{aligned}\right\} \Rightarrow x_1 = -\frac{f_c}{\frac{1}{\sqrt{2}} + \sqrt{2}} =$$

$$= -\frac{\sqrt{2} \cdot f_c}{1+2} = \underline{\frac{\sqrt{2}}{3} f_c}$$

$$y_1 = -\frac{f_c}{3}$$

$$\cos\theta = \frac{r}{f_c}$$

$$r = \sqrt{\frac{2}{3}} \cdot f_c$$

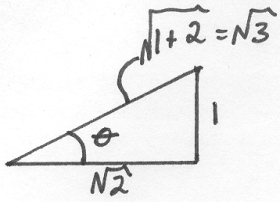

$$\cos\theta = \frac{\sqrt{2}}{\sqrt{3}}$$

- **Point A**

$$x_A = -2 \cdot \sin\theta \cdot r = -2 \frac{1}{\sqrt{3}} \cdot \frac{\sqrt{2}}{\sqrt{3}} \cdot f_c = -\frac{2\sqrt{2}}{3} \cdot f_c$$

$$y_A = -\sqrt{2}\left(-\frac{2\sqrt{2}}{3} \cdot f_c\right) - f_c = \frac{f_c}{3}$$

- **Curve B** $(ax+b)$

1) $[B](-1{,}16 \cdot \sqrt{2} \cdot f_c, 0)$

$$0 = a\left(-1.16 \cdot \sqrt{2} \cdot f_c\right) + b$$

$$b = 1.16 \cdot \sqrt{2} \cdot f_c \cdot a$$

2) $$\frac{f_c}{3} = -a \cdot \frac{2\sqrt{2}}{3} \cdot f_c + 1.16 \cdot \sqrt{2} \cdot f_c \cdot a$$

$$\Rightarrow \quad a \approx 0.47777$$

$$b \approx 12.82270$$

- **Intersectionpoint** x_2, y_2

$$\left.\begin{aligned} y &= 0{,}4777x + 12.8227 \\ y &= \frac{1}{\sqrt{2}} x \end{aligned}\right\} \Rightarrow \begin{aligned} x_2 &= 55.9134 \\ y_2 &= 39.5367 \end{aligned}$$

- **Distance** $x_2, y_2 \rightarrow x_1, y_1$

$$R = \sqrt{(55.9134 + 7{,}7122)^2 + (39.5367 + 5.4533)^2} = 77{,}925$$

$$\phi = \arctan\left(\frac{13{,}3579}{R}\right) = \underline{\underline{9.727°}}$$

E.1 Residual flexural tensile strength

Batch: B1a

The calculation of the residual flexural tensile strength is based on the following report:

"Stålfiberarmering i betong - Veiledning for prosjektering, utførelse og kontroll."
Høringsutkast Mai 2006

but modified to account for used specimen geometry:

Test specimens cast in accordance with the following governing standard:

NS-EN 14651:2005 Test method for metallic fibre concrete
Measuring the flexural tensile strength

Input: Load level at 0.6667mm and 3.3333mm deflection of test specimens.

$F_{\delta 1.1} := 5980N$	$F_{\delta 1.2} := 4810N$	$F_{\delta 1.3} := 4400N$
$F_{\delta 2.1} := 4480N$	$F_{\delta 2.2} := 3860N$	$F_{\delta 2.3} := 3510N$
$L_1 := 500mm$	$L_2 := 500mm$	$L_3 := 500mm$
$b_1 := 150mm$	$b_2 := 150mm$	$b_3 := 150mm$
$d_1 := 125mm$	$d_2 := 125mm$	$d_3 := 125mm$
$h_1 := 150mm$	$h_2 := 150mm$	$h_3 := 150mm$

3 specimens: $k_n := 1.89$

Output:

Specimen 1:

$$F_{\delta 12.1} := \frac{F_{\delta 1.1} + F_{\delta 2.1}}{2}$$

$F_{\delta 12.1} = 5.23 \cdot kN$ Mean load level

$$M_{\delta 12.1} := \frac{F_{\delta 12.1} \cdot L_1}{4}$$

$M_{\delta 12.1} = 6.537 \times 10^5 \cdot N \cdot mm$

$$f_{ftk.eq.1} := \frac{6 \cdot M_{\delta 12.1}}{b_1 \cdot {d_1}^2}$$

$f_{ftk.eq.1} = 1.674 \cdot MPa$

Specimen 2:

$$F_{\delta 12.2} := \frac{F_{\delta 1.2} + F_{\delta 2.2}}{2}$$

$F_{\delta 12.2} = 4.335 \cdot kN$ Mean load level

$$M_{\delta 12.2} := \frac{F_{\delta 12.2} \cdot L_2}{4}$$

$M_{\delta 12.2} = 5.419 \times 10^5 \cdot N \cdot mm$

$$f_{ftk.eq.2} := \frac{6 \cdot M_{\delta 12.2}}{b_2 \cdot {d_2}^2}$$

$f_{ftk.eq.2} = 1.387 \cdot MPa$

Specimen 3:

$$F_{\delta 12.3} := \frac{F_{\delta 1.3} + F_{\delta 2.3}}{2}$$

$F_{\delta 12.3} = 3.955 \cdot kN$ Mean load level

$$M_{\delta 12.3} := \frac{F_{\delta 12.3} \cdot L_3}{4}$$

$M_{\delta 12.3} = 4.944 \times 10^5 \cdot N \cdot mm$

$$f_{ftk.eq.3} := \frac{6 \cdot M_{\delta 12.3}}{b_3 \cdot {d_3}^2}$$

$f_{ftk.eq.3} = 1.266 \cdot MPa$

$f_{ftk.snitt} := mean(f_{ftk.eq.1}, f_{ftk.eq.2}, f_{ftk.eq.3})$ $f_{ftk.snitt} = 1.442 \cdot MPa$ Average

$f_{ftk.stdev} := stdev(f_{ftk.eq.1}, f_{ftk.eq.2}, f_{ftk.eq.3})$ $f_{ftk.stdev} = 0.171 \cdot MPa$ Standard deviation

$f_{ftk.eq} := f_{ftk.snitt} - k_n \cdot f_{ftk.stdev} = 1.119 \cdot MPa$ Average residual flexural tensile strength

$f_{ftk.res} := f_{ftk.eq} \cdot 0.37$ $f_{ftk.res} = 0.414 \cdot MPa$ Average residual tensile strength

Average residual tensile strength, not corrected with respect to standard deviation:

$f_{ftk.res.nocorr} := f_{ftk.snitt} \cdot 0.37$ $f_{ftk.res.nocorr} = 0.534 \cdot MPa$

E.2 Residual flexural tensile strength

Batch: B2a

The calculation of the residual flexural tensile strength is based on the following report:

"Stålfiberarmering i betong - Veiledning for prosjektering, utførelse og kontroll."
Høringsutkast Mai 2006

but modified to account for used specimen geometry:

Test specimens cast in accordance with the following governing standard:

NS-EN 14651:2005 Test method for metallic fibre concrete
Measuring the flexural tensile strength

Input: Load level at 0.6667mm and 3.3333mm deflection of test specimens.

$F_{\delta 1.1} := 8660N$	$F_{\delta 1.2} := 8410N$	$F_{\delta 1.3} := 8940N$
$F_{\delta 2.1} := 5310N$	$F_{\delta 2.2} := 5520N$	$F_{\delta 2.3} := 5760N$
$L_1 := 500mm$	$L_2 := 500mm$	$L_3 := 500mm$
$b_1 := 150mm$	$b_2 := 150mm$	$b_3 := 150mm$
$d_1 := 125mm$	$d_2 := 125mm$	$d_3 := 125mm$
$h_1 := 150mm$	$h_2 := 150mm$	$h_3 := 150mm$

3 speimens: $k_n := 1.89$

Output:

Specimen 1:

$$F_{\delta 12.1} := \frac{F_{\delta 1.1} + F_{\delta 2.1}}{2} \qquad F_{\delta 12.1} = 6.985 \cdot kN$$ Mean load level

$$M_{\delta 12.1} := \frac{F_{\delta 12.1} \cdot L_1}{4} \qquad M_{\delta 12.1} = 8.731 \times 10^5 \cdot N \cdot mm$$

$$f_{ftk.eq.1} := \frac{6 \cdot M_{\delta 12.1}}{b_1 \cdot {d_1}^2} \qquad f_{ftk.eq.1} = 2.235 \cdot MPa$$

Specimen 2:

$$F_{\delta 12.2} := \frac{F_{\delta 1.2} + F_{\delta 2.2}}{2} \qquad F_{\delta 12.2} = 6.965 \cdot kN$$ Mean load level

$$M_{\delta 12.2} := \frac{F_{\delta 12.2} \cdot L_2}{4} \qquad M_{\delta 12.2} = 8.706 \times 10^5 \cdot N \cdot mm$$

$$f_{ftk.eq.2} := \frac{6 \cdot M_{\delta 12.2}}{b_2 \cdot {d_2}^2} \qquad f_{ftk.eq.2} = 2.229 \cdot MPa$$

Specimen 3:

$$F_{\delta 12.3} := \frac{F_{\delta 1.3} + F_{\delta 2.3}}{2} \qquad F_{\delta 12.3} = 7.35 \cdot kN$$ Mean load level

$$M_{\delta 12.3} := \frac{F_{\delta 12.3} \cdot L_3}{4} \qquad M_{\delta 12.3} = 9.188 \times 10^5 \cdot N \cdot mm$$

$$f_{ftk.eq.3} := \frac{6 \cdot M_{\delta 12.3}}{b_3 \cdot {d_3}^2} \qquad f_{ftk.eq.3} = 2.352 \cdot MPa$$

$f_{ftk.snitt} := mean(f_{ftk.eq.1}, f_{ftk.eq.2}, f_{ftk.eq.3})$ $f_{ftk.snitt} = 2.272 \cdot MPa$ Average

$f_{ftk.stdev} := stdev(f_{ftk.eq.1}, f_{ftk.eq.2}, f_{ftk.eq.3})$ $f_{ftk.stdev} = 0.057 \cdot MPa$ Standard deviation

$f_{ftk.eq} := f_{ftk.snitt} - k_n \cdot f_{ftk.stdev} = 2.165 \cdot MPa$ Average residual flexural tensile strength

$f_{ftk.res} := f_{ftk.eq} \cdot 0.37$ $f_{ftk.res} = 0.801 \cdot MPa$ Average residual tensile strength

Average residual tensile strength, not corrected with respect to standard deviation:

$f_{ftk.res.nocorr} := f_{ftk.snitt} \cdot 0.37$ $f_{ftk.res.nocorr} = 0.841 \cdot MPa$

E.3 Residual flexural tensile strength

Batch: B3

The calculation of the residual flexural tensile strength is based on the following report:

"Stålfiberarmering i betong - Veiledning for prosjektering, utførelse og kontroll."
Høringsutkast Mai 2006

but modified to account for used specimen geometry:

Test specimens cast in accordance with the following governing standard:

NS-EN 14651:2005 Test method for metallic fibre concrete
Measuring the flexural tensile strength

Input: Load level at 0.6667mm and 3.3333mm deflection of test specimens.

$F_{\delta 1.1} := 15770N$ $F_{\delta 1.2} := 13380N$ $F_{\delta 1.3} := 13100N$

$F_{\delta 2.1} := 12160N$ $F_{\delta 2.2} := 9350N$ $F_{\delta 2.3} := 9910N$

$L_1 := 500mm$ $L_2 := 500mm$ $L_3 := 500mm$

$b_1 := 150mm$ $b_2 := 150mm$ $b_3 := 150mm$

$d_1 := 125mm$ $d_2 := 125mm$ $d_3 := 125mm$

$h_1 := 150mm$ $h_2 := 150mm$ $h_3 := 150mm$

3 specimens: $k_n := 1.89$

Output:

Specimen 1:

$$F_{\delta 12.1} := \frac{F_{\delta 1.1} + F_{\delta 2.1}}{2}$$

$F_{\delta 12.1} = 13.965 \cdot kN$ Mean load level

$$M_{\delta 12.1} := \frac{F_{\delta 12.1} \cdot L_1}{4}$$

$M_{\delta 12.1} = 1.746 \times 10^6 \cdot N \cdot mm$

$$f_{ftk.eq.1} := \frac{6 \cdot M_{\delta 12.1}}{b_1 \cdot {d_1}^2}$$

$f_{ftk.eq.1} = 4.469 \cdot MPa$

Specimen 2:

$$F_{\delta 12.2} := \frac{F_{\delta 1.2} + F_{\delta 2.2}}{2}$$

$F_{\delta 12.2} = 11.365 \cdot kN$ Mean load level

$$M_{\delta 12.2} := \frac{F_{\delta 12.2} \cdot L_2}{4}$$

$M_{\delta 12.2} = 1.421 \times 10^6 \cdot N \cdot mm$

$$f_{ftk.eq.2} := \frac{6 \cdot M_{\delta 12.2}}{b_2 \cdot {d_2}^2}$$

$f_{ftk.eq.2} = 3.637 \cdot MPa$

Specimen 3:

$$F_{\delta 12.3} := \frac{F_{\delta 1.3} + F_{\delta 2.3}}{2}$$

$F_{\delta 12.3} = 11.505 \cdot kN$ Mean load level

$$M_{\delta 12.3} := \frac{F_{\delta 12.3} \cdot L_3}{4}$$

$M_{\delta 12.3} = 1.438 \times 10^6 \cdot N \cdot mm$

$$f_{ftk.eq.3} := \frac{6 \cdot M_{\delta 12.3}}{b_3 \cdot {d_3}^2}$$

$f_{ftk.eq.3} = 3.682 \cdot MPa$

$f_{ftk.snitt} := mean(f_{ftk.eq.1}, f_{ftk.eq.2}, f_{ftk.eq.3})$ $f_{ftk.snitt} = 3.929 \cdot MPa$ Average

$f_{ftk.stdev} := stdev(f_{ftk.eq.1}, f_{ftk.eq.2}, f_{ftk.eq.3})$ $f_{ftk.stdev} = 0.382 \cdot MPa$ Standard deviation

$f_{ftk.eq} := f_{ftk.snitt} - k_n \cdot f_{ftk.stdev} = 3.207 \cdot MPa$ Average residual flexural tensile strength

$f_{ftk.res} := f_{ftk.eq} \cdot 0.37$ $f_{ftk.res} = 1.187 \cdot MPa$ Average residual tensile strength

Average residual tensile strength, not corrected with respect to standard deviation:

$f_{ftk.res.nocorr} := f_{ftk.snitt} \cdot 0.37$ $f_{ftk.res.nocorr} = 1.454 \cdot MPa$

F.1 Moment Capacity of Homogenous Concrete Section

All references done in the margin are related to NS-EN 1992 (Eurcode 2) unless otherwise is specified

All calculations are done with mean measured values in the laboratory

Only calculations done for beam B2B are shown in detail. Calculations for beam B1B and B0
are performed equally, but with their respective input parameters. The results are summarized in the main report.

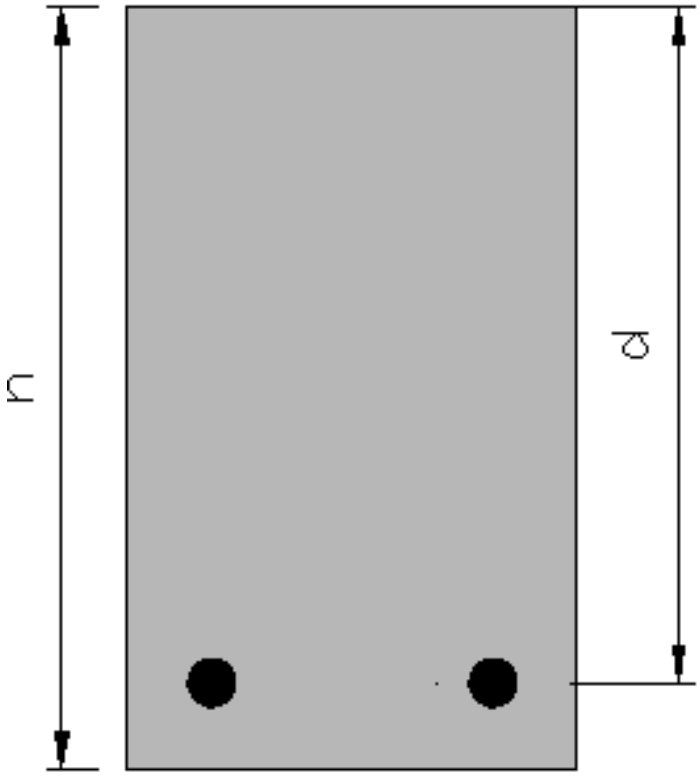

Input:

$\gamma_m := 1.0$

Dimensions:

$h := 250mm$

$b := 150mm$

$d := 221mm$

Concrete Parameters:

Table 3.1

$f_{cm} := 10.66MPa$

$f_{cd} := f_{cm}$ $\quad f_{cd} = 10.66 \cdot MPa$

NA.3.1.6

$\rho := 900 \frac{kg}{m^3}$

$E_{cm} := 8400MPa$

$\eta_1 := 0.4 + 0.6 \cdot \frac{\rho}{2200 \frac{kg}{m^3}}$

$\varepsilon_{cu2} := 0.0035 \cdot \eta_1$ $\quad \varepsilon_{cu2} = 2.259 \times 10^{-3}$

$\varepsilon_{c0} := 0.002$

$f_{ftk.res} := 0.801MPa$

Longitudinal reinforcement:

$f_{sk} := 500MPa$

$E_s := 200000MPa$

$\varepsilon_{sy} := \frac{f_{sk}}{E_s}$ $\quad \varepsilon_{sy} = 2.5 \times 10^{-3}$

$\phi := 16mm$ $\quad n := 2$

$A_s := n \cdot \pi \cdot \left(\frac{\phi}{2}\right)^2$ $\quad A_s = 402.124 \cdot mm^2$

$\varepsilon_{su} := 0.01$

Output:

Balanced reinforcement amount:

$$\alpha_b := \frac{\varepsilon_{cu2}}{\varepsilon_{cu2} + \varepsilon_{sy}}$$

$\alpha_b = 0.475$

Antar fullt utnyttet trykksone

3.1.7(3)

$$A_{s.b} := \frac{0.8 \cdot f_{cd} \cdot b \cdot d \cdot \alpha_b}{f_{sk}}$$

$A_{s.b} = 268.393 \cdot mm^2$

$$\text{Armeringsmengde} := \begin{cases} \text{"Underarmert"} & \text{if } A_s \le A_{s.b} \\ \text{"Overarmert"} & \text{otherwise} \end{cases}$$

Armeringsmengde = "Overarmert"

Moment Capacity:

$$\alpha := \begin{cases} \alpha_{under} & \text{if } A_s \le A_{s.b} \\ \alpha_{over} & \text{otherwise} \end{cases}$$

$\alpha = 0.542$

$0.8 \cdot \alpha \cdot d = 95.885 \cdot mm$

$$M_{Rk} := 0.8 \cdot \alpha \cdot b \cdot d \cdot f_{cd} \cdot (d - 0.5 \cdot 0.8 \cdot \alpha \cdot d)$$

$M_{Rk} = 26.533 \cdot kN \cdot m$

Reinforcement strain:

$$\varepsilon_s := \frac{1 - \alpha}{\alpha} \cdot \varepsilon_{cu2}$$

$\varepsilon_s = 1.906 \times 10^{-3}$

$$\text{Tøyning} := \begin{cases} \text{"Overskrider bruddtøyning"} & \text{if } \varepsilon_s > 0.01 \\ \text{"Ok mtp. bruddtøyning"} & \text{otherwise} \end{cases}$$

Tøyning = "Ok mtp. bruddtøyning"

$M_{Rk} = 26.533 \cdot kN \cdot m$

$p := 1.1 - \frac{0.7 \cdot h}{1000mm}$ $\quad p = 0.925$

$M_{Rk.fiber} := 0.4 \cdot f_{ftk.res} \cdot b \cdot h^2 \cdot p$ $\quad M_{Rk.fiber} = 2.778 \cdot kN \cdot m$

$M_{Rk.tot} := M_{Rk} + M_{Rk.fiber}$ $\quad M_{Rk.tot} = 29.312 \cdot kN \cdot m$

F.2 Shear Capacity of Homogenous Concrete Section

All references done in the margin are related to NS-EN 1992 (Eurcode 2) unless otherwise is specified

All calculations are done with mean measured values in the laboratory

Only calculations done for beam B2B are shown in detail. Calculations for beam B1B and B0
are performed equally, but with their respective input parameters. The results are summarized in the main report.

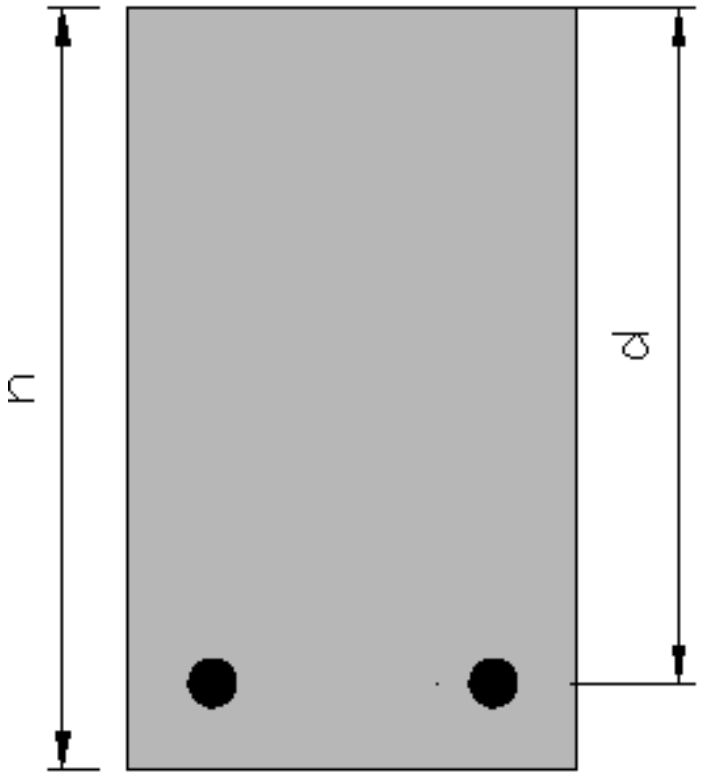

Input:

$\gamma_m := 1.0$

Dimensions:

$h := 250mm$

$b := 150mm$

$d := 221mm$

$d_{max} := 10mm$

Axial Force:

$N_{Ed} := 0 \cdot kN$

Concrete Parameters:

Table 3.1

NA.3.1.6

$f_{cm} := 10.66MPa$

$f_{cd} := f_{cm}$

$f_{cd} = 10.66 \cdot MPa$

$\rho := 900 \frac{kg}{m^3}$

$E_{cm} := 8400MPa$

$\eta_1 := 0.4 + 0.6 \cdot \frac{\rho}{2200 \frac{kg}{m^3}}$

$\varepsilon_{cu2} := 0.0035 \cdot \eta_1$

$\varepsilon_{cu2} = 2.259 \times 10^{-3}$

$\varepsilon_{c0} := 0.002$

$f_{ftk.res} := 0.801MPa$

Reinforcement:

$f_{sk} := 500MPa$

$E_s := 200000MPa$

$\varepsilon_{sy} := \frac{f_{sk}}{E_s}$ $\quad \varepsilon_{sy} = 2.5 \times 10^{-3}$

$\phi := 16mm$ $\quad n := 2$

$A_s := n \cdot \pi \cdot \left(\frac{\phi}{2}\right)^2$ $\quad A_s = 402.124 \cdot mm^2$

$\varepsilon_{su} := 0.01$

Output:

6.2.2(1)
NA6.2.2

$$C_{rd.c} := \begin{cases} 0.18 & \text{if } d_{max} \geq 16mm \\ 0.15 & \text{otherwise} \end{cases}$$

$C_{rd.c} = 0.15$

$$k := \begin{cases} \left(\left(1 + \sqrt{\frac{200mm}{d}}\right)\right) & \text{if } \left(1 + \sqrt{\frac{200mm}{d}}\right) \leq 2 \\ 2 & \text{otherwise} \end{cases}$$

$k = 1.951$

$$\rho_1 := \begin{cases} \frac{A_s}{b \cdot d} & \text{if } \left(\frac{A_s}{b \cdot d}\right) \leq 0.02 \\ 0.02 & \text{otherwise} \end{cases}$$

$\rho_1 = 0.012$

$$\sigma_{cp} := \begin{cases} \left(\left(\frac{N_{Ed}}{b \cdot h}\right)\right) & \text{if } \left(\frac{N_{Ed}}{b \cdot h}\right) < 0.2 \cdot f_{cd} \\ \left(0.2 \cdot f_{cd}\right) & \text{otherwise} \end{cases}$$

$\sigma_{cp} = 0\,Pa$

$$k_1 := 0.15$$

$$v_{min} := 0.028 \cdot k^{\frac{3}{2}} \cdot \sqrt{f_{cm}} \cdot \sqrt{MPa}$$

$v_{min} = 0.249 \cdot MPa$

$$V_{Rk.c} := \left[C_{rd.c} \cdot k \cdot \left(100 \cdot \rho_1 \cdot f_{cm}\right)^{\frac{1}{3}} \cdot (MPa)^{\frac{2}{3}} + k_1 \cdot \sigma_{cp}\right] \cdot b \cdot d$$

$$V_{Rk.c} := \begin{cases} V_{Rk.c} & \text{if } V_{Rk.c} \geq \left[\left(v_{min} + k_1 \cdot \sigma_{cp}\right) \cdot b \cdot d\right] \\ \left[\left(v_{min} + k_1 \cdot \sigma_{cp}\right) \cdot b \cdot d\right] & \text{otherwise} \end{cases}$$

$V_{Rk.c} = 22.774 \cdot kN$

$$p := 1.1 - \frac{0.7 \cdot h}{1000mm}$$

$p = 0.925$

$$V_{Rk.c.fiber} := 0.8 \cdot f_{ftk.res} \cdot b \cdot d \cdot p$$

$V_{Rk.c.fiber} = 19.649 \cdot kN$

$$V_{Rk.tot} := V_{Rk.c} + V_{Rk.c.fiber}$$

$V_{Rk.tot} = 42.424 \cdot kN$

F.3 Control Anchorage Capacity, Homogenous Concrete Section.

All references done in the margin are related to NS-EN 1992 (Eurocode 2) unless otherwise is specified.

All calculations are done with mean measured values in the laboratory.

Only calculations done for beam B2B are shown in detail. Calculations for beam B1B and B0.
are performed equally, but with their respective input parameters. The results are summarized in the main report.

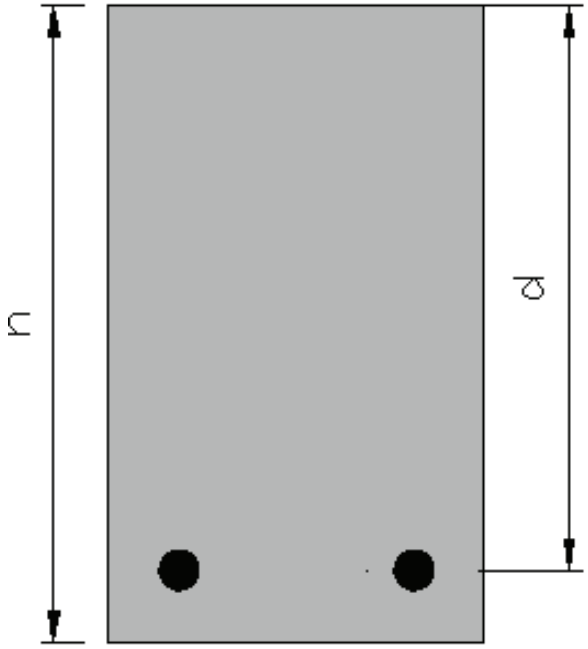

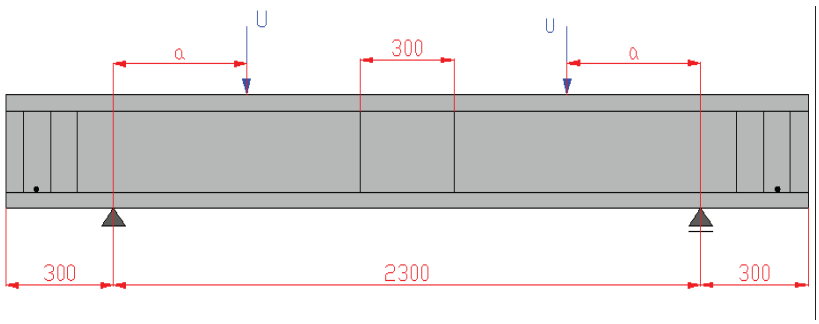

Input:

$\gamma_m := 1.0$

Dimensions:

$h := 250mm$

$b := 150mm$

$d := 221mm$

$d_{max} := 10mm$

Axial Force:

$N_{Ed} := 0 \cdot kN$

Concrete Parameters Bottom Layer:

Table 3.1

NA.3.1.6

$f_{cm} := 10.66MPa$

$f_{cd} := f_{cm}$

$f_{cd} = 10.66 \cdot MPa$

$f_{ctk} := 1.7437MPa$

$\rho := 900 \frac{kg}{m^3}$

$E_{cm} := 8400MPa$

$\eta_1 := 0.4 + 0.6 \cdot \frac{\rho}{2200 \frac{kg}{m^3}}$

$\varepsilon_{cu2} := 0.0035 \cdot \eta_1$

$\varepsilon_{cu2} = 2.259 \times 10^{-3}$

$\varepsilon_{c0} := 0.002$

Reinforcement:

$f_{sk} := 500MPa$

$E_s := 200000MPa$

$\varepsilon_{sy} := \frac{f_{sk}}{E_s}$ $\quad \varepsilon_{sy} = 2.5 \times 10^{-3}$

$\phi := 16mm$ $\quad n := 2$

$A_s := n \cdot \pi \cdot \left(\frac{\phi}{2}\right)^2$ $\quad A_s = 402.124 \cdot mm^2$

$\varepsilon_{su} := 0.01$

Reference:Y:\Håndberegninger\Skjærbjelker\B2b\Fullt utnyttet trykksone\PrinteArk\Momentkapasitet Homogent t

Reference:Y:\Håndberegninger\Skjærbjelker\B2b\Fullt utnyttet trykksone\PrinteArk\Skjærkapasitet Homogent tv.s

$M_{Rk.tot} = 29.312 \cdot kN \cdot m$

$V_{Rk.tot} = 42.424 \cdot kN$

$a := 3 \cdot d$ $\quad a = 663 \cdot mm$

Output:

$$P_{maks.mom} := \frac{M_{Rk.tot}}{a}$$

$P_{maks.mom} = 44.211 \cdot kN$

$$Dimensjonerende := \begin{cases} \text{"Moment"} & \text{if } P_{maks.mom} \le V_{Rk.tot} \\ \text{"Skjær"} & \text{otherwise} \end{cases}$$

$Dimensjonerende = \text{"Skjær"}$

$$P_{maks} := \begin{cases} V_{Rk.tot} & \text{if } V_{Rk.tot} < P_{maks.mom} \\ P_{maks.mom} & \text{otherwise} \end{cases}$$

$P_{maks} = 42.424 \cdot kN$

Control Anchorage Capacity:

8.4.2

Table 8.2

$\eta_1 := 1$ $\alpha_1 := 1$ $\alpha_3 := 1$ $\alpha_5 := 1$

$\eta_2 := 1$ $\alpha_2 := 1$ $\alpha_4 := 0.7$

$$f_{bk} := 2.25 \cdot \eta_1 \cdot \eta_2 \cdot f_{ctk}$$

$f_{bk} = 3.923 \cdot MPa$

$$\sigma_s := \frac{P_{maks} \cdot \cot\left(\frac{\pi}{4}\right)}{A_s}$$

$\sigma_s = 105.499 \cdot MPa$

8.4.3

$$l_{b.rqk} := \left(\frac{\phi}{4}\right) \cdot \left(\frac{\sigma_s}{f_{bk}}\right)$$

$l_{b.rqk} = 107.561 \cdot mm$

8.4.4

$$l_{b.min} := \max\left(0.3 l_{b.rqk}, 10 \cdot \phi, 100mm\right)$$

$l_{b.min} = 160 \cdot mm$

$$l_{bk} := \max\left(\alpha_1 \cdot \alpha_2 \cdot \alpha_3 \cdot \alpha_4 \cdot \alpha_5 \cdot l_{b.rqk}, l_{b.min}\right)$$

$l_{bk} = 160 \cdot mm$

F.4 Control Anchorage Capacity, Homogenous Concrete Section. (Old Norwegian Standard)

All references done in the margin are related to NS 3473 (Old Norwegian Standard) unless otherwise is specified.

All calculations are done with mean measured values in the laboratory.

Only calculations done for beam B2B are shown in detail. Calculations for beam B1B and B0.
are performed equally, but with their respective input parameters. The results are summarized in the main report.

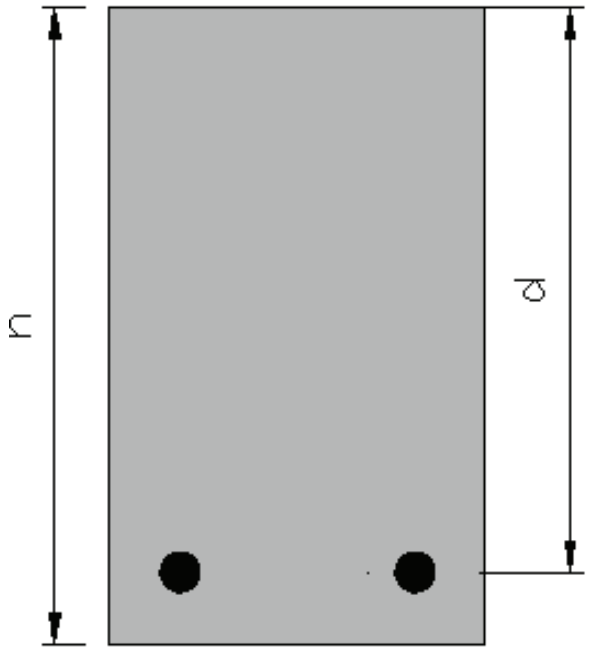

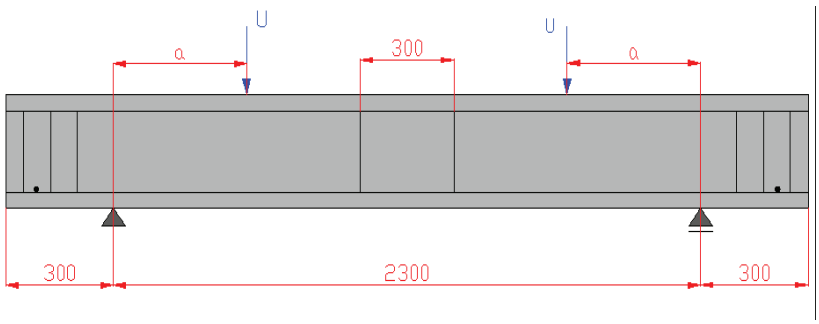

Input:

$\gamma_m := 1.0$

Dimensions:

$h := 250mm$

$b := 150mm$

$d := 221mm$

$d_{max} := 10mm$

Axial Force:

$N_{Ed} := 0 \cdot kN$

Concrete Parameters Bottom Layer:

$f_{cm} := 10.66MPa$

$f_{cd} := f_{cm}$

$f_{cd} = 10.66 \cdot MPa$

$f_{ctk} := 1.7437MPa$

$\rho := 900 \frac{kg}{m^3}$

$E_{cm} := 8400MPa$

$\eta_1 := 0.4 + 0.6 \cdot \frac{\rho}{2200 \frac{kg}{m^3}}$

$\varepsilon_{cu2} := 0.0035 \cdot \eta_1$

$\varepsilon_{cu2} = 2.259 \times 10^{-3}$

$\varepsilon_{c0} := 0.002$

Reinforcement:

$f_{sk} := 500MPa$

$E_s := 200000MPa$

$\varepsilon_{sy} := \frac{f_{sk}}{E_s}$ $\quad \varepsilon_{sy} = 2.5 \times 10^{-3}$

$\phi := 16mm$ $\quad n := 2$

$A_s := n \cdot \pi \cdot \left(\frac{\phi}{2}\right)^2$ $\quad A_s = 402.124 \cdot mm^2$

$\varepsilon_{su} := 0.01$

Reference:Y:\Håndberegninger\Skjærbjelker\B2b\Fullt utnyttet trykksone\PrinteArk\Momentkapasitet Homogent t

Reference:Y:\Håndberegninger\Skjærbjelker\B2b\Fullt utnyttet trykksone\PrinteArk\Skjærkapasitet Homogent tv.s

$M_{Rk.tot} = 29.312 \cdot kN \cdot m$

$V_{Rk.tot} = 42.424 \cdot kN$

$a := 3 \cdot d$ $\quad a = 663 \cdot mm$

Output:

$$P_{maks.mom} := \frac{M_{Rk.tot}}{a} \qquad P_{maks.mom} = 44.211 \cdot kN$$

$$Dimensjonerende := \begin{cases} \text{"Moment"} & \text{if } P_{maks.mom} \le V_{Rk.tot} \\ \text{"Skjær"} & \text{otherwise} \end{cases}$$

$Dimensjonerende = \text{"Skjær"}$

$$P_{maks} := \begin{cases} V_{Rk.tot} & \text{if } V_{Rk.tot} < P_{maks.mom} \\ P_{maks.mom} & \text{otherwise} \end{cases} \qquad P_{maks} = 42.424 \cdot kN$$

Control Anchorage Capacity:

12.8.5

Tabell 8

$k_1 := 1.4$

$s := 92mm$

$c := 13mm$

$$k_2 := \begin{cases} 1.6 & \text{if } s > \max[9 \cdot \phi, (6 \cdot c + \phi)] \\ 1.0 & \text{if } s < \max[5 \cdot \phi, (3 \cdot c + \phi)] \\ \left[1.6 - 0.6 \cdot \left[\frac{\max[9 \cdot \phi, (6c + \phi)] - s}{\max[9 \cdot \phi, (6 \cdot c + \phi)] - \max[5 \cdot \phi, (3 \cdot c + \phi)]}\right]\right] & \text{otherwise} \end{cases}$$

$k_2 = 1.113$

$k_3 := 20MPa$

$s_t := 200mm$ $\quad A_{st} := 314.16mm^2$

$$f_{bc} := k_1 \cdot k_2 \cdot f_{ctk} \cdot \left(\frac{1}{3} + \frac{2 \cdot c}{3 \cdot \phi}\right) \qquad f_{bc} = 2.376 \cdot MPa$$

$$f_{bs} := \begin{cases} 0 & \text{if } s_t \le 0 \\ \min\left(k_3 \cdot \frac{A_{st}}{s_t \cdot \phi}, 1.5\text{MPa}\right) & \text{otherwise} \end{cases}$$

$f_{bs} = 1.5 \cdot \text{MPa}$

$$f_{bd} := \min\left(f_{bc} + f_{bs}, 2 \cdot k_1 \cdot f_{ctk}\right)$$

$f_{bd} = 3.876 \cdot \text{MPa}$

12.3.4.1 $$\sigma_s := \frac{P_{maks}}{A_s}$$

$\sigma_s = 105.499 \cdot \text{MPa}$

$$l_{b.min} := 0.25 \cdot \phi \cdot \frac{\sigma_s}{f_{bd}} + 3 \cdot \phi$$

$l_{b.min} = 156.864 \cdot \text{mm}$

G.1 Moment Capacity of Concept CSS With Top Cast

All references done in the margin are related to NS-EN 1992 (Eurcode 2) unless otherwise is specified.

All calculations are done with mean measured capacity values in the laboratory. Assumptions made when calculating the capacity are summarized together with the results in the main report.

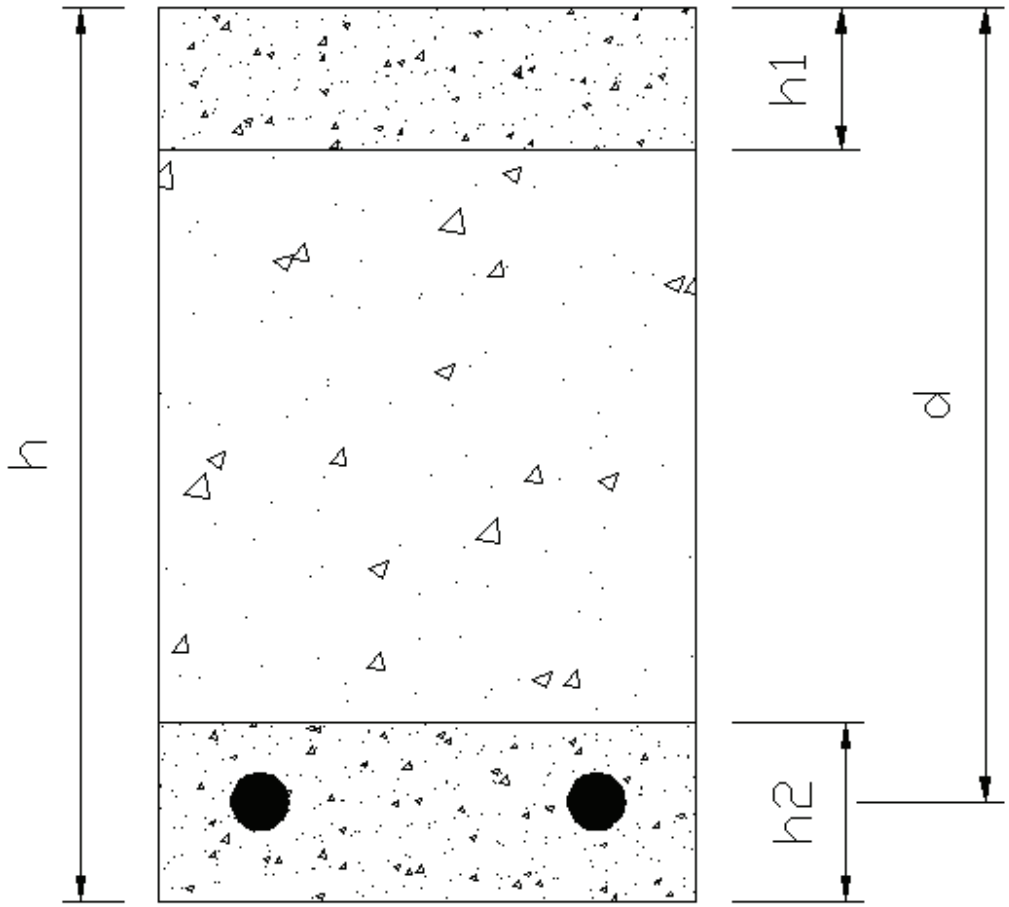

Input:

$\gamma_m := 1.0$

Dimensions:

$h := 250mm$

$b := 150mm$

$h1 := 50mm$ $h2 := 50mm$ $h_{midt} := 150mm$

$\phi := 12mm$

$d := 216mm$

Concrete Parameters:

Top Layer:

$f_{ck.h1} := 25.47MPa$ $f_{cd.h1} := \frac{f_{ck.h1}}{\gamma_m}$ $f_{cd.h1} = 25.47 \cdot MPa$

$\rho_{h1} := 2400 \frac{kg}{m^3}$

$E_{cm.h1} := 29130MPa$

$\varepsilon_{cu1.h1} := 0.0035$

$\varepsilon_{c0.h1} := 0.002$

Bottom Layer:

$f_{ck.h2} := 26.8MPa$ $f_{cd.h2} := \frac{f_{ck.h2}}{\gamma_m}$ $f_{cd.h2} = 26.8 \cdot MPa$

$\rho_{h2} := 2400 \frac{kg}{m^3}$

$E_{cm.h2} := 29570MPa$

$\varepsilon_{cu1.h2} := 0.0035$

$\varepsilon_{c0.h2} := 0.002$

Middle Layer:

$f_{cm.midt} := 11.6MPa$

$f_{cm.midt} := \frac{f_{cm.midt}}{\gamma_m}$

$f_{cm.midt} = 11.6 \cdot MPa$

$\rho_{midt} := 1250 \frac{kg}{m^3}$

$E_{cm.midt} := 11700MPa$

$\eta_1 := 0.4 + 0.6 \cdot \frac{\rho_{midt}}{2200 \frac{kg}{m^3}}$

$\varepsilon_{cu2.midt} := 0.0035 \cdot \eta_1$

$\varepsilon_{cu2.midt} = 2.593 \times 10^{-3}$

$\varepsilon_{c0.midt} := 0.002$

$\eta_1 := \frac{E_{cm.midt}}{E_{cm.h1}}$

$\eta_1 = 0.402$

$f_{ftk.res} := 0.840MPa$

Reinforcement:

$f_{sk} := 500MPa$

$E_s := 200000MPa$

$\varepsilon_{sy} := \frac{f_{sk}}{E_s}$

$\varepsilon_{sy} = 2.5 \times 10^{-3}$

$n := 2$

$A_s := n \cdot \pi \cdot \left(\frac{\phi}{2}\right)^2$

$A_s = 226.195 \cdot mm^2$

$\varepsilon_{su} := 0.01$

Output:

Balansert armeringsmengde:

$$\alpha_b := \frac{\varepsilon_{cu1.h1}}{\varepsilon_{cu1.h1} + \varepsilon_{sy}} \qquad \alpha_b = 0.583$$

Antar fullt utnyttet trykksone:

$$h_{maxit.trykk} := 0.8\alpha_b \cdot d - h1 \qquad h_{maxit.trykk} = 50.8 \cdot mm$$

T.c = S

$$A_{s.b} := \frac{\left(f_{cd.h1} \cdot b \cdot h1 + f_{cm.midt} \cdot b \cdot h_{maxit.trykk}\right)}{f_{sk}} \qquad A_{s.b} = 558.834 \cdot mm^2$$

$$\text{Armeringsmengde} := \begin{cases} \text{"Underarmert"} & \text{if } A_s \le A_{s.b} \\ \text{"Overarmert"} & \text{otherwise} \end{cases}$$

Armeringsmengde = "Underarmert"

Moment Capacity:

The contribution from the steel fibers on the tensile side has conservatively been neglected.

$$\alpha := \frac{A_s \cdot f_{sk}}{0.8 \cdot d \cdot b \cdot f_{cd.h1}} \qquad \alpha = 0.171 \qquad 0.8 \cdot \alpha \cdot d = 29.603 \cdot mm$$

$$M_{Rk} := 0.8 \cdot \alpha \cdot b \cdot d \cdot f_{cd.h1} \cdot (d - 0.5 \cdot 0.8 \cdot \alpha \cdot d) \qquad M_{Rk} = 22.755 \cdot kN \cdot m$$

$$p := 1.1 - 0.7 \cdot \frac{h}{1000mm} \qquad p = 0.925$$

$$M_{Rk.fiber} := 0.4 \cdot f_{ftk.res} \cdot b \cdot (h - h2)^2 \cdot p \qquad M_{Rk.fiber} = 1.865 \cdot kN \cdot m$$

Reinforcement strain:

$$\varepsilon_s := \frac{1-\alpha}{\alpha}\cdot\varepsilon_{cu1.h1} \qquad \varepsilon_s = 0.017$$

$$\text{Tøyning} := \begin{cases} \text{"Overskrider bruddtøyning"} & \text{if } \varepsilon_s > 0.01 \\ \text{"Ok mtp. bruddtøyning"} & \text{otherwise} \end{cases}$$

Tøyning = "Overskrider bruddtøyning"

OBS: Lamellmetode/iterasjonsmetode kun utført mtp. kravet om maks armeringstøyning i NS 3473. Dette kravet finnes ikke i Eurocode 2.

Reference:Y:\Håndberegninger\Hybridbjelke\Forhåndsdimensjonering\Hybriddekke\Faktiske fastheter, korrekt ber

Lamellmetode gir ny betongtrykktøyning og momentkapasitet som følger:

Betongtrykktøyning som oppfyller tøyningskrav armering: $\varepsilon_c = 2.4\times 10^{-3}$

$M_{Rk2} = 22.898\cdot kN\cdot m$

Final Moment Capacity:

Etter Eurocode 2: $M_{Rk.tot} := M_{Rk} + M_{Rk.fiber}$ $\qquad M_{Rk.tot} = 24.62\cdot kN\cdot m$

Etter NS3473: $M_{Rk.tot2} := M_{Rk2} + M_{Rk.fiber}$ $\qquad M_{Rk.tot2} = 24.763\cdot kN\cdot m$

CSS Weight:

$$\rho_{tot} := \rho_{h1}\cdot h1 + \rho_{h2}\cdot h2 + \rho_{midt}\cdot h_{midt} \qquad \rho_{tot} = 427.5\,\frac{kg}{m^2}$$

G.2 Lamellmetode/Iterasjonsmetode

Lamellmetode beregninger er kun gjort med tanke på kravet om maksimalt 1% armeringstøyning i NS 3473. Dette kravet eksisterer ikke i Eurocode 2.

Reference:Y:\Håndberegninger\Hybridbjelke\Forhåndsdimensjonering\Hybriddekke\Faktiske fastheter, korrekt bereg

Prøver med: $\varepsilon_{cu} := 0.0024$

$\delta\varepsilon := 0.000024$

Antall lameller: $l := \frac{\varepsilon_c}{\delta\varepsilon}$ $l = 100$

Antall lameller full flyt:

$l_{flyt1} := \frac{\varepsilon_c - \varepsilon_{c0.h1}}{\delta\varepsilon}$ $l_{flyt} := \begin{cases} l_{flyt1} & \text{if } l_{flyt1} \geq 0 \\ 0 & \text{otherwise} \end{cases}$ $l_{flyt} = 16.667$

Antall lameller delvis utnyttet:

$l_{delvis} := l - l_{flyt}$ $l_{delvis} = 83.333$

Kraft i armering:

$S := f_{sk} \cdot A_s$ $S = 113.097 \cdot kN$

Trykksonehøyde:

$\alpha := \frac{\varepsilon_c}{\varepsilon_c + \varepsilon_{su}}$ $\alpha \cdot d = 41.806 \cdot mm$

Lamellhøyde

$h_{lamell} := \frac{\alpha \cdot d}{l}$ $h_{lamell} = 0.418 \cdot mm$

Lamellkrefter:

$T_{c.full} := l_{flyt} \cdot h_{lamell} \cdot f_{cd.h1} \cdot b$ $\quad T_{c.full} = 26.62 \cdot kN$

$T_{c.delvis}(k) :=$
$\quad sum \leftarrow 0$
$\quad i \leftarrow 1$
$\quad \varepsilon_0 \leftarrow \begin{cases} \varepsilon_c & \text{if } \varepsilon_c \le 0.002 \\ 0.002 & \text{otherwise} \end{cases}$
$\quad$ for $i \in 1 .. l_{delvis}$
$\quad\quad \varepsilon_i \leftarrow \varepsilon_{(i-1)} - \delta\varepsilon$
$\quad\quad f_i \leftarrow \frac{\varepsilon_i}{\varepsilon_{c0.h1}} \cdot \left(2 - \frac{\varepsilon_i}{\varepsilon_{c0.h1}} \right)$
$\quad\quad sum \leftarrow sum + f_i \cdot f_{cd.h1} \cdot b \cdot h_{lamell}$
$\quad\quad i \leftarrow i + 1$
$\quad$ return sum

$T_{c.delvis}(1) = 8.794 \times 10^4\,N$

$f_{cd.h1} = 2.547 \times 10^7\,Pa$

$h_{lamell} = 0.418 \cdot mm$

$T_c := T_{c.delvis}(1) + T_{c.full}$ $\quad T_c = 1.146 \times 10^5\,N$

$T_c - S = 1.46 \times 10^3\,N$

$$M_{Rk.delvis}(k) := \left| \begin{array}{l} sum \leftarrow 0 \\ i \leftarrow 1 \\ \varepsilon_0 \leftarrow \left| \begin{array}{ll} \varepsilon_c & \text{if } \varepsilon_c \le 0.002 \\ 0.002 & \text{otherwise} \end{array} \right. \\ a \leftarrow d - 0.5 \cdot h_{lamell} - l_{flyt} \cdot h_{lamell} \\ \text{for } i \in 1 .. l_{delvis} \\ \quad \left| \begin{array}{l} \varepsilon_i \leftarrow \varepsilon_{(i-1)} - \delta\varepsilon \\ f_i \leftarrow \dfrac{\varepsilon_i}{\varepsilon_{c0.h1}} \cdot \left(2 - \dfrac{\varepsilon_i}{\varepsilon_{c0.h1}} \right) \\ sum \leftarrow sum + f_i \cdot f_{cd.h1} \cdot b \cdot h_{lamell} \cdot a \\ a \leftarrow a - h_{lamell} \\ i \leftarrow i + 1 \end{array} \right. \\ \text{return } sum \end{array} \right.$$

$$M_{Rk.delvis}(1) = 1.724 \times 10^7 \cdot N \cdot mm$$

$$M_{Rk.full} := T_{c.full} \cdot \left(d - 0.5 \cdot l_{flyt} \cdot h_{lamell} \right)$$

$$M_{Rk2} := M_{Rk.delvis}(1) + M_{Rk.full} \qquad M_{Rk2} = 2.29 \times 10^7 \cdot N \cdot mm$$

G.3 Shear Capacity of Concept CSS With Top Cast

All references done in the margin are related to NS-EN 1992 (Eurcode 2) unless otherwise is specified.

All calculations are done with mean measured capacity values in the laboratory. Assumptions made when calculating the capacity are summarized together with the results in the main report.

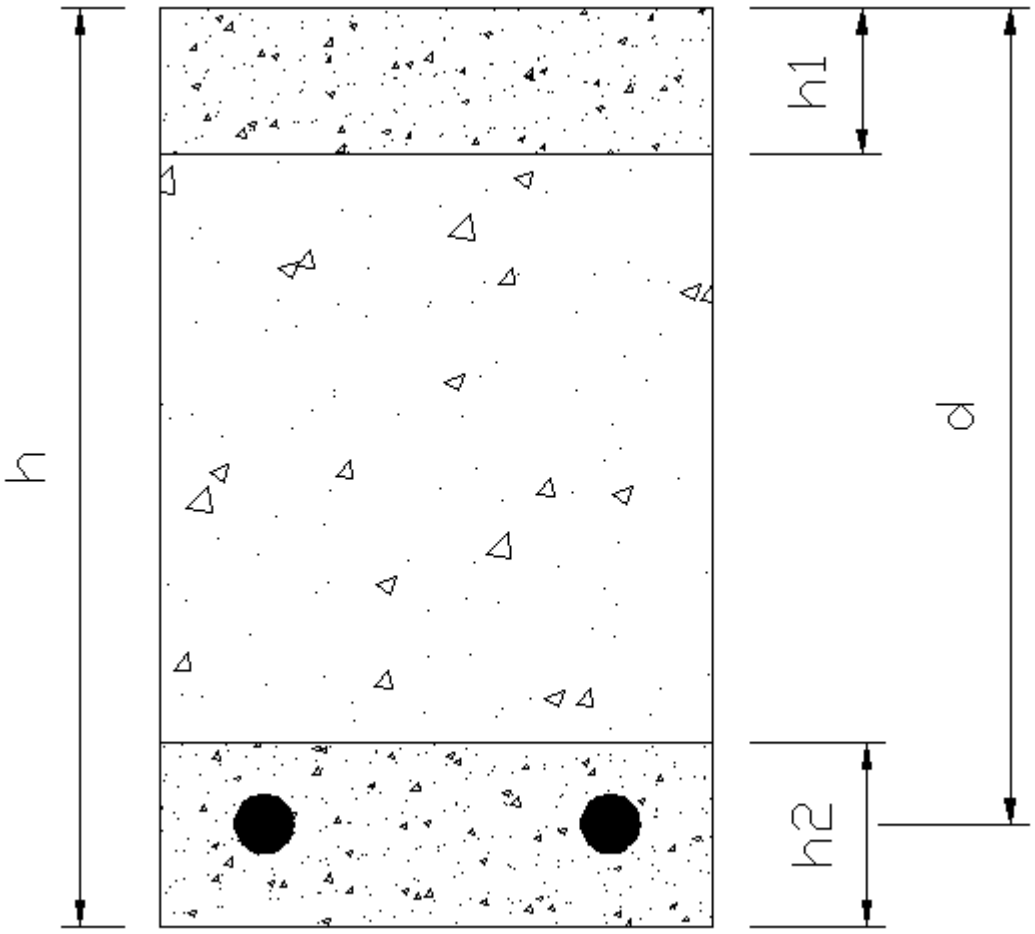

Input:

$\gamma_m := 1.0$

Dimensions:

$h := 250mm$

$b := 150mm$

$d := 216mm$

$d_{max} := 10mm$

$h_{midt} := 150mm$

Axial Force:

$N_{Ed} := 0 \cdot kN$

Concrete Parameters:

$f_{lctm} := 1.26MPa$; from tension tests done in lab

Table 3.1

$$f_{ck.equiv} := 10.39133 \cdot \left(f_{lctm}\right)^{\frac{3}{2}} \cdot (MPa)^{\frac{-1}{2}}$$

NA.3.1.6

$f_{ck.equiv} = 14.697 \cdot MPa$

$$f_{cd} := \frac{f_{ck.equiv}}{\gamma_m}$$

$f_{cd} = 14.697 \cdot MPa$

$\rho := 1250 \frac{kg}{m^3}$

Table 11.3.1

$E_{cm} := 11700MPa$

$$\eta_1 := 0.4 + 0.6 \cdot \frac{\rho}{2200 \frac{kg}{m^3}}$$

$\varepsilon_{cu2.midt} := 0.0035 \cdot \eta_1$

$\varepsilon_{cu2.midt} = 0.002593$

$\varepsilon_{c0} := 0.002$

$f_{ftk.res} := 0.840MPa$

Reinforcement:

$f_{sk} := 500MPa$

$E_s := 200000MPa$

$\varepsilon_{sy} := \frac{f_{sk}}{E_s}$ $\quad \varepsilon_{sy} = 2.5 \times 10^{-3}$

$\phi := 12mm$ $\quad n := 2$

$A_s := n \cdot \pi \cdot \left(\frac{\phi}{2}\right)^2$ $\quad A_s = 226.195 \cdot mm^2$

$\varepsilon_{su} := 0.01$

Output:

6.2.2(1)
NA6.2.2

$$C_{rd.c} := \begin{cases} 0.18 & \text{if } d_{max} \geq 16mm \\ 0.15 & \text{otherwise} \end{cases}$$

$C_{rd.c} = 0.15$

$$k := \begin{cases} \left(\left(1 + \sqrt{\frac{200mm}{d}}\right)\right) & \text{if } \left(1 + \sqrt{\frac{200mm}{d}}\right) \leq 2 \\ 2 & \text{otherwise} \end{cases}$$

$k = 1.962$

$$\rho_1 := \begin{cases} \frac{A_s}{b \cdot d} & \text{if } \left(\frac{A_s}{b \cdot d}\right) \leq 0.02 \\ 0.02 & \text{otherwise} \end{cases}$$

$\rho_1 = 6.981 \times 10^{-3}$

$$\sigma_{cp} := \begin{cases} \left(\left(\frac{N_{Ed}}{b \cdot h}\right)\right) & \text{if } \left(\frac{N_{Ed}}{b \cdot h}\right) < 0.2 \cdot f_{cd} \\ \left(0.2 \cdot f_{cd}\right) & \text{otherwise} \end{cases}$$

$\sigma_{cp} = 0\,Pa$

$k_1 := 0.15$

$$v_{min} := 0.028 \cdot k^{\frac{3}{2}} \cdot \sqrt{f_{ck.equiv}} \cdot \sqrt{MPa}$$

$v_{min} = 0.295 \cdot MPa$

$$V_{Rk.c} := \left[C_{rd.c} \cdot k \cdot \left(100 \cdot \rho_1 \cdot f_{ck.equiv}\right)^{\frac{1}{3}} \cdot (MPa)^{\frac{2}{3}} + k_1 \cdot \sigma_{cp}\right] \cdot b \cdot d$$

$$V_{Rk.c1} := \begin{cases} V_{Rk.c} & \text{if } V_{Rk.c} \geq \left[\left(v_{min} + k_1 \cdot \sigma_{cp}\right) \cdot b \cdot d\right] \\ \left[\left(v_{min} + k_1 \cdot \sigma_{cp}\right) \cdot b \cdot d\right] & \text{otherwise} \end{cases}$$

$V_{Rk.c1} = 20.723 \cdot kN$

$$p := 1.1 - 0.7 \cdot \frac{h}{1000mm}$$

$p = 0.925$

$V_{Rk.c.fiber} := f_{ftk.res} \cdot b \cdot h_{midt} \cdot p$

$V_{Rk.c.fiber} = 17.483 \cdot kN$

$V_{Rk.c.tot} := V_{Rk.c1} + V_{Rk.c.fiber}$

$V_{Rk.c.tot} = 38.205 \cdot kN$

G.4 Control Anchorage Capacity, Concept CSS Beams

All references done in the margin are related to NS-EN 1992 Eurocode 2 unless otherwise is specified.

All calculations are done with mean measured capacity values in the laboratory. Assumptions made when calculating the capacity are summarized together with the results in the main report.

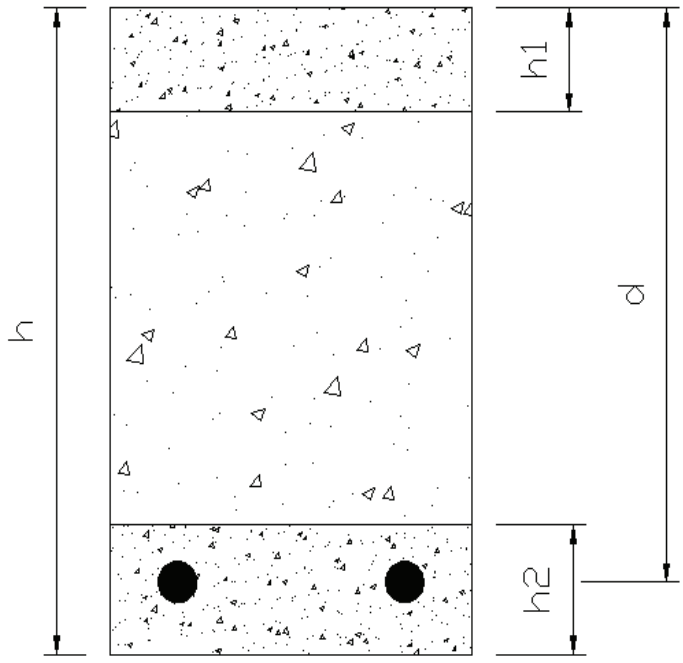

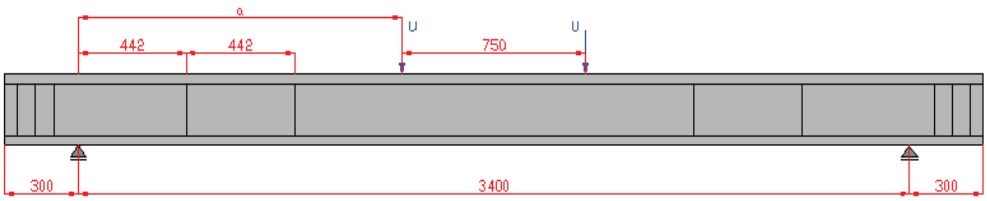

Input:

$\gamma_m := 1.0$

Dimensions:

$h := 250mm$

$b := 150mm$

$d := 216mm$

$d_{max} := 16mm$

$a := 1325mm$

Axial Force:

$N_{Ed} := 0 \cdot kN$

$a = 1325 \cdot mm$

Concrete Parameters Bottom Layer:

Table 3.1

NA.3.1.6

$f_{ck} := 26.8MPa$

$f_{cd} := f_{ck}$

$f_{cd} = 26.8 \cdot MPa$

$f_{ctk} := 2.1MPa$

$\rho := 2400 \frac{kg}{m^3}$

$E_{cm} := 29570MPa$

$\varepsilon_{cu1} := 0.0035$

$\varepsilon_{c0} := 0.002$

Reinforcement:

$f_{sk} := 500MPa$

$E_s := 200000MPa$

$\varepsilon_{sy} := \frac{f_{sk}}{E_s}$ $\quad \varepsilon_{sy} = 2.5 \times 10^{-3}$

$\phi := 12mm$ $\quad n := 2$

$A_s := n \cdot \pi \cdot \left(\frac{\phi}{2}\right)^2$ $\quad A_s = 226.195 \cdot mm^2$

$\varepsilon_{su} := 0.01$

Reference:Y:\Håndberegninger\Hybridbjelke\Forhåndsdimensjonering\Hybriddekke\Faktiske fastheter, korrekt ber

Reference:Y:\Håndberegninger\Hybridbjelke\Forhåndsdimensjonering\Hybriddekke\Faktiske fastheter, korrekt ber

$M_{Rk.tot} = 2.462 \times 10^4 \cdot N \cdot m$

$V_{Rk.c.tot} = 38.205 \cdot kN$

Output:

$$P_{maks.mom} := \frac{M_{Rk.tot}}{a} \qquad P_{maks.mom} = 18.581 \cdot kN$$

$$Dimensjonerende := \begin{cases} \text{"Moment"} & \text{if } P_{maks.mom} \le V_{Rk.c.tot} \\ \text{"Skjær"} & \text{otherwise} \end{cases}$$

$$Dimensjonerende = \text{"Moment"}$$

$$P_{maks} := \begin{cases} V_{Rk.c.tot} & \text{if } V_{Rk.c.tot} < P_{maks.mom} \\ P_{maks.mom} & \text{otherwise} \end{cases} \qquad P_{maks} = 18.581 \cdot kN$$

Control Anchorage Capacity:

8.4.2
Table 8.2

$\eta_1 := 1$ $\quad \alpha_1 := 1$ $\quad \alpha_3 := 1$ $\quad \alpha_5 := 1$

$\eta_2 := 1$ $\quad \alpha_2 := 1$ $\quad \alpha_4 := 0.7$

$$f_{bk} := 2.25 \cdot \eta_1 \cdot \eta_2 \cdot f_{ctk} \qquad f_{bk} = 4.725 \cdot MPa$$

$$\sigma_s := \frac{P_{maks} \cdot \cot\left(\frac{\pi}{4}\right)}{A_s} \qquad \sigma_s = 82.146 \cdot MPa$$

8.4.3

$$l_{b.rqk} := \left(\frac{\phi}{4}\right) \cdot \left(\frac{\sigma_s}{f_{bk}}\right) \qquad l_{b.rqk} = 52.156 \cdot mm$$

8.4.4

$$l_{b.min} := \max\left(0.3 l_{b.rqk}, 10 \cdot \phi, 100mm\right) \qquad l_{b.min} = 120 \cdot mm$$

$$l_{bk} := \max\left(\alpha_1 \cdot \alpha_2 \cdot \alpha_3 \cdot \alpha_4 \cdot \alpha_5 \cdot l_{b.rqk}, l_{b.min}\right) \qquad l_{bk} = 120 \cdot mm$$

G.5 Control Anchorage Capacity, Concept CSS Beams (Old Norwegian Standard)

All references done in the margin are related to NS 3473 (old Norwegian standard) unless otherwise is specified.

All calculations are done with mean measured capacity values in the laboratory. Assumptions made when calculating the capacity are summarized together with the results in the main report.

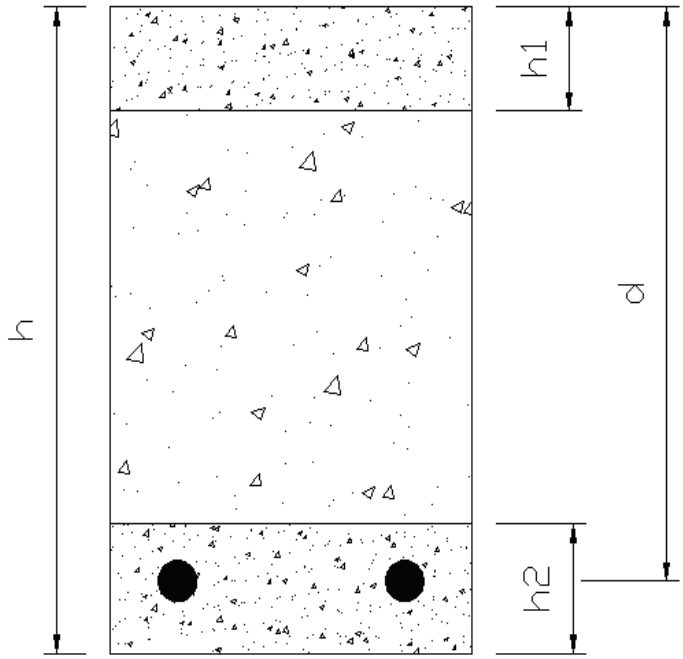

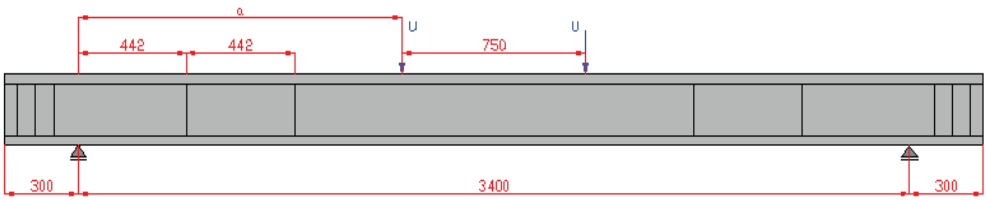

Input:

$\gamma_m := 1.0$

Dimensions:

$h := 250mm$

$b := 150mm$

$d := 216mm$

$d_{max} := 16mm$

$a := 1325mm$

Axial Force:

$N_{Ed} := 0 \cdot kN$

$a = 1325 \cdot mm$

Concrete Parameters Bottom Layer:

Table 3.1

NA.3.1.6

$f_{ck} := 26.8MPa$

$f_{cd} := f_{ck}$

$f_{cd} = 26.8 \cdot MPa$

$f_{ctk} := 2.1MPa$

$\rho := 2400 \frac{kg}{m^3}$

$E_{cm} := 29570MPa$

$\varepsilon_{cu1} := 0.0035$

$\varepsilon_{c0} := 0.002$

Reinforcement:

$f_{sk} := 500MPa$

$E_s := 200000MPa$

$\varepsilon_{sy} := \frac{f_{sk}}{E_s}$ $\quad \varepsilon_{sy} = 2.5 \times 10^{-3}$

$\phi := 12mm$ $\quad n := 2$

$A_s := n \cdot \pi \cdot \left(\frac{\phi}{2}\right)^2$ $\quad A_s = 226.195 \cdot mm^2$

$\varepsilon_{su} := 0.01$

Reference:Y:\Håndberegninger\Hybridbjelke\Forhåndsdimensjonering\Hybriddekke\Faktiske fastheter, korrekt ber

Reference:Y:\Håndberegninger\Hybridbjelke\Forhåndsdimensjonering\Hybriddekke\Faktiske fastheter, korrekt ber

$M_{Rk.tot} = 2.462 \times 10^4 \cdot N \cdot m$

$V_{Rk.c.tot} = 38.205 \cdot kN$

Output:

$$P_{maks.mom} := \frac{M_{Rk.tot}}{a} \qquad P_{maks.mom} = 18.581 \cdot kN$$

$$Dimensjonerende := \begin{cases} \text{"Moment"} & \text{if } P_{maks.mom} \le V_{Rk.c.tot} \\ \text{"Skjær"} & \text{otherwise} \end{cases}$$

$$Dimensjonerende = \text{"Moment"}$$

$$P_{maks} := \begin{cases} V_{Rk.c.tot} & \text{if } V_{Rk.c.tot} < P_{maks.mom} \\ P_{maks.mom} & \text{otherwise} \end{cases} \qquad P_{maks} = 18.581 \cdot kN$$

Control Anchorage Capacity:

12.8.5

Tabell 8

$k_1 := 1.4$

$s := 70mm$

$c := 20mm$

$$k_2 := \begin{cases} 1.6 & \text{if } s > \max[9 \cdot \phi, (6 \cdot c + \phi)] \\ 1.0 & \text{if } s < \max[5 \cdot \phi, (3 \cdot c + \phi)] \\ \left[1.6 - 0.6 \cdot \left[\frac{\max[9 \cdot \phi, (6c + \phi)] - s}{\max[9 \cdot \phi, (6 \cdot c + \phi)] - \max[5 \cdot \phi, (3 \cdot c + \phi)]}\right]\right] & \text{otherwise} \end{cases}$$

$k_2 = 1$

$k_3 := 20MPa$

$s_t := 0mm$ $\quad A_{st} := 0mm^2$

$$f_{bc} := k_1 \cdot k_2 \cdot f_{ctk} \cdot \left(\frac{1}{3} + \frac{2 \cdot c}{3 \cdot \phi}\right) \qquad f_{bc} = 4.247 \cdot MPa$$

$$f_{bs} := \begin{cases} 0 & \text{if } s_t \le 0 \\ \min\left(k_3 \cdot \frac{A_{st}}{s_t \cdot \phi}, 1.5\text{MPa}\right) & \text{otherwise} \end{cases}$$

$f_{bs} = 0 \cdot \text{MPa}$

$$f_{bd} := \min\left(f_{bc} + f_{bs}, 2 \cdot k_1 \cdot f_{ctk}\right)$$

$f_{bd} = 4.247 \cdot \text{MPa}$

12.3.4.1 $$\sigma_s := \frac{P_{maks}}{A_s}$$

$\sigma_s = 82.146 \cdot \text{MPa}$

$$l_{b.min} := 0.25 \cdot \phi \cdot \frac{\sigma_s}{f_{bd}} + 3 \cdot \phi$$

$l_{b.min} = 94.031 \cdot \text{mm}$

H.1 Moment Capacity of Concept CSS Without Top Cast

All references done in the margin are related to NS-EN 1992 (Eurcode 2) unless otherwise is specified.

All calculations are done with mean measured capacity values in the laboratory. Assumptions made when calculating the capacity are summarized together with the results in the main report.

No calculations has been carried out regarding anchorage capacity of the beams without the top cast. This is because the capacity for the beams with the topcast was sufficient.

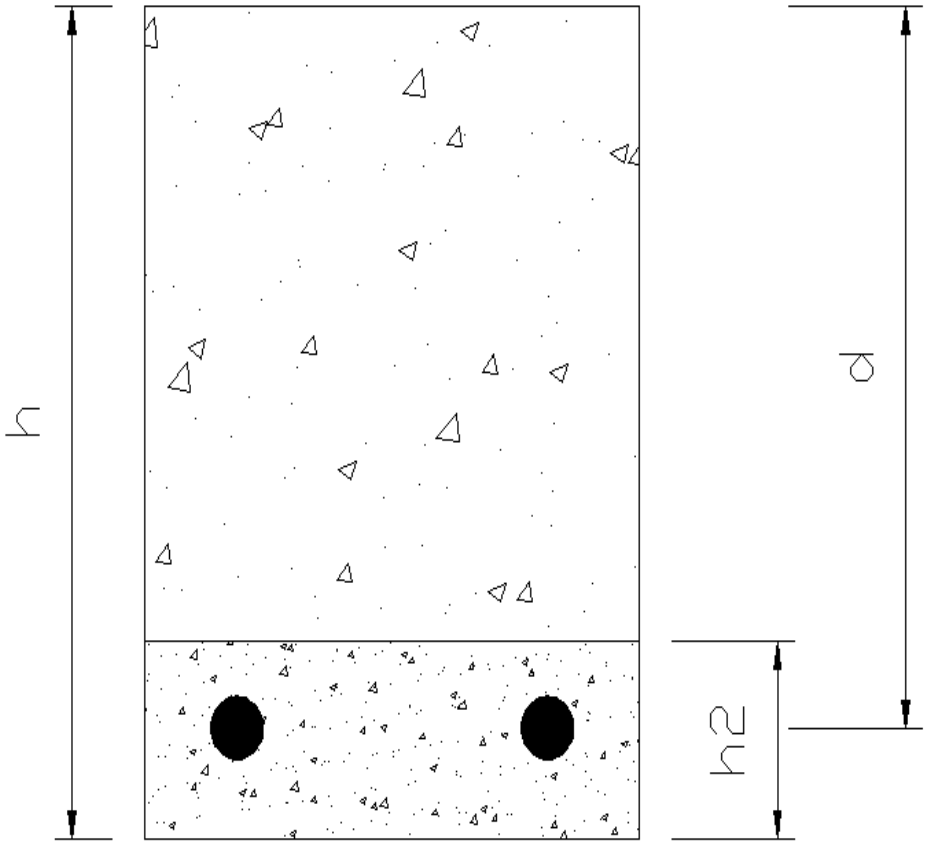

Input:

$\gamma_m := 1.0$

Dimensions:

$h := 200mm$

$b := 150mm$

$h1 := 0mm$ $h2 := 50mm$ $h_{midt} := 150mm$

$\phi := 12mm$

$d := 166mm$

Concrete Parameters:

Top Layer:

$f_{ck.h1} := 11.6MPa$ $f_{cd.h1} := \frac{f_{ck.h1}}{\gamma_m}$ $f_{cd.h1} = 11.6 \cdot MPa$

$\rho_{h1} := 1250 \frac{kg}{m^3}$

$E_{cm.h1} := 11700MPa$

$\eta_1 := 0.4 + 0.6 \cdot \frac{\rho_{h1}}{2200 \frac{kg}{m^3}}$

$\varepsilon_{cu2.h1} := 0.0035 \cdot \eta_1$ $\varepsilon_{cu2.h1} = 2.593 \times 10^{-3}$

$\varepsilon_{c0.h1} := 0.002$

Bottom Layer:

$f_{ck.h2} := 25.47MPa$

$f_{cd.h2} := \frac{f_{ck.h2}}{\gamma_m}$

$f_{cd.h2} = 25.47 \cdot MPa$

$\rho_{h2} := 2400 \frac{kg}{m^3}$

$E_{cm.h2} := 29570MPa$

$\varepsilon_{cu1.h2} := 0.0035$

$\varepsilon_{c0.h2} := 0.002$

Middle Layer:

$f_{cm.midt} := 11.6MPa$

$f_{cm.midt} := \frac{f_{cm.midt}}{\gamma_m}$

$f_{cm.midt} = 11.6 \cdot MPa$

$\rho_{midt} := 1250 \frac{kg}{m^3}$

$E_{cm.midt} := 11700MPa$

$\eta_1 := 0.4 + 0.6 \cdot \frac{\rho_{midt}}{2200 \frac{kg}{m^3}}$

$\varepsilon_{c0.midt} := 0.002$

$\varepsilon_{cu2.midt} := 0.0035 \cdot \eta_1$

$\varepsilon_{cu2.midt} = 0.00259$

$f_{ftd.res} := 0.840MPa$

Reinforcement:

$f_{sk} := 500MPa$

$E_s := 200000MPa$

$\varepsilon_{sy} := \frac{f_{sk}}{E_s}$

$\varepsilon_{sy} = 2.5 \times 10^{-3}$

$n := 2$

$A_s := n \cdot \pi \cdot \left(\frac{\phi}{2}\right)^2$

$\varepsilon_{su} := 0.01$

Output:

Balansert armeringsmengde:

$$\alpha_b := \frac{\varepsilon_{cu2.midt}}{\varepsilon_{cu2.midt} + \varepsilon_{sy}}$$

$\alpha_b = 0.509$

T.c = S

$$A_{s.b} := \frac{\left(0.8 f_{cm.midt} \cdot b \cdot \alpha_b \cdot d\right)}{f_{sk}}$$

$A_{s.b} = 235.3 \cdot mm^2$

$$\text{Armeringsmengde} := \begin{cases} \text{"Underarmert"} & \text{if } A_s \le A_{s.b} \\ \text{"Overarmert"} & \text{otherwise} \end{cases}$$

Armeringsmengde = "Underarmert"

Moment Capacity:

The contribution from the steel fiber on the tensile side has conservatively been neglected.

$$\alpha := \frac{A_s \cdot f_{sk}}{0.8 \cdot d \cdot b \cdot f_{cm.midt}}$$

$\alpha = 0.489$

$0.8 \cdot \alpha \cdot d = 64.998 \cdot mm$

$$M_{Rk} := 0.8 \cdot \alpha \cdot b \cdot d \cdot f_{cm.midt} \cdot (d - 0.5 \cdot 0.8 \cdot \alpha \cdot d)$$

$M_{Rk} = 15.099 \cdot kN \cdot m$

$$p := 1.1 - 0.7 \cdot \frac{h}{1m}$$

$p = 0.96$

$$M_{Rk.fiber} := 0.4 \cdot f_{ftd.res} \cdot b \cdot (h - h2)^2 \cdot p$$

$M_{Rk.fiber} = 1.089 \cdot kN \cdot m$

$$M_{Rk.tot} := M_{Rk} + M_{Rk.fiber}$$

$M_{Rk.tot} = 16.187 \cdot kN \cdot m$

Reinforcement strain:

$$\varepsilon_s := \frac{1-\alpha}{\alpha}\cdot\varepsilon_{cu2.h1} \qquad \boxed{\varepsilon_s = 2.705\times 10^{-3}}$$

$$\text{Tøyning} := \begin{cases} \text{"Overskrider bruddtøyning"} & \text{if } \varepsilon_s > 0.01 \\ \text{"Ok mtp. bruddtøyning"} & \text{otherwise} \end{cases}$$

$$\text{Tøyning} = \text{"Ok mtp. bruddtøyning"}$$

CSS Weight:

$$\rho_{tot} := \rho_{h1}\cdot h1 + \rho_{h2}\cdot h2 + \rho_{midt}\cdot h_{midt} \qquad \boxed{\rho_{tot} = 307.5\,\frac{kg}{m^2}}$$

H.2 Shear Capacity of Concept CSS Without Top Cast

All references done in the margin are related to NS-EN 1992 (Eurcode 2) unless otherwise is specified.

All calculations are done with mean measured capacity values in the laboratory. Assumptions made when calculating the capacity are summarized together with the results in the main report.

No calculations has been carried out regarding anchorage capacity of the beams without the top cast. This is because the capacity for the beams with the topcast was sufficient.

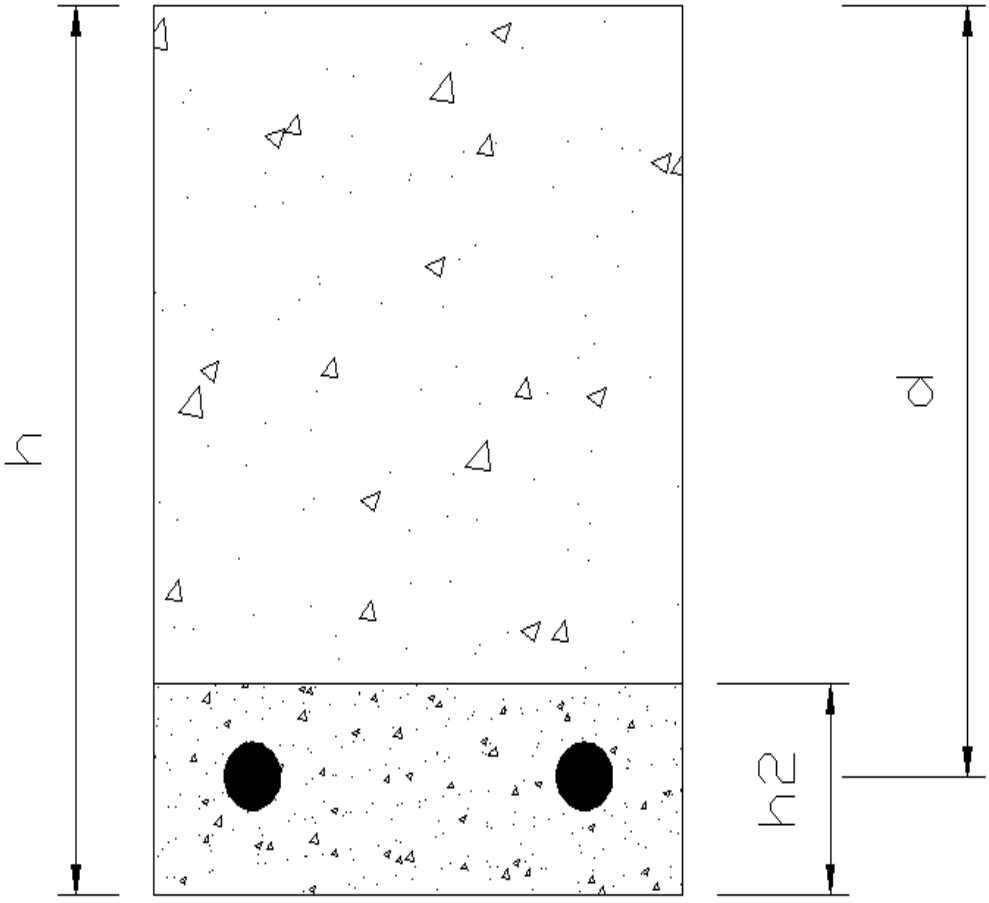

Input:

$\gamma_m := 1.0$

Dimensions:

$h := 200mm$

$b := 150mm$

$d := 166mm$

$d_{max} := 10mm$

$h_{midt} := 150mm$

Axial Force:

$N_{Ed} := 0 \cdot kN$

Concrete Parameters:

$f_{lctm} := 1.26MPa$; from tension tests done in lab

$f_{ftd.res} := 0.840MPa$

Table 3.1

$$f_{ck.equiv} := 10.39133 \cdot \left(f_{lctm}\right)^{\frac{3}{2}} \cdot (MPa)^{\frac{-1}{2}}$$

NA.3.1.6

$$f_{ck.equiv} = 14.697 \cdot MPa$$

$$f_{cd} := \frac{f_{ck.equiv}}{\gamma_m}$$

$$f_{cd} = 14.697 \cdot MPa$$

$\rho := 1250 \frac{kg}{m^3}$

Table 11.3.1

$E_{cm} := 11700MPa$

$$\eta_1 := 0.4 + 0.6 \cdot \frac{\rho}{2200 \frac{kg}{m^3}}$$

$$\varepsilon_{cu2.midt} := 0.0035 \cdot \eta_1$$

$$\varepsilon_{cu2.midt} = 0.002593$$

$\varepsilon_{c0} := 0.002$

Reinforcement:

$f_{sk} := 500MPa$

$E_s := 200000MPa$

$\varepsilon_{sy} := \frac{f_{sk}}{E_s}$ $\quad \varepsilon_{sy} = 2.5 \times 10^{-3}$

$\phi := 12mm$ $\quad n := 2$

$A_s := n \cdot \pi \cdot \left(\frac{\phi}{2}\right)^2$ $\quad A_s = 226.195 \cdot mm^2$

$\varepsilon_{su} := 0.01$

Output:

6.2.2(1)

NA6.2.2

$$C_{rd.c} := \begin{cases} 0.18 & \text{if } d_{max} \geq 16mm \\ 0.15 & \text{otherwise} \end{cases}$$

$C_{rd.c} = 0.15$

$$k := \begin{cases} \left(\left(1 + \sqrt{\frac{200mm}{d}}\right)\right) & \text{if } \left(1 + \sqrt{\frac{200mm}{d}}\right) \leq 2 \\ 2 & \text{otherwise} \end{cases}$$

$k = 2$

$$\rho_1 := \begin{cases} \frac{A_s}{b \cdot d} & \text{if } \left(\frac{A_s}{b \cdot d}\right) \leq 0.02 \\ 0.02 & \text{otherwise} \end{cases}$$

$\rho_1 = 9.084 \times 10^{-3}$

$$\sigma_{cp} := \begin{cases} \left(\left(\frac{N_{Ed}}{b \cdot h}\right)\right) & \text{if } \left(\frac{N_{Ed}}{b \cdot h}\right) < 0.2 \cdot f_{cd} \\ \left(0.2 \cdot f_{cd}\right) & \text{otherwise} \end{cases}$$

$\sigma_{cp} = 0\,Pa$

$$k_1 := 0.15$$

$$v_{min} := 0.028 \cdot k^{\frac{3}{2}} \cdot \sqrt{f_{ck.equiv}} \cdot \sqrt{MPa}$$

$v_{min} = 0.304 \cdot MPa$

$$V_{Rk.c} := \left[C_{rd.c} \cdot k \cdot \left(100 \cdot \rho_1 \cdot f_{ck.equiv}\right)^{\frac{1}{3}} \cdot (MPa)^{\frac{2}{3}} + k_1 \cdot \sigma_{cp}\right] \cdot b \cdot d$$

$$V_{Rk.c1} := \begin{cases} V_{Rk.c} & \text{if } V_{Rk.c} \geq \left[\left(v_{min} + k_1 \cdot \sigma_{cp}\right) \cdot b \cdot d\right] \\ \left[\left(v_{min} + k_1 \cdot \sigma_{cp}\right) \cdot b \cdot d\right] & \text{otherwise} \end{cases}$$

$V_{Rk.c1} = 17.721 \cdot kN$

Høringsutkast
Mai 2006

$$p := 1.1 - 0.7 \cdot \frac{h}{1000mm}$$

$$V_{Rk.c.fiber} := 0.8 \cdot f_{ftd.res} \cdot b \cdot h_{midt} \cdot p$$

$$V_{Rk.c.tot} := V_{Rk.c1} + V_{Rk.c.fiber}$$

$V_{Rk.c.tot} = 32.236 \cdot kN$